Recognizing critically damaged quay wall structures using a three-dimensional numerical model.

Master's Thesis

C.P.A. van Hulten




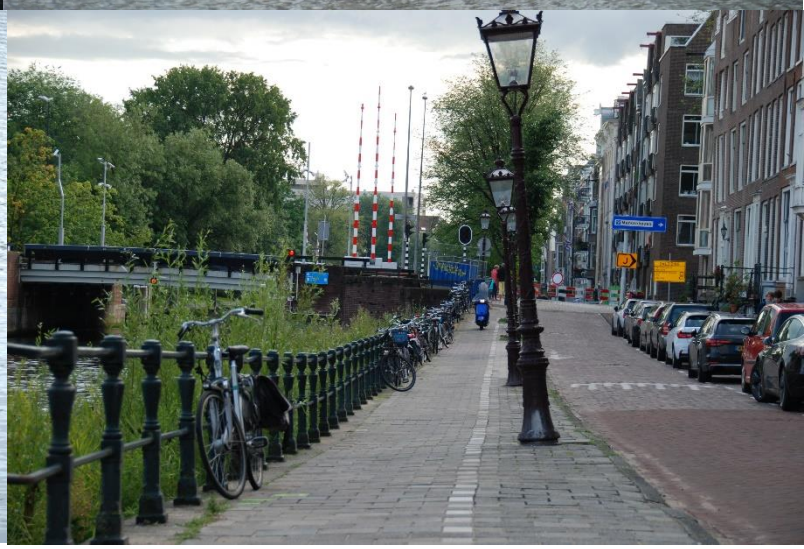

TU Delft Delft University of Technology

SWECO

Delft University of Technology

Recognizing critically damaged quay wall structures using a three-dimensional numerical model

Author:
Chris van Hulten

To obtain the degree of Master of Science at the Delft University of Technology

Thesis duration: 19/10/2020 - 30/11/2021

Thesis committee composition:

Dr.ir. M. Korff (chair)	TU Delft, Faculty of Civil Engineering and Geosciences
Ir. P.A. Korswagen	TU Delft, Faculty of Civil Engineering and Geosciences
Ir. M.J. Hemel	TU Delft, Faculty of Civil Engineering and Geosciences
Dr. Elisa Ragno	TU Delft, Faculty of Civil Engineering and Geosciences
Ir. R. Roggeveld	Sweco NL

Preface

This master's thesis is written to complete my master degree in Hydraulic Engineering at the Delft University of Technology. This work is written in cooperation with the engineering firm Sweco, where I had been active for a while before commencing my master´s thesis trajectory. Together we have chosen to dive deeper into the subject of quay walls. The part which made this subject interesting is due to the fact that the poor quality of Amsterdam´s quay walls is a contemporary and relatively urgent issue. Although I was initially inexperienced with finite element modelling, I have always been interested in automation and in building parametric models. I am grateful I was able to learn to work with these types of software and being able to build a parametric model with it, which is a skill I value and would like to apply in my future career.

This thesis is written for those who have a particular interest in the current quay wall problem in Amsterdam. It can be used to provide better insight on how quay walls with poor quality present themselves in real life and what the cause might be. Hopefully, it will be possible to improve recognition of quay walls which find themselves in critical condition, which can then be prioritized for renovations.

The thesis trajectory took place in the middle of the COVID-19 pandemic. Unfortunately, most of my work had to be written remotely and I had little physical contact with Sweco and the university, which I experienced as a less-than-ideal situation. I would like to acknowledge my thesis committee who, despite these limitations, were still able to help me complete this process successfully.

First of all, I would like to thank Mandy Korff for being the chair of my committee and providing advice on how to approach the topic scientifically. Mart-Jan Hemel for helping me better understand the physical behaviour of quay wall structures. Paul Korswagen for his expertise on masonry and how to go about numerically interpreting the behaviour of masonry. Elisa Ragno for providing tips on reporting and talking about my progress along the way. Lastly, Richard Roggeveld for teaching me to work with DIANA FEA.

I would also like to thank Sweco in general and Arjan Frens who introduced me to this company, where I have enjoyed working dearly. Including my colleagues, who provided a positive atmosphere in the workplace. Lastly, I would like to thank my friends and family who have made my life more fun in these times.

Chris van Hulten
Rotterdam, November 23, 2021

Summary

Many quay walls in Amsterdam have surpassed their structural lifetime and have started showing signs of damage. The city of Amsterdam is currently tackling the problem and have published a plan of action. This plan includes the renovation of hundreds of kilometres of quay walls. Given this enormous amount, it is necessary to prioritize certain quay walls over others based on the severity of their damage. Some quay walls have reached total collapse, of which the most recent case involves the "Grimburgwal" quay.

The municipality has no accurate view of the current condition of quay walls in Amsterdam. On top of that, the vast majority of quay walls have not been assessed on their safety. It is known that the most vulnerable quay walls types consist of masonry walls, supported by wooden foundation structures. Given that the quay wall renovation project requires prioritisation, it is necessary to gain more information on how the most vulnerable walls are recognised. Preferably, a method should be developed in which only visual cues given by the masonry wall are required, as it is quick and relatively cheap. To gain information on what these visual cues might be, a three-dimensional finite element model is made to run simulations on possible behaviours of quay walls. In this thesis, it is attempted to model a quay wall as realistically as possible. Several different deterioration conditions will be applied to see how the masonry responds.

The 3D model is built using a parametric model coded in Python. This code can be used to run simulations in the finite element software DIANA FEA. Many behavioural aspects have been incorporated into the model, with the purpose to make the model more realistic. The model consists of a masonry wall, planks on which the wall rests, and supporting piles. The behaviour of each component has been applied in the code and have been obtained through other literature and European norms. The model is loaded by simulating the weight of the soil and its effect on the quay wall structure. The masonry is simulated using a smeared cracking model (macro-model). Long-term deterioration of quay walls is simulated by changing the material properties of each respective component. This thesis focuses on three deterioration conditions:

1. Non-uniform pile degradation: application of broken piles, simulated by removal of those piles from the model. This is subdivided into two categories: removal of entire rows (a row consisting of a front, middle and end pile) and removal of front piles only.

2. Non-uniform soil removal: formation of soil pits at the foundation level, which result in decreased bedding around the foundation piles.

3. Uniform degradation: application of uniform deterioration along a stretch of quay walls.

The simulations yield fairly consistent cracking patterns, in which the same crack fields appear in each simulation depending on the chosen case mentioned before. Displacement patterns are also documented and presented in all cases. The quay wall model is able to display in-plane and out-of-plane movement simultaneously. The effect of each parameter on the crack/displacement patterns are analysed as well. This includes masonry and wood quality. The results show that the largest in-plane settlements are reached by damaged piles, while the largest

out-of-plane displacements are caused by a loss of soil bedding around the piles.

The results can be used to provide better insight on how quay walls with poor quality present themselves in real life and what their cause might be. This research contributes to the possibility of improving recognition of quay walls which find themselves in critical condition, which can then be prioritized for renovations. For future research, it is recommended to see whether time-dependent simulations can be run, to see if it makes a difference in the outcome of displacement/cracking patterns. Another important recommendation is to look into deterioration rates of materials, which could be used as another indicator for critically damaged quay walls.

Contents

1

Introduction

1.1. Background

One of the reasons that drive tourists to Amsterdam is its well-preserved 17th-century architecture and the canals surrounding it. Historically, the canals were built as a way to manage the water of the Amstel river and to add more dry land to the city. The canals also proved to be ideal to use as transport routes and as a line of defence against foreign armies. The water in the canal is surrounded by quay walls, which are vertical soil retaining walls designed to manage the canal water. Most of these walls are more than a hundred years old. At present time, over 600 km worth of quay walls exist in Amsterdam, of which approximately 200 km are founded on wooden piles (Dijstelbloem et al., 2019).

Today, the city is suffering from structural damage of quay walls and bridges. Many quay walls started showing signs of damage and required immediate attention, while several quay walls seemed to unexpectedly collapse. The reason why the city is now forced to reactively handle the situation can be attributed to the fact that the city has postponed its necessary maintenance activities for too long. On top of that, these structures, most of which are over a hundred years old, are not designed for their present-day use. The city has become busier and traffic has become heavier, which exacerbates the problem even further (Dijstelbloem et al., 2019).

The problem regarding the condition of Amsterdam's quay walls has been known for several decades. In 1985, the municipality had already determined that the quay walls were due for maintenance. The funds that were made available for this project have eventually been spent on different matters. This negligence has created the current quay wall problems the municipality is facing. Hundreds of millions of euros have to be invested to tackle the problem of damaged quay walls and bridges (Kruidhof, 2019).

Several quay walls have already collapsed, notable examples are Nassaukade (March 2018) and Grimburgwal (September 2020). According to the municipality, the city has no accurate view of the current state of the quay walls and bridges in Amsterdam. As of January 2020, approximately 90 per cent of the quay walls of Amsterdam have not been assessed on their safety. In 2017, five calamities have taken place regarding quay walls. The municipality was aware of the critical condition of only one out of these five, while the other four remained

unnoticed. On top of that, the municipality predicts that more collapses will occur in the future (Brannan, 2020).

Figure 1.1: Grimburgwal before collapse (Amsterdam) in feb. 2018 (Google Street View).

Figure 1.2: Collapsed quay wall at the Grimburgwal (Amsterdam) on September 1st 2020 (RTLNieuws, 2020).

The municipality has published a plan of action that describes the process of handling the situation. One such publication, which will be regularly referenced in this report, is the action

plan regarding bridges and quay walls "Actieplan bruggen en kademuren" (Dijstelbloem et al., 2019).

This project includes 850 bridges and approximately 200 km worth of quay walls. Many old quay wall constructions in Amsterdam are masonry walls structures on wooden platforms, supported by wooden pile foundations (de Gijt et al., 2013). These structures currently have a considerable risk of failure and are put on high priority regarding renovations (Dijksma, 2019). The municipality has planned out twenty years for this project, which constitutes the reparation or replacement of every vulnerable quay wall and bridge in Amsterdam.

There have been many cases where measures have been taken to control the situation of critically unstable quay walls and bridges. Steel sheet piles have been placed at the most vulnerable parts to prevent total collapse. The municipality also attempts to prevent structural overloading by restricting the type and amount of traffic using vulnerable areas (Dijstelbloem et al., 2019).

There is still a large information gap regarding the safety of the quay walls in Amsterdam. Because of the urgency of this problem, more research is being done on this matter. This report intends to contribute to solving this problem by providing more insight regarding the behaviour of quay walls using a 3-dimensional numerical model.

1.2. Research objective

Ultimately, the purpose of this research is to provide more insight into how critically damaged quay walls can be visually recognised. A three-dimensional finite element model will be used to indicate what the displacement and damage patterns can tell about the quality of the quay wall structure. The central research question can be formulated as follows:

"How to recognize critically damaged quay wall structures using a three-dimensional finite element model."

The following sub-questions have been formulated, designed to contribute to answering the main question.

1. How do long-term phenomena affect the quality of the quay wall structure?
2. How should the numerical model be set up?
3. Based on the numerical model, which tell-tale signs could be observed that can help better detect critical quay walls defects?
4. To what extent can the quay wall deteriorate before it starts to portray visually detectable signs of damage?
5. Which factor contributes the most to cause the displacement of quay walls?

Section 1.3 explains how the report is structured in relation to these questions.

The baseline model is based on the properties of the quay wall at the "Nieuwe Herengracht" in Amsterdam. Quay walls generally vary a lot from each other, such as dimensions, number

of piles and soil retaining wall position. However, only the properties of the "Nieuwe Herengracht" quay wall will be used in this thesis.

This research will mainly focus on uniform conditions, non-uniform pile damage and non-uniform soil removal around the piles.

1.3. Thesis outline

The formulated research questions will be addressed in the given order. The first two questions are purely focused on information gathered from the literature. Question 1 will be theoretically answered in chapter 2. Question 2 will be answered using a combination of theory and logical reasoning. Properties and physical behavioural aspects regarding quay wall structures will be derived from literature and European norms. All relevant information regarding this aspect is outlined in chapter 3.

The next step is to verify whether the finite element model produces realistic results. In chapter 4, various relevant behavioural aspects of quay walls will be verified. This regards the behaviour of masonry as a material, but also the quay wall in general.

When all modelling prerequisites have been defined and verified, they will all be incorporated into the finite element model. A three-dimensional parametric model of a quay wall will be produced in DIANA FEA. The purpose of the model is to mimic reality to a sufficient degree. Because it is parametric, it is possible to run many simulations in a relatively short time. The parametric model will be written in Python. DIANA FEA is capable of reading Python files. Therefore, incremental changes can quickly be made and applied, each producing a unique set of output parameters.

The last three questions are answered based on the output of the finite element model, all of which can be found in chapter 5. Question 3 and 4 require cracks to be induced. In this thesis, cracks will be induced in two ways: as a result of non-uniform pile properties and non-uniform soil properties. Question 5 requires uniform conditions, but results gathered from non-uniform simulations will be used to address this question as well. A qualitative comparison will also be made between the results found in this thesis and the real-life cases of the quay walls at "Nieuwe Herengracht" and "Grimburgwal" (chapter 6).

The next step is to discuss the results, in which the strengths and limitations will be outlined (chapter 7). It is important to outline all important assumptions and simplifications that were made throughout the process and to discuss their impact on the final results. Finally, the conclusions and recommendations are made in chapter 8.

2

Quay Wall Structures

This section provides theoretical background on quay walls in Amsterdam. The following topics will be discussed:

1. Quay walls in general
2. Loads and failure mechanisms
3. Foundation structure
4. Amsterdam soil profile
5. Masonry wall

2.1. Quay walls

Quay walls are built with a soil and water-retaining purpose, using a vertical wall. Its shape allows docking of ships and its paved surface allows for the loading and unloading of goods and passengers. In the Netherlands, they also surround the iconic canals flowing through its historic inner cities.

2.1.1. History

The Netherlands has been building inner-city canals for centuries. Their initial purpose goes beyond water management, as they were also used as a line of defence. As more canal rings were excavated, the inner rings have become more useful for the transportation of goods. Their vertical design also provides the possibility for mooring boats and ships. The first quay walls of Amsterdam date back to the 13th century. Since then, technological advancements have allowed the design of quay walls to evolve to accommodate new functional requirements, which have continuously changed over time (de Gijt et al., 2013). An overview of the development of inner-city quay walls is shown in figure 2.1.

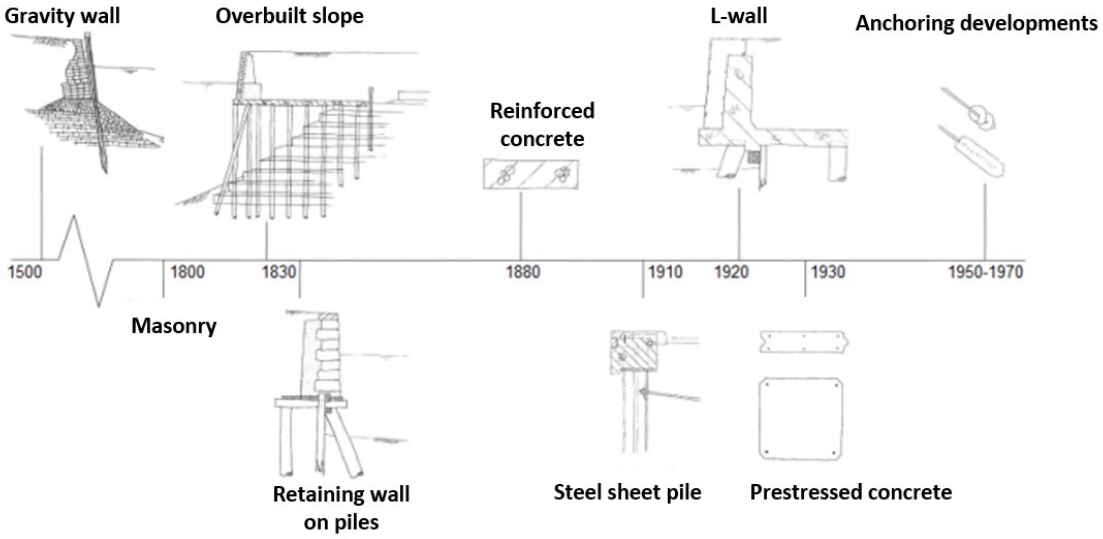

Figure 2.1: An overview of the development of inner-city quay walls in history (de Gijt et al., 2013)

2.1.2. Quay wall types

In the SBRCURnet publication "Binnenstedelijke kademuren" (Inner city quay walls), four different types of quay walls have been described as they currently exist in the Netherlands (de Gijt et al., 2013):

1. Gravity wall supported by shallow foundations.
2. Gravity wall supported by pile foundations.
3. L-shaped wall supported by pile foundations.
4. Sheet pile wall made from steel/concrete.

Most old quay wall constructions in Amsterdam fall under the second category. The gravity structure is mostly made out of masonry which is supported by wooden platforms and wooden piles (de Gijt, 2010). A schematisation of a quay wall structure is illustrated in figure 2.2.

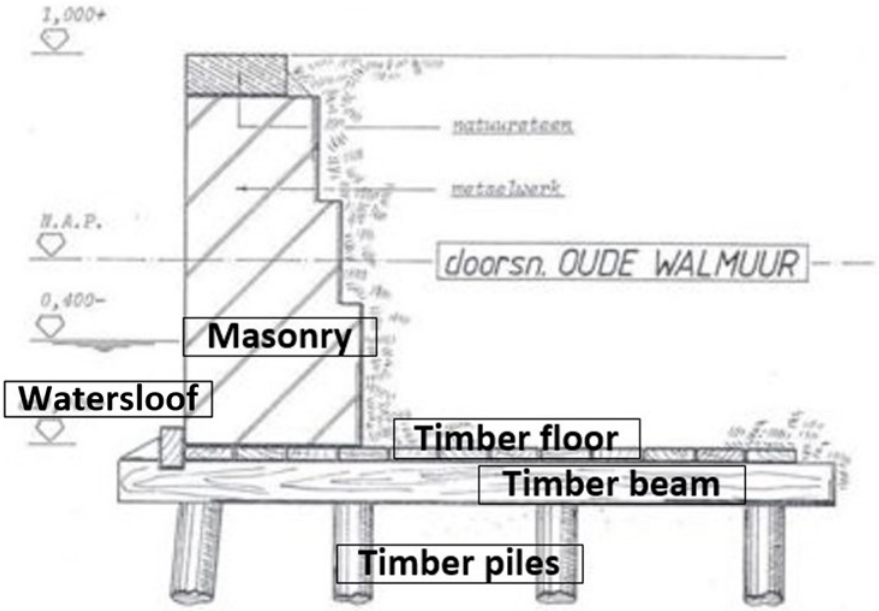

Figure 2.2: Schematisation of a typical gravity wall on wooden foundations.

2.2. Loads and failure mechanisms

This section describes loads and failure mechanisms to which quay walls are subjected. First of all, the main loads, which are taken into account when making a design, will be mentioned. Secondly, possible failure mechanisms that a quay wall may experience will be summarised.

2.2.1. Loads

Designing a quay wall requires load quantification. The main loads on which quay walls are currently designed have been summarized in a publication from SBRCURnet (Stichting Bouwresearch) in the following order (de Gijt et al., 2013):

- Soil loads.
- Surface and traffic loads.
- Difference between surface water level and groundwater level.
- Tree loads.
- Ice loads.
- Mooring loads (impact loads).
- Hawser loads (rope used to moor ships).
- Jet stream loads (from ships).
- Loads as a result of earthquakes and vibrations.
- Loads as a result of soil compaction.
- Loads as a result of soil swelling.

- Loads as a result of temperature changes.

When it comes to historic quay walls in Amsterdam which are still in use today, several changes in loads have taken place, which have not been taken into account in their initial design. Most notably, shipping loads have been greatly reduced as most shipping activity has been moved outside of the historic city centre. More importantly, surface loads have increased over the last decades (see figure 2.3), as traffic loads and intensity have substantially risen (de Gijt et al., 2013).

Figure 2.3: Heavy traffic on historical quay walls, from TLN Nederland

A crude schematisation of the loads acting on a quay wall is shown in figure 2.4.

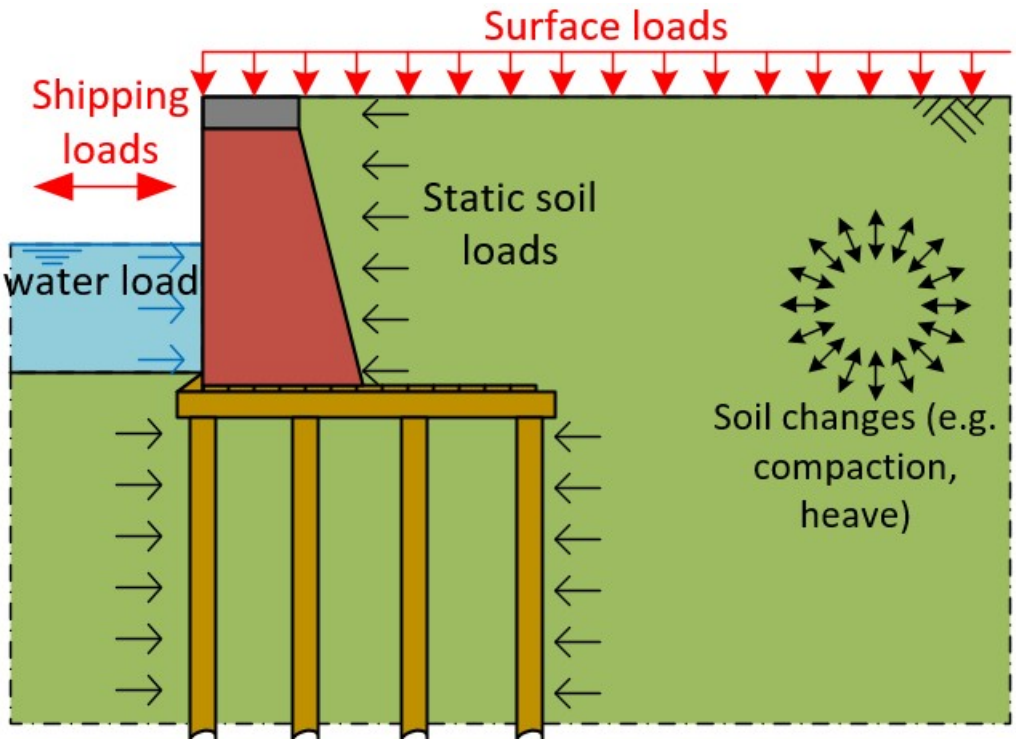

Figure 2.4: Schematisation of loads acting on a quay wall structure (Changes in load in recent decades are indicated in red)

2.2.2. Failure mechanisms

Since quay walls supported by wooden piles are deemed vulnerable, the possible failure mechanisms regarding these kinds of structures will be further elaborated. The main relevant failure mechanisms, valid for gravity walls supported by foundation piles, are classified as follows (de Gijt et al., 2013):

1. Exceedance of the compressive bearing capacity of a pile (no rupture).
2. Exceedance of the tensile bearing capacity of a pile (no rupture).
3. Failure of the soil as a result of horizontal loading on the pile foundation.
4. Exceedance of the general stability.
5. Structural failure of the retaining wall.
6. Structural failure of the piles as a result of pressure, tension, bending, buckling or shear.
7. Failure of the structure as a result of large pile displacements.
8. Failure as a result of internal erosion or piping.

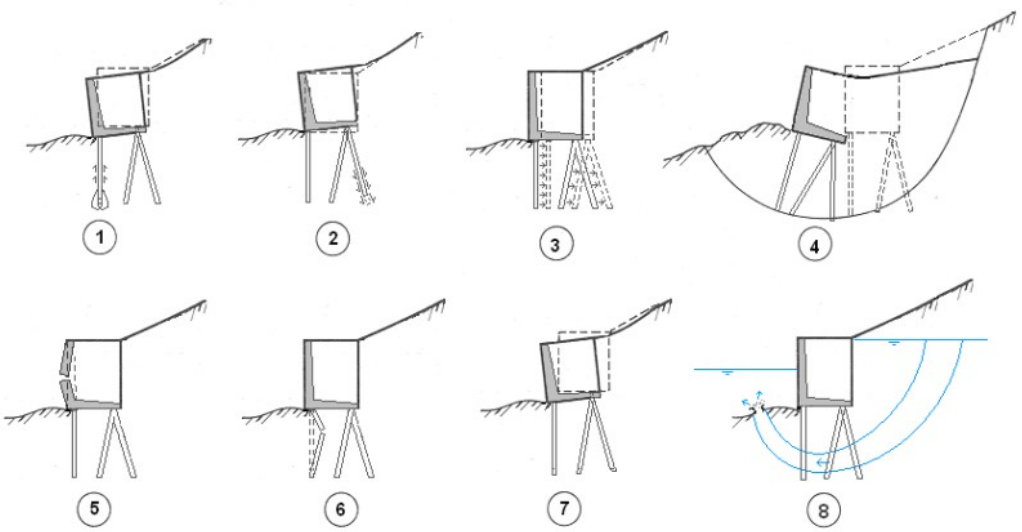

Figure 2.5: Possible failure mechanisms (de Gijt et al., 2013).

The before-mentioned items are shown in figure 2.5. When it comes to quay walls, multiple failure mechanisms may be taking place at the same time. The focus in this thesis will mainly lie with pile fracture and soil failure and their consequence on the masonry wall.

2.2.3. Inspection regime

Approximately 200 km worth of quay walls need renovation. The municipality states that it is impossible to exactly know the condition of every quay wall or bridge in the city (Brannan, 2020). It is costly, labour-intensive and time-consuming to assess every quay wall thoroughly, making it an unrealistic approach. Therefore, the city is forced to prioritize renovations based on the damage the quay walls are currently showing.

Currently, the municipality of Amsterdam is performing risk-oriented investigations to gain insight into the state of its quay walls and bridges (Dijstelbloem, 2020). Inspected structures are divided into three risk categories, depending on the severity of their condition. Based on these categories, more thorough research will be done depending on how dangerous a structure is perceived to be. The three categories are:

1. The state of the structure seems adequate: no changes in approach are necessary.
2. The state of the structure remains unknown: further research is necessary.
3. The state of the structure is unsatisfactory: quick and qualitative action must be taken.

However, according to the engineering firm of the municipality of Amsterdam (Ingenieursbureau Amsterdam), the current method of inspecting does not provide full insight into the condition of the quay walls. The inspection regime is done as follows (van der Linde, 2018):

1. The first step is to check the condition of a quay wall. This is done by checking for obvious signs such as cracks or settlements with a boat or a bicycle.
2. If a wall shows signs, a more thorough inspection will take place by taking measurements using professional divers.

3. Lastly, a judgement will be made on what measures to take to increase the remaining lifespan of a wall.

According to the inspection regime, these judgements are fundamentally based on visual inspections. This can cause a pitfall, namely that failure mechanisms could be taking place, while the wall is not showing clear signs of damage. In other words, there is a real chance that structures are being misjudged. Several calamities, in which structures have unexpectedly collapsed, have already taken place. On top of that, the municipality states that, unfortunately, unexpected collapses are very likely to occur again in the future (Dijstelbloem et al., 2019).

2.3. Foundation structure

2.3.1. Background

Quay walls in their worst condition are prioritised for renovations. Most of those quay walls are supported by wooden foundations (Dijksma, 2019). Figure 2.6 shows a photo of the quay wall and its wooden foundation taken at Da Costakade in 2018. In Amsterdam's inner city, wood is commonly used in support structures for the masonry gravity walls. The reason that wood is commonly found is that concrete and steel foundation piles only came into existence after the 1920s. Before that, wood was the only available construction material for foundation elements (de Gijt, 2010). Most pre-Second World War foundation piles are on average approximately 12 or 13 meters long, which were driven into the first sand layer (van Kasteren, 2009).

Figure 2.6: Wooden foundation structure from an old quay wall undergoing renovation (taken at Da Costakade, december 2018), retrieved from the municipality of Amsterdam.

2.3.2. Material degradation

The old age of many quay walls indicates that a significant amount of them are approaching, or have already surpassed, their structural lifetime. A clear example is the before-mentioned quay at Da Costakade, where the tilt in the foundation piles is quite noticeable (see figure 2.6). When designing and maintaining wooden foundations, the effect of wood degradation on its structural integrity must be taken into account. There are several ways in which the

foundation structure may lose its initial properties. They can be summarised by mechanical and biological degradation (de Gijt et al., 2013).

2.3.2.1 Mechanical degradation

Mechanical degradation refers to a loss of structural integrity as a result of long-term loading. It is caused by specific high-loading events leading to wood damage such as rupture or shear. On top of that, wood loses some of its initial strength and stiffness when it is subjected to long-term overloading (creep). Wood behaves as a visco-elastic material when subjected to permanent loads. This leads to an increasing deformation over time (Granello and Palermo, 2019). Due to the deformation of wooden foundation piles, their strength and stiffness may have been reduced considerably and it may contribute to the deformation of the quay wall structure. Only by inspection can the degree of mechanical degradation be accurately estimated (de Gijt et al., 2013).

2.3.2.2 Biological degradation

Biological degradation can develop in multiple ways. The wooden platform and piles are affected by various organisms (such as bacteria and fungi), which will lead to wood decay. For piles, this leads to a smaller bearing diameter, followed by a weaker bearing capacity. Ultimately, this can lead to pile fracture, which is a common appearance in Amsterdam. When it comes to the wooden platform, the wood may have degraded to such a level that a foundation pile can punch through the weakened wood (de Gijt et al., 2013). In any case, wood decay contributes to the loss of stability of the entire structure.

The way in which biological factors influence timber quality is well documented. The wooden foundation structure lies below water level most of the time. However, the water level can drop significantly during dry periods, which leads to direct exposure to air. High oxygen levels caused by exposure makes wood vulnerable to some types of fungi. The degree to which the fungi affect the structure depends on the water content of the wood. The lower the water content, the more vulnerable it is to fungal attacks. Other organisms which cause degradation are mainly bacteria. These organisms affect the wood at any time and everywhere below the water table. Bacteria become active as a result of water flow in the wood. The degree of bacterial degradation is relatively low when there is no water flow present. The degree to which bacteria affect the wood, therefore, depends on location, wood type and wood quality (de Gijt et al., 2013).

2.4. Soil profile

2.4.1. Characteristics

A significant part of the Netherlands, including Amsterdam, is covered with peat, which is a relatively weak soil. Peat is prone to subsidence, especially as a result of dewatering practices. These practices were performed by early settlers near the Amstel river. Historically, the ground surface was situated at about 2-3 m above NAP (Normaal Amsterdam's Peil). Today, it is situated around 1-2 m below NAP. For reference, NAP is equivalent to the average sea level in the North Sea.

It is relatively difficult to construct on peat because of its weakness and high moisture content. For that reason, the ground level has been elevated with a sandy layer. This layer provides a much stronger foundation to build on while compensating the previously mentioned historic subsidence. However, the weight of the sand resting on the peat often leads to even more

subsidence of the soil. Therefore, there is a limit on how much sand is allowed to be placed. Also, uneven settlements are taking place all over the city, because the thickness of the sandy surface is not equal at every location (de Gans, 2011).

Today, the soil in Amsterdam consists of a peat layer of around 2-3 meters thick, underneath which lies a large clay layer of around 7-8 m thick. Both layers have been deposited during the Holocene era. Because these are relatively weak soils, man-made structures are required to be built on foundation piles. These piles must reach deeper levels, where stronger soil layers are situated. At approximately 12-13 meters below NAP, the first natural sand layer is found, which originated from the Pleistocene era. This is the layer in which most foundation piles were/are driven (de Gans, 2011). Another clay layer is found beneath the first sand layer, below which another sand layer is found between approximately 17-24 meters below NAP. Larger and more modern structures, which were built after the Second World War, are supported on these deeper sand layers.

According to geologists from the Dutch public real-estate service (Rijksvastgoedbedrijf), the before-mentioned composition of soil layers is an approximate idea of the soil in Amsterdam, differences are depending on location. The depth in which these layers are found varies across the area, sometimes as well as their presence in the first place. When it comes to designing structural foundations, thorough research on the area's soil composition is necessary to avoid unintended consequences (de Baar, 2009). A soil sample with a depth of 12 meters from an Amsterdam geotechnical boring test is shown in figure 2.7.

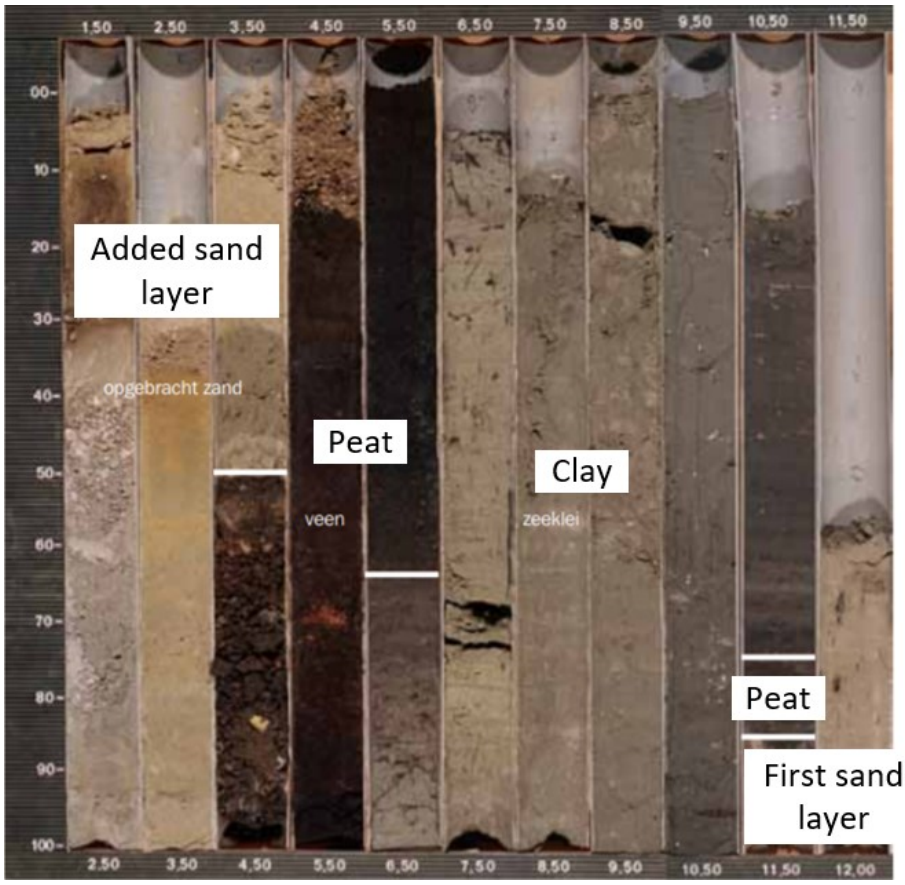

Figure 2.7: Soil sample from Amsterdam, retrieved from de Gans, 2011

2.4.2. Soil degradation

Quay walls are both supported and loaded by the soil. Therefore, the behaviour of a quay wall must be dependent on the behaviour of the soil. Most of the time, soil deformations are deemed unfavourable to the stability of the structure. Several factors are leading to soil deformations, most of which are gradual processes.

- **Primary settlement:** When placing a structure on soil, the increased loading cause the soil particles to come closer together as water particles are being dissipated. The maximum primary settlement time is considered to be approximately 30 years after construction (Molenaar and Voorendt, 2017).
- **Creep:** Also referred to as secondary settlement, is the permanent deformation of soil caused by long-term or persistent loading, causing the properties of the soil to change. Secondary settlement practically lasts forever. Usually, the effect of creep is taken into account when designing structures (Molenaar and Voorendt, 2017). Logically, when structures are undergoing creep effects for too long without some form of compensation, serious deformations can occur in the long run.
- **Frost:** Another way soil can deform is through frost heave, which is a natural phenomenon. When the soil starts to freeze, the moisture particles within the soil will start to expand. This leads to soil expansion, which may result in permanent displacements of nearby structures. Soils that retain water effectively, such as clay or peat, are the most

susceptible soil types to experience frost heave effects (Kasprick, 2019). This makes Amsterdam's quay walls susceptible to this phenomenon, given that the soil mostly consists of clay and peat (de Gans, 2011).

All of the before-mentioned long-term soil effects could lead to a significant loss in strength and stiffness in the soil. Which, in turn, directly affects the structural integrity of the entire quay wall structure.

Another real danger is the formation of sinkholes, some of which led to complete collapses. A notable example is the quay wall at the Grimburgwal (Korff et al., 2020). Over long periods, the foundation piles may lose soil support due to it being washed away by the water flow in the canal. This process usually takes a long time, but its effect can be drastic, as the Grimburgwal case has proven.

2.5. Masonry wall

2.5.1. Background

Masonry is a composite material that consists of stacked individual units, which are held together by mortar. The first masonry quay walls date back to many thousands of years ago. In Northern Europe, brick structures on wooden foundations came to widespread application around 1500 AD. Even today, masonry as a construction material is still applied, given its reputation as a durable material (de Gijt, 2010). In Amsterdam's inner city, historic retaining walls are usually made of masonry with a layer of natural stone on top. The long brick structures are occasionally interrupted by dilation joints (figure 2.8), which absorb expansion induced by variations in temperature.

Figure 2.8: Damaged quay wall near a dilation joint, retrieved from (de Gijt et al., 2013).

2.5.2. Masonry degradation

Over a long time, masonry will lose its initial properties. This fact is natural and applicable to practically any material. Creep in masonry is dependent on several factors, for example: how much loading it has endured during its lifetime, continuous changes in temperature, moisture content and the type of mortar (Sayed-Ahmed et al., 1997). The fact that the masonry wall is partly submerged most of the time poses an extra damage risk, since moisture speeds up the deterioration process, as it promotes damaging chemical reactions with the material (Maljaee et al., 2013). Not to mention that weaknesses in masonry allow the growth of plants and mosses (see figure 2.8). All of these factors eventually influence the strength and stiffness of the masonry structure.

2.5.3. Stability, stiffness and strength

As mentioned in section 2.2.3, the current inspection regime judges the condition of quay walls based on the appearance of the masonry. Specifically, the part which is situated above water level. Symptoms of damage of quay walls include deformations, cracks and tilts (de Vent, 2011). The latter is caused by a lack of external stability. Deformations and cracks arise from loads acting directly on the wall. The extent to which masonry deforms and cracks depends on the stiffness and strength of the material respectively.

Every material is subjected to deformations. Large deformations are a result of a lack of stiffness of the material. Masonry structures can develop in-plane and out-of-plane deformations. In-plane deformations take place in the plane of the wall, meaning that they do not deviate perpendicular to the wall. Out-of-plane deformations are in- or outward deformations, such as buckling or bulging. Examples of in-plane and out-of-plane deformations are provided in figure 2.9. The direction in which the wall deforms is usually a consequence of loading originating from the same direction. However, this is not always the case. Out-of-plane deformations may occur as a result of differences in moisture content and/or temperature within the structure. Buckling may also occur, which are out-of-plane deformations as a result of in-plane overloading (de Vent, 2011).

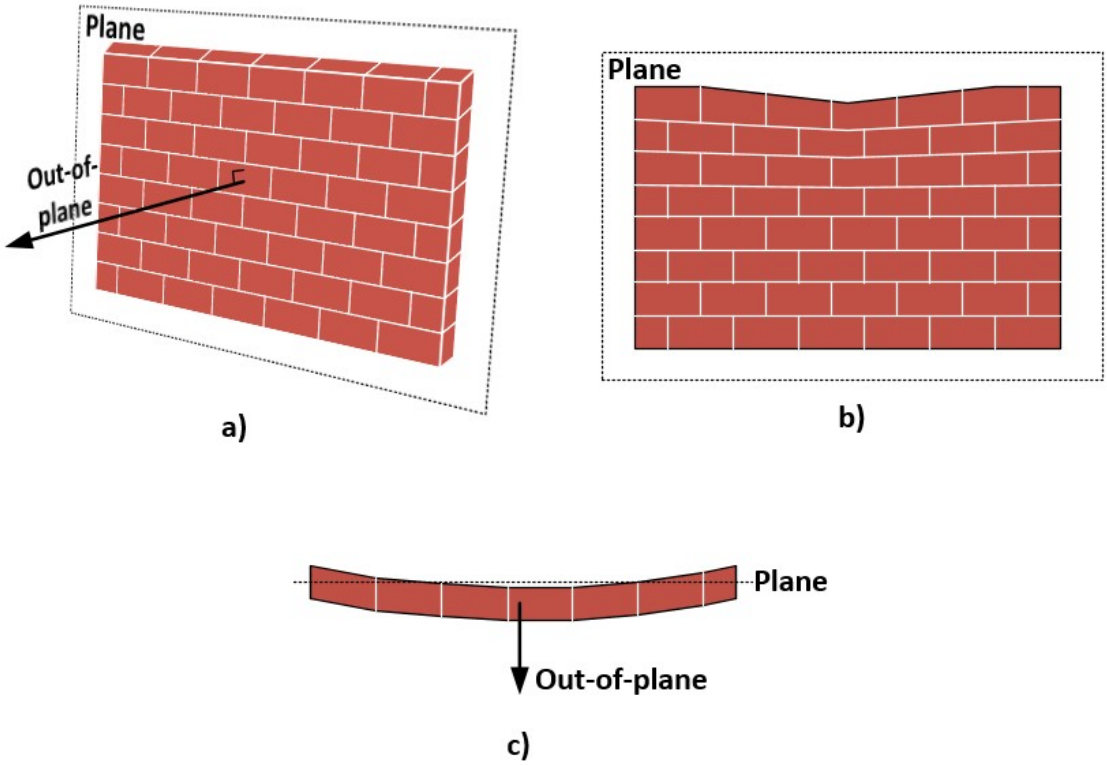

Figure 2.9: (a) Visualisation of in-plane and out-of-plane directions; (b) In-plane example: local settlement; (c) Out-of-plane example: bulging

Aside from deformations, structural overloading (or lack of strength) of masonry leads to the development of cracks as well. Cracks can develop as a result of many different loading conditions. Some features which should be taken into account when analysing a crack include: crack direction, size, deformation as a result of crack and crack depth. A crack pattern analysis may indicate the possible reasons for its development. Many possible crack patterns exist, even combinations of multiple patterns (de Vent, 2011).

3

3D Model Setup

This chapter focuses on all modelling aspects regarding the quay wall structure. The structural behaviour of wood, soil and masonry will be elaborated as well. How each element is modelled in the finite element software will be explained in detail. The chapter is divided into several sections:

- Model schematisation
- Pile modelling
- Masonry modelling
- Loading

3.1. Model schematisation

3.1.1. Structural elements

The quay wall structure consists of many structural elements. To reduce complexity, not every element can be assessed in great detail. The build-up of the model will be described in this section.

3.1.1.1 Quay wall simplification

The purpose of this thesis is to model the out-of-plane behaviour of masonry and piles. Therefore, this research will focus solely on the behaviour of the masonry wall and the wooden foundation piles. In reality, the foundation structure is made up of several kinds of wooden elements. A description has been provided on every element, along with a description of how they are elaborated in this thesis.

- **Foundation piles:** The scope of this thesis is limited to structural failure of the foundation piles and its effect on the lateral behaviour of the masonry wall. The model will therefore primarily focus on foundation piles.
- **Soil retaining wall:** To prevent soil movement, a wooden soil retaining wall is often placed underneath the wooden floor. Failure of this wall is dangerous as soils can wash away, which leads to general instability. Because of its contribution to the stability of the quay wall, its effect will be included in the model.

- **Lateral support beams:** Individual piles are interconnected through a wooden support beam ("kesp" in Dutch) resting on top. These beams contribute to the stability of the structure by ensuring evenly distributed loading on the foundation piles. Failure of these beams leads to eccentric loading directly on the piles, which leads to the development of horizontal forces and may even lead to pile fracture (Sas, 2007). Since the focus of the thesis lies with the failure of foundations piles, the beams themselves will not be modelled to reduce complexity.

- **Longitudinal support beams:** These beams rest on top of the lateral support beams (kesp) and consist of wooden floor plates and a wooden beam.

    1. **Floor plates:** The wooden floor plates are used as the first layer of support for the masonry wall. Failure of these beams usually leads to the masonry wall sinking through the floor but does not lead to calamities (Sas, 2007). The focus does not lie on the failure of these floor elements. However, they do contribute to the behaviour of masonry, as there is an interface present between the wood and the bricks. Therefore, its effect should be taken into account as an interface condition. This interface condition will be elaborated upon in section 3.3.
    2. **Wooden beam:** The wooden beam, which is usually slightly embedded into the underlying lateral support beam, is used as a horizontal constraint for the masonry wall (Sas, 2007). This beam contributes to additional horizontal support. However, considering the degree of material degradation the structure has undergone through its lifetime, it is assumed that the beam does not provide any substantial structural value anymore.

When it comes to structural behaviour, only the foundation piles and the masonry wall will be elaborated upon.

3.1.1.2 Pile model

The foundation pile is a circular beam, completely supported by the surrounding soil. The head of the pile is connected with the wooden support structure on which the masonry wall rests. This connection is assumed to be hinged. As a result, there is a direct correlation between the movement of the pile tip and the movement of the masonry wall. The extent to which the *pile tip* displaces is dependent on several factors, which is the reason why the pile is assessed in a separate section. The surrounding soil behaviour will be treated as a boundary condition for the pile.

3.1.1.3 Masonry model

The masonry model consists of a masonry wall with boundary and interface conditions. The foundation piles will be simulated by placing them at each pile location. After imposing out-of-plane loading against the wall, several kinds of simulations can be performed, each with a different outcome regarding the behaviour of the masonry. The main focus lies in comparing wall displacements with crack formation.

3.1.2. Reference case

Although most inner-city quay walls of Amsterdam have a similar set-up, there are still differences in the exact dimensions. For this thesis, the quay wall at "Nieuwe Herengracht" has been chosen as a reference case. This quay wall is known for experiencing critical damage in its foundation and already has experienced noticeable deformations according to the municipality of Amsterdam (IBA). The dimensions of this quay wall are summarised in table 3.1. These

values have been determined based on the archives of the municipality of Amsterdam. The distance between the dilation joints (see figure 2.8) is assumed to be about 20 m. Based on the municipality's archives, the piles' centre-to-centre distances have been set to 1.0 m to reduce complexity. However, in reality, it varies between 0.8 and 1.3 m.

Dimension	**Value [m]**
Wall height	1.6
Wall thickness	0.66
Wall length	20 (assumed)
Floor thickness	0.2 (kesp) 0.05 (floor)
Floor length	2.75
Pile diameter	0.18
Pile length	to be determined
No. of piles (in cross-section)	3
C.t.c. pile distance (in cross-section)	1
C.t.c. pile distance (longitudinally)	1

Table 3.1: Nieuwe Herengracht quay wall dimensions, retrieved from IBA.

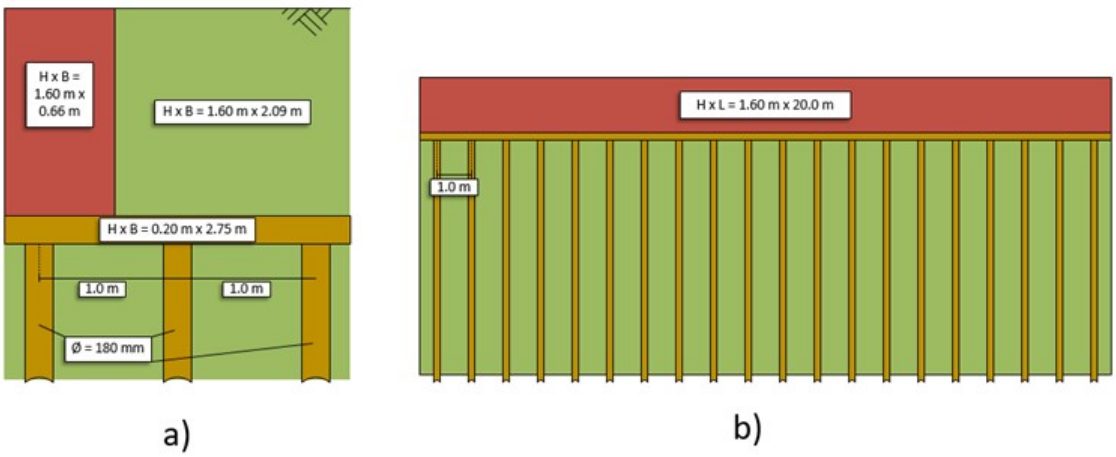

Figure 3.1: Visualisation of table 3.1.

3.2. Pile modelling

Modelling a foundation pile requires some prior knowledge of its behaviour. This section is divided into several topics:

- Pile behaviour (which will be modelled)
- Material properties
- Available material models in DIANA
- Boundary conditions: soil

3.2.1. Modelling pile behaviour

Before modelling the pile, it is necessary to understand the behaviour of timber as a result of external loading. Structural elements bend and deform when subjected to loads. The extent to which it deforms depends on which material is used. Wood (or timber) initially experiences linear elastic behaviour, just like most other materials. This means that the imposed load (stress) on the material is linearly proportionate to its deformation (strain). Another property of linear elasticity is that the original state of the material will be restored when the specified load is removed. Most materials will permanently deform when a critical load has been reached. Usually, this is also paired with the loss of the linear relationship between stress and strain. From this point, the material experiences non-linear plastic behaviour.

Eurocode 5 provides guidelines on how to design and assess wooden structures. It also provides strength characteristics for many wood types. According to Eurocode 5, the characteristic strength parameters have been determined under the assumption that the pile does not experience plastic behaviour. In other words, the pile will experience a linear stress-strain relationship until it breaks (brittle behaviour). The stress-strain relationship assumed in Eurocode 5 is illustrated in figure 3.2.

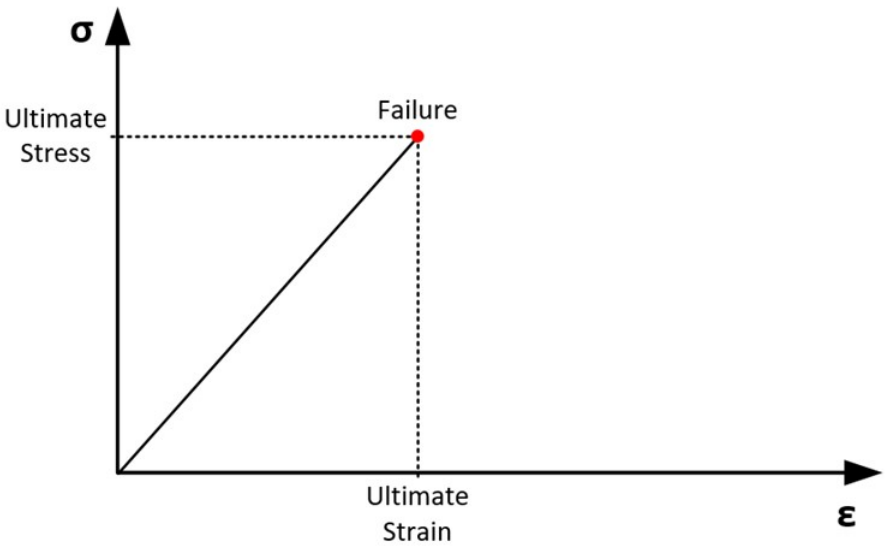

Figure 3.2: Stress-strain relationship of wood assumed in Eurocode 5.

Eurocode 5 does not provide any rules when it comes to assessing plastic behaviour, when in fact, material tests conclude that timber does show its presence. Experiments with timber, performed at TU Delft, show a negligible plastic trajectory for timber in tension, while non-linear behaviour in compression is approximately perfectly plastic (Hoekstra, 2020). This trajectory will therefore be incorporated into the model.

3.2.2. Material models

DIANA does not offer material models specifically for timber structures. However, since no complicated material models are necessary in this case, it is sufficient to create a structural non-linear model with user-specified material input.

The foundation pile will be treated as a 1-dimensional beam with a circular cross-section. The only DIANA material model allowing for non-linear input, which is also compatible with beams,

is the uni-axial non-linear elasticity model. It asks for linear elastic parameters, such as Young's modulus and mass density. The user can specify a custom stress-strain diagram. The diagram must include stress-strain relations in compression (negative) as well as in tension (positive), as a result of bending (see figure 3.3). The compressive side will behave ideally plastic after the bending strength has reached, while the tensile side will behave almost perfectly brittle after this value. In the material model, when the bending capacity in tension has been reached, the strain will continue to increase by 10 per cent until it breaks completely. This is an assumption made in accordance with the assumption that it is "almost" perfectly brittle.

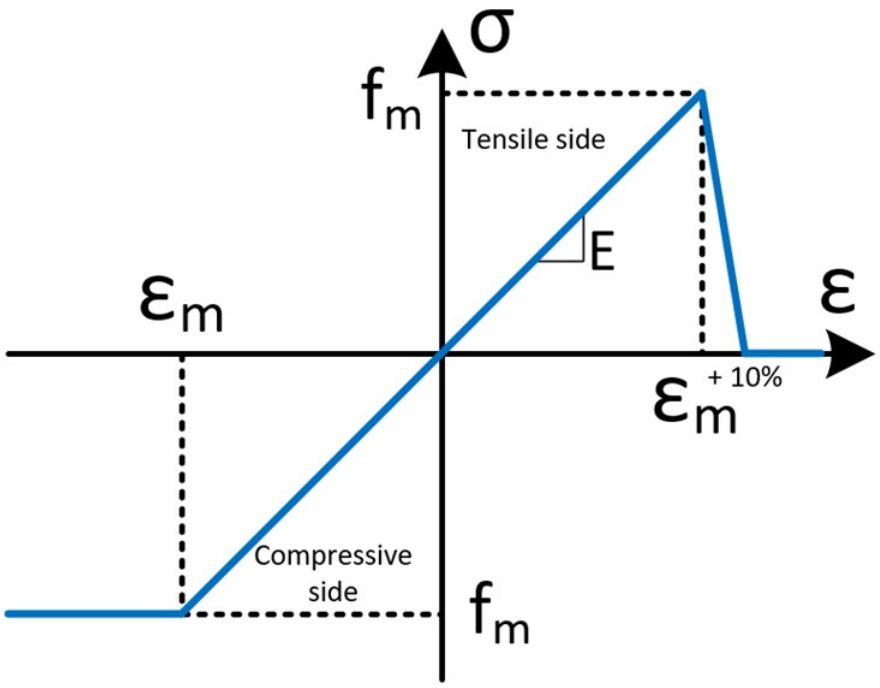

Figure 3.3: Stress-strain relationship of wood in bending, as input in DIANA.

3.2.3. Properties

The most commonly used wood types in Dutch foundation piles are spruce and pine, both of which are examples of softwood (Klaassen, 2007). In the Netherlands and the European Union, different wood types have been classified in Eurocode 5 (Eurocode, 2017). European pine and spruce from the North-North Eastern region are described in four different strength classes: C14, C18, C24 and C30. Each number indicates the bending capacity of each softwood class in [N/mm^2]. In this thesis, class C18 will be assumed for the model. Its relevant strength characteristics are provided in appendix A.1. Some of the more relevant characteristic values are represented in table 3.2. These values will be used to represent a wooden pile in its fresh (new) state. The values of table 3.2 are representative values used as a baseline for structural engineers. Note that these are characteristic values and are likely an overestimation of the actual structural value. These values will be considered an "upper limit" of wood structural properties.

Material property	Value	Unit
Young's modulus (E)	6000	N/mm^2
Mass density (ρ)	320	kg/m^3
Flexural strength (f_m)	18.0	N/mm^2

Table 3.2: Characteristic properties of a fresh foundation pile used in DIANA.

When assessing wooden structures, Eurocode 5 provides several guidelines as to how to determine the material properties. This is mostly done by including safety factors into characteristic properties. Characteristic strength values are assessed using the following formula:

$$X_d = k_{mod}\frac{X_k}{\gamma_M} \tag{3.1}$$

Where:

X_d = Design value of a strength property [N/mm^2] or [MPa]
X_k = Characteristic value of a strength property [MPa]
k_{mod} = A factor taking load duration and moisture content into account. Permanent loading and the maximum value for moisture is assumed, leading to a value of 0.5 [-].
γ_M = A partial safety factor. Used for designing a new structure, therefore dismissed.

As a result of decades of consistent loading and being in contact with moisture, the original stiffness has also been greatly reduced. According to Eurocode 5, the characteristic Young´s modulus must be reduced according to equation 3.2. This formula applies to the assessment of wooden structures in their ultimate limit state.

$$E_{mean,fin} = \frac{E_{mean}}{1 + \psi_2 k_{def}} \tag{3.2}$$

Where:

$E_{mean,fin}$ = Design value for the Young's modulus [MPa]
E_{mean} = Characteristic Young's modulus [MPa]
ψ_2 = A factor taking load duration of its highest load into account. If that loading is permanent, a value of 1 is assumed.
k_{def} = A creep factor, in this case 2.0 [-].

Since the Young's modulus E and the flexural (bending) strength capacity σ are known, the ultimate strain ε of wood can be calculated with equation 3.3, given the linear stress-strain relationship shown in figure 3.2.

$$\varepsilon = \frac{\sigma}{E} \tag{3.3}$$

The resulting design values of the material properties of the pile are summarised in table 3.3. The design flexural strength calculated using equation 3.1 is rounded off to the nearest first decimal.

Material property	Value	Unit
Young's modulus (E)	3000	N/mm^2
Mass density (ρ)	320	kg/m^3
Flexural strength (f_m)	9.0	N/mm^2
Ultimate strain (ε_m)	3.0·10^{-3}	mm/mm

Table 3.3: Design properties of the foundation pile used in DIANA.

Although these values are based on European norms, one must be careful to use these values to represent reality. Structural engineers use this approach to make sure that upcoming projects are structurally sound and safe. In reality, it is reasonable to assume that these design values are probably underestimating the real capacity of the material. The purpose of these values is to act as a "lower limit" of the wood properties in the finite element model.

3.2.4. Boundary conditions

Foundation piles are supported by the surrounding soil layers. Therefore, the surrounding soil conditions will be defined as the boundary conditions in the pile model. The extent to which the pile deforms is dependent on the stiffness of the soil. The higher the soil stiffness, the smaller the pile displacement will be, as stiffer soils require a larger load to force movement of the pile. In the finite element model, soil stiffness as a boundary condition will be modelled as a spring system. The horizontal movement will be constrained using uncoupled distributed horizontal springs, while vertical movement will be constrained by a single uncoupled vertical spring.

3.2.4.1 Soil composition

The extent to which a foundation pile displaces or deforms is dependent on the soil characteristics. Soil characteristics at "Nieuwe Herengracht" will be used as a reference case. Soil profiles from all around the Netherlands are publicly accessible at DINOloket, which is a database containing information on Dutch soil. Table 3.4 summarises the relevant soil parameters at "Nieuwe Herengracht", interpreted based on the cone penetration test (CPT) provided by DINOloket. The full results of the performed CPT can be found in appendix A.2.

Based on the cone resistance and friction ratio, the soil type can be determined based on the classification chart developed by Peter Robertson in 2010 (Molenaar and Voorendt, 2017). The chart can be found in appendix A.2.

Layer	Depth + NAP [m]	Cone resistance [MPa]	Friction ratio [%]	Soil type
1	-1.0 to -3.5	0.5	4.0	Clay
2	-3.5 to -6.5	0.5	12.0	Peat
3	-6.5 to -9.0	2.0	1.0	Silt
4	-9.0 to -11.5	0.5	2.5	Clay
5	-11.5 to -14.5	15.0	1.0	Dense sand

Table 3.4: Soil properties at "Nieuwe Herengracht" to be used for the DIANA model, interpreted from data acquired at DINOloket.

To incorporate the given soil profile into the finite element model, a few assumptions are made:

- According to the CPT diagram, the surface level lies at NAP + 0.75 m, while the first measurements appear at NAP - 1.0 m. Based on the general soil composition in Amsterdam, which has been elaborated in section 2.4, it is assumed that the missing top layer is made up of sand.
- The height of the quay wall and the thickness of the wooden foundation slab together is roughly equal to the thickness of this sandy top layer ($\approx$ 1.80 m). Therefore, it is assumed that the pile begins at NAP - 1.0 m exactly.
- Based on the theory in section 2.4, it is assumed that the pile is supported by the first sand layer (which has a high cone resistance). For the finite element model, it is assumed that the pile is embedded up to 0.5 m into this sand layer (NAP - 12.0 m). Therefore, the length of the pile adds up to 11 m.

3.2.4.2 Lateral boundary

The soil exhibits non-linear stiffness behaviour. Numerically, the lateral behaviour of a foundation pile is typically approached by using so-called *p-y* curves. Where p is described as the horizontal soil resistance (varying in-depth) and y as the horizontal displacement of the pile. These *p-y* curves describe the non-linear spring behaviour (Fayyazi et al., 2014). A typical p-y curve is shown in figure 3.4. To reduce numerical complexity, the *p-y* curve which will be used in this thesis will be simplified according to figure 3.5. To analyse the horizontal behaviour of foundation piles, three considerations have to be taken into account:

1. The stiffness of the soil resulting from pile displacement.
2. The ultimate horizontal resistance of soil against piles.
3. The effect of piles in a group as opposed to a single pile.

With these considerations taken into account, it is assumed that the *p-y* curve exhibits linear elastic behaviour in the beginning. When the ultimate horizontal resistance has been reached, the soil behaviour is assumed to behave ideally plastic.

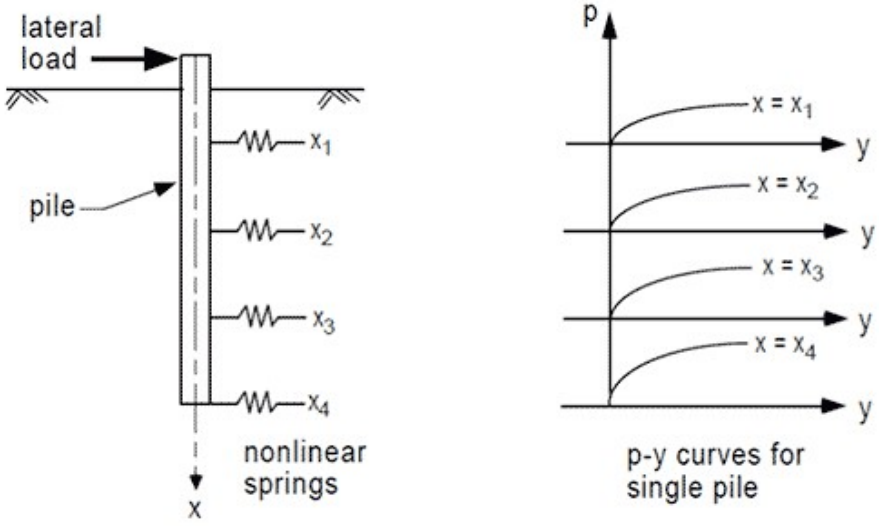

Figure 3.4: A typical *p-y* curve for a single pile model, retrieved from FHWA Manual (2010)

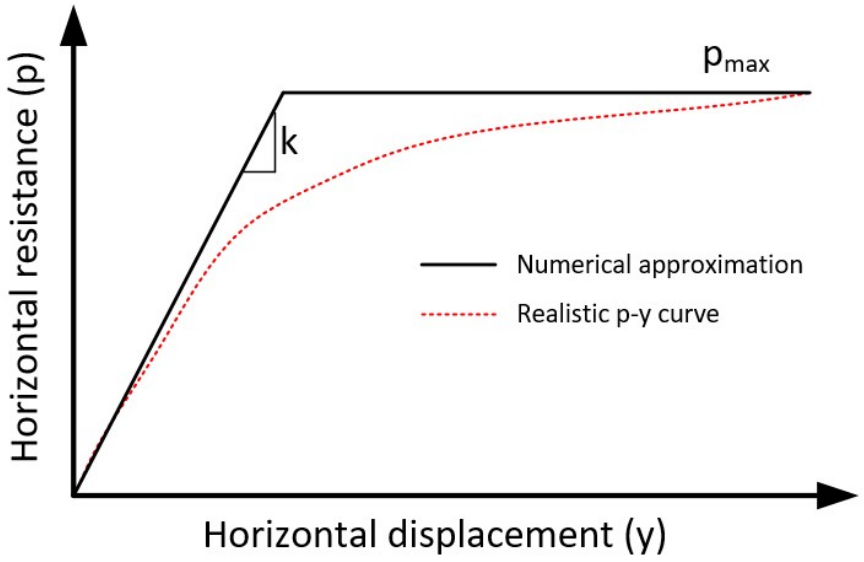

Figure 3.5: Numerical approximations for the *p-y* curve for a single pile model.

The horizontal modulus of sub-grade reaction is used for laterally loaded piles. The spring stiffness is determined using the approach described by Ménard (Molenaar and Voorendt, 2017). It is an empirical relationship, in which a relation is established between the horizontal stiffness of the soil K_h [MN/m^3] and the soil's cone resistance (q_c) [MPa]. The horizontal spring constant can be calculated according to formula 3.4. This equation is only applicable to piles with diameters smaller than 0.60 m (Molenaar and Voorendt, 2017).

$$\frac{1}{k_h} = \frac{2R}{E_p}\left[\frac{4.0\,(2.65)^{\alpha} + 3\alpha}{18}\right] \tag{3.4}$$

Where:

R = pile radius [m]
E_p $\approx$ $\beta \cdot q_c$ (Modulus of elasticity according to Ménard [MPa])
α, β = Rheological factors according to Ménard [-]

Soil type	α **[-]**	β **[-]**
Peat	1	3.0
Clay	2/3	2.0
Silt	1/2	1.0
Sand	1/3	0.7
Gravel	1/4	0.5

Table 3.5: Rheological factors according to Ménard (Hoefsloot, 2008).

Based on cone resistance values and soil types from table 3.4, the modulus of sub-grade reaction according to Ménard can be calculated for various pile diameters. The results are shown in table 3.7.

Layer	Soil type	Thickness [m]	q_c [MPa]	α	β
1	Clay	2.5	0.5	2/3	2.0
2	Peat	3.0	0.5	1	3.0
3	Silt	2.5	2.0	1/2	1.0
4	Clay	2.5	0.5	2/3	2.0
5	Sand	0.5	15.0	1/3	0.7

Table 3.6: Overview of soil layers with corresponding parameters required for the Ménard approach.

Layer	Soil type	k_h [MN/m^3]; $D = 0.18m$	k_h [MN/m^3]; $D = 0.16m$	k_h [MN/m^3]; $D = 0.14m$	k_h [MN/m^3]; $D = 0.12m$
1	Clay	7.6	8.3	9.1	10.2
2	Peat	11.2	12.7	14.5	16.9
3	Silt	15.3	16.3	17.6	19.1
4	Clay	7.6	8.3	9.1	10.2
5	Sand	80.5	84.2	88.6	93.9

Table 3.7: Horizontal stiffness values obtained through the approach of Ménard for various pile diameters.

A method to determine the ultimate resistance of soil against horizontally loaded piles has been described by Brinch Hansen in 1961. The method of Brinch Hansen is used to determine passive soil coefficients, in which a distinction is made between the contribution of the internal friction coefficient ϕ and cohesion c. Equation 3.5 is used to obtain the ultimate resistance of soil against horizontally loaded piles (Hoefsloot, 2008). The entire set of formulas used in the approach by Brinch Hansen are shown in appendix A.3:

$$p_{max} = K_q \cdot \sigma'_v + K_c \cdot c \tag{3.5}$$

Where:

K_q = Soil coefficient for the angle of friction ϕ [-]
K_c = Soil coefficient for the cohesion c [-]
σ'_v = Vertical effective soil pressure [kPa]
c = Cohesion of the soil [kPa]

According to Brinch Hansen, the value p_{max} is dependent on the soil characteristics, pile diameter and local depth. This results in an uneven distribution across the entire pile length. For each soil layer, the average p_{max} will be calculated (at the centre of each layer) and smeared out over the entire thickness in each soil layer. The soil characteristics needed to calculate p_{max} are summarised in table 3.8. These soil characteristics are obtained from Eurocode 7 (Molenaar and Voorendt, 2017). Since the outcome of p_{max} is dependent on several more variables, the results will not be discussed in this section.

Soil type	**Vol. weight [kN/m^3]**	ϕ **[rad]**	c' **[kPa]**
Peat	12	15.0	2.5
Clay	17	17.5	5.0
Silt	20	27.5	1.0
Sand	20	32.5	0

Table 3.8: Soil characteristics needed to obtain p_{max} according to the method of Brinch Hansen

Lastly, there is a difference in behaviour between a horizontally loaded single pile compared to piles in a group. Because of their proximity to each other, their "spheres of influence" overlap with each other (Walsh, 2005). This effect is illustrated in figure 3.6. A relatively simple solution is to multiply the *p-y* curve by a pile group reduction factor P. This factor is dependent on several aspects of the pile group: centre-to-centre distance between piles, the position of the pile, soil characteristics and whether the pile head is fixed or hinged. The larger the spacing between the piles, the less interaction there is between them due to reduced interference. Also, the position of the pile within the group is of importance. The piles in the leading row experience group effects the least due to the shadowing effect as shown in figure 3.6 (Fayyazi et al., 2014). The effect of the pile group reduction factor (also referred to as "P-multiplier") is illustrated in figure 3.7.

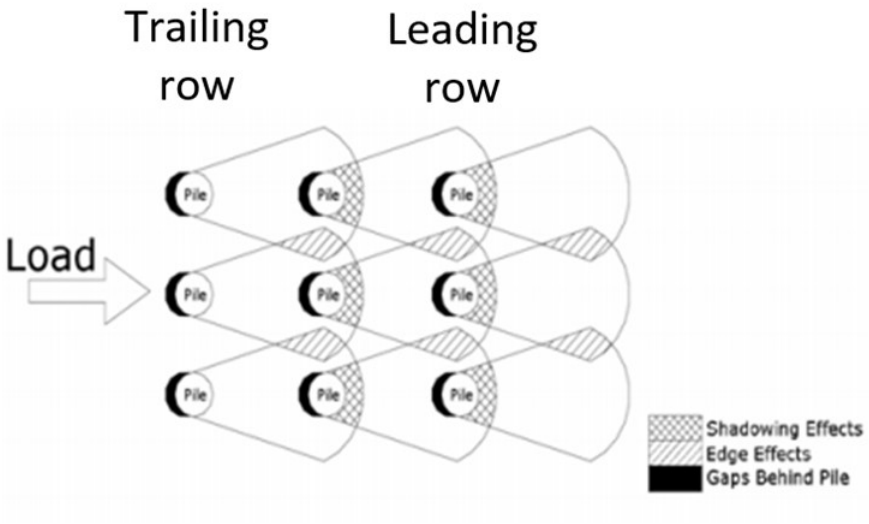

Figure 3.6: Illustration of individual piles influencing each other, retrieved from Walsh, 2005.

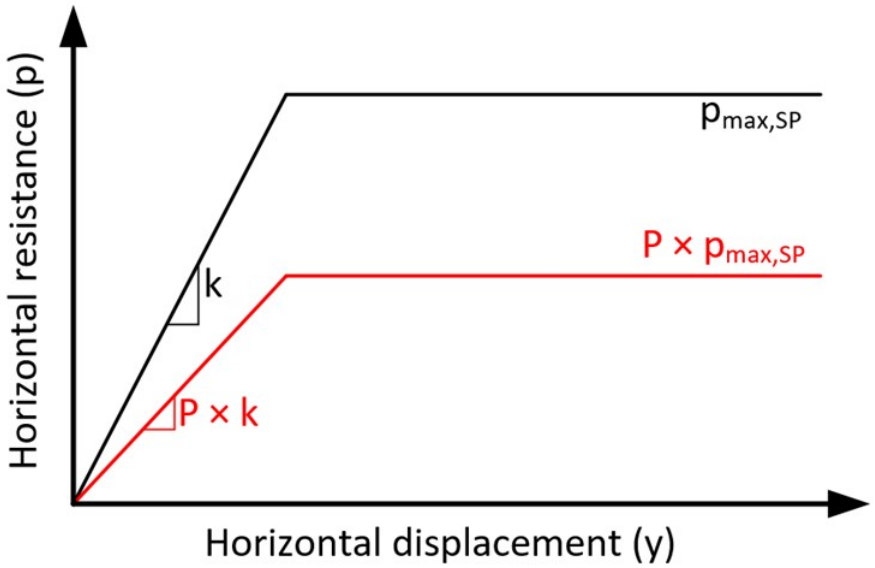

Figure 3.7: The influence of group effects on the *p-y* curve.

Many physical experiments have been done, as well as numerical analyses, to attempt to quantify the P-multipliers. P-multiplier values are dependent on many factors. Several things are known that help to predict such a value, according to Fayyazi et al., 2014:

- Larger relative spacing results in higher P-factors. Relative spacing is calculated by dividing the centre-to-centre distance by the pile diameter.
- A free pile head condition results in higher P-factors compared to a fixed connection.
- Higher soil friction angles ϕ lead to lower P-factors.

For pile groups with three rows (as is the case of "Nieuwe Herengracht"), values for P range from as low as 0.3 for the trailing rows to as high as 1 for the leading rows (Fayyazi et al., 2014).

3.2.4.3 Axial boundary

The pile tip is vertically constrained by the sand layer. However, applying an axial load leads to vertical pile displacement, since sand is not infinitely stiff. This effect can be modelled by applying a single vertical translational spring at the pile tip. The stiffness [N/m] of this spring is determined by relating the settlement [m] of the pile head to the exerted normal force [N] on top of it. The settlement of the pile head s_{head} is determined by two factors:

1. The settlement of the pile **head** s_{el} as a result of elastic deformation of the pile itself.
2. The settlement of the pile tip **tip** s_b as a result of the limited strength and stiffness capacity of the sand layer.

$$s_{head} = s_{el} + s_b \tag{3.6}$$

Elastic deformation of the pile due to axial forces is calculated according to equation 3.7.

$$s_{el} = L_{pile}\varepsilon = L_{pile}\frac{\sigma}{E} = L_{pile}\frac{F}{EA} \tag{3.7}$$

The Dutch norm NEN 9997-1 will be used to approximate the vertical settlement of the pile tip. NEN9997-1 defines a relation between the pile settlement and the exerted force, which is shown in figure 3.8. The curves which are marked by "1" should be applied as they are intended for wooden piles. It is a curve that progresses exponentially until the maximum bearing capacity is reached. These capacities need to be determined.

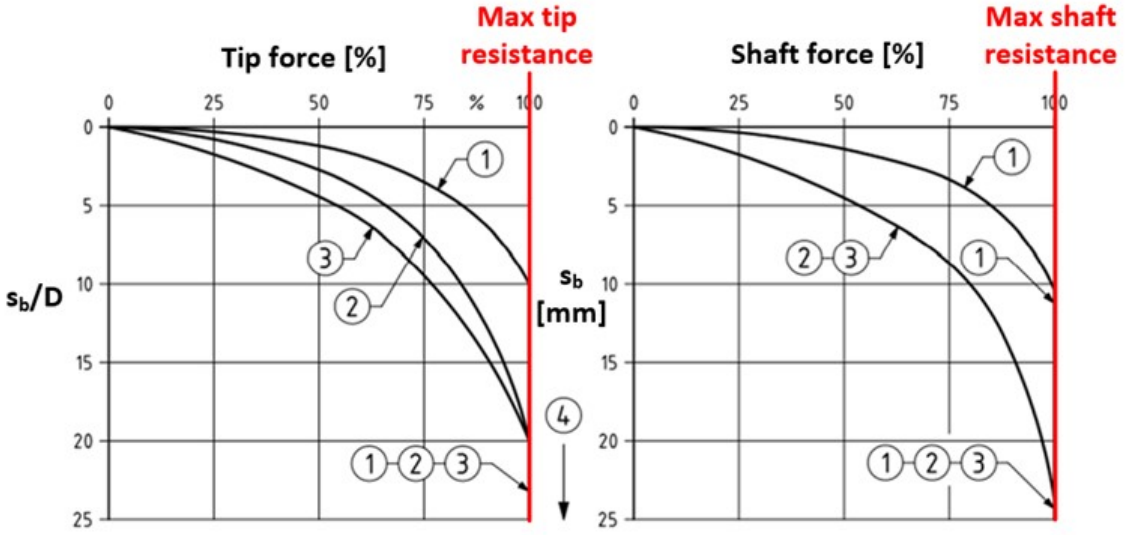

Figure 3.8: Settlement curves according to NEN 9997-1. Left: Pile tip; Right: Pile shaft.

In the Dutch norms (NEN 9997-1), the method of Koppejan is used to determine the vertical compressive bearing capacity of a foundation pile. This method uses the cone resistance values obtained from the local cone penetration test, which can be found in appendix A.2. The Koppejan method is subdivided into two parts: the maximum resistance of the pile tip $F_{r;max;tip}$ in [N] and the maximum resistance along the pile shaft $F_{r;max;shaft}$ in [N]. They are calculated using equation 3.8 and 3.9 respectively (Molenaar and Voorendt, 2017). Apart from these pile resistance parameters, negative shaft friction may be present as well. This is a result of soil settlements in which the soil hangs against the pile shaft (Molenaar and Voorendt, 2017). The first equation is for the tip resistance:

$$F_{r;max;tip} = A_{tip}\frac{1}{2}\alpha_p\beta s\left(\frac{q_{c;I;avg} + q_{c;II;avg}}{2} + q_{c;III;avg}\right) \tag{3.8}$$

Where:

A_{tip}	=	Pile cross-sectional area at the tip [m^2]
α_p	=	Pile class factor: 0.7 [-] for driven wooden piles.
β	=	Pile tip shape factor: 1.0 [-] for a uniform circular cross-section.
s	=	Pile tip cross-sectional shape factor: 1.0 [-] for a circular cross-section.
$q_{c;I;avg}$	=	Average cone resistance in section I, from pile tip level to a level of $0.7D$ to $4D$ deeper. The bottom is determined in such a way that the average cone resistance is minimal. Result: 14 MPa.
$q_{c;II;avg}$	=	Average cone resistance in section II, from the bottom of section I to pile tip level. Going upwards, the cone resistance cannot increase. Result: 14 MPa.
$q_{c;III;avg}$	=	Average cone resistance in section III, from pile tip level to a level of $8D$ higher Going upwards, the cone resistance cannot increase. Result: 3.8 MPa.

The calculation processes behind the cone resistance values $q_{c;I;avg}$, $q_{c;I;avg}$ and $q_{c;I;avg}$ are elaborated in appendix A.2. The pile class and shape factors have been acquired from NEN 9997-1. Next is the shaft resistance:

$$F_{r;max;shaft} = O_{p;avg} \int_0^L \alpha_s q_{c;z;a} \, dz \tag{3.9}$$

Where:

$O_{p;avg}$	=	Average pile circumference [m]
L	=	Pile length [m]
α_s	=	Pile class factor: 0.010 for sand, 0.02 for clay, 0.025 for silt, 0 for peat.
$q_{c;z;a}$	=	Average cone resistance per layer [MPa]

The pile class factors have been acquired from NEN 9997-1. The cone resistance values per layer can be found in table 3.4. The results of the total vertical pile bearing capacity are shown in table 3.9.

Pile diameter [mm]	$F_{r;max;tip}$ **[kN]**	$F_{r;max;shaft}$ **[kN]**	$F_{r;max;total}$ **[kN]**
180	158.5	141.4	300
126 (30% reduction)	76.5	98.2	175

Table 3.9: Total vertical bearing capacity of a single pile according to the Koppejan method.

Another axial constraint directly resulting from soil is negative shaft friction. It is a downward working shear force, progressing along a foundation pile. Negative shaft friction is caused by consolidation of soil, which leads to the pile being dragged along downwards (Hamakareem, n.d.). This drag results in an extra downwards force acting on the piles, which contributes to a reduction of the vertical pile bearing capacity. Similarly to the determination of the pile tip settlement, the negative shaft friction is determined according to NEN 9997-1 (section 7.3.2.2). The friction at the outer pile rows will be determined using formulas for single rows/piles. The friction at the middle pile row will be determined using formulas for pile groups. Due to the presence of the planks, the added sand layer and any surcharge at the surface will not have any effect on negative shaft friction on the piles below, since the piles are shielded by a soil retaining wall (figure 3.9).

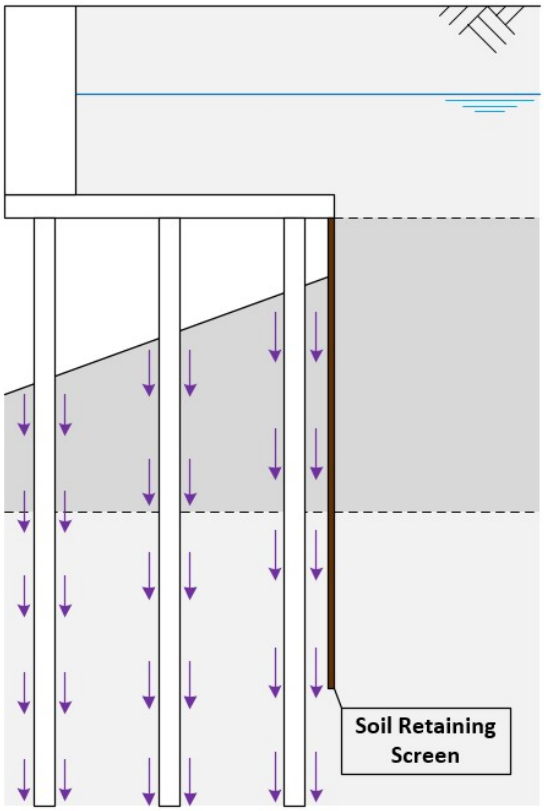

Figure 3.9: The effect of negative shaft friction along the piles.

The following equations are used to calculate the characteristic negative shaft friction for the outer pile rows:

$$F_{nk;k} = O_{s;avg} \times \sum_{j=1}^{j=n} d_j \times K_{0;j;k} \times tan(\delta_{j;k}) \times \frac{\sigma'_{v;j-1;k} + \sigma'_{v;j;k}}{2} \tag{3.10}$$

With:

$$K_{0;j;k} = 1 - sin(\phi_{j;k}) \tag{3.11}$$

And:

$$\sigma'_{v;j;k} = \sum_{j=1}^{j\leq n} d_j \times \gamma'_{j;k} \tag{3.12}$$

The following equations are used to calculate the characteristic negative shaft friction for the middle pile row:

$$F_{nk;k} = A \times \sum_{j=1}^{j=n} \left(\sigma'_{v;j;sur;k} - \sigma'_{v;j;k}\right) \tag{3.13}$$

And:

$$\sigma'_{v;j;sur;k} = \sigma'_{v;j-1;k} + d_j \gamma'_{j;k} \tag{3.14}$$

And:

$$\sigma'_{v;j;k} = \frac{\gamma'_{j;k}}{m_j} \times (1 - exp\,(-m_j \times d_j)) + \sigma'_{v;j-1;k} \times exp\,(-m_j \times d_j) \tag{3.15}$$

With:

$$m_j = \frac{O_{s;avg}}{A} \times (1 - sin(\phi_{j;k})) \times tan(\delta_{j;k}) \tag{3.16}$$

Where:

$F_{nk;k}$	=	Characteristic negative shaft friction [kN]
A	=	Area of the soil around each pile [1 m^2]
$O_{s;avg}$	=	Average pile circumference [m]
d_j	=	Thickness of layer *j* [m]
j	=	Layer number with negative friction
n	=	Total number of layers with negative friction
$K_{0;j;k}$	=	Characteristic neutral soil factor in layer *j*
$\phi'_{j;k}$	=	Characteristic angle of friction *j*
$\delta_{j;k}$	=	$0.75 \times \phi'_{j;k}$
$\sigma_{v;j;k}$	=	Characteristic vertical effective stress under layer *j*
$\gamma_{j;k}$	=	Characteristic effective volumetric weight of the soil at layer *j*

3.3. Masonry modelling

Modelling the masonry wall requires some prior knowledge of its behaviour. This section is divided into several topics:

- Masonry behaviour (to be modelled)
- Material properties
- Available material models in DIANA
- Boundary conditions: dilation joints and brick/wood interface

3.3.1. Modelling masonry behaviour

First of all, to be able to model masonry as a material, it is necessary to understand how masonry responds to external loading.

3.3.1.1 Plasticity

Like other construction materials, masonry experiences linear elastic behaviour. This means that the deformation of the material is linearly proportionate to the exerted force on the material. With linear elasticity, the material usually returns to its original state when it is unloaded. However, when forces are great enough, the material will experience non-linear plastic behaviour. This implies permanent deformations in which the material experiences a higher deformation rate compared to the elastic phase. With ductile materials like steel, the stiffness of the material is decreasing, but the applicable load can initially still increase. Once a material's peak strength has surpassed, it will result in a subsequent loss in strength, which may result in complete failure. The relation between load and deformation is different for each material, but it also depends on the type of loading (e.g. compressive or tensile). A generalised stress-displacement is shown in figure 3.10.

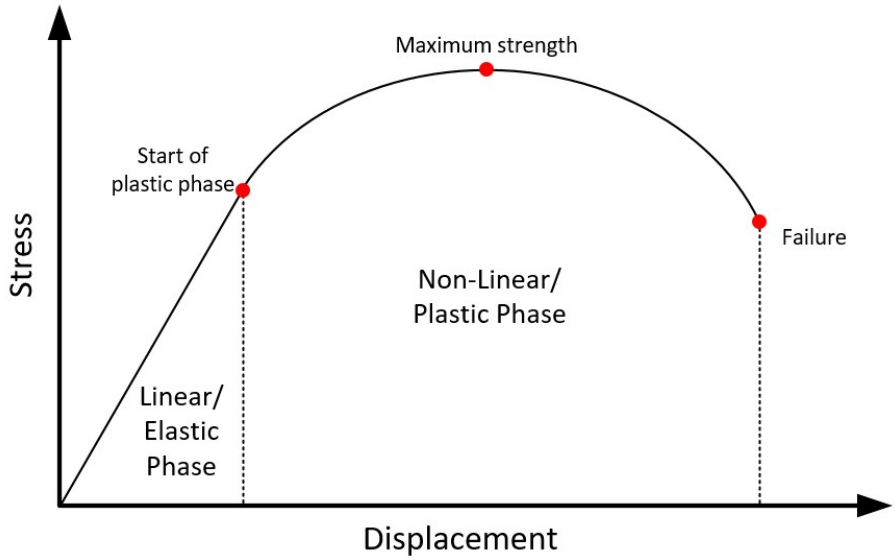

Figure 3.10: Generalised stress-displacement diagram of a material.

3.3.1.2 Quasi-brittle behaviour

Unlike steel, brick is considered to be a quasi-brittle material. It falls under the same category as, for instance, rock and concrete. This means that the material will deform as a result of the development of micro-cracks instead of yielding. Micro-cracks are already present in the material even before loading (Lourenço, 1996). Micro-cracks will develop in proportion to material deformation. When the material's peak strength is reached, macro-cracks will develop, leading to a substantial decrease in material strength (Lourenço, 1996). The process of strength loss is also referred to as "softening". Generalised stress-displacement diagrams of quasi-brittle materials are shown in figure 3.11, for different types of loading situations. The graphs describe the behaviour of these materials in compression, tension and shear respectively.

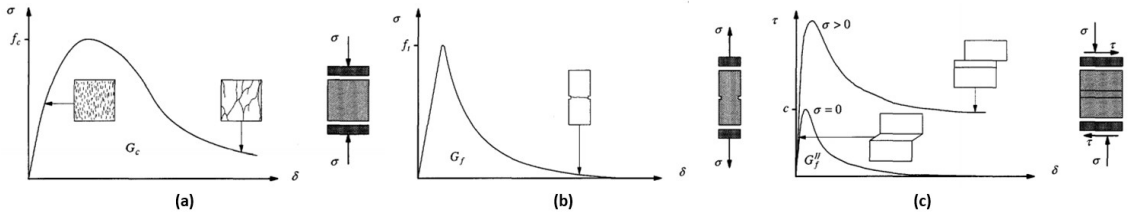

Figure 3.11: Behaviour of quasi-brittle materials in (a) compression, (b) tension and (c) shear (Lourenço, 1996)

In compression, quasi-brittle materials can absorb increased loading even after plasticity has begun, this process is referred to as "hardening". Macro-cracks start appearing once the peak compressive strength f_c is reached. In tension, the material shows a more sudden loss in strength after its peak tensile strength f_t is reached. In shear, the behaviour depends on the presence of a compressive force ($\sigma > 0$), which contributes to shear resistance. When this force is absent ($\sigma = 0$), the shear strength depends on cohesion c only (Lourenço, 1996).

3.3.2. Modelling options

Traditionally, designers would use empirical formulae and rules-of-thumb to predict the behaviour of a masonry object. However, the rise of sophisticated numerical tools contributed to

the change of approaching the behaviour of masonry, as well-established models were absent beforehand (Lourenço, 1996). There are several approaches towards computational modelling of masonry structures, all of which vary in degree of complexity.

3.3.2.1 Micro- and Macro-Modelling

Given that masonry is a composite material consisting of relatively small unit and mortar geometries, it is possible to assess the material on different levels of complexity (Lourenço et al., 1995):

1. **detailed micro-modelling:** A highly elaborated method, which includes the modelling of the unit, the mortar as a continuous element and the unit-mortar interface as a discontinuous element (joint). Material properties of both the unit and mortar are included and the behaviour of the unit-mortar interface is taken into account, which leads to a relatively detailed result.

2. **simplified micro-modelling:** In this method, the unit is still treated as a continuous element, while the mortar and the unit-mortar interface are combined into a discontinuous element (joint) as a so-called "average" interface. The size of the unit is increased in order to maintain the geometry. This method requires less computing time than the detailed micro-model but sacrifices its accuracy.

3. **macro-modelling:** The unit, mortar and unit-mortar interface are combined to represent a continuous anisotropic composite material. Anisotropy in a material is described as a variation in property dependent on direction. When it comes to macro-modelling, the individual units and the mortar joints are therefore not distinguished. Instead, the masonry is modelled as a continuum with average strains and stresses within the material.

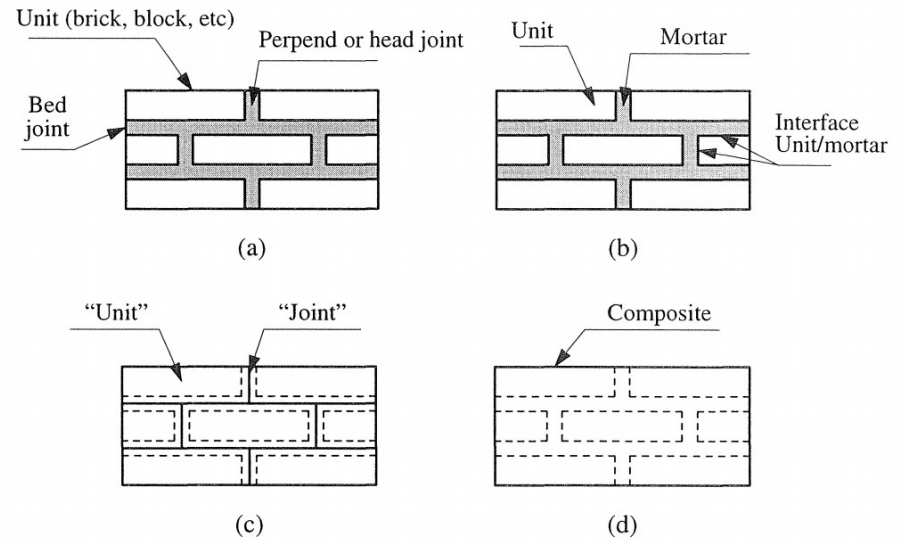

Figure 3.12: Modeling strategies for masonry structures: (a) masonry sample; (b) detailed micro-modeling; (c) simplified micro-modeling; (d) macro-modeling. Acquired from Lourenço et al., 1995

The proposed models are illustrated in figure 3.12. Micro-models are generally suitable for analysing small structural elements. they are used to model the behaviour of masonry with

a magnified view. Macro-models can be used to analyse larger-scale structures, as: "In large and practice-oriented analyses the knowledge of the interaction between units and mortar is, generally, negligible for the global structural behaviour." Macro-models can be applied to solid walls with sufficient size. Aside from being more time-efficient, the meshing process is also more user-friendly, compared to the micro-model (Lourenço et al., 1995). For these reasons, the macro-model is deemed applicable in the context of this research.

3.3.2.2 Material models

DIANA offers several macro-modelling options for quasi-brittle materials as so-called "smeared crack models", meaning that the cracked solid is treated as a continuum. All of these modelling options are described in the software user manual (DIANA, 2017). Smeared crack modelling options, offered by DIANA, which do not apply to masonry will neither be considered nor mentioned in this thesis.

1. **Multi-Directional Fixed Crack Model:** A model applicable to both concrete and masonry. Applicable on 3D solids, however, it only takes tensile cracking into account.

2. **Total Strain Crack Model:** Originally developed for modelling concrete. However, it is also applicable to masonry structures (van Noort, 2012). It is applicable to 3D solids. However, the model assumes isotropic behaviour, meaning that the material properties are the same in each direction in the 3D space.

3. **Engineering Masonry Model:** Compared to the Total Strain Crack Model, the Engineering Masonry Model describes the behaviour of masonry as a result of cyclic loading more realistically. Cyclic loading is described as the repetition or fluctuation of stresses on a structure. The energy absorbed by the masonry as a result of cyclic loading is underestimated in the Total Strain Crack Model. Furthermore, the Engineering Masonry Model allows for anisotropic input parameters, while the Total strain Cracking Model does not. A drawback of the Engineering Masonry Model is that it does not allow the modelling of 3D solids.

Based on the available material models, the Engineering Masonry Model seems to be the most suitable choice. The first option does not take cracking as a result of compression and shear behaviour into account, which makes it an undesirable option. Furthermore, The Engineering Masonry Model has proven to have a better accuracy compared to the Total Strain Crack Model. However, since the scope of this thesis is to build a 3D model, the best choice has become the Total Strain Crack Model by process of elimination. This model will therefore be further elaborated.

3.3.3. Total Strain Crack Model

The Total Strain Crack Model (TSCM) is a macro-model, using a smeared crack approach (Vecchio and Collins, 1986). When cracks occur in a point, they are smeared out and extrapolated over the represented area around the point in which the crack occurs. Besides, it allows for modelling of 3D solids and it allows for input for compressive, tensile and shear behaviour.

In DIANA, the Total Strain Crack Model asks for the following input:

- Linear material properties
- Total strain crack propagation
- Tensile behaviour

- Compressive behaviour
- Shear behaviour

3.3.3.1 Linear elasticity and crack propagation

Linear material properties only include the Young's Modulus, Poisson's ratio and mass density. All other parameters describe the masonry's non-linear behaviour. The Total Strain Crack Model describes two types of crack propagation: fixed and rotating. If a fixed model is chosen, the direction in which the crack develops remains fixed after initial cracking. If a rotating model is chosen, the change in direction of crack development corresponds to the changes in the stress-strain relationship (van Noort, 2012). When modelling an entire masonry wall, it is to be expected that the direction of crack propagation will not remain fixed once the first cracks are shown. Therefore, when it comes to building the model, a rotating model seems more appropriate. Additionally, it is no longer required to define input for shear behaviour according to the software.

3.3.3.2 Tension and compression

DIANA offers a number of predefined tensile stress-strain curves in TSCM, all of which are shown in appendix B. Most predefined curves are either energy-based or strain-based. Strain-based curves will be dismissed since more information is available regarding tensile fracture energy. All relevant energy-based tensile curves, which to a reasonable degree fit the tensile curve of quasi-brittle materials (figure 3.11), are shown in figure 3.13.

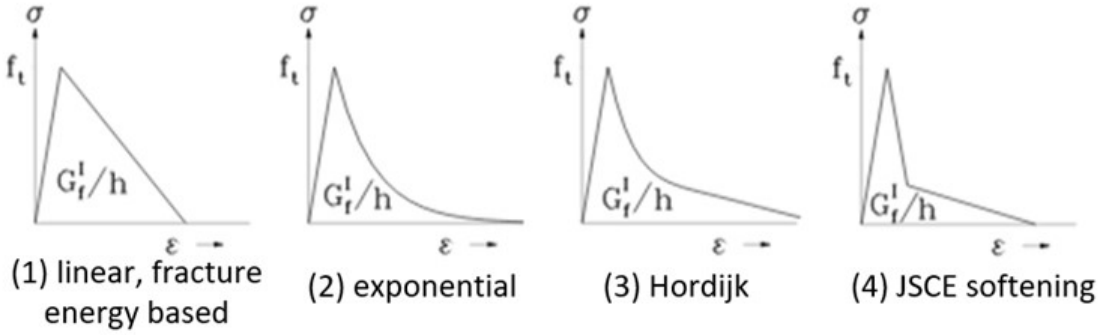

Figure 3.13: Options for energy-based tensile curves for masonry, acquired from the DIANA manual.

These predefined tensile softening curves can be compared to the tensile curve of quasi-brittle materials shown in figure 3.11. The predefined functions which show the closest resemblance would be the exponential curve, and to a slightly lesser extent, the Hordijk curve. In case it is only necessary to define when macro-cracks appear, it might not be necessary to represent the softening process to an exact degree (process after tensile strength capacity is reached). A linear approximation might prove to be sufficiently accurate. It is a simplified approximation of reality, but the main benefit of choosing a linear curve is an increase in computational speed.

DIANA offers a number of predefined stress-strain curves for compression as well, all of which can be found in appendix B. All relevant compressive curves, which to a reasonable degree fit the compressive curve of quasi-brittle materials (figure 3.11), are shown in figure 3.14. Strain-based curves are again dismissed for a similar reason as the tensile part.

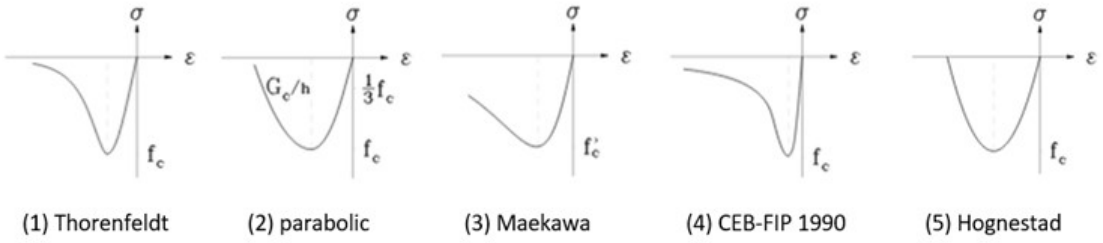

Figure 3.14: Options for compressive curves for masonry, acquired from the DIANA manual.

The Thorenfeldt curve most closely resembles the compressive curve of quasi-brittle materials shown in figure 3.11. It is known that the compressive strength is much stronger than the tensile strength in brittle and quasi-brittle materials. According to table 3.10, the compressive strength capacity is 85 times the tensile strength capacity. Also, the compressive fracture energy is up to 200 times the tensile fracture energy. Given the significant disparity between compressive and tensile strength, it is likely that the masonry will have developed significant macro-cracks before the compressive strength capacity is reached. As a result, it can be concluded that incorporating compressive linear elastic behaviour to masonry may prove to be sufficiently accurate in this case. The main benefit of applying linear elasticity for compression is less numerical complexity. Combining the compressive and tensile curves result in a stress-strain relationship shown in figure 3.15. The stress-strain curve resembling reality the most is a combination of the Thorenfeldt curve in compression and the exponential curve in tension. Possibly, the curve can be simplified and approximated by combining linear elasticity in compression and the linear, fracture energy-based curve in tension.

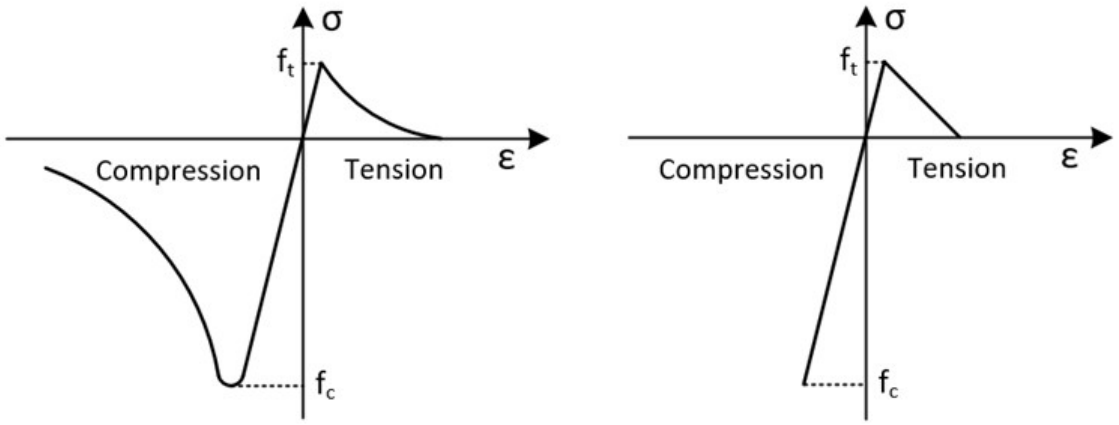

Figure 3.15: Realistic stress-strain curve (left), simplified stress-strain curve (right). Not to scale.

3.3.3.3 Crack bandwidth

It has been found that the energy dissipation during the process of crack formation is dependent on the size of the finite elements in smeared models. In an attempt to eliminate the influence of the mesh size, the crack bandwidth value l has been introduced (Slobbe, 2015).

This value is required as input in the Total Strain Cracking Model under tensile behaviour. When it comes to crack development, the crack bandwidth value is linked to the crack energy (G_f/l). The area underneath the tensile curve equals the division of the crack energy by the

crack bandwidth (figure 3.16). Given this relation, it can be concluded that the bandwidth has a direct effect on the slope of the softening curve (post-peak behaviour). Larger crack bandwidth values lead to quicker energy dissipation, resulting in brittler behaviour.

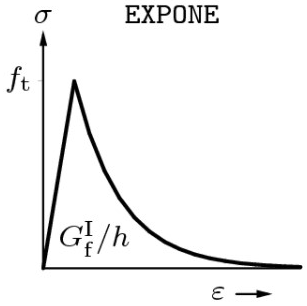

Figure 3.16: The area under the tensile curve is equal to the crack energy divided by the crack bandwidth. This graph is retrieved from the DIANA FEA software manual.

Because of the effect that the bandwidth has on the post-peak behaviour, it can be used to counteract the effect the mesh size has on crack development. The crack bandwidth should therefore be dependent on the mesh size in order to get consistent cracking patterns (and thus minimising the dependency on the element sizes) (Slobbe, 2015). The Total Strain Cracking Model offers three ways to specify these values: according to the theory of Rots, the theory of Govindjee et al. and user-specified values. According to the DIANA FEA manual, the crack bandwidth according to Rots is equal to the cubic root of the volume of an element $\sqrt[3]{V}$. Govindjee's method is more elaborate, by also taking the element aspect ratio and the crack orientation into account. For this reason, the method of Govindjee will be implemented.

3.3.4. Properties

Amsterdam quay walls are made of unreinforced masonry. Accurate and detailed information on old Amsterdam masonry properties is, as of the time this research is conducted, unavailable. However, there is a bulk of data available on the properties of unreinforced Groningen masonry, which have undergone major damages as a result of local earthquakes. Extracted samples from existing masonry structures in that area have undergone destructive tests to characterise the material properties (Jafari et al., 2017). However, the material properties of masonry can also be derived from Dutch norms, which provides average values for assessing existing masonry structures. The norm states that if the material properties are not determined by testing of local samples, the values provided by NPR9998:2020 can be used as a baseline (NPR9998, 2020). The values provided by NPR9998:2020 will be used as a baseline for the numerical model.

There are some values that NPR9998:2020 does not provide, namely the Poisson's ratio and the mass density. Research done by Van Noort provides values based on research done on how to computationally model masonry. When it comes to masonry, Poisson's ratio is not the same in each direction (anisotropic). Therefore, Poisson's ratio from x- and y-direction have been combined into a single value, using formulas obtained from Pande et al., 1994. Van Noort also provides the density of masonry, which is the weighted average of the densities of the mortar and the bricks (van Noort, 2012). It must be noted that these values are likely different from reality. However, since the properties of Amsterdam's quay wall masonry are unknown, the density provided by Van Noort will be adopted nonetheless. Poisson's ratio can be calculated

using the following relation between the Young's modulus and the shear modulus:

$$G = \frac{E}{2(1+\nu)} \tag{3.17}$$

The values directly derived from NEN9998 are assumed to be the structural value of "fresh" (new) masonry, built before 1945. The relevant values are summarised in table 3.10. In NEN9998 it is specified that the fracture energy value is dependent on the mesh size, which should be used in accordance with a crack bandwidth. The specification of the crack bandwidth has been elaborated in the previous section.

Material property	**Value**	**Unit**
Young's modulus (E)	5000	N/mm^2
Shear modulus (G)	2000	N/mm^2
Poisson's ratio (ν)	0.25	-
Mass density (ρ)	1800	kg/m^3
Tensile strength (f_t)	0.35	N/mm^2
Tensile fracture energy (G_t)	0.035	N/mm
Compressive strength (f_c)	8.5	N/mm^2
Compressive fracture energy (G_c)	20	N/mm

Table 3.10: Average masonry properties of masonry before 1945, derived from NEN9998.

According to NEN9998, the average strength, stiffness and energy values summarised in table 3.10 may be reduced by 40 per cent if the masonry shows clear signs of bad quality. In that case, the values in table 3.11 are used. These values will be used as a lower limit for the masonry quality.

Material property	**Value**	**Unit**
Young's modulus (E)	3000	N/mm^2
Shear modulus (G)	1200	N/mm^2
Poisson's ratio (ν)	0.25	-
Mass density (ρ)	1800	kg/m^3
Tensile strength (f_t)	0.21	N/mm^2
Tensile fracture energy (G_t)	0.021	N/mm
Compressive strength (f_c)	5.1	N/mm^2
Compressive fracture energy (G_c)	12	N/mm

Table 3.11: Weak masonry properties of masonry before 1945, with the exception of the Poisson's ratio, derived from NEN9998.

3.3.5. Boundary conditions

Two kinds of boundaries connected to the masonry wall can be identified:

1. **Dilation joints:** As mentioned before, quay walls are longitudinally separated from each other with dilation joints.

2. **Brick/wood interface:** When quay walls were being constructed, the foundation structure was built first, with wooden floor plates functioning as the first layer of support for the masonry wall. Bricks were laid on top of the wooden floor (no mortar in between),

resulting in direct contact between wood and bricks (Sas, 2007). With no special connection between the wall and the foundation, the interface connection is based solely on friction between the two materials.

3.3.5.1 Dilation joints

Dilation joints act as a separation line between two quay wall structures or between a quay wall structure and a different hydraulic structure (e.g. bridges). The presence of this joint may cause two separate structures to shear alongside each other vertically and laterally. However, rotation in all directions and horizontal movement in the longitudinal direction of the wall is constrained. The effect of full fixation and free vertical and lateral movement, as illustrated in figure 3.17, will be analysed in the finite element model.

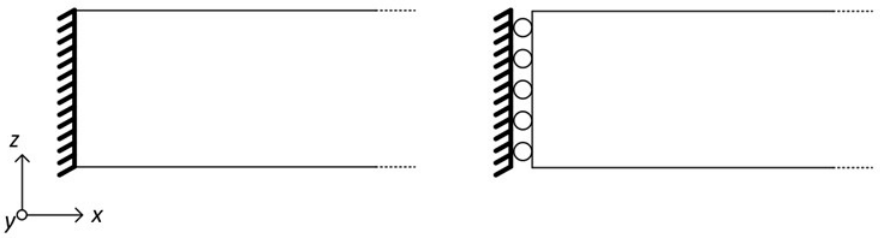

Figure 3.17: Fully fixed boundary (left) and boundary with free shear movement (right).

3.3.6. Brick/wood interface

DIANA offers many interface material models, each describing different kinds of interfaces. Coulomb friction is an approximate model which describes the motion between two surfaces in contact with each other (DIANA, 2017). The Coulomb Friction Model is available in DIANA FEA. It is also the most suitable option for modelling the interface between two structural parts, given that the behaviour of the contact surface between masonry and wood is governed by friction/sliding.

3.3.6.1 Coulomb Friction Model

Coulomb friction assumes the following relation:

$$F_f \leq \mu F_N \tag{3.18}$$

The friction force F_f works in the opposite direction to the motion-inducing force. Both forces negate each other, resulting in a zero-sum net force until the threshold of μF_N has been reached. Once the friction force reaches this level, the surfaces start to slide over each other. The friction force is related to the normal force F_N as shown in equation 3.3.6.1. Both forces are visualised in figure 3.18. The friction coefficient μ is an empirical coefficient indicating roughness between two surfaces.

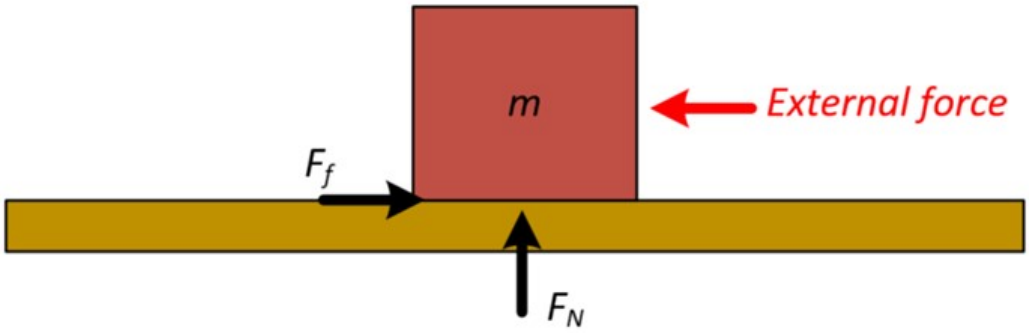

Figure 3.18: Visualisation of coulomb friction.

In DIANA FEA, the Coulomb Friction Model assumes non-linear friction behaviour. The linear elastic input defines the force required to move the wall. The force required to trigger sliding is called the friction force F_f. It is related to the normal force F_N as shown in equation 3.3.6.1. The Coulomb Friction Model in DIANA FEA requires the application of the friction angle ϕ instead of the friction coefficient μ. Both parameters are directly related to each other according to the following relation:

$$tan(\phi) = \mu \tag{3.19}$$

3.3.6.2 System properties

Several studies and experiments have been done when it comes to defining the sliding properties of masonry. However, not much is known about the interface between masonry and wood. Several wet sliding experiments of masonry on wood have been performed by I. Strikvoort with the intent of understanding the behaviour of old quay walls (Strikvoort, 2014). It is preferred to assume values that represent reality the most, even though it is difficult to represent reality with full accuracy. Strikvoort determined several values as a result of horizontal shear tests with varying consolidation times. The cases in which the longest consolidation time have been imposed, while still remaining wet, have been assumed for the finite element analyses performed in this thesis. The horizontal friction coefficient μ and friction angle ϕ are of importance in this case. The friction coefficients varied between 0.81 and 0.89 and the friction angles varied between 38.9 and 41.1 degrees (Strikvoort, 2014). Therefore, the following values have been assumed for the finite element analyses: $\mu = 0.85$ and $\phi = 40°$ or 0.7 rad. Both values correspond to each other according to the relation presented by equation 3.3.6.1.

In DIANA FEA, another available parameter is the cohesion c [N/m^2]. In the Coulomb Friction Model, the cohesion value represents an extra interface strength parameter. In other words, adding cohesion results in larger withstand-able loads before sliding is induced. In the case of historical quay walls, longitudinal wooden support beams (watersloof, see figure 2.2) are usually present which aid in horizontal stability Sas, 2007. Assuming a shear strength of 3.4 N/mm^2 (C18 wood) and a width of 100 mm, it results in an extra capacity of 340 N/mm (in the longitudinal direction). Since the cohesion value applies to the entire masonry/wood interface, this value should be divided by the wall thickness (0.7 m at the base). This leads to a value of 0.485 MPa. However, if the wooden foundation structure has been severely degraded, this extra horizontal protection will have little structural value left (Sas, 2007). In the finite element model, it is assumed that when the foundation has been severely degraded,

the cohesion value will be reduced to zero.

3.4. Loading

Existing loads on quay wall structures are mentioned in section 2.2.

3.4.1. Loading configuration

When the shapes of the finite element model are defined, and their material models (behaviour) have been assigned, it is necessary to define the loading configurations. The model requires forces to which it can respond. It is necessary to understand which forces the quay wall is subjected to and to determine their quantity. The forces acting on the structure will be divided into three categories:

1. Self-weight: Downward forces resulting from the mass of the structure itself.
2. Permanent loads: Forces that are continuously acting on the quay wall. Examples include: the weight of the soil pushing downward and against the masonry wall; the presence of water; the presence of other semi-permanent forces such as trees.
3. Variable loads: Forces that act on the quay wall but occur for a short(er) amount of time. Examples include: passing/parked traffic, layers of snow, passing people.

One must keep in mind that the variable loads which are exerted on the quay wall are not the same at each location. Some quay walls allow the passing of heavy traffic while others only accommodate passing people. As stated before in this thesis, the increase in traffic loads has significantly contributed to the degradation of quay walls. Therefore, these loads will be studied more thoroughly. The quay at "Nieuwe Herengracht" contains several trees behind the masonry wall. However, these trees are scattered point loads and the distance between some are over 10 meters long. As a means to reduce the complexity of the loading configuration, the local effect of trees is not taken into account. The finite element model will therefore consist of the following load configuration:

- Self-weight of the masonry wall and the wooden foundation structure (including piles).
- Permanent soil loads resulting from the soil resting directly against the wall and on top of the wooden planks, as well as the soil behind the structure.
- Added surcharge directly behind the masonry wall, as well as behind the entire structure, resulting from traffic.

The vertical masonry wall, together with the horizontal planks, represents an L-shaped cantilever wall. The only differences between a historical quay wall and a modern cantilever wall are the use of different materials and the type of connection between the vertical and the horizontal component (see figure 3.19).

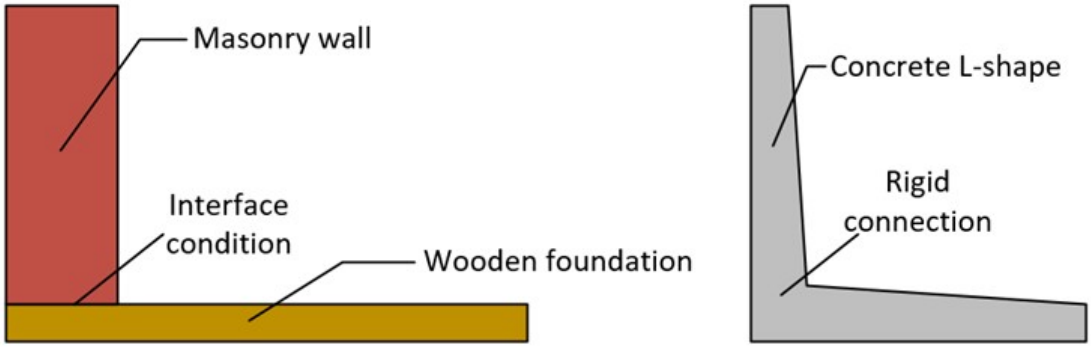

Figure 3.19: Notice the L-shape in the historical quay wall and a modern concrete cantilever wall (representation).

3.4.2. Soil loading

The soil rests against the masonry wall and the soil retaining wall in the horizontal direction, and it rests on top of the planks in the vertical direction. The water table is set at NAP (Normal Amsterdam Level), although it is not constant. It is assumed that the soil is permeable enough so that the water table differences inside the canal and behind the quay wall are minimal and short-lasting. Therefore, the model assumes equal water pressure from both sides, resulting in a net force of zero. The forces resulting from the soil can be divided into two parts (figure 3.20), which will be further elaborated upon:

- The soil column influencing the stability of the quay wall (located behind the L-shape).
- The soil column resting directly against the masonry wall and on top of the planks.

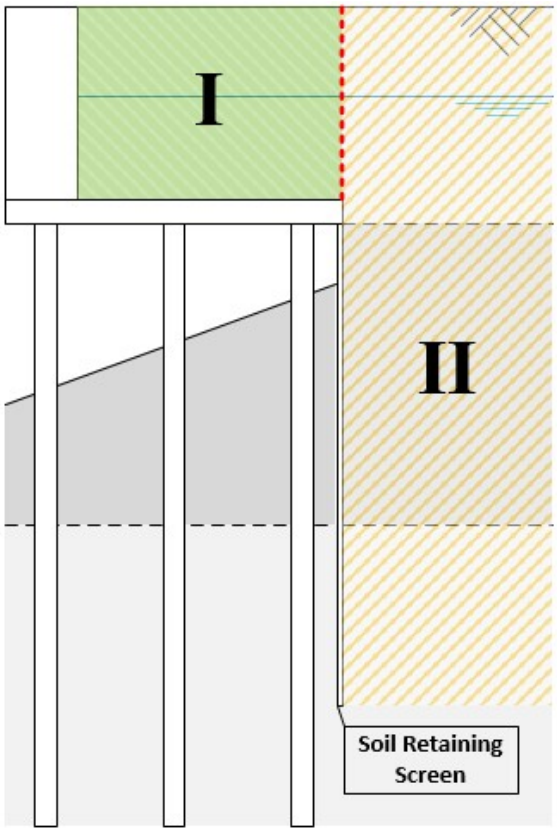

Figure 3.20: a) I: Soil directly behind the masonry wall; II: Soil behind the foundation structure.

3.4.2.1 External stability

In assessing the external stability of a cantilever wall, the load configuration presented in figure 3.21 is assumed (Nematollahi et al., 2014). It shows the forces relevant for general stability and the position of the "virtual boundary" and the horizontal forces.

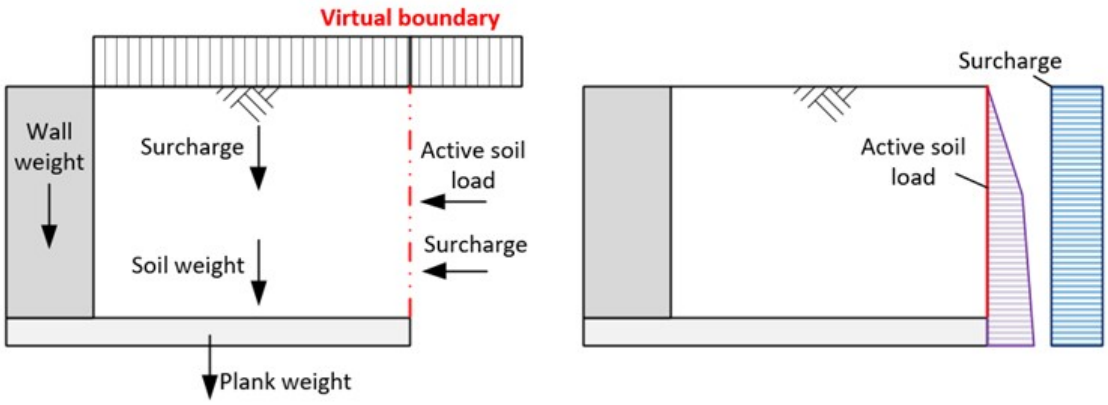

Figure 3.21: Left) Forces contributing to instability; Right) Horizontal forces acting against the virtual boundary.

The soil column behind this virtual boundary pushes directly against the foundation structure (soil retaining wall). These forces will be transferred to the planks and the piles, resulting in potential movement in the horizontal direction. This has a major impact on the stability of

the structure as a whole (see figure 3.22.

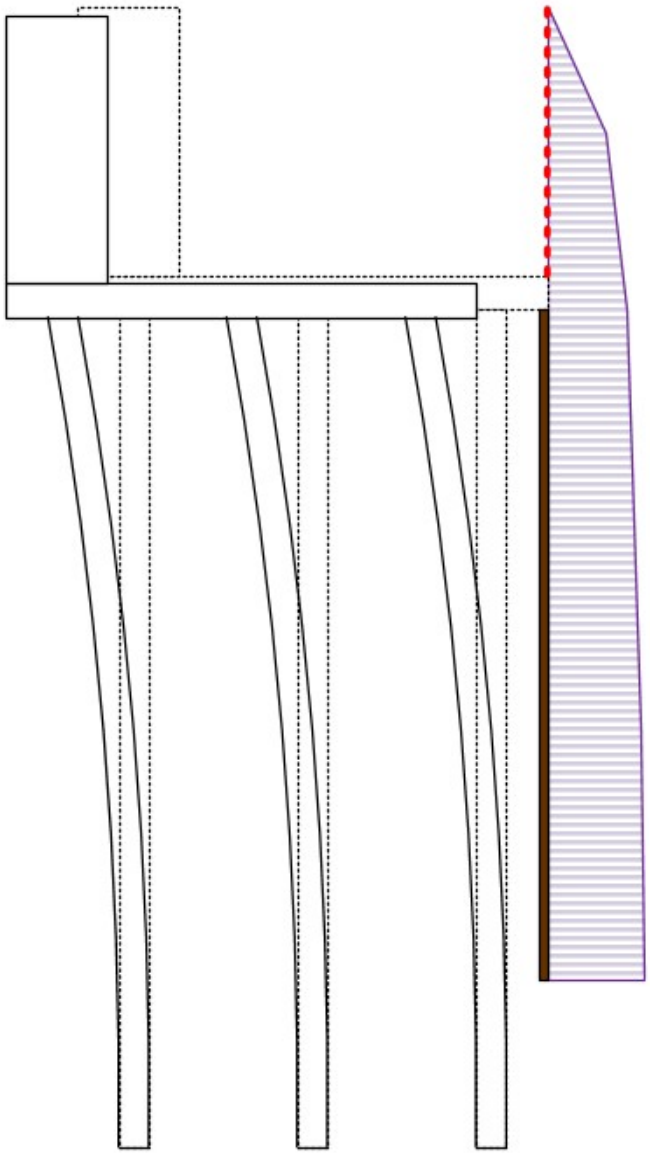

Figure 3.22: Expected response of the structure after applying loads behind the foundation structure.

3.4.2.2 Internal stability

As mentioned in section 3.3.6, the masonry and planks are connected with a friction/sliding interface condition. Because of this interconnected L-shape, it is assumed that the soil resting on top of the planks cannot result in horizontal displacement of the foundation structure. Rather, this soil column will instead push against the masonry wall which results in an increase in friction within the brick/wood interface, according to this assumption. Vertically, the soil rests on top of the planks, resulting in vertical displacements of the foundation structure. If the force in this area of the soil becomes too large, the masonry wall will either start to slide off the foundation structure horizontally, or the structure will settle too much vertically (see figure 3.23).

The "table" analogy is used to illustrate the assumption that the foundation does not move laterally as a result of forces directly behind the masonry wall. This is done by imagining the foundation structure (with piles) as a table and the masonry wall as an object standing on top of it. The soil column, which is resting directly on top of the planks, acts as a subject standing on the table, pushing against the masonry wall. While the subject tries to push the object away, the table itself will not displace. Future references to this analogy will be clarified by using the term "table effect".

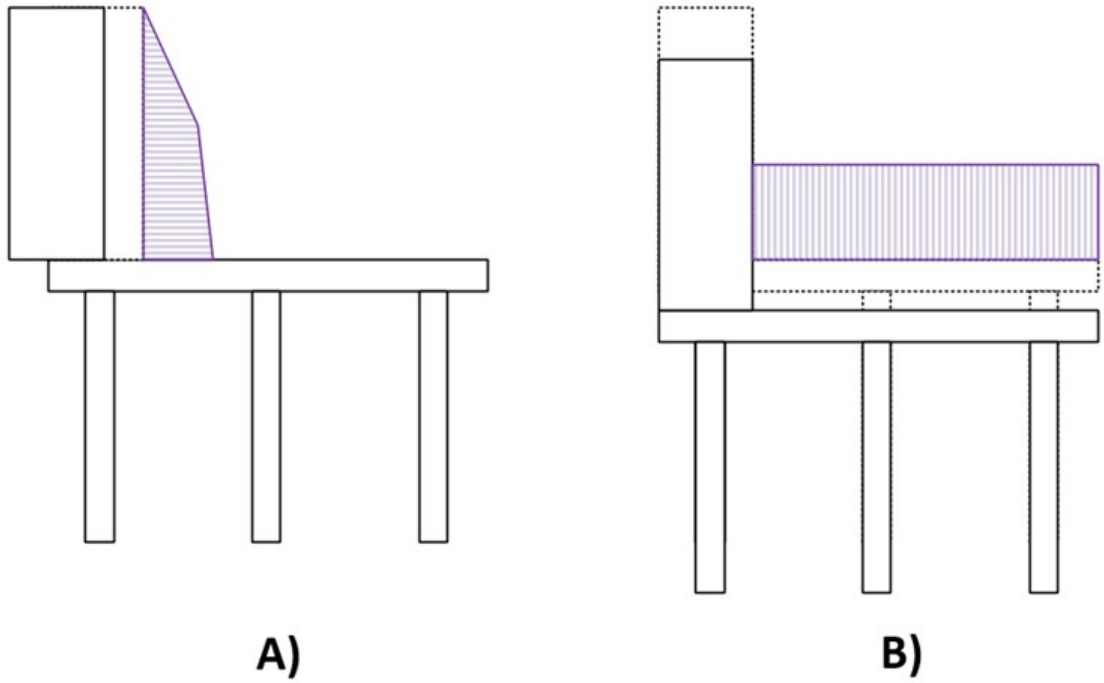

Figure 3.23: Response of the structure after applying loads behind the masonry wall. a) horizontal; b) vertical.

3.4.3. Modelling of loads

The first step was to define the loads, the next step is to introduce them into the finite element model correctly. In the previous paragraph, it has been determined that the quay wall structure responds to the loads in two different mechanisms. Firstly, the soil directly behind the masonry wall rests against it, causing it to "push" the wall in the direction of the free water. Secondly, the soil further behind the masonry structure pushes against the soil retaining wall, causing it to "push" the entire foundation structure in the direction of the free water. In other words, the first mechanism is the internal stability of the masonry wall and its connection to the foundation. The second mechanism is the external stability of the entire quay wall including its foundation structure.

3.4.3.1 Soil column I

Forces resulting from the area directly behind the quay wall (column I) cause the internal stability mechanism as described before. The forces which will be considered in the model are the soil forces (horizontal and vertical) and possible surcharge in this area (load above the surface). Furthermore, the self-weight of the masonry wall and the wooden foundation structure should be taken into account. The wooden floor and the masonry wall carry the

weight of both the soil and the water. However, as mentioned previously, it is assumed that the soil is permeable enough so that the water table differences inside the canal and behind the quay wall are minimal and short-lasting. Therefore, the model assumes equal water pressure from both sides, resulting in a net force of zero.

Because of the limitations of DIANA, it has proven to be difficult to model the two described mechanisms at once. When loads are applied behind the masonry wall, the entire structure (including the piles) will displace, because the wall is directly connected to the foundation structure. To overcome this limitation, a virtual boundary will be implemented at the trailing edge of the planks, which represents the red line in figure 3.20. The forces exerted on the masonry wall will be complemented by an equal force against this virtual boundary, in the opposite direction. Theoretically, this balance in forces should make any displacements in the piles negligibly small, resulting in a more accurate representation of the "table effect".

The loading configuration is shown in figure 3.24. The relevant values needed for calculations are summarised in table 3.12. It has been established in section 3.2.4 that the soil is composed of sand. The properties of sand have been derived from Eurocode 7 NEN-EN9997, within the category of "clean, moderate sand".

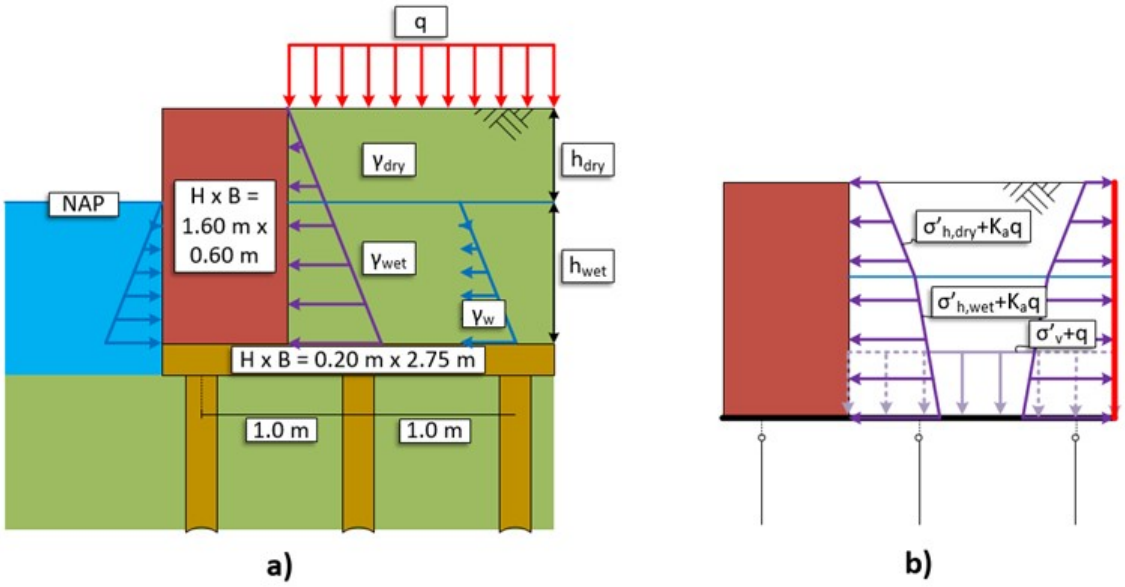

Figure 3.24: a) Load configuration on the quay wall structure; b) Load configuration applied to the finite element model.

Property	Value	Unit	Source
Volumetric weight: dry sand (γ_{dry})	18	kN/m^3	NEN-EN9997
Volumetric weight: wet sand (γ_{wet})	20	kN/m^3	NEN-EN9997
Volumetric weight: water (γ_w)	10	kN/m^3	
Angle of friction: sand (ϕ)	32.5	degrees	NEN-EN9997
Dry height (h_{dry})	0.75	m	Figure A.2
Wet height (h_{wet})	0.85	m	1.60 m - 0.75 m

Table 3.12: Overview of load properties and their corresponding dimensions.

The effective vertical soil stress on the wooden floor (σ'_v) is the summation of the effective stress above and below the water table at NAP. The effective stress above the water table is equal to the total stress, the effective stress below the water table is equal to the total stress minus the pore water pressure. The result is equation 3.20.

$$\sigma'_v = \gamma_{dry} h_{dry} + (\gamma_{wet} - \gamma_w) h_{wet} = 22 \text{ kPa} \tag{3.20}$$

Horizontal effective pressure is calculated by multiplying the vertical effective pressure with a soil pressure coefficient (K [-]). The value of this coefficient is dependent on the soil behaviour resulting from the displacement of the masonry wall. If the wall moves away from the soil column, the soil becomes less compacted, resulting in stress reduction (active stress). Similarly, if the wall moves towards a soil column, the soil becomes compressed, resulting in a stress increase (passive stress) (Molenaar and Voorendt, 2017). In this case, the soil is only present at the right side of the cross-section, pushing the quay wall in the direction of the canal. Therefore, only active soil deformation is assumed according to Rankine's theory of soil behaviour (Molenaar and Voorendt, 2017). The active soil coefficient is calculated using equation 3.21.

$$K_a = \frac{1 - sin(\phi)}{1 + sin(\phi)} \approx 0.30 \text{ [-]} \tag{3.21}$$

The load q is an applied external load on top of the quay wall, which will be used to represent traffic in the finite element model. Vertically, the acting total load will increase by q. Horizontally, the acting total load will increase by $+K_a q$ or $+0.3q$.

3.4.3.2 Soil column II

Forces resulting from the area behind the soil retaining screen (column II) cause the external stability mechanism as described before. The forces which will be considered in the model are the soil forces (horizontal only) and possible surcharge directly on top of this column. The horizontal soil forces, which are transferred to the foundation structure, will be determined using the same principles as done in the Grimburgwal case. The horizontal soil forces will be partially absorbed by the lateral beams (kesp) and partially by the foundation piles. Horizontal forces resulting from the top sand layer (A) are all transferred to the lateral beams, as well as part of the loads acting on the soil retaining screen (B). The part of the soil which is absorbed by the piles is assumed to come from the reaction force of the soil between the first pile and the soil retaining screen (C). This reaction force is transferred to the piles using the soil as a medium. It happens at a depth of 2/3 L_{screen} until L_{screen}, this part represents the estimated clamped depth (inklemmingsdiepte) (Korff et al., 2020). The load configuration is presented in figure 3.25.

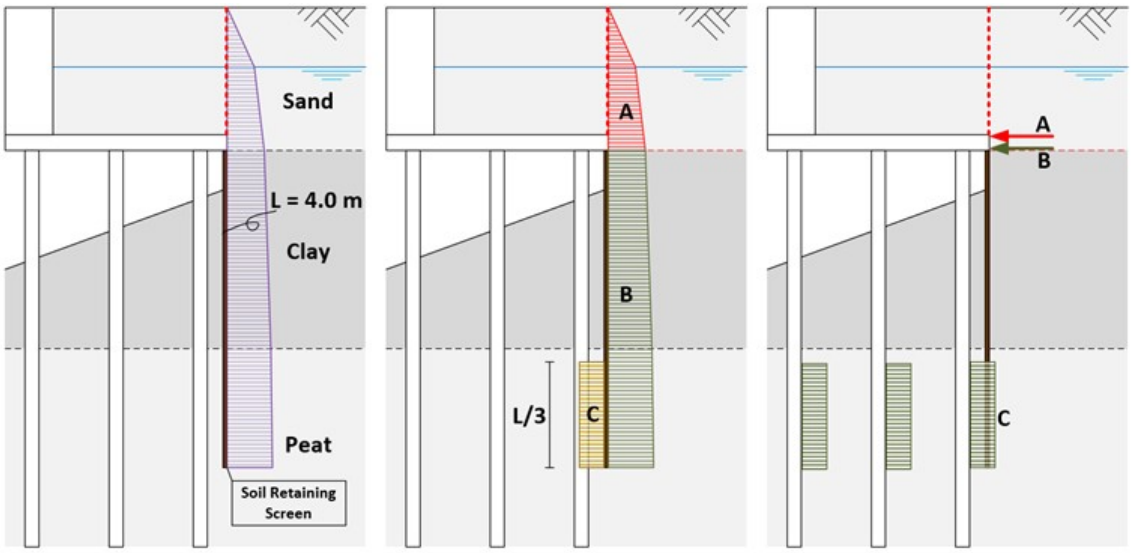

Figure 3.25: Left) Active soil — Middle) Force distribution — Right) Transfer of forces

The yet unknown force "C" and the force that is absorbed by the lateral beams are determined by calculating the balance of moments around the lateral beam. The mechanism acts as a cantilever beam, hinged at the lateral beam (see figure 3.26).

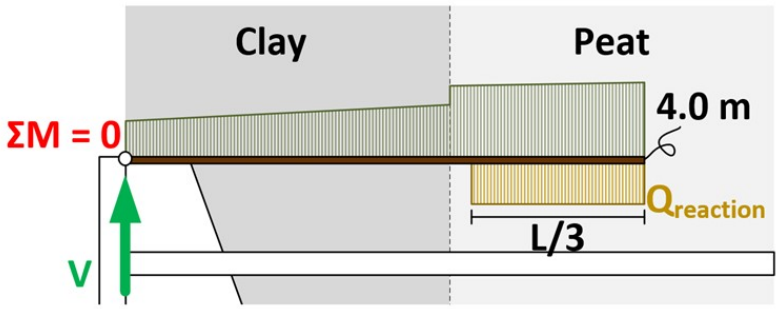

Figure 3.26: Soil retaining screen as a cantilever beam: balance of forces (rotated 90 degrees to the left).

It is assumed that force "C" (or $Q_{reaction}$) will be completely transferred through the soil towards all the piles. The nearest piles will transfer the largest part of this load, due to the fact that the other piles are positioned directly behind it (shadowing effect) (Korff et al., 2020). It is assumed that the nearest pile will absorb 50%, the piles after that will absorb 30% and 20% respectively (see figure 3.27; left). If soil is washed away below the level of the retaining wall, the piles are unable to transfer any loads. However, due to the absence of passive soil resistance, the soil retaining wall will start to arch towards the nearest piles. Because of this, $Q_{reaction}$ will be completely transferred to the nearest piles (see figure 3.27; right) (Korff et al., 2020).

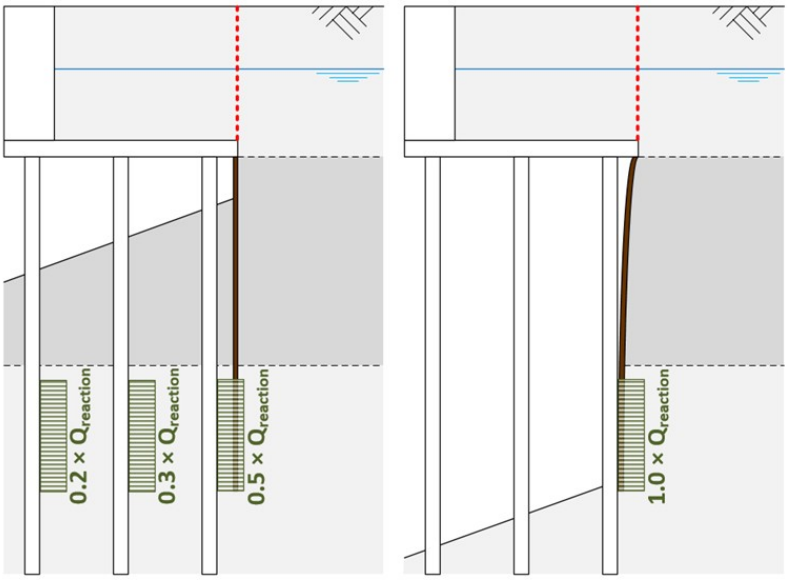

Figure 3.27: Left) Pile force distribution. Right) In case of lack of passive soil.

The relevant values needed for calculations are summarised in table 3.13. Since the depth of the soil retaining wall is assumed to be four meters (NAP - 1.0 to NAP - 5.0), it crosses the first clay layer and the peat layer only. The soil characteristics have been previously determined in table 3.8.

Property	**Value**	**Unit**	**Source**
Volumetric weight: clay (γ_{clay})	17	kN/m^3	NEN-EN9997
Volumetric weight: peat (γ_{peat})	12	kN/m^3	NEN-EN9997
Volumetric weight: water (γ_w)	10	kN/m^3	
Angle of friction: clay (ϕ_{clay})	17.5	degrees	NEN-EN9997
Angle of friction: peat (ϕ_{peat})	15.0	degrees	NEN-EN9997
Clay thickness (d_{clay})	2.5	m	Figure A.2
Peat thickness (d_{clay})	1.5	m	Until NAP - 5.0

Table 3.13: Overview of load properties and their corresponding dimensions.

4

Model Verification

One of the aims of this thesis is to approach the behaviour of a historical Amsterdam quay wall as realistically as possible. This can be achieved by incorporating as many behavioural aspects as possible, as has been done in chapter 3. These aspects are translated into the finite element model in DIANA, using Python code to build a parametric model. This section aims to verify whether the output of the model corresponds with the baseline theory which has been elaborated in chapter 3. The following behavioural aspects within the model will be verified:

1. The behaviour of masonry in general. This relates to cracking patterns, strength parameters and softening behaviour.
2. The behaviour of the masonry/wood interface, which is governed by friction and sliding.
3. The behaviour of the quay wall structure after introducing external loads. The behaviour as described in section 3.4.2 will be verified (external and internal stability).

4.1. Numerical input and analysis

Before any behavioural aspect of the finite element model can be analysed, it is necessary to establish what input is given to it. This section summarises the used numerical analysis properties and the baseline properties of the model itself.

4.1.1. Analysis settings

Once the model dimensions and properties have been set in DIANA FEA, it will run through built-in non-linear numerical analyses. The model will respond according to the selected loads. The analysis will be set in such a way that the model always responds to permanent loads first, and then to any variable loads. The analysis settings of both load cases are the same and are summarised in table 4.1.

Analysis property	Setting
Max. number of iterations	100
Method	Secant (Quasi-Newton)
Line search	Enabled
Convergence norms	Energy and displacement
Convergence tolerance	0.01
In case of no convergence	Terminate

Table 4.1: Analysis settings in DIANA FEA.

The mesh size is set to be 100 mm in the z- and y-direction (width and height). In x-direction, it will be 250 mm. This is done to reduce computational time, and because the number of elements allowed in DIANA FEA is restricted.

4.1.2. Baseline properties

This section discusses the baseline properties of the structure as it will be incorporated into the finite element model. In chapter 3, it has already been discussed which choices have been made when it comes to modelling the quay wall structure. This section aims to summarise all modelling prerequisites, this refers to the dimensions, material models and material properties of all elements.

4.1.2.1 Dimensions

The dimensions of the parametric model are summarised in table 4.2, based on table 3.1. It has already been determined in section 3.2.4 that each foundation pile is 11 meters in length. The width of the support beam was determined to be 0.2 m. However, the support beams will not be included in the model. The width of the planks is assumed to be 5 cm in thickness. The quay wall length is arbitrary and might be different depending on which case is simulated. The length of the quay wall is essentially built up by 1-meter segments with one pile row in the middle. Meaning that a 20-meter wall will have 20 rows of piles (60 piles).

Material property	Value (new)	Unit
Wall height	1.60	m
Wall thickness	0.6	m
Wall length	arbitrary	-
Plank width	2.80	m
Plank thickness	0.05	m
Plank length	arbitrary	-
Pile length	11.0	m
Pile c.t.c. distance	1.0	m
No. of rows	3	-
Virtual boundary height	1.60	m
Virtual boundary total length	21	m
Virtual boundary segment length	0.20	-

Table 4.2: Model dimensions

The appearance of the finite element model is shown in figure 4.1. In this figure, the red/brown

masonry wall, the brown planks and the large number of foundation piles are easily distinguishable. The yellow plate at the back represents the "virtual boundary" which separates the soil columns into two parts. The purpose is to be able to simulate the before-mentioned table effect. This virtual boundary is divided into segments with a thickness of the mesh size each (0.25 m). This choice is made to force the model to mesh properly.

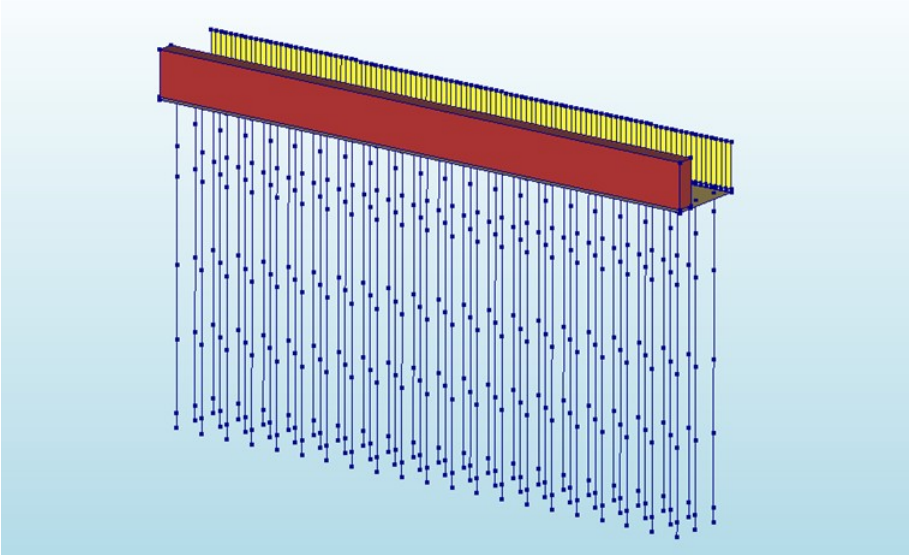

Figure 4.1: Quay wall structure represented in DIANA FEA.

In the baseline model, the piles have no free height, as is assumed to be the case at the time when the historical quay wall was newly built.

4.1.2.2 Material Models

Chapter 3 describes the process of choosing the material models in detail. This subsection aims to summarise these modelling types and to which elements these types are applied. A concise summary is made by subdividing the model into three parts: Shapes, interface connections and boundary conditions.

As is visible in figure 4.1, four shapes can be distinguished: The masonry wall, planks, piles and the virtual soil boundary. The behaviour of masonry is approached using a smeared crack model. The attention towards the planks will not be thorough in this thesis, therefore it will be approached using a simple linear elastic model. The piles will be approached using a non-linear elastic model, with a force-elongation diagram. Since the virtual boundary is factually not present as a real screen, it will also be considered to be linear elastic. Table 4.3 summarises the shapes and their properties according to the terminology of the DIANA FEA program.

Geometry	Element type	Element type code	Modelling
Masonry	Structural solid	CHX60	Total Strain Cracking
Planks	Curved shell	CQ40S	Linear Elasticity
Piles	Class-III beam	CL18B	Uniaxial Non-Linear Elasticity
Virtual boundary	Curved shell	CQ40S	Linear Elasticity

Table 4.3: Baseline modelling properties of all shapes.

Since the model is composed of the wall, planks and piles, two relatively clear interface connection types can be distinguished. One is the interface layer between the masonry and the planks underneath it, the other is the connection between the planks and the foundation piles underneath. Less obvious interface conditions are the connections between the planks and the virtual boundary surface and the connections between the virtual boundary segments. The masonry-planks interface is modelled using a friction/sliding model. The connection between the pile and the planks is assumed to be hinged, meaning that they are connected in translation but free in rotational movements. The connection between the planks and the virtual boundary is completely rigid, and the connection between the virtual boundary segments is completely free. The reasoning behind these choices lies behind the idea that the virtual boundary is able to bend freely in the longitudinal direction, while it can absorb forces in the normal (perpendicular) direction. Free bending in the longitudinal direction results in no restrictions in the bending capabilities of the planks. Table 4.4 summarises the connections and their properties according to the terminology of the DIANA FEA program.

Connections	Element type	Element type code	Modelling
Masonry-Planks Interface	Interface	CQ48I	Coulomb Friction
Pile-Planks Connection	Hinge	-	Free rotation/Fixed translation
Virtual Boundary-Planks Interface	Rigid	-	Fixed rotation/Fixed translation
Virtual Boundary Segments Interface	Free	-	Free rotation/Free translation

Table 4.4: Baseline modelling properties of all interface connections.

Lastly, all boundary conditions will be summarised. The boundary conditions comprise all connections between the shapes and their environment. These comprise the boundary at both ends of the masonry wall in the longitudinal direction, as well as the lateral and longitudinal connection between the piles and the surrounding soil. When it comes to the masonry and planks, it is obvious that movements in longitudinal and rotational direction should be restricted, since it is neighboured by another hydraulic structure. The degree of mobility in lateral or vertical direction depends on the structure to which the quay wall is connected. In case a quay wall is neighboured by another quay wall on each side with a dilation joint in between, movement in these directions will be considered to be free. A completely fixed connection may be considered in case a quay wall is connected with a different hydraulic structure (e.g. a bridge). Connections between piles and soil are modelled using non-linear spring systems.

Table 4.5 summarises the boundaries and their properties according to the terminology of the DIANA FEA program.

Connections	**Element type**	**Element type code**	**Modelling**
Pile-Soil Interface	Boundary interface	CL18IS	Non-Linear Elasticity
Pile tip-Soil Interface	Translation spring	SP1TR	Force-elongation diagram
Masonry boundary (longitudinal)	Fixed or Free	-	Fixed rotation/Restricted translation

Table 4.5: Baseline modelling properties

4.2. Masonry

This section is dedicated to determining the actual behaviour of masonry and comparing it to the behaviour of masonry in the finite element model built in DIANA. The purpose of this comparison is to determine whether the behaviour of the masonry wall shown by the model shows a realistic pattern. The focus will primarily lie with cracking behaviour, however, attention will also be given to the strength parameters of masonry.

4.2.1. Cracking patterns

Unfortunately, not much is known about the behaviour of thick masonry quay walls. The main reason is the lack of research available in this area. However, research has been done dedicated to predicting cracking patterns in masonry buildings. These usually regard relatively thin masonry walls on regular buildings, such as housing or larger structures. Expected cracking patterns on different wall configurations will be further elaborated in this section. One thing to note is that these elements more closely resemble a two-dimensional plane, while a quay wall more closely resembles a beam. The main purpose of analysing several wall configurations is to determine whether the Total Strain Cracking Model shows some validity when it comes to showing realistic cracking patterns in masonry.

Several masonry wall configurations will be replicated in DIANA by creating a 3-dimensional element using the Total Strain Cracking Model. Conclusions will be drawn based on the following steps:

1. Determine the expected cracking patterns of the given configuration.
2. Recreate the given configuration in DIANA FEA using the Total Strain Cracking Model.
3. Compare the cracking patterns produced in DIANA FEA to the expected cracking patterns and draw conclusions.

The focus will lie on configurations with out-of-plane loading conditions. The following configurations will be considered based on a study done by C.R. Willis (Willis, 2004):

- One-way supported wall; supported on two edges.
- Two-way supported wall; supported on three edges.
- Two-way supported wall; supported on four edges.
- Two-way supported wall with a window in the centre; supported on three edges.

4.2.1.1 One-way supported wall; two edges

A regular wall supported by the two opposite vertical edges, and its failure mode resulting from out-of-plane loading, are shown in figure 4.2. A rectangular wall produces a vertical crack through the middle of the wall (Willis, 2004).

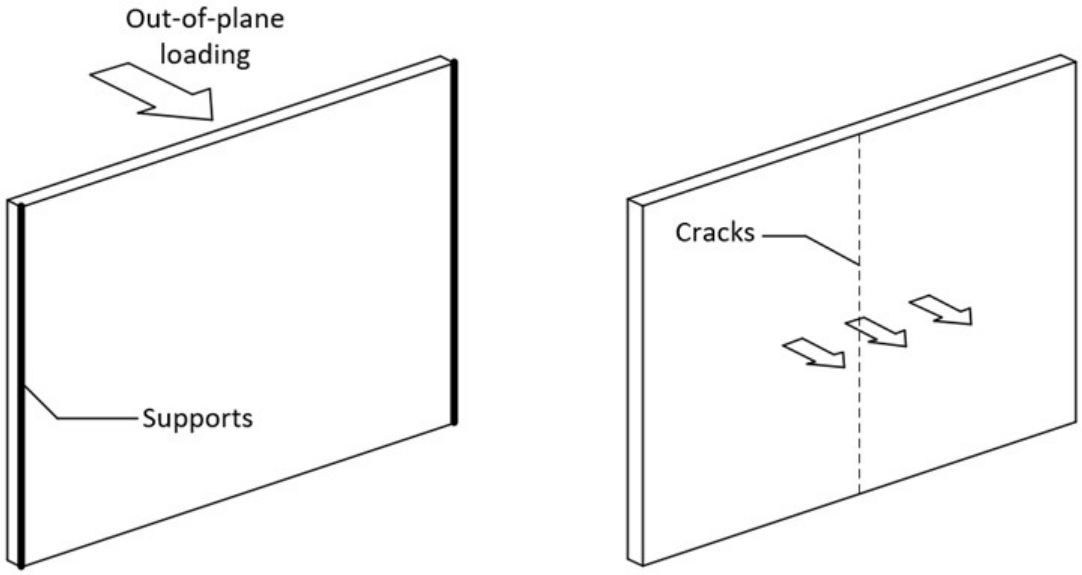

Figure 4.2: left) two edge supported wall; right) expected cracking patterns at failure (Willis, 2004).

This configuration will be modelled in DIANA, with the parameters summarised in table 4.6.

Parameter	**Value**	**Unit**
Height	3.0	m
Length	4.0	m
Thickness	0.1	m
Young's modulus	5000	N/mm^2
Poisson's ratio	0.25	-
Tensile strength	0.35	N/mm^2
Tensile fracture energy	0.035	N/mm

Table 4.6: Relevant model parameters.

According to the finite element model, applying an incrementally increasing homogeneous out-of-plane load yields the crack propagation as shown in figures 4.3 and 4.4.

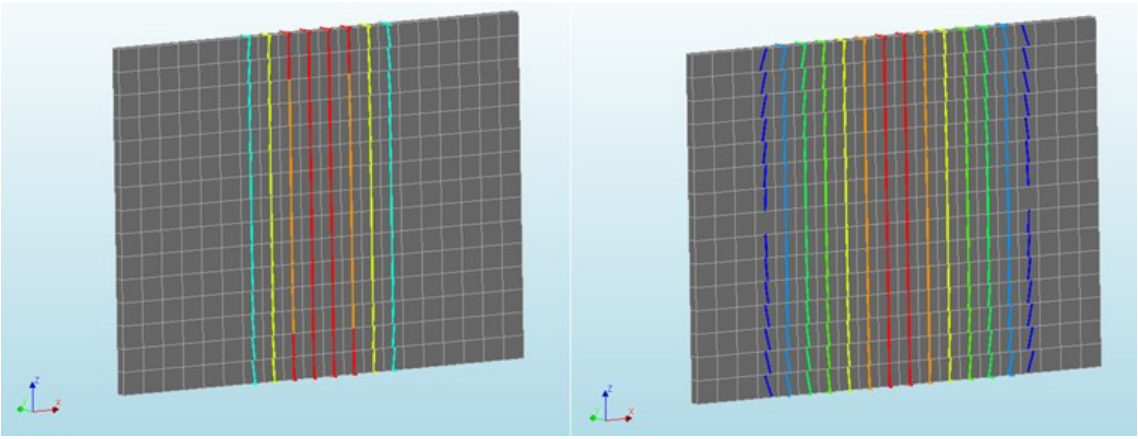

Figure 4.3: left) Initial cracks; right) crack propagation.

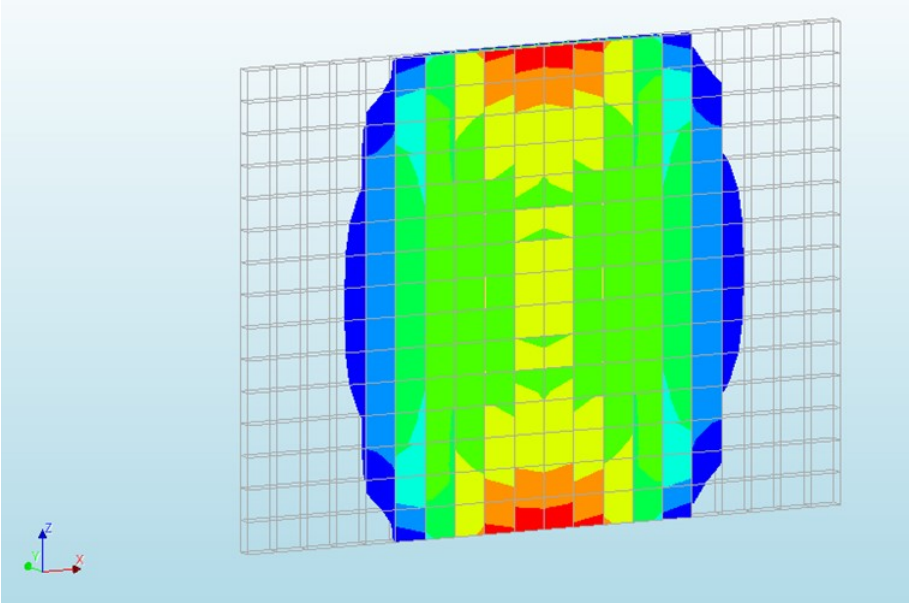

Figure 4.4: Cracking patterns after no numerical convergence.

The cracking patterns according to the Total Strain Cracking Model follow a similar path compared to the expected crack patterns.

4.2.1.2 Two-way supported wall; three edges

A regular wall supported by three edges (with a free upper edge), and its failure mode resulting from out-of-plane loading, are shown in figure 4.5. A rectangular wall produces a vertical crack in the middle with diagonal cracks reaching each lower corner (Willis, 2004).

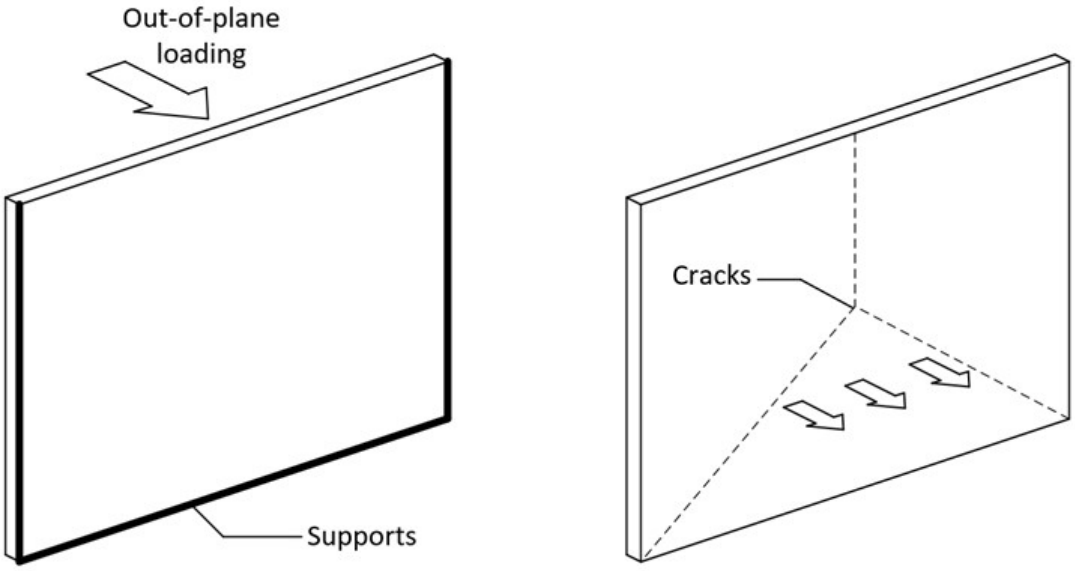

Figure 4.5: left) three edge supported wall; right) expected cracking patterns at failure (Willis, 2004).

This configuration will be modelled in DIANA, with the same parameters as the previous configuration, summarised in table 4.6. According to the finite element model, applying an incrementally increasing homogeneous out-of-plane load yields the crack propagation as shown in figures 4.6 and 4.7.

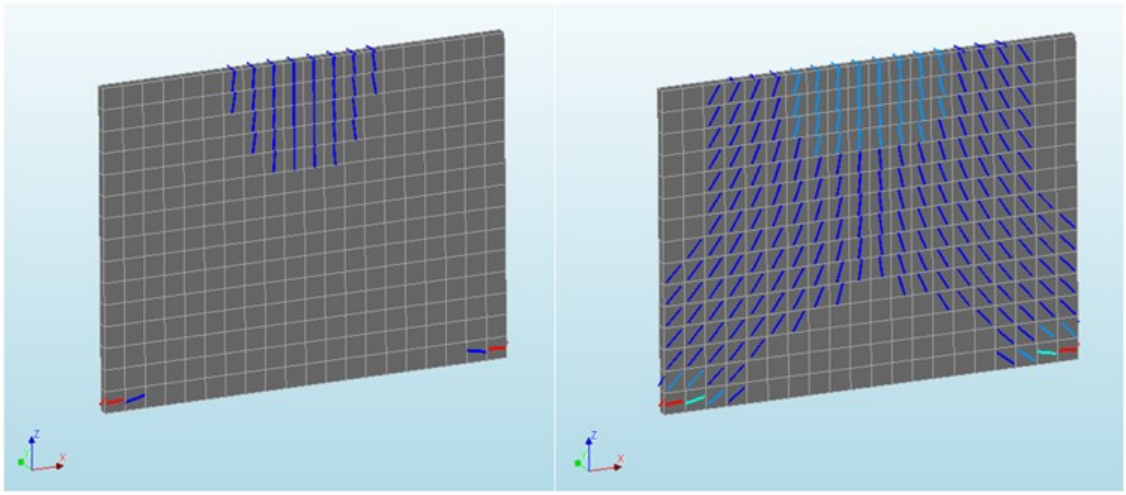

Figure 4.6: left) Initial cracks; right) crack propagation.

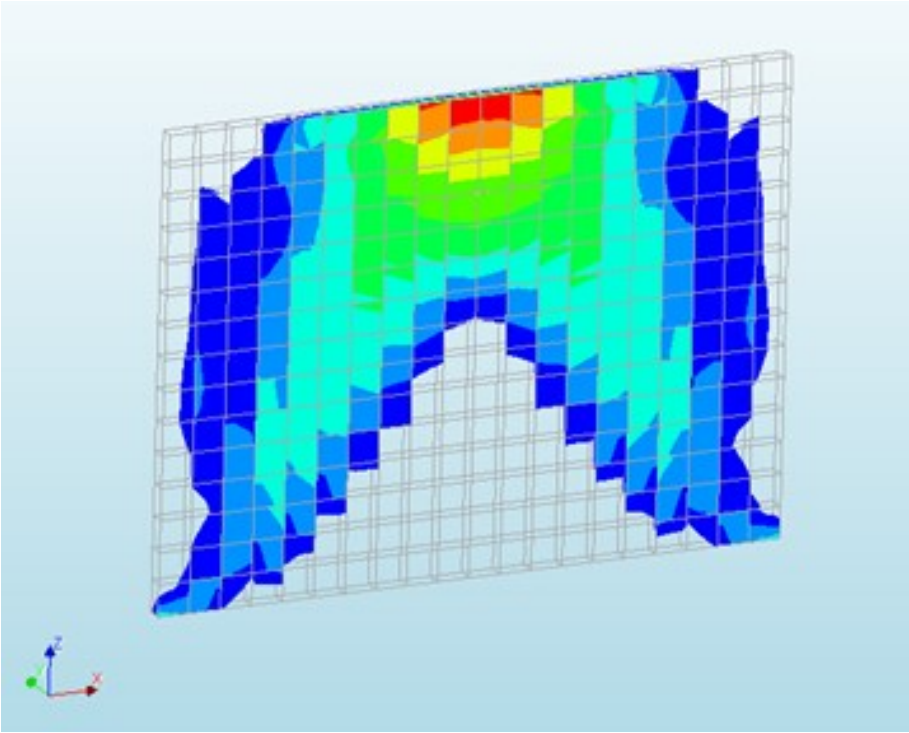

Figure 4.7: Cracking patterns after no numerical convergence.

The cracking patterns according to the Total Strain Cracking Model follow a similar path compared to the expected crack patterns.

4.2.1.3 Two-way supported wall; four edges

A regular wall supported by four edges, and its failure mode resulting from out-of-plane loading, are shown in figure 4.8. A rectangular wall, with a wider base compared to height, produces a horizontal crack in the middle with diagonal cracks reaching each corner (Willis, 2004).

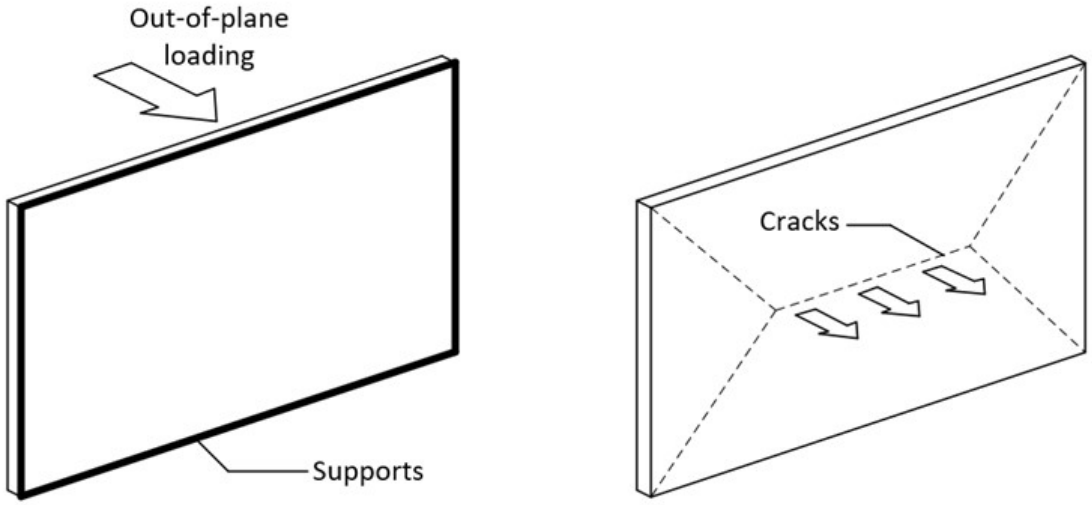

Figure 4.8: left) four edge supported wall; right) expected cracking patterns at failure (Willis, 2004).

This configuration will be modelled in DIANA, with the parameters summarised in table 4.7.

Parameter	**Value**	**Unit**
Height	2.0	m
Length	5.0	m
Thickness	0.1	m
Young's modulus	5000	N/mm^2
Poisson's ratio	0.25	-
Tensile strength	0.35	N/mm^2
Tensile fracture energy	0.035	N/mm

Table 4.7: Relevant model parameters.

According to the finite element model, applying an incrementally increasing homogeneous out-of-plane load yields the crack propagation as shown in figures 4.9 and 4.10.

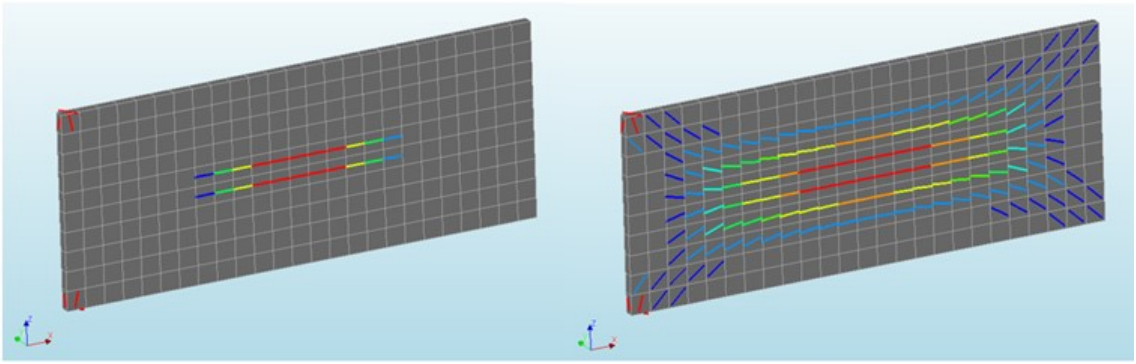

Figure 4.9: left) Initial cracks; right) crack propagation.

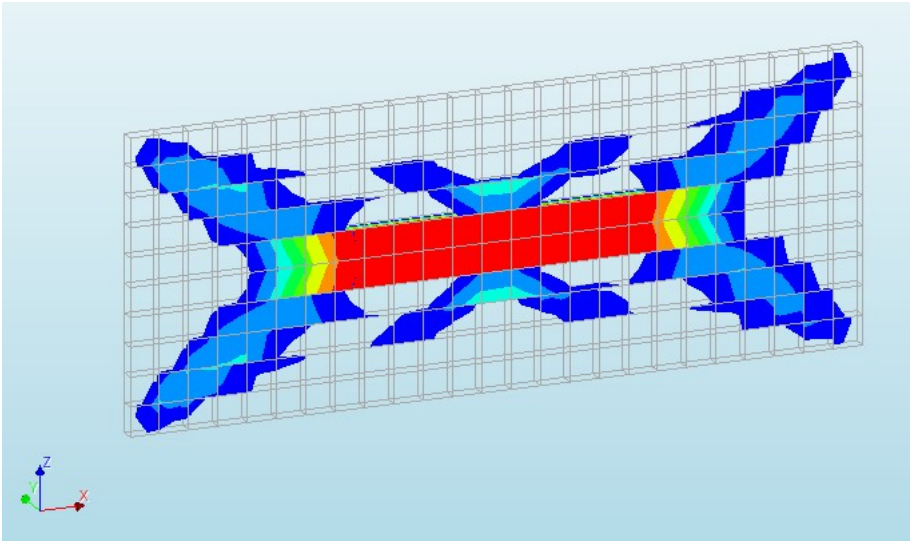

Figure 4.10: Cracking patterns after no numerical convergence.

The cracking patterns according to the Total Strain Cracking Model follow a similar path

compared to the expected crack patterns.

4.2.1.4 Two-way supported wall with a window; three edges.

A windowed wall supported by three edges (with a free upper edge), and its failure mode resulting from out-of-plane loading, are shown in figure 4.11. A rectangular wall produces a vertical crack in the middle above the window, with diagonal cracks reaching each lower corner below the window (Willis, 2004). Basically, the cracking patterns are similar to the two-way supported wall which is supported on three edges, except with a hole in the middle representing a window.

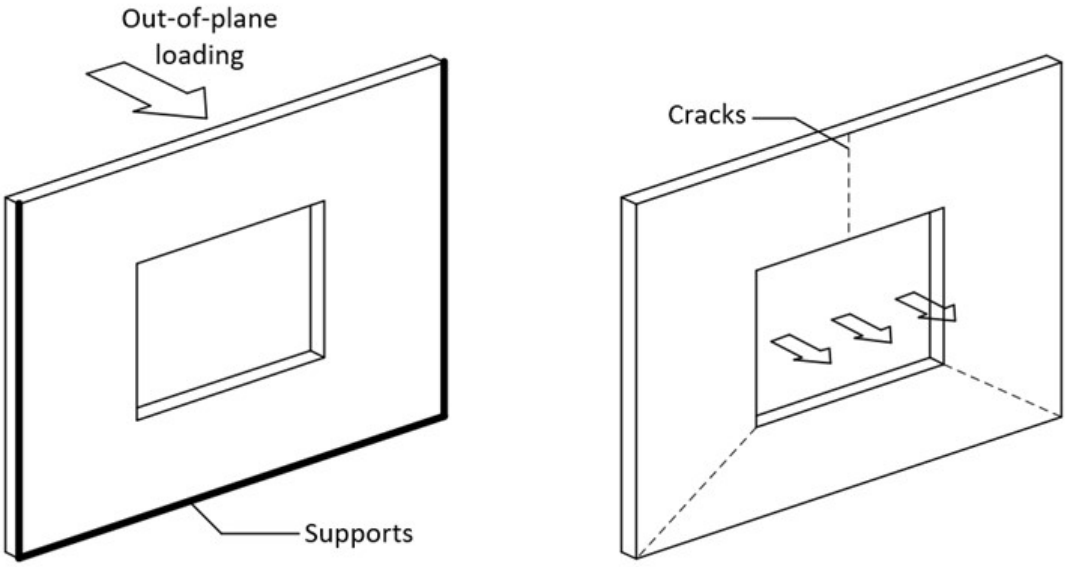

Figure 4.11: left) four edge supported wall; right) expected cracking patterns at failure (Willis, 2004).

This configuration will be modelled in DIANA, with the parameters summarised in table 4.8.

Parameter	**Value**	**Unit**
Height	5.0	m
Length	5.0	m
Window	2.0 x 2.0	m^2
Thickness	0.1	m
Young's modulus	5000	N/mm^2
Poisson's ratio	0.25	-
Tensile strength	0.35	N/mm^2
Tensile fracture energy	0.035	N/mm

Table 4.8: Relevant model parameters.

According to the finite element model, applying an incrementally increasing homogeneous out-of-plane load yields the crack propagation as shown in figures 4.12 and 4.13.

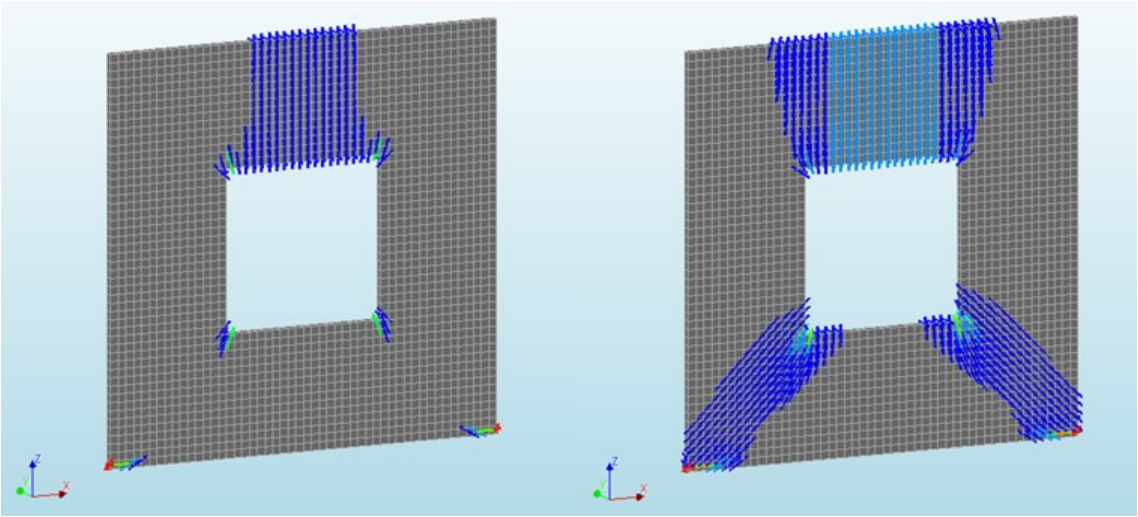

Figure 4.12: left) Initial cracks; right) crack propagation.

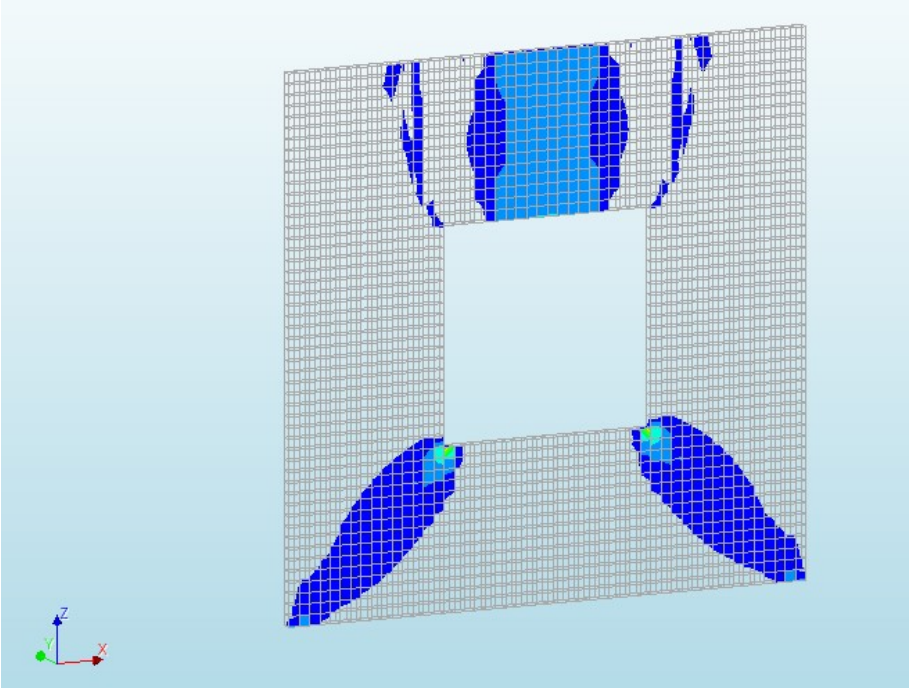

Figure 4.13: Cracking patterns after no numerical convergence.

The cracking patterns according to the Total Strain Cracking Model follow a similar path compared to the expected crack patterns.

4.2.1.5 Conclusions

Based on the performed comparisons, it can be concluded that the cracking patterns in masonry shown by the Total Strain Cracking Model (TSCM) follow a realistic path. Based on this conclusion, the following assumption is made: if a masonry wall, with dimensions resembling a historical quay wall, would be modelled with TSCM in DIANA FEA, the results will show realistic cracking patterns.

4.2.2. Strength and cracking: masonry beam

In reality, a historical quay wall resembles more of a beam rather than a 2D plane, because of its dimensions (small cross-section compared to length). For this reason, it is useful to find out how a beam is expected to behave when its strength capacity has been reached.

As mentioned before, little research is available regarding the expected cracking behaviour of masonry beams. The expected cracking patterns of a concrete beam will be used as an alternative form of reference. The behaviour of concrete and masonry can be reasonably compared for the following reasons:

- Both concrete and masonry are quasi-brittle materials. Deformations are therefore governed by the development of micro-cracks. Concrete is also subjected to softening after its peak strength has been reached, just like masonry. All quasi-brittle materials have a similar stress-strain curve (see section 3.3.1.2).
- The Total Strain Cracking Model is applicable to both masonry and concrete (van Noort, 2012). Because it is a macro-model, masonry will be treated as a homogeneous material. Since concrete is inherently homogeneous, the model will treat both materials similarly. Therefore, cracking patterns in concrete are expected to be similar to the expected cracking patterns in masonry.
- Lots of research available regarding cracking in concrete beams.

Results from a failure analysis of a plain (unreinforced) concrete beam, performed by M. Słowik (2018), will be used as a reference case. This experimental setup will be replicated in DIANA by creating a 3-dimensional element using the Total Strain Cracking Model. Conclusions will be drawn based on the following steps:

1. Summarise the failure analysis results from the experimental set-up performed by M. Słowik.
2. Recreate the given configuration in DIANA FEA using the Total Strain Cracking Model.
3. Compare the results produced in DIANA FEA to the failure analysis results from the real experiment and draw conclusions.

4.2.2.1 Reference case results

In the reference case, a four-point bending test has been performed on a plain concrete beam. The set-up as described in this experiment is shown in figure 4.14. The relevant material properties are summarised in table 4.9. Poisson's ratio and mass density are not given, instead, the general average value of concrete is used.

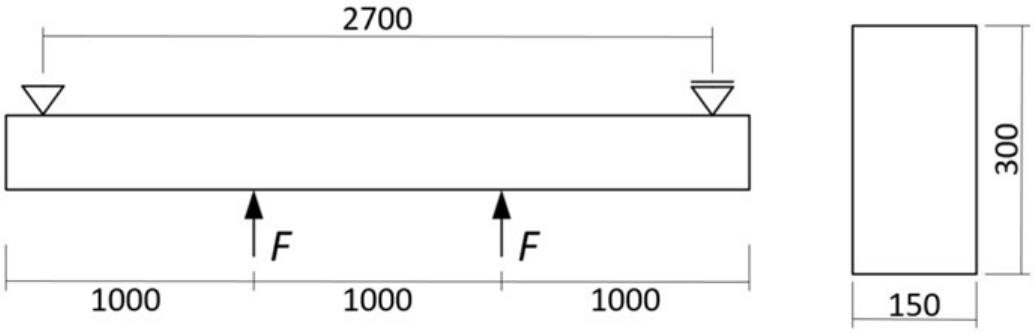

Figure 4.14: Experimental set-up of the reference case (**concrete**).

Parameter	**Value**	**Unit**
Young's modulus	22118	N/mm^2
Poisson's ratio	0.15	-
Mass density	2400	kg/m^3
Tensile strength	1.48	N/mm^2
Tensile fracture energy	0.083	N/mm

Table 4.9: Material properties of the concrete beam described in the reference case (**concrete**).

In the reference case, three similar samples have been tested, in which a sudden brittle failure has been observed following the appearance of the first flexural crack. The crack develops vertically, commencing from the tensile region (upper side). The location of the crack appears to be off-centre, near the location of one of the point loads in all three cases. The cracking pattern in each sample is presented in figure 4.15. Furthermore, the experiment showed that the average cracking load at the point loads was 5.02 kN.

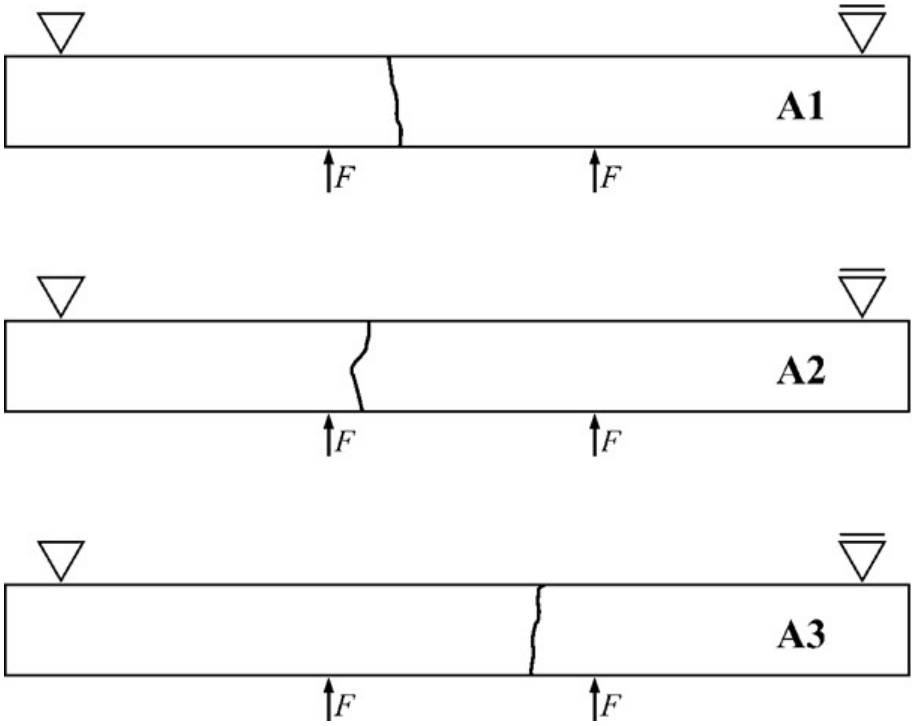

Figure 4.15: Crack locations in each sample, retrieved from **concrete**.

4.2.2.2 Finite element model results

The experiment is replicated in DIANA FEA using the exact dimensions and the parameters according to table 4.9. The point loads are incrementally increased with steps of 190 N until failure. Figure 4.16 shows the location of the initial crack according to the model. The locations of the cracks are consistent with the experiment in the reference case (see figure 4.15), they are located at 1100 mm from each end. Note that the model shows the large flexural crack at both sides, while it only happens at one side in the real samples. One hypothetical explanation is the fact that the experiment reports brittle failure right after the onset of cracking, resulting in a rapid redistribution of forces within the beam. This takes place right after the formation of the first crack. For this reason, the crack at the other side had no opportunity to start developing. On the other hand, the finite element model is perfectly symmetrical. In that case, equal behaviour of both halves is to be expected. However, real-life is never perfectly symmetrical, leading to this discrepancy. The simulation in the model has proven that this specific crack may develop at either side, but never at both sides.

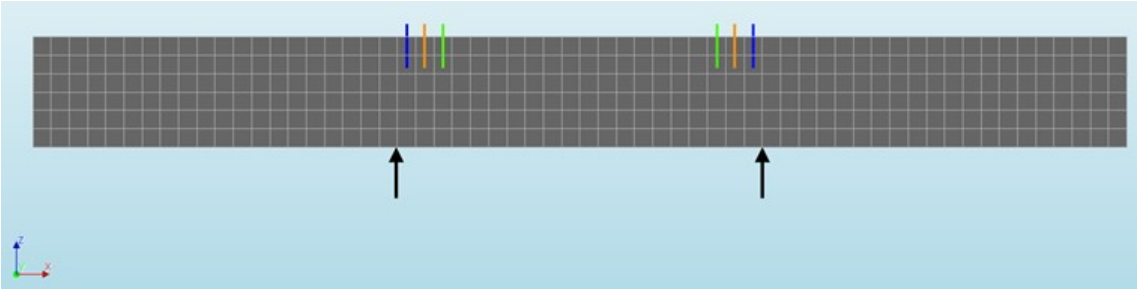

Figure 4.16: The onset of cracking according to DIANA FEA, with the loads indicated by the black arrows.

According to the experiment, the beam fails as soon as the crack appears. In the model, the first cracks appear at a point load of 5.06 kN, compared to 5.02 kN in the reference case. This proves that the strength capacity in the model is accurate compared to reality. However, the model does not show brittle failure as described by the experiment. The model allows for crack development until convergence is lost at a point load of 7.3 kN. The reason behind this is the fact that the model assumes that softening takes place. It was a valid assumption, given that the crack energy was provided by the researcher behind the reference case (83 N/m). Given that the test samples show brittle failure, it can be concluded that the given crack energy value is highly overestimated.

4.2.2.3 Interpreting cracks from DIANA FEA

DIANA FEA consistently shows cracking patterns at their expected locations and their expected orientations. In the previously discussed failure modes, one clearly visible crack appears at each expected location. However, DIANA FEA presents the cracking patterns at each expected location as a collection of cracks that are spread over a larger area. The reason behind this spreading is that the tensile strength of the material has been reached at every node within this area, which results in the development of a macro-crack in each element, according to the material model (however small they might be). But, the crack strains (and widths) are always the highest at the centre of these areas. This results in the earliest and largest crack occurring at the centre, or at least at the location with the highest strains. Therefore, when a distinguishable crack field can be identified within the model, it will be interpreted as one large crack at the location with the highest crack strains. The interpretation of these crack fields is visualised in figure 4.17.

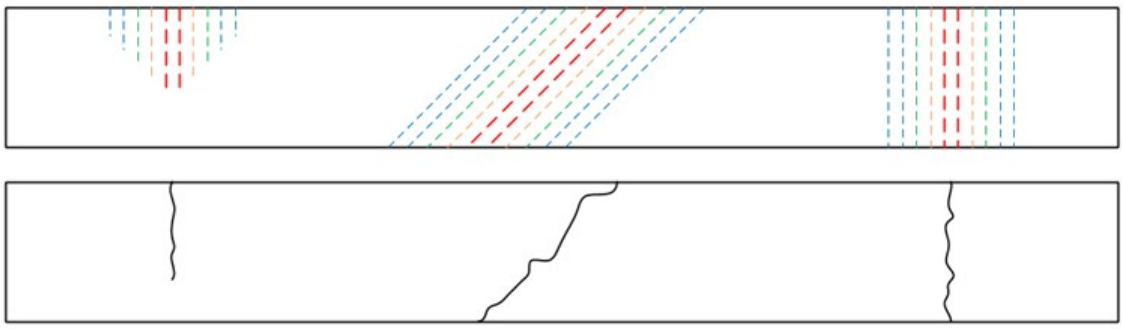

Figure 4.17: Up) Cracking patterns presented by DIANA FEA; Down) Crack interpretation based on expected cracking patterns.

Sometimes, multiple local maximum values exist in the same crack field. In that case, each local maximum will be represented by a single crack. The width of each crack is determined as follows:

1. Calculate the crack width sum of the entire crack field. This is done by multiplying the total crack strain with the mesh size.
2. Determine the location and the nodal crack width of each maximum. Each maximum will be represented by a single crack.
3. Allocate a part of the total crack width to every single crack depending on the size of each maximum.

4.2.2.4 Conclusions

The first conclusion is that the Total Strain Cracking Model is quite reliable when it comes to modelling the strength capacity and cracking patterns of a material. One caveat is that care must be taken when it comes to dealing with very brittle materials, which leads to the next conclusion.

The second conclusion is that symmetrical models produce symmetrical crack development. In the reference case, cracks develop asymmetrically. Because of the extreme brittleness of the used samples, the material will fail quickly after one crack starts developing. For this reason, care must be taken when using symmetrical finite element models with brittle materials, especially when drawing conclusions.

The last conclusion is that the crack energy provided by the experiment is likely highly overestimated given the lack of plastic (softening) behaviour.

4.2.3. Numerical convergence

When the analysis in DIANA FEA reaches numerical convergence, it can approach every model solution accurately. It has been found that the cracking patterns from each failure mode most accurately represents the finite element results when the analysis can no longer converge (which then terminates the analysis). When the model no longer converges, it is usually paired with large and abrupt increases in displacements and crack widths. Based on these findings, it will be assumed that when the numerical analysis terminates due to no convergence, the structure is failing.

4.3. Masonry/wood interface

This section is dedicated to verifying the interaction between masonry and wood, which is governed by Coulomb friction. First of all, the expected behaviour of this interface will be discussed. In the end, the goal is to replicate this behaviour in DIANA FEA.

4.3.1. Expected behaviour

Coulomb Friction as described in section 3.3.6 is used to define the behaviour of the masonry/wood interface. When applied to the quay wall, it assumes that the masonry wall will not start sliding from the planks as long as the following criterion is met:

$$F_f \leq \mu F_N \tag{4.1}$$

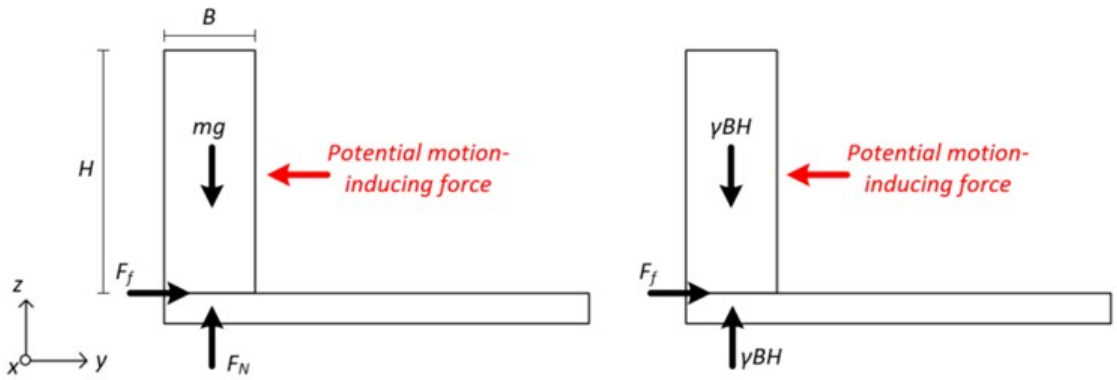

Figure 4.18: Visualisation of friction on a historical quay wall.

The forces leading to friction between masonry and wood on a historical quay wall is visually presented in figure 4.18. In order to verify whether the Coulomb Friction Model produces realistic results, a relatively simple example will be tested, where a plate of bricks is put on top of wooden planks (see figure ... below). The following dimensions are assumed for the plate: $L = B = 0.5$ m and $H = 0.1$ m. The properties of masonry are assumed.

Figure 4.19: Example case to verify the Coulomb Friction Model and its representation in DIANA FEA.

As determined in section 3.3.6, $\mu = 0.85$ (which leads to $\phi = 0.7$ rad). The normal force F_N is the upward reaction force as a result of the weight of the masonry plate [N]. The density of masonry ρ is approximately 1800 kg/m^3. The expected force required to move the wall (or maximum friction force) can now be calculated as follows:

$$F_f = \mu \rho g L B H = 375.2 \text{ N} \tag{4.2}$$

In other words, if the force in the interface reaches this value, the plate will start to slide off. Structures that experience large horizontal loads and which are relatively tall compared to their base may also be prone to tilting and overturning. However, it is assumed that in the case of historical quay walls, the masonry wall does not lose contact with the plank layer.

4.3.2. Replication in DIANA FEA

The next step is to replicate the expected behaviour of the masonry/wood interface into DIANA FEA. The built-in Coulomb Friction Model works as a non-linear spring system acting over the entire interface (see figure 4.20). It is required to enter linear stiffness parameters as well as parameters related to Coulomb friction.

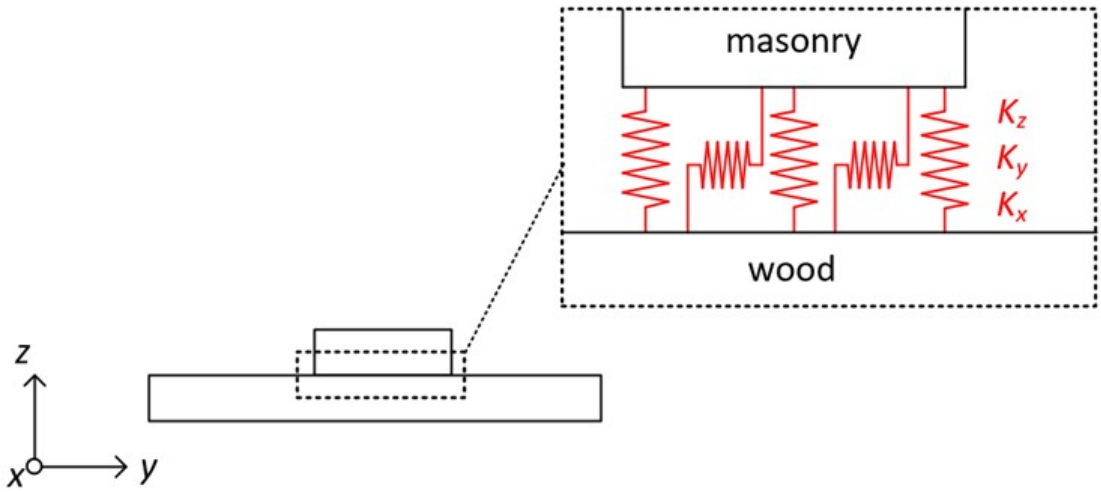

Figure 4.20: Brick/Wood interface condition.

The following relevant input parameters are required:

- Normal stiffness modulus K_z [N/m^3]
- Shear stiffness modulus (longitudinal) K_x [N/m^3]
- Shear stiffness modulus (cross-sectional) K_y [N/m^3]
- Cohesion [N/m^2]
- Friction angle ϕ [rad]
- Interface opening model

It is assumed that the bricks will not slide off until the maximum friction force has been reached. Also, it is assumed that the bricks will not lose contact with the wood. Based on these assumptions, it has been determined that the linear stiffness should be extremely high, and there will be no interface opening model used. A stiffness value in the order of 10^9 N/m^3 has been chosen to fit these requirements.

In DIANA FEA, the cohesion value adds extra strength to the interface. In other words, adding cohesion leads to the ability of the interface to withstand larger loads before sliding is induced. In the example case, it is set to zero. The friction angle is already known (0.7 rad).

The set-up of the simulation is presented in figure 4.19. The material properties are set to be linear elastic, in order to isolate the friction mechanism. The object will be incrementally (and horizontally) loaded with steps of 0.2 kPa. Running the simulation results in no convergence after the 38th step (or after a horizontal load of 7.6 kPa has been exerted). This load is pushing against a surface of $0.5 \times 0.1 = 0.05$ m^2. Therefore, the force becomes 380 N, which is approximately the same as the expected friction force. The Coulomb Friction Model has thus simulated the sliding phenomenon accurately, and can therefore be applied to the quay wall model. It is assumed that when the finite element model stops converging in the interface, the quay wall has started sliding off.

4.4. External loads

This section verified whether the quay wall responds to applied loads as expected. The two mechanisms described in section 3.4 will be discussed: internal and external stability.

4.4.1. Internal stability: table effect

A full description of the table effect has been provided in section 3.4.2. The idea is that the soil directly on top of the planks (column I), combined with the surcharge on top of this area pushes the masonry wall in the direction of the canal. However, the assumption has been made that these loads will not lead to the horizontal movement of the piles underneath. This mechanism is modelled by applying a 'virtual boundary' which corresponds to the boundary of this soil column. This virtual boundary is clearly visible on the right side in figure 4.21.

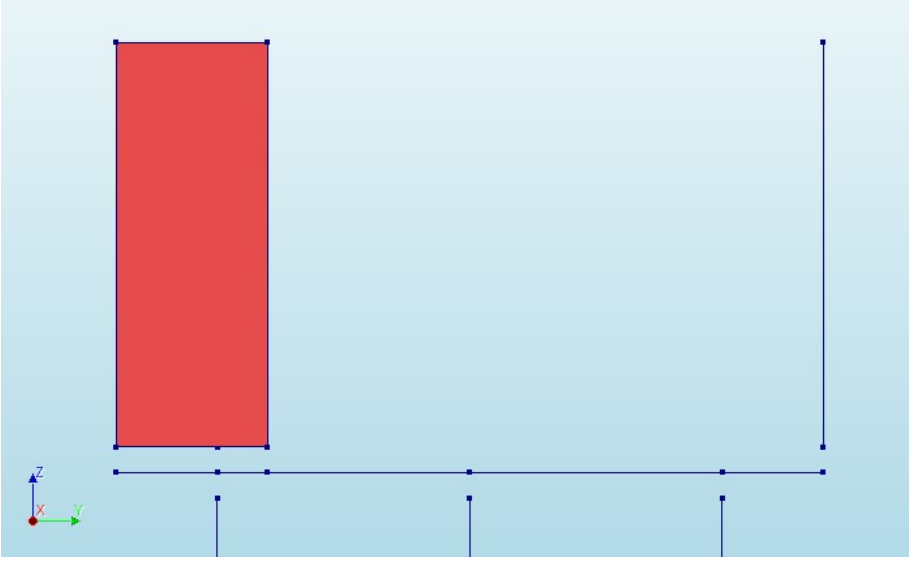

Figure 4.21: Quay wall structure represented in DIANA FEA in cross-sectional view.

The loads acting on the masonry wall are counteracted by applying identical loads in opposite directions normal to the virtual boundary. This should result in the ability of the masonry wall to slide while keeping the piles horizontally in their place. The following analyses have been performed:

1. Applying loads with incrementally increasing surcharge on the masonry wall with the virtual boundary present.
2. Applying loads with incrementally increasing surcharge on the masonry wall without the virtual boundary to counteract these loads.

The aim is to illustrate the effect of the virtual boundary. To test this mechanism in full isolation, all other loads will be disregarded. Meaning that there are no loads present resulting from soil outside of the specified column. First, the permanent loads resulting from the specific soil column between the masonry wall and the virtual boundary will be applied. Secondly, a surcharge will be applied, acting on the same soil column. Lastly, the surcharge will be incrementally increased by 6 kPa per load step until the model stops running, essentially meaning failure. The results are shown in figure 4.22.

The straight horizontal blue line shows the horizontal displacement of the pile head after incrementally increasing lateral loads, with the presence of the virtual boundary. The exponentially increasing red line represents the same, except without the presence of the virtual boundary. These are relative displacements, relative to the position of the pile head connection.

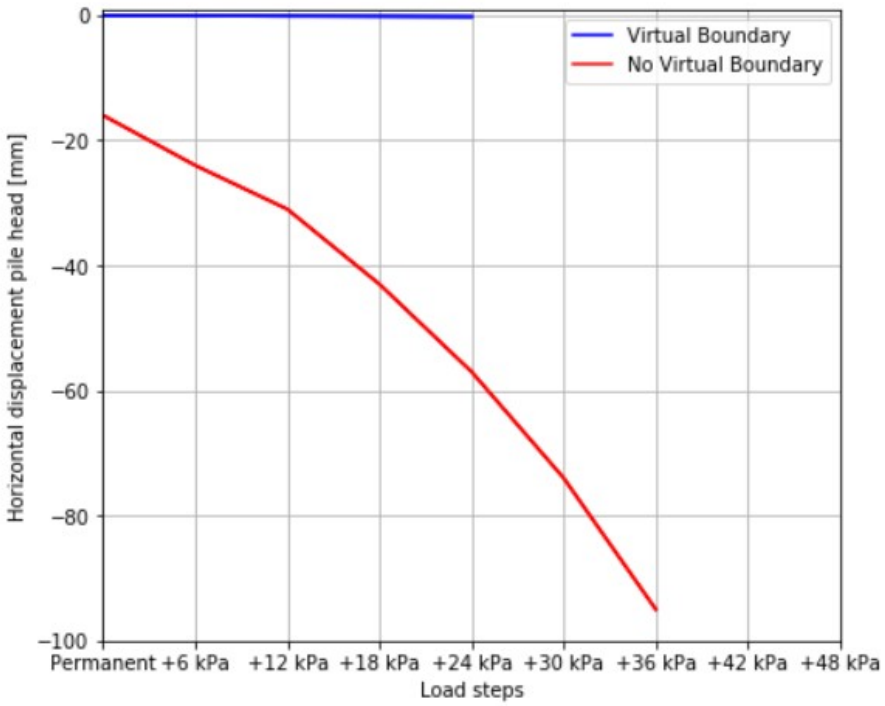

Figure 4.22: Horizontal displacement of the pile heads after applying loads. Blue: Virtual boundary; Red: No virtual boundary. Note that these are relative displacements and not absolute.

According to these results, the conclusion can be drawn that the table effect mechanism, resulting in no lateral movement of the pile heads, can be simulated using the virtual boundary wall.

In these same simulations, it is also possible to look at the behaviour of the masonry wall in relation to the planks. The lateral displacement of the masonry wall at the base is compared to the lateral displacement of the planks in both simulations. This is to show to what degree the masonry slides off of the planks. The results are shown in figure 4.23. Again, these are relative displacements, relative to the position of the pile head connection.

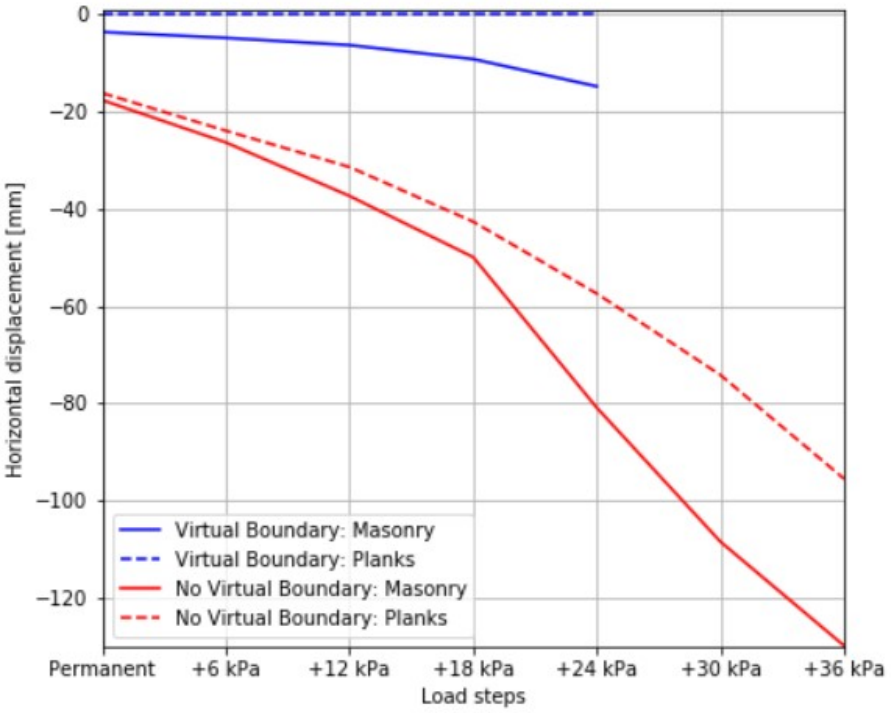

Figure 4.23: Horizontal displacement of the base of the masonry wall and the planks after applying loads. Blue: Virtual boundary; Red: No virtual boundary. Note that these are relative displacements and not absolute.

When applying the virtual boundary, it is expected that the planks will not move laterally, since it is fully connected to the piles in translation. In both cases, the masonry slides over the planks.

4.4.2. External stability

The soil column outside of the virtual boundary (column II) pushes against the foundation structure, leading to lateral movement of the entire structure (including piles). These loads come from permanent loads due to the presence of the soil and the added surcharge above the surface at this location. When it comes to performing numerical analysis, the expectation is that the masonry wall will not slide off the planks as a result of these loads alone. To test this mechanism in full isolation, all other loads will be disregarded. Two situations will be compared:

1. The lateral displacement of the base of the masonry and the planks, as a result of loading from only soil column I.
2. The lateral displacement of the base of the masonry and the planks, as a result of loading from only soil column II.

First of all, the permanent loads resulting from the specific soil column outside of the virtual boundary will be applied. Secondly, a surcharge will be applied, acting on the same soil column. Lastly, the surcharge will be incrementally increased by 6 kPa per load step until the model stops running, essentially meaning failure. The results are shown in figure 4.24.

The blue diverging lines represent the lateral movement of the piles/planks (dashed line) and the bottom of the masonry wall (solid line), while the virtual boundary is present. The red

non-diverging lines represent the same, except without the presence of the virtual boundary. Again, these are relative displacements, relative to the position of the pile head connection.

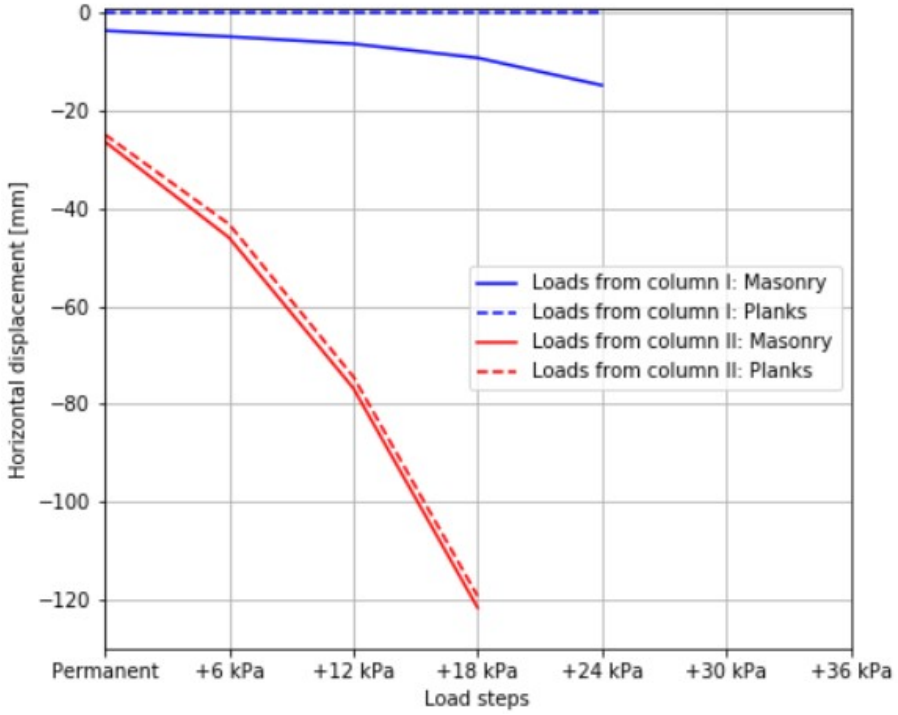

Figure 4.24: Horizontal displacement of the base of the masonry wall and the planks after applying loads. Blue: Column I; Red: Column II. Note that these are relative displacements and not absolute.

One must keep in mind that since the planks are connected to the piles, the translation of the planks equals the translation of the piles. It is visible that loads resulting from soil column I, do not result in any lateral movement of the planks. Any movement of the masonry is a direct result of the interaction between the masonry and the planks. The loads that result from soil column II, cause a much larger displacement of the masonry wall, but the displacement of the planks is roughly equal to that of the masonry wall. This is due to the fact that there is no direct loading on the masonry wall. As a result, the masonry wall tends not to slide off the planks.

5

Results

5.1. Cases

The produced results from the finite element model will be presented in this chapter. The finite element model is built to answer the following questions:

- On the basis of the numerical model, which tell-tale signs could be observed that can help better detect critical quay walls defects?
- To what extent can the quay wall degrade before it starts to portray visually detectable signs of damage?
- Which factor contributes the most to cause the displacement of quay walls?

The finite element model in DIANA FEA is presented in figure 5.1.

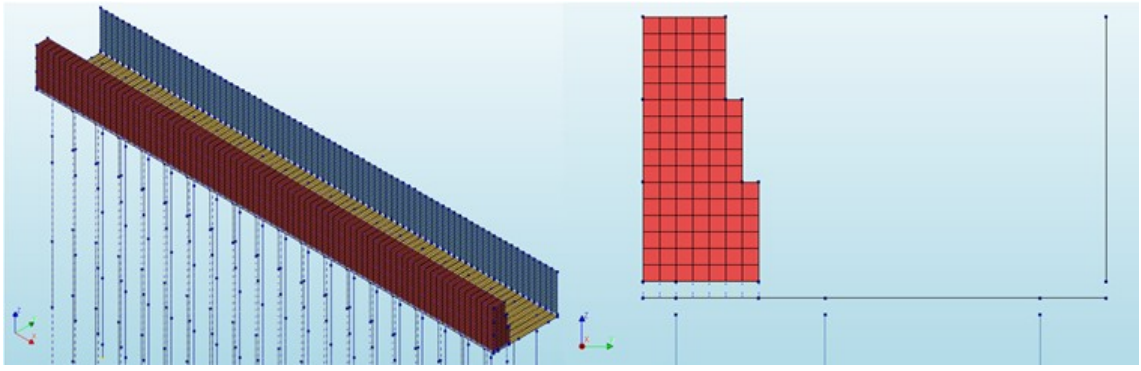

Figure 5.1: The quay wall model represented in DIANA FEA (Mesh: 0.25 m x 0.1 m x 0.1 m)

In order to observe damage patterns in the masonry, it is necessary to run simulations of realistic cases which may trigger the formation of cracks. This thesis will focus mainly on two cases, including some variations within each case.

1. Non-uniform pile degradation.

2. Non-uniform soil removal.

Non-uniform pile degradation is the idea that over the course of many years, not every pile degrades at an equal rate. In the finite element model, this aspect is simulated by selecting pile rows and assigning them different properties (see figure 5.2). It is necessary to mention that two important terms will be often mentioned in this chapter, namely 'pile rows' and 'soil removal'. These terms could be perceived as confusing without an elaboration. The definition of these two terms are as follows:

- Pile row: a row of piles perpendicular to the quay wall. Meaning that one row consists of three piles (front, middle, end), unless stated otherwise. In this thesis, a pile row is therefore NOT defined as a row in the direction parallel to the canal.
- Soil removal: a decrease in soil level around the foundation piles, or a decrease in pile embedding. It must therefore NOT be confused with a loss of soil behind the masonry wall and on top of the foundation planks. This aspect has not been incorporated into the model code.

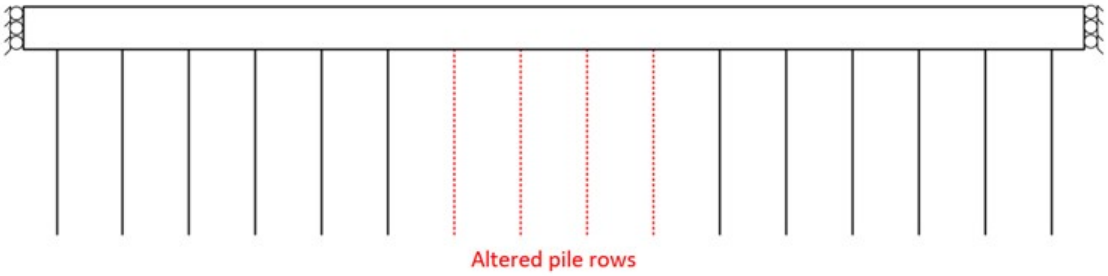

Figure 5.2: Non-uniform pile degradation will be simulated by altering pile row properties in the finite element model.

Non-uniform soil removal is the idea that over the course of many years, the soil surrounding the piles washes away, although not at an equal rate at every location. In the finite element model, this aspect is simulated by selecting pile rows and lowering the soil level locally (see figure 5.3).

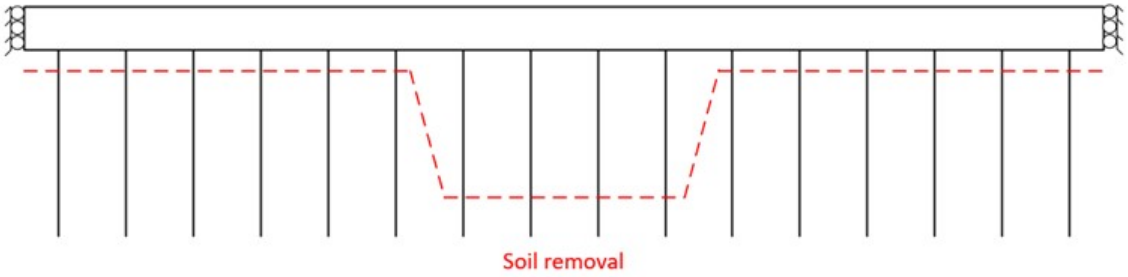

Figure 5.3: Non-uniform soil removal will be simulated by lowering the soil surrounding the pile in the finite element model.

Eventually, the goal is to document cracking and displacement patterns within the masonry. These patterns may be used to predict a specific defect within an existing quay wall.

Lastly, one more case will be simulated, which is total uniformity over the entire domain of the quay wall structure. This means that the properties at every pile row is exactly the same throughout the entire length of the quay wall. All relevant parameters will be assessed separately, in order to understand which parameter affects the displacement of the masonry wall the most according to the model.

5.2. Material Properties

This section aims to summarise the material properties used in the finite element model, as they are established in chapter 3. Three different material types can be distinguished: masonry, wood and the virtual boundary properties. The quality of masonry and wood can vary greatly depending on their state. Upper and lower bounds of masonry and wood have been determined in chapter 3. The upper bound material properties are set to be the characteristic values from European norms and regulations. The lower bound material properties are set to be design values according to the same European norms, which are based on environmental and time dependent factors among other things. It must be noted that these are baseline values. It is likely, and therefore assumed, that the strong characteristics are an overestimation of the quality of the materials, while the weak characteristics are an underestimation.

The virtual boundary is not present in reality, it is purely modelled to simulate more or less the same effects as the retained soil would have on the quay wall. Therefore, the virtual boundary is mass-less and rigid (infinite stiffness). The properties put in DIANA FEA are summarised in table 5.1.

Material property	**Value**	**Unit**
Young's modulus (E)	10^6	N/mm^2
Mass density (ρ)	1	kg/m^3

Table 5.1: Properties of the virtual boundary.

In the DIANA model, the masonry is modelled using the Total Strain Cracking Model with a rotating crack orientation. The model assumes linear elasticity in compression and an exponential hardening curve in tension. The properties are summarised in table 5.2.

Material property	**Value (max.)**	**Value (min.)**	**Unit**
Young's modulus (E)	5000	3000	N/mm^2
Poisson's ratio (ν)	0.25	0.25	-
Mass density (ρ)	1800	1800	kg/m^3
Tensile strength (f_t)	0.35	0.21	N/mm^2
Tensile fracture energy (G_t)	0.035	0.021	N/mm

Table 5.2: Maximum and minimum masonry properties used in the analyses.

Similarly to masonry, wood quality is bounded by a maximum and a minimum value, based on the quality of the material. These values are also based on European norms and regulations. Again, the strong characteristics are likely an overestimation, while the weak characteristics are likely an underestimation. When it comes to pile group effects, it reduces the soil capacity with a factor of 0.9, 0.8 and 0.7 for the respective pile rows (front to back). According to the

inspection report of the Nieuwe Herengracht, half of all piles have had a reduction in diameter of 30 %, resulting into a value of 70 % of 180 millimeters (Schol-Calingacion and Bosveld, 2016).

Material property	**Value (max.)**	**Value (min.)**	**Unit**
Young's modulus (E)	6000	3000	N/mm^2
Mass density (ρ)	320	320	kg/m^3
Flexural strength (f_m)	18.0	9.0	N/mm^2
Diameter (D)	180	126	mm

Table 5.3: Maximum and minimum pile properties used in the analyses.

5.3. The base case

The results of the simulations will be compared to a newly built quay wall, in order to quantify the changes that can occur according to the model. To simulate a newly built quay wall, the following assumptions have been made:

- Uniform conditions: the pile, masonry and soil properties are assumed to be the same at every location.
- The piles and the masonry wall have material properties in the upper bound. In other words, the materials used are new, therefore no degradation has taken place yet.
- No soil has been washed away yet, meaning that all piles are fully embedded.
- The pile head connection to the planks has not degraded yet, meaning that this connection is assumed to be rigid.
- The length of the quay wall section is set to 40 meters.

Dilation joints are present at both boundaries, which is modelled as an interface along which free sliding is permitted. Due to the presence of symmetry in the model, only one half is sufficient to simulate. The results will be the same, but calculation effort and time will be greatly reduced. This principle is illustrated in figure 5.4 below.

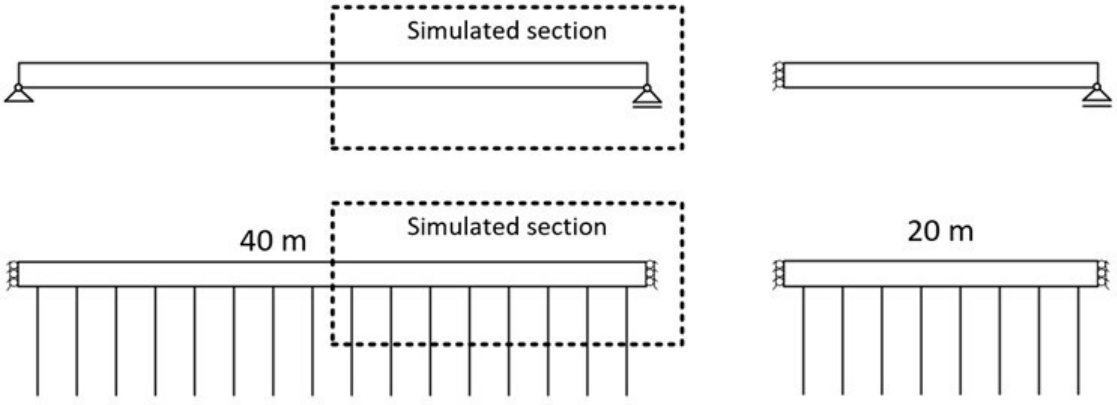

Figure 5.4: UP: Principle of symmetry — DOWN: Applied to free sliding boundaries.

Both results are presented in figure 5.5. A free sliding boundary results into uniform displacement of the structure. A fixed boundary results into the largest displacements being at the midpoint of the wall, while they are zero at the edge.

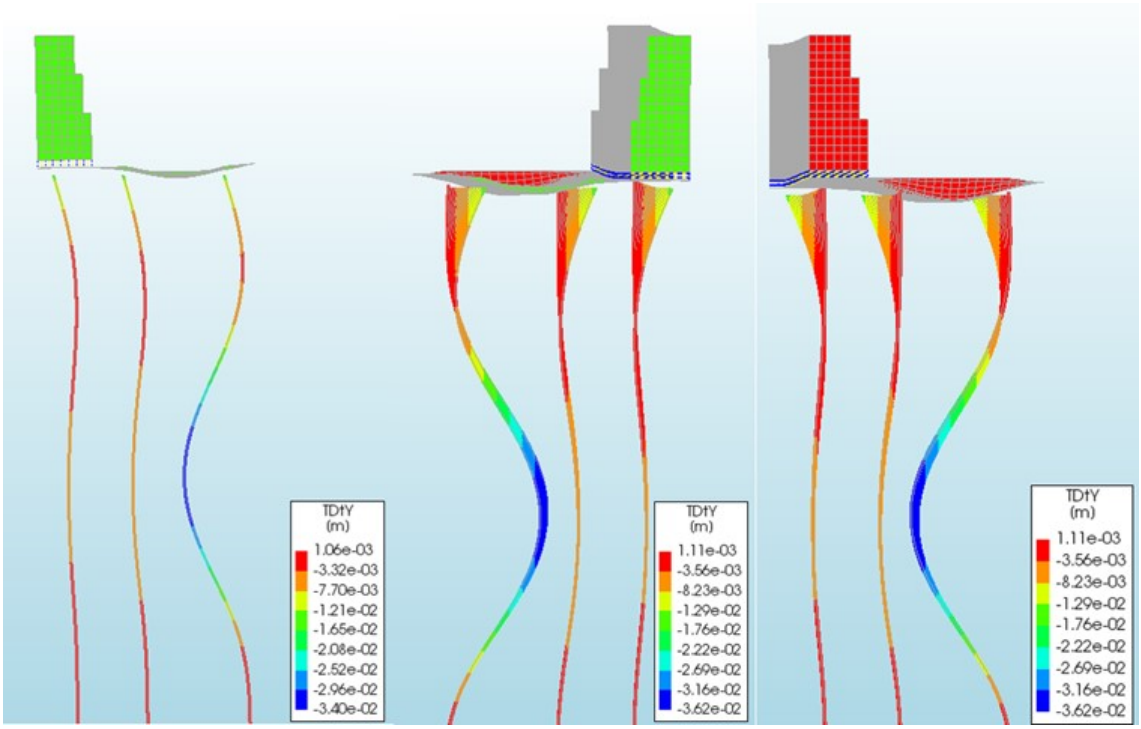

Figure 5.5: LEFT: Sliding boundary — MIDDLE: Fixed boundary at midpoint — RIGHT: Fixed boundary at the edge

5.4. Non-uniform pile degradation

In reality, foundation piles will likely not experience degradation at the same rate at every location. In other words, over the course of decades or centuries, not all piles will have degraded at an equal rate. The development of damage patterns in the masonry wall due to non-uniform pile degradation will be discussed in this section. The following aspects will be closely looked at:

1. The effect of breaking piles.
2. The effect of reducing the diameter of the piles.
3. The effect of reducing the stiffness of the piles.
4. The effect of lowering the pile-supporting soil.
5. The comparison between qualities of masonry.

5.4.1. Cracking patterns

This subsection presents and discusses the crack fields induced by loss of pile capacity. The focus only lies on the location and direction of induced cracks. On top of that, several different model parameters will be compared with each other, in order to establish a relation between crack development and the corresponding parameter. In the upcoming analyses, an arbitrary

degraded quay wall will be used as a baseline. These initial properties used in the analyses are summarised in table 5.4 below. Most of these parameters will thereafter be assessed individually in order to document their influence on the quay wall.

Property	**Value**	**Unit**
Masonry: Young's modulus	3000	N/mm^2
Masonry: Shear modulus	1200	N/mm^2
Masonry: Poisson's ratio	0.25	-
Masonry: Mass density	1800	kg/m^3
Masonry: Tensile strength	0.21	N/mm^2
Masonry: Tensile fracture energy	0.021	N/mm
Pile: Young's modulus	4000	N/mm^2
Pile: Flexural strength	16	N/mm^2
Pile: Mass density	320	kg/m^3
Pile: Diameter	160	mm
Pile head connection	Hinged	-
Free height: Front pile	0	m
Free height: Middle pile	0	m
Free height: End pile	0	m

Table 5.4: Initial properties used in the upcoming analyses (degraded properties).

In some analyses, a healthy quay wall will be used as the baseline. The properties of such a structure are summarised in 5.5 below.

Property	**Value**	**Unit**
Masonry: Young's modulus	5000	N/mm^2
Masonry: Shear modulus	2000	N/mm^2
Masonry: Poisson's ratio	0.25	-
Masonry: Mass density	1800	kg/m^3
Masonry: Tensile strength	0.35	N/mm^2
Masonry: Tensile fracture energy	0.035	N/mm
Pile: Young's modulus	6000	N/mm^2
Pile: Flexural strength	18	N/mm^2
Pile: Mass density	320	kg/m^3
Pile: Diameter	180	mm
Pile head connection	Rigid	-
Free height: Front pile	0	m
Free height: Middle pile	0	m
Free height: End pile	0	m

Table 5.5: Initial properties used in the upcoming analyses (healthy properties).

5.4.1.1 Cracking due to pile fracture

Broken piles practically do not have any structural value left. Therefore, a broken pile is simulated simply by removing it from the model. Three different pile positions are considered in the model: front, middle and end piles. The front piles are positioned closest to the canal, while the end piles are the furthest away from it. The effect of removing an entire row will be discussed, as well as the effect of removing the front and middle piles and the effect of

removing the front piles only (see figure 5.6). As mentioned before, a 'pile row' is defined as a row of piles perpendicular to the wall.

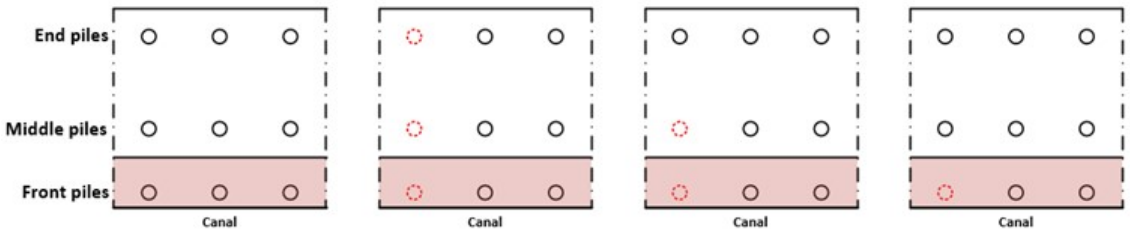

Figure 5.6: Pile positions and subsequent pile removal cases (three cases). The red-dotted circles indicate a removed pile.

A quay wall of 40 meters long will be considered, with dilation joints at both ends. Note that the dilation joints allow for free lateral and vertical movement, but restricts rotation and horizontal movement in longitudinal direction (parallel to the canal). Pile rows will be removed starting at the midpoint of the 40 meter wall. Due to symmetry at both sides, the finite element model can be halved in size. The midpoint is replaced by a boundary allowing free lateral and vertical movement, while restricting rotation and horizontal movement in longitudinal direction. Essentially, this boundary condition is the same as if one would replace the midpoint with another dilation joint. In other words, simulating a 40 meter long quay wall with dilation joints at both ends, yields the same results as simulating a 20 meter long quay wall with dilation joints at both ends. This is only the case given that piles are removed from the midpoint of the 40 meter wall (or from the edge of the 20 m wall). The situation is presented in figure 5.7.

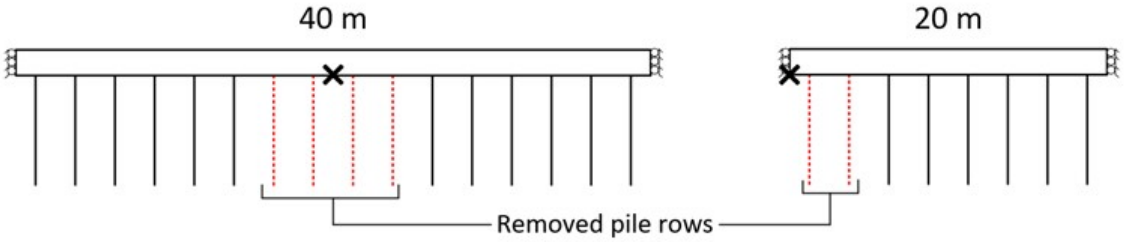

Figure 5.7: Quay wall schematisation (dilation joints at both ends). The schematisation on the left yields similar results compared to the schematisation on the right.

In the upcoming analyses, the quay wall structure will be assumed to be in a weak state (properties derived from table 5.4). This translates to lower strength and stiffness values. This is done to represent the present-day situation more realistically. After each simulation has been performed, the following information will be extracted:

- The damage/cracking patterns.
- The horizontal displacement of the masonry wall at ground surface level, at the location where the displacement is maximum. This location is indicated by the "X" in figure 5.7.
- The horizontal displacement of the masonry wall at the bottom of the masonry wall, at the same location.

- The vertical displacement of the masonry wall at ground surface level, at the same location.

The analyses will be performed with the following steps:

1. Remove the two middle piles rows of the 40 meter long quay wall entirely, and run the analysis. Removal must occur in pairs in order to retain symmetry.
2. Remove two neighboring pile rows (one at each side). Run the analysis.
3. Repeat step 2, until the model collapses.
4. Repeat step 1 until 3. Instead of removing the entire row, only remove the middle and front piles of said row.
5. Repeat step 1 until 3. Instead of removing the entire row, only remove the front pile of said row.

These steps are visualised in figure 5.8 below.

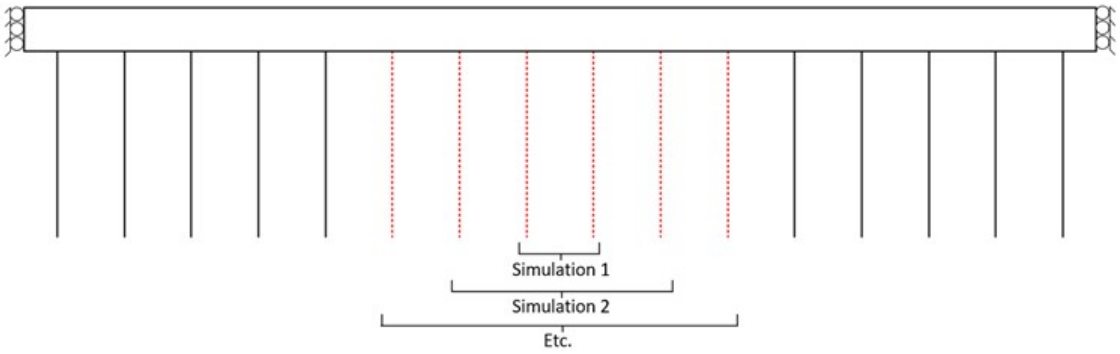

Figure 5.8: Visualisation of how the simulations will be performed.

Removing three pile rows entirely (or six accounting for symmetry), results into the crack fields presented in figure 5.9. Each line represents the crack strain per element.

Figure 5.9: Cracking patterns after removal of three pile rows (e.g. nine individual piles). Note that only one half or 20 m has been simulated.

According to the model output, changing the number of removed pile rows results into variations of the cracking patterns shown in figure 5.9 above. The cracks induced by pile removal can thus be described generalised crack fields. Generally, two crack fields can be distinguished: one directly surrounding the defected piles, the other further away from the defected piles (see figures 5.10 and 5.11).

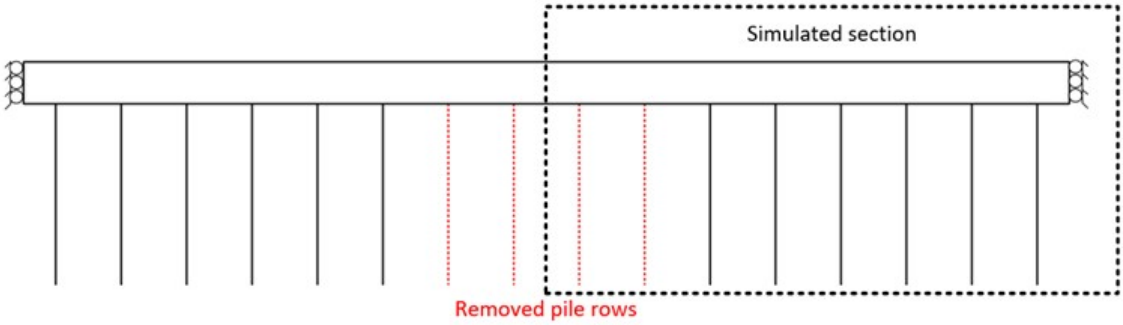

Figure 5.10: Pile removal modelling.

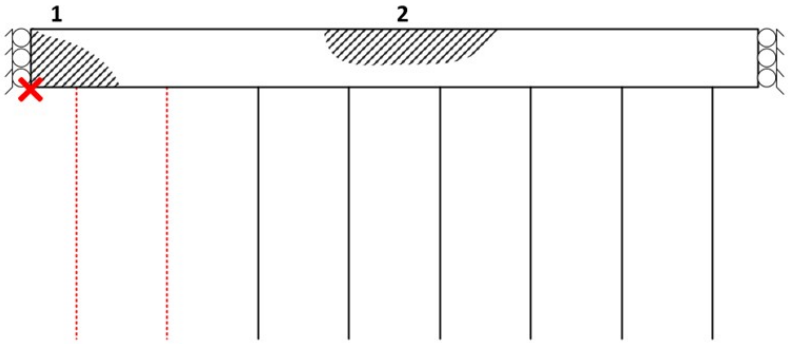

Figure 5.11: Schematic view of the primary (1) and secondary (2) cracking area as a result of pile removal.

The crack fields will also be visualised using plots. Given that the cracks propagate from either the top or the bottom of the masonry wall, the nodal values should be the largest at these positions. The plotted nodes and their graphic interpretation are illustrated in figure 5.12.

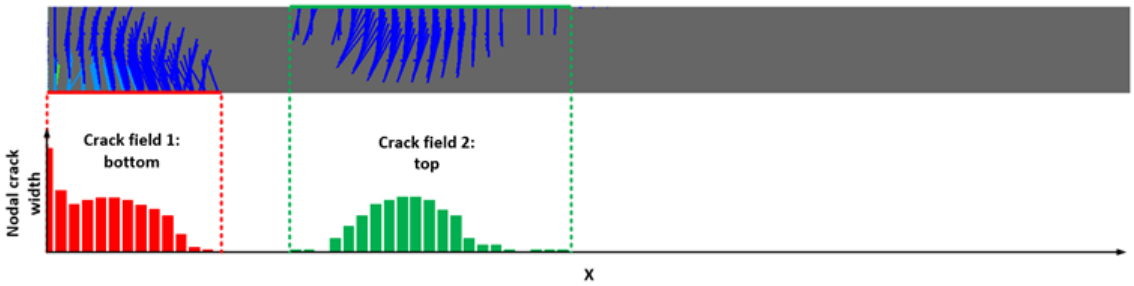

Figure 5.12: The node positions which will be plotted, including their graphic interpretation.

As an example, figure 5.13 shows the development of both crack fields in the case of total pile row removal. All results can be found in appendix C.1.

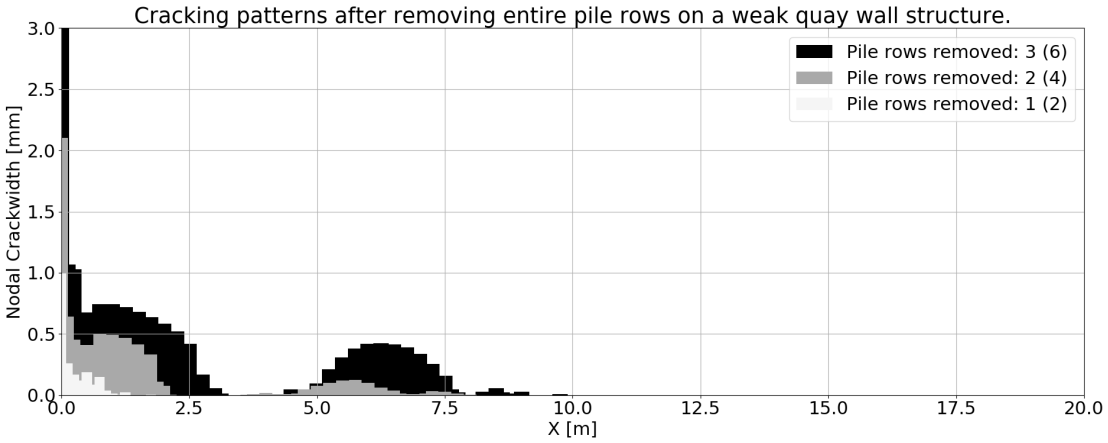

Figure 5.13: Nodal crack width values after removal of entire rows at the nodes presented in figure 5.12.

The two crack fields are easily distinguishable from the graph. The largest peak is in the middle of the quay wall (X = 0 m). The secondary peak lies around X = 6 m. Notice that the secondary peak is non-existent in the case where only two pile rows were removed. Therefore, it can be concluded that the crack in the middle is induced first, followed by the secondary area as pile damage progresses. The model output shows that the secondary cracks have an in-plane character, given that the crack progression is similar at both the canal side and the inner side. The primary cracks are induced due to a combination of both in-plane and out-of-plane movement of the masonry wall. This is due to the fact that the cracks at the canal side are significantly larger compared to those at the inner side. Also, the cracks at the bottom are wider than those at the top of the masonry wall (see figure 5.14). To summarise, the cracks are induced by the following aspects:

- The primary crack field has an in-plane component, due to the relatively large vertical settlements as a result of pile removal (due to lack of vertical support).
- The primary crack field has an out-of-plane component. The masonry wall can bulge towards the canal, due to a lack of horizontal support caused by the absence of piles.
- The secondary crack fields have an in-plane character. Due to relatively large vertical settlements at the primary crack field, secondary cracks will start to appear further away, where another bending moment peak is present.
- The out-of-plane component of the secondary crack field is present, but negligibly small.

Lastly, the more pile rows are removed, the larger the crack field spreads, and the larger the crack width values become. On top of that, removing more pile rows results into the secondary crack field to move away from the midpoint (X = 0). In figure 5.14, the generalised cracking patterns are presented in 3D.

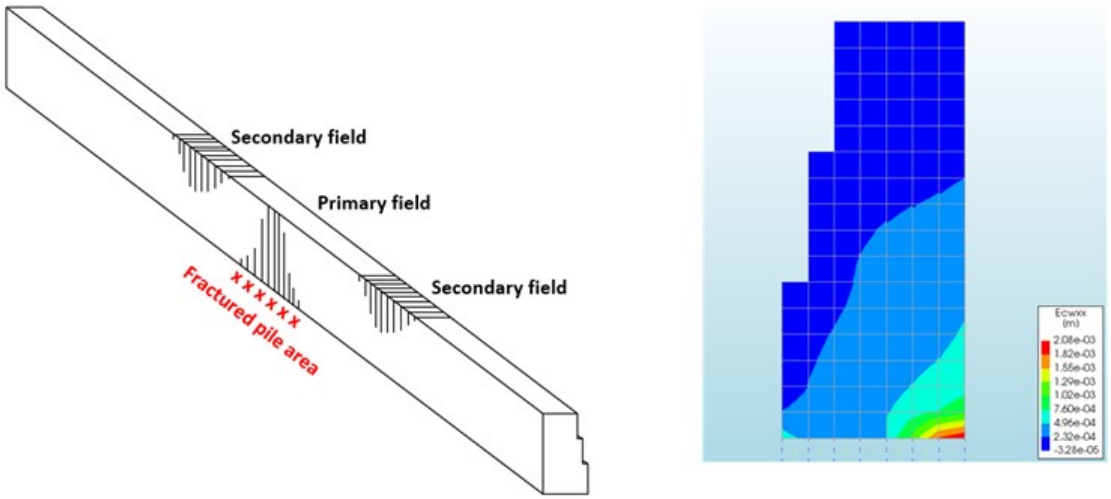

Figure 5.14: Left) Generalised cracking patterns due to pile removal — Right) Crack development in the middle of the primary crack field

5.4.1.2 Cracking due to pile diameter reduction

It is common sense that the pile diameter has an effect on the overall strength and stiffness of an element. Changing the diameter of the pile also has a direct effect on how a pile interacts with the surrounding soil. Changing the diameter has the following additional consequences according to the model code:

- Decreasing the diameter results into less pile tip and shaft friction, leading to decreased vertical soil stiffness and vertical bearing capacity.
- Decreasing the diameter results into a change of the Ménard stiffness values [N/m^3] and the horizontal bearing capacity.

The following simulations use the same base parameters as presented in table 5.4. Three piles will stay removed, in order to retain cracking patterns. The effect that the general pile diameter has on the cracking patterns have been documented. They are presented in figure 5.15, full results are presented in appendix C.1.

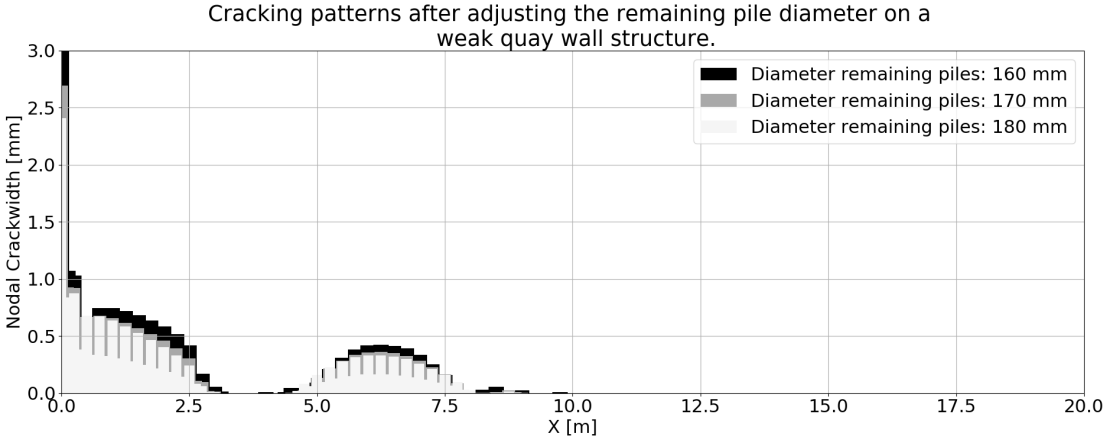

Figure 5.15: The effect of changing the pile diameter of the non-broken piles on the nodal crack width values at the nodes presented in figure 5.12.

According to figure 5.15, changing the pile diameter has a negligible effect on the position of the crack fields, although a larger diameter seems to slightly decrease the spread of the field. Smaller diameters lead to slightly larger crack widths in the secondary crack field, while it causes a more significant increase in the primary field.

5.4.1.3 Cracking due to pile stiffness reduction

In the model code, the stiffness of wood not only affects the piles, but also the planks. The following simulations use the same base parameters as presented in table 5.4. Three piles will stay removed, in order to retain cracking patterns. A change in these patterns by changing the wood stiffness have been recorded, which are presented in figure 5.16. The visual results are presented in appendix C.1.

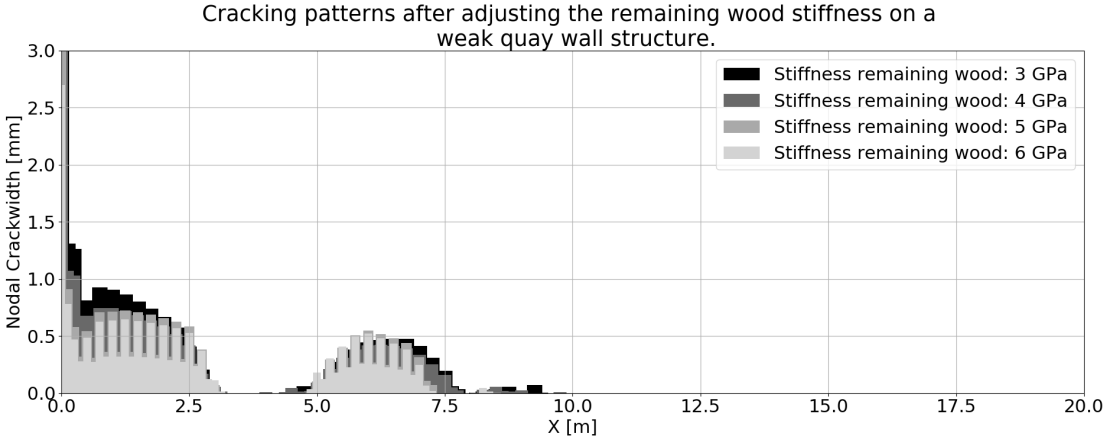

Figure 5.16: The effect of changing the wood stiffness of the non-broken piles/planks on the nodal crack width values at the nodes presented in figure 5.12.

According to figure 5.16, reducing the wood stiffness leads to a larger spread of the secondary crack field. Also, this crack field moves away from the midpoint at $X = 0$. The spread in the primary crack field stays more or less the same, although smaller pile stiffness values lead to

larger crack width values there.

5.4.1.4 Cracking due to a decrease in pile bedding

Lowering the soil level has the following consequences according to the model code:

- Less horizontal coverage of springs, resulting into less horizontal soil support.
- Less soil leads to less vertical friction, resulting into less vertical soil support.

The quay wall does not tolerate any removal of soil, if the base parameters are used according to table 5.4 and when three piles rows are removed. However, when only the three front piles are removed, the model allows for limited soil removal of 0.5 m at the front pile location. The results are presented in figure 5.17.

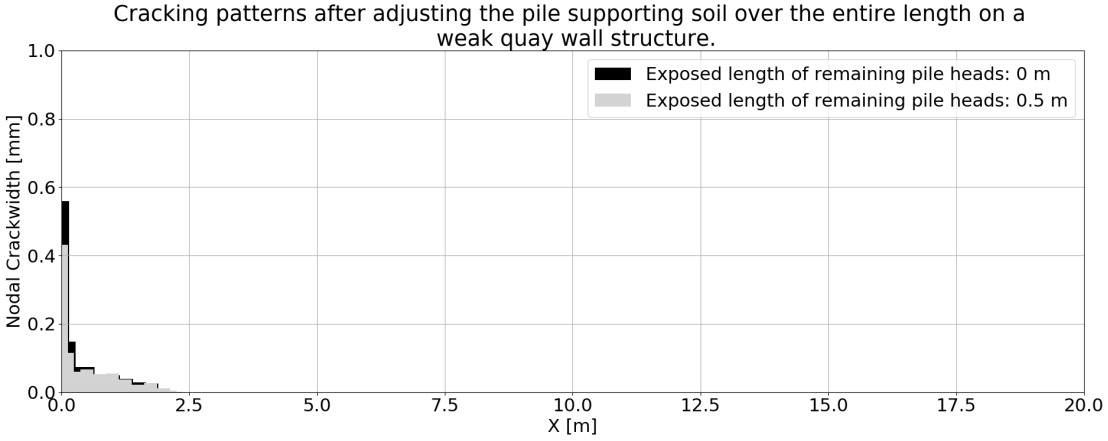

Figure 5.17: The effect of lowering the pile supporting soil around the non-broken piles on the nodal crack width values at the nodes presented in figure 5.12.

According to the obtained data, increasing the free height of the piles seems to have a favourable effect when it comes to damage to the masonry wall. It is difficult to draw conclusions based on these two data sets alone, given that the outcome is counter-intuitive.

5.4.1.5 Cracking due to masonry degradation

The following simulations use the same base parameters as presented in table 5.4. The properties of healthy masonry and weak masonry will be compared. These properties are summarised in table 5.2. Three piles will stay removed, in order to retain cracks. A change in these patterns by changing the masonry properties will be recorded. The results are presented in figure 5.18.

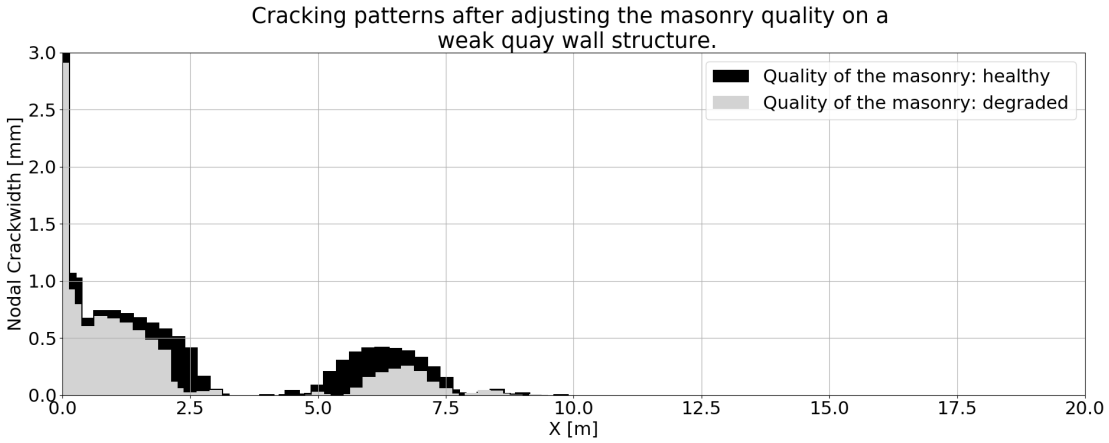

Figure 5.18: The effect of changing the quality of the masonry on the nodal crack width values at the nodes presented in figure 5.12.

As expected, masonry of a higher quality shows a smaller crack field spread and thinner cracks. Bad quality masonry leads the secondary crack field to move slightly closer to the primary field.

5.4.2. Displacement patterns

This subsection presents and discusses the displacement patterns induced by loss of pile capacity. Evidently, the largest displacements are found at the location where piles have been removed in the model. Therefore, the displacement output will mainly be focused in that location. From here on, this position will be referred to as the point of maximum displacement or "P.M.D." (see figure 5.19). In this case, it is situated in the middle of the primary crack area. The results have been obtained from the same simulations from which the cracking patterns have been determined. Therefore, the same model input has been used, which is given in table 5.4. Note that six pile rows have been removed in running these simulations, unless stated otherwise.

Figure 5.19: Left: Quay wall schematisation with the point of maximum displacement — Right: Plotted wall section in the upcoming graphs

5.4.2.1 Displacements due to pile fracture

When pile capacity is lost, the masonry wall will lack local vertical and horizontal support. The graphs in figure 5.20 below display the stance of the quay wall after incrementally removing pile rows. Three scenarios will be presented: one where entire pile rows are removed, one where only the front and middle piles are removed, and one where only the front pile is removed.

These results are as the position of maximum displacement (P.M.D.). The lines represent the absolute displacements of the front of the masonry wall (see figure 5.19).

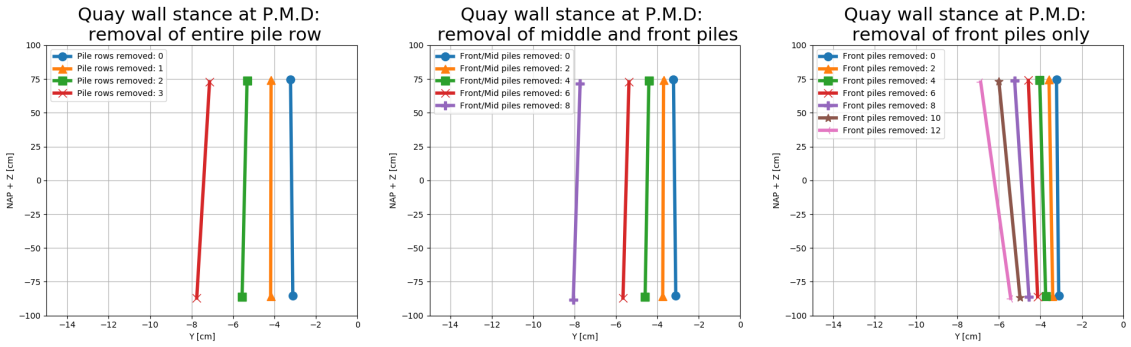

Figure 5.20: Quay wall stance at the P.M.D., left) entire row removal — middle) front and middle pile removal — right) front pile removal (not to scale).

As more piles are removed, it is visible that the displacement increases exponentially, meaning that the rate of displacement increases as pile fracture progresses. A notable finding is that the quay wall starts tilting backwards when entire rows are removed. When the front and middle piles are removed, this backwards tilt is almost negligible. Removing only the front piles result into frontward tilting. One possible explanation for the backwards tilt is the fact that the thin wood layer settles more easily compared to a thick masonry unit. The brick wall has a bending capacity of its own, so the wood layer underneath this wall is not absorbing as much bending load as the wood behind the wall. The consequence of the sagging planks behind the wall is that the wall will start to tilt backwards. When only the front pile is removed, the planks behind the masonry wall are still supported, while the support directly underneath the masonry wall is lost, causing the forward tilting.

5.4.2.2 Displacements due to pile degradation

The effect of pile degradation on the displacement at the P.M.D. is presented in figure 5.21. The graphs below have been obtained by removing the entire pile row (front, middle and end piles).

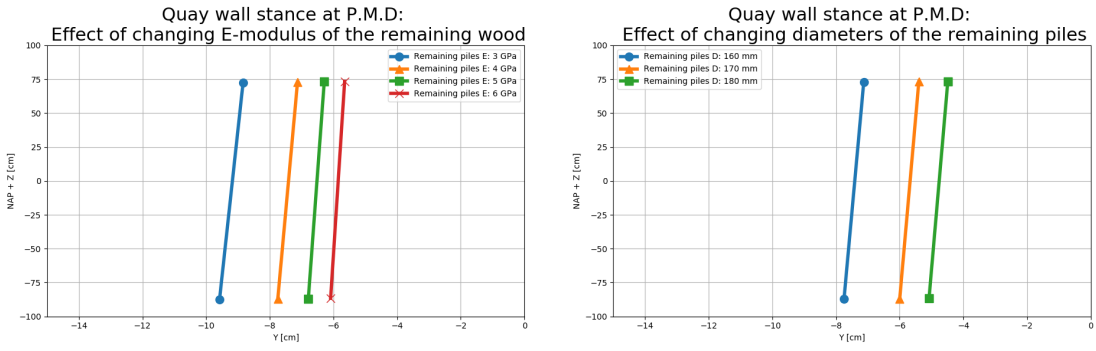

Figure 5.21: Quay wall stance at the P.M.D., left) influence of wood stiffness — right) influence of pile diameter (not to scale).

Changing the pile diameter has a similar effect on the quay wall as changing the wood stiffness (E-modulus). The tilt of the wall barely changes at all and the displacement progresses

exponentially. Figure 5.22 shows the combined effect of stiffness and diameter reduction in the following cases: when the middle and front piles are removed and when only the front piles are removed.

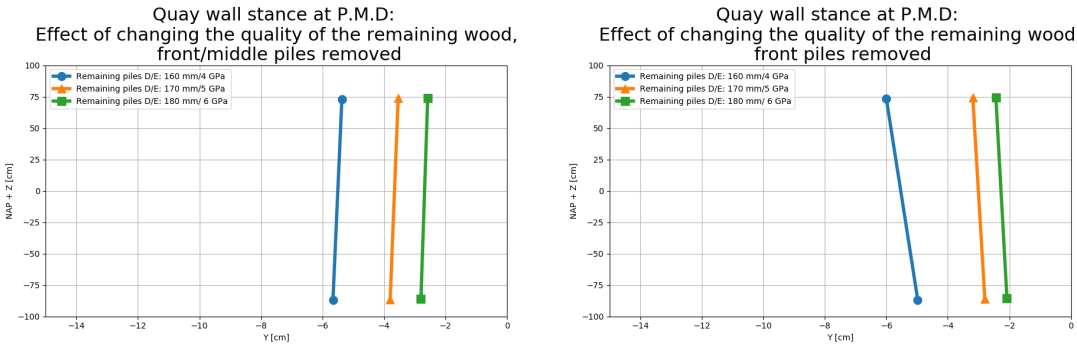

Figure 5.22: Quay wall stance at the P.M.D., left) front and middle pile removal — right) front pile removal (not to scale).

In both cases, the tilt orientation is maintained, the frontward tilt even increases in the case of front pile removal.

5.4.2.3 Displacements due to a decrease in pile bedding

As mentioned before, the quay wall model with properties from table 5.4, does not tolerate any soil removal when three entire rows are removed. However, limited soil removal is permitted when three front piles are removed. The results are presented in figure 5.23 below.

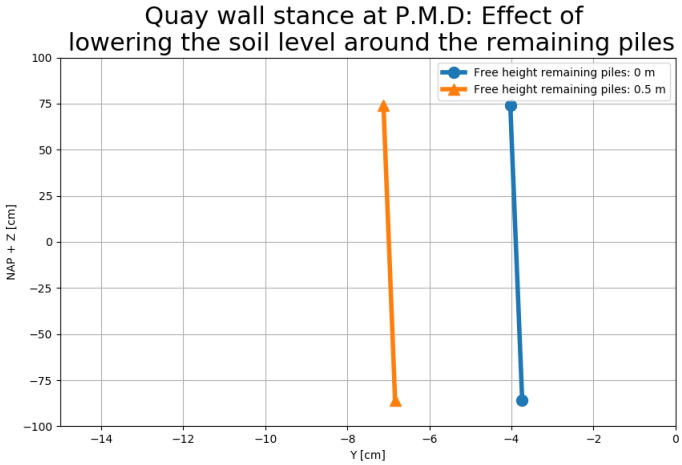

Figure 5.23: Quay wall stance at the P.M.D., left) front and middle pile removal — right) front pile removal (not to scale).

Even a limited loss of supporting soil leads to a significant increase in horizontal displacement. This increase in displacement may explain why the crack development at the P.M.D. is limited.

5.4.3. Visible cracks

This subsection is dedicated to providing an indication of masonry wall cracking visible to the naked eye. As mentioned in the problem analysis, quay walls are initially assessed using visual indicators. It is impossible to classify the simulation results as objective reality, but at least

it gives a rough indication on how much a quay wall structure is able to degrade before any outward damage is visible.

5.4.3.1 Pile removal: degraded quay wall

The damage patterns visible due to removal of piles have been discussed in section 5.4.1. Two pile removal cases will be presented here: one where the entire row is removed, and one where only the front piles are removed. The nodal crack width values and the combined crack value are presented in figure 5.24. In the figures below, properties from table 5.4 have been assigned. So in this case, the quay wall is already in a weak state.

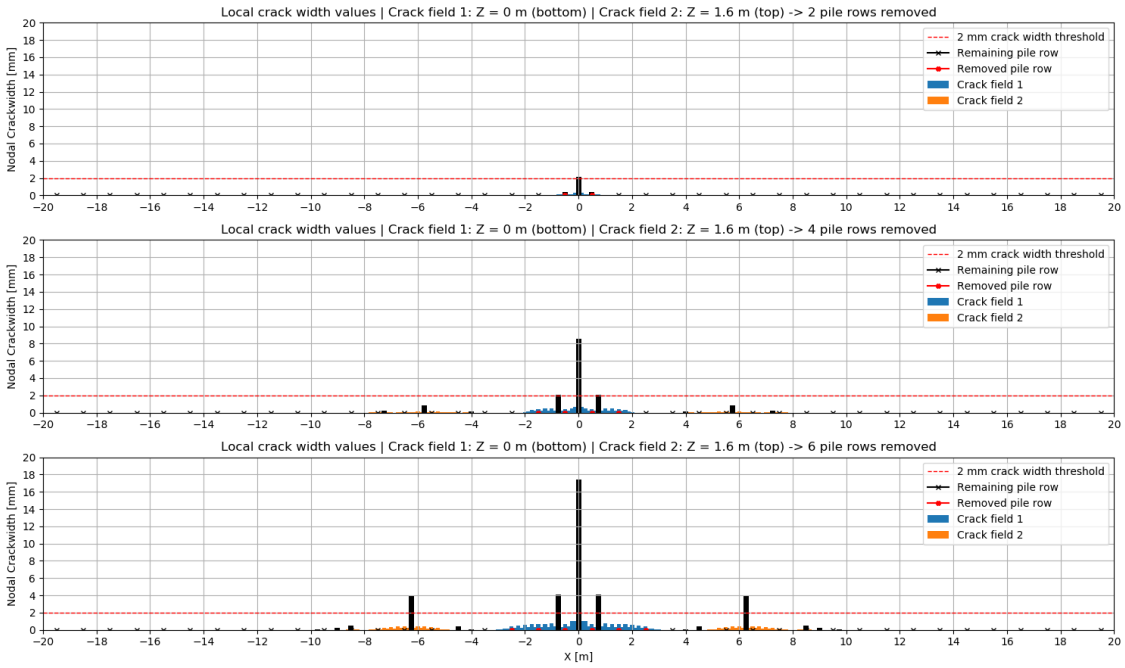

Figure 5.24: Crack width values at the bottom (1st crack area) and the top (2nd crack area) of the masonry wall. Pile rows have been incrementally removed on a weak quay wall structure.

Figure 5.24 above shows that when a quay wall is already considerably weak, removing two entire pile rows will cause a single visible crack at the center of removal. Once six pile rows are removed, the secondary cracks become more visible. The model does not allow any more pile removal than six rows, indicating that the appearance of the secondary cracks is relatively dangerous in this case. The cracking patterns at the onset of the first crack and at the onset of secondary cracks are presented in figure 5.25 below. The mean water table is indicated by the blue line running through Z = 0.85 m.

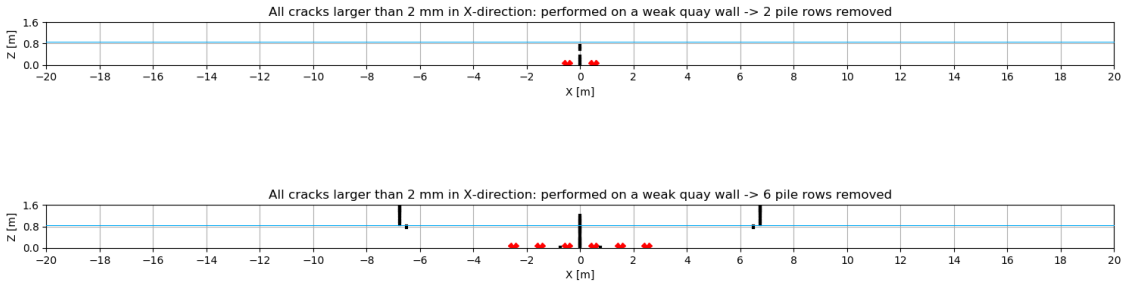

Figure 5.25: Cracking patterns when two pile rows are removed and when six pile rows are removed. The quay wall is in a weak state. Removal of more than six pile rows results into failure.

Figure 5.26 shows the DIANA FEA output of the lower graph from figure 5.25.

Figure 5.26: DIANA FEA output of the case when six pile rows are removed from a weak quay wall structure.

Figures 5.27 and 5.28 show the same model properties as before. However, only the front piles have been removed instead of all three. The mean water table is indicated by the blue line running through Z = 0.85 m in figure 5.28.

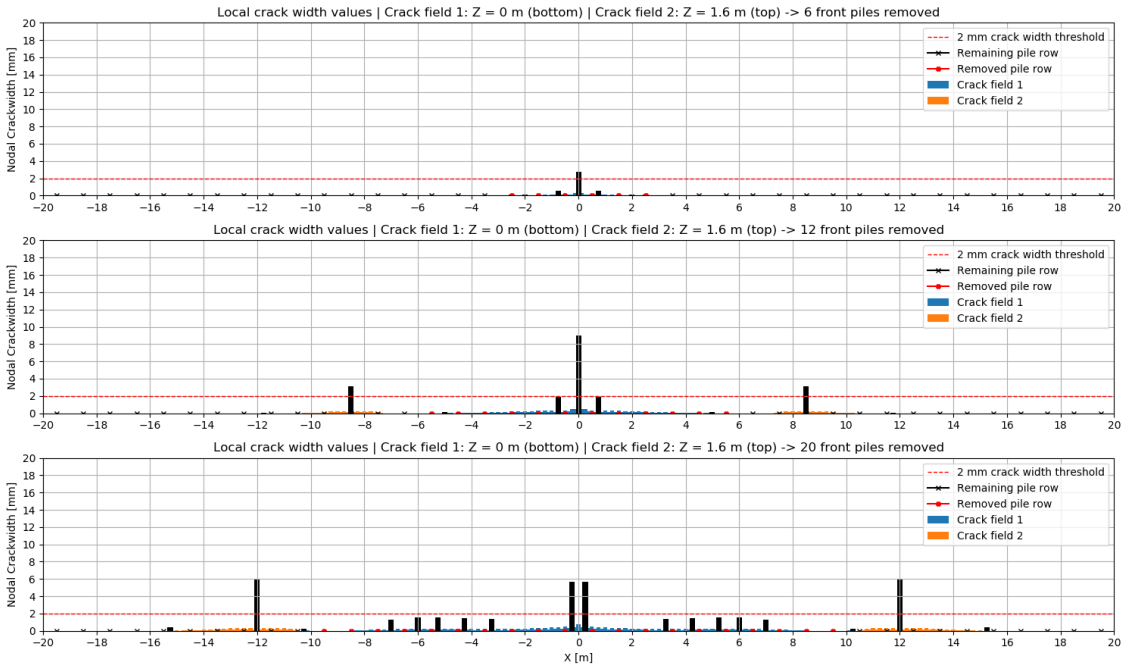

Figure 5.27: Crack width values at the bottom (1st crack area) and the top (2nd crack area) of the masonry wall. Front piles have been incrementally removed on a weak quay wall structure.

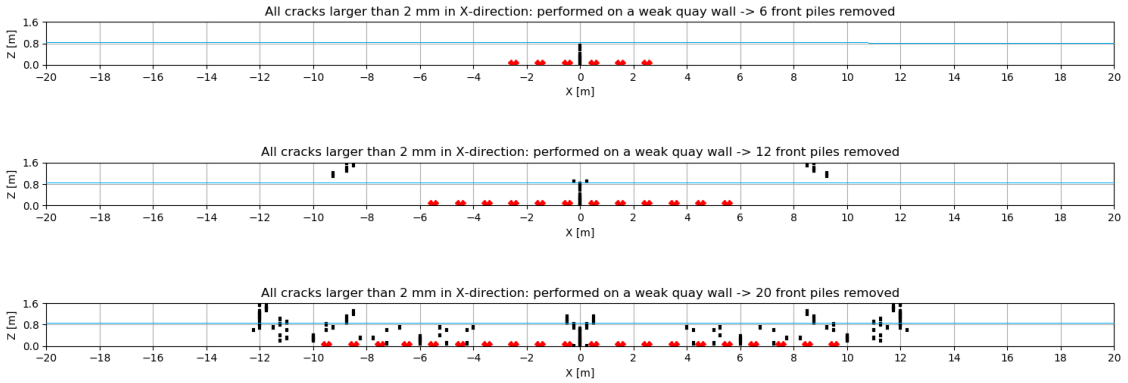

Figure 5.28: Cracking patterns when six, twelve and twenty front piles are removed. The quay wall is in a weak state. Removal of more than twenty pile rows results into failure.

Figure 5.29 shows the DIANA FEA output of the lower graph from figure 5.28.

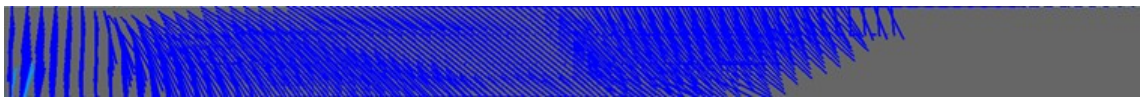

Figure 5.29: DIANA FEA output of the case when twenty front piles are removed from a weak quay wall structure.

It is clear that removing the front piles only results into a larger overall capacity of the quay

wall, compared to removing entire pile rows. The crack orientation is different in both crack areas when comparing to removing entire rows. If entire rows are removed, the primary crack goes vertically. If only the front pile is removed, resulting in frontward tilting of the masonry wall, the primary crack starts to diverge sideways. The crack direction of the secondary cracks are opposite when comparing both cases. Based on these results, the order of crack induction can be predicted. Figure 5.30 shows the generalised crack progression when entire pile rows are removed, figure 5.31 shows the generalised crack progression when only front piles are removed. The numbers indicate the likely order of appearance.

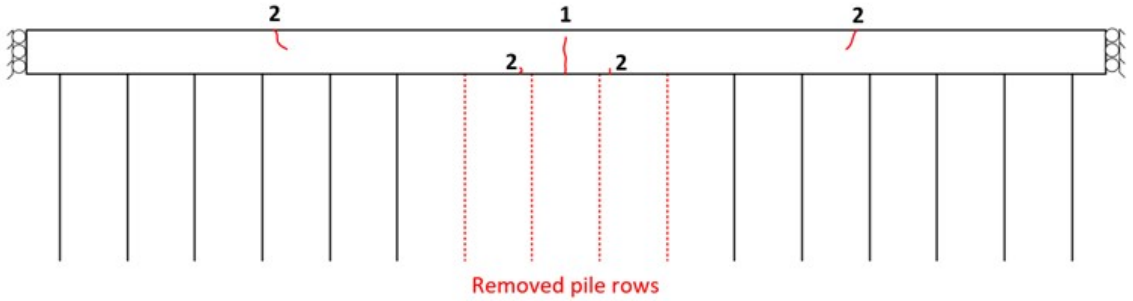

Figure 5.30: Crack progression caused by the incremental removal of all three piles.

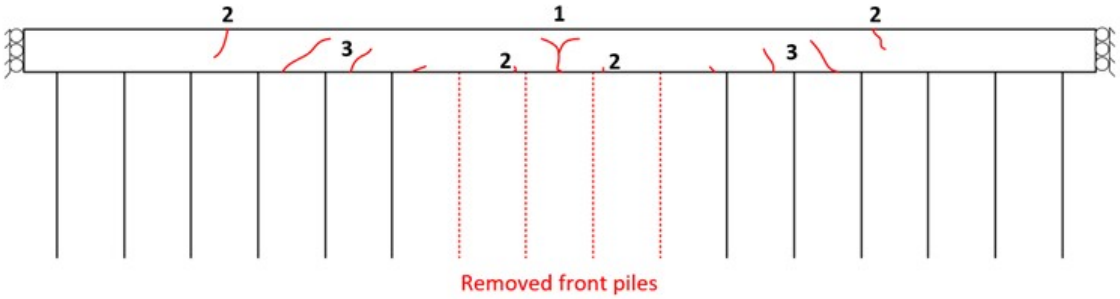

Figure 5.31: Crack progression caused by the incremental removal of front piles only.

Note that the cracks from the secondary crack field progress in opposite direction when comparing both cases. This is likely a consequence of the tilt of the quay wall. According to the model, when entire pile rows are removed, the quay wall will start to tilt backwards. However, when only the front piles are removed, the quay wall will tilt forwards. The tilt variation along the wall causes a torsional load in the masonry wall. The direction of the secondary crack depends on the direction of the torsional forces.

5.4.3.2 Pile removal: healthy quay wall

The same analyses will now be performed, except a healthy quay wall will be assessed instead of a degraded one. Two pile removal cases will be presented here: one where the entire row is removed, and one where only the front piles are removed. The nodal crack width values and the combined crack value are presented in figure 5.24. In the figures below, properties from table 5.5 have been assigned. So in this case, the quay wall is healthy.

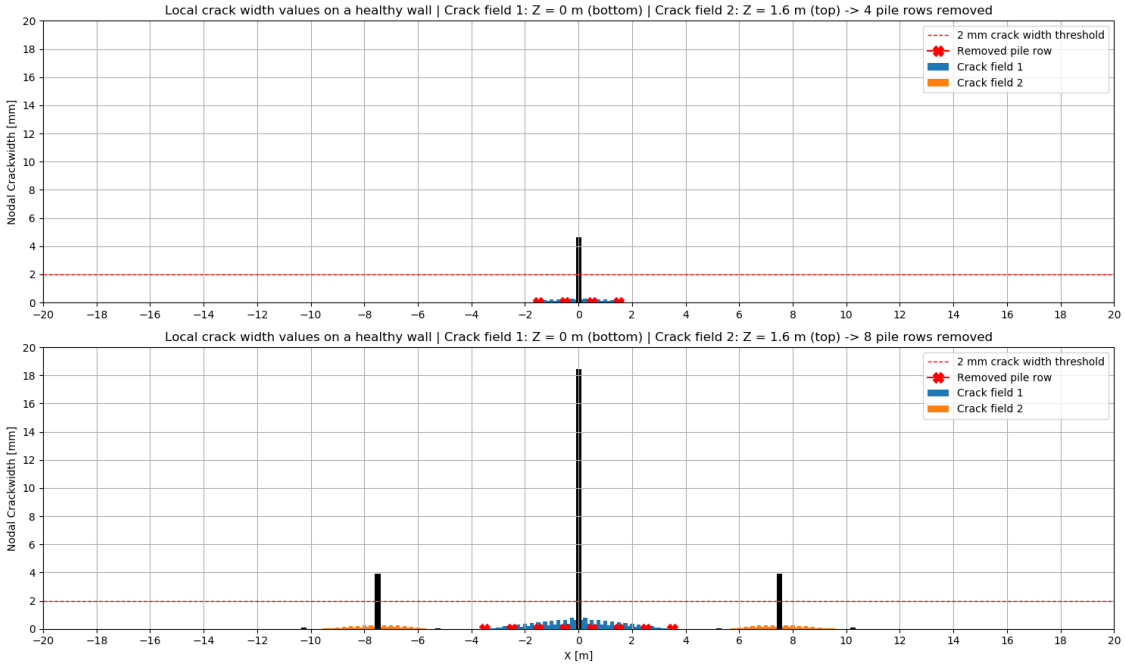

Figure 5.32: Crack width values at the bottom (1st crack area) and the top (2nd crack area) of the masonry wall. Pile rows have been incrementally removed on a strong quay wall structure.

Figure 5.32 above shows that a strong quay wall can lose much more foundation strength before it shows visible dangerous cracks compared to a weak wall. The onset of cracking begins later. Also, the primary crack area is represented by a single crack, instead of multiple cracks in the case of a weak wall. This might be explained due to the fact that strong masonry has a larger tensile strength and stiffness value. The primary crack reaches its 2 mm threshold when four pile rows have been removed. The secondary crack shows itself when eight pile rows have been removed. The cracking patterns at the onset of the first crack and at the onset of secondary cracks are presented in figure 5.33 below. The mean water table is indicated by the blue line running through Z = 0.85 m.

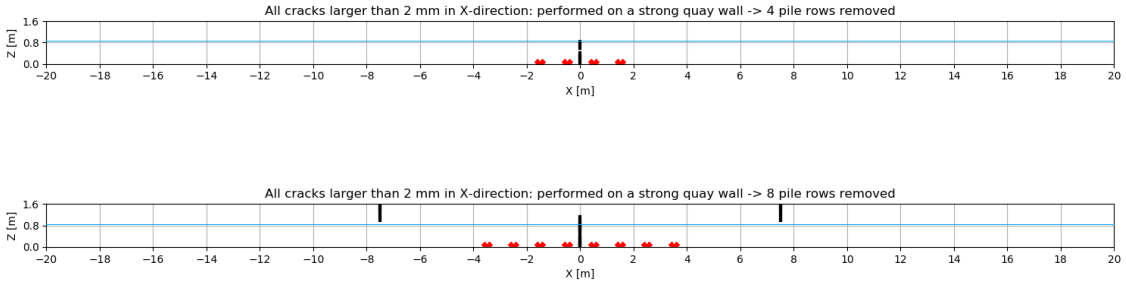

Figure 5.33: Cracking patterns when four pile rows are removed and when eight pile rows are removed. The quay wall is in a strong state. Removal of more than eight pile rows results into failure.

Figures 5.34 and 5.35 show the same model properties as before. However, only the front piles have been removed instead of all three. The mean water table is indicated by the blue line running through Z = 0.85 m in figure 5.35.

Figure 5.34: Crack width values at the bottom (1st crack area) and the top (2nd crack area) of the masonry wall. Front piles have been incrementally removed on a strong quay wall structure.

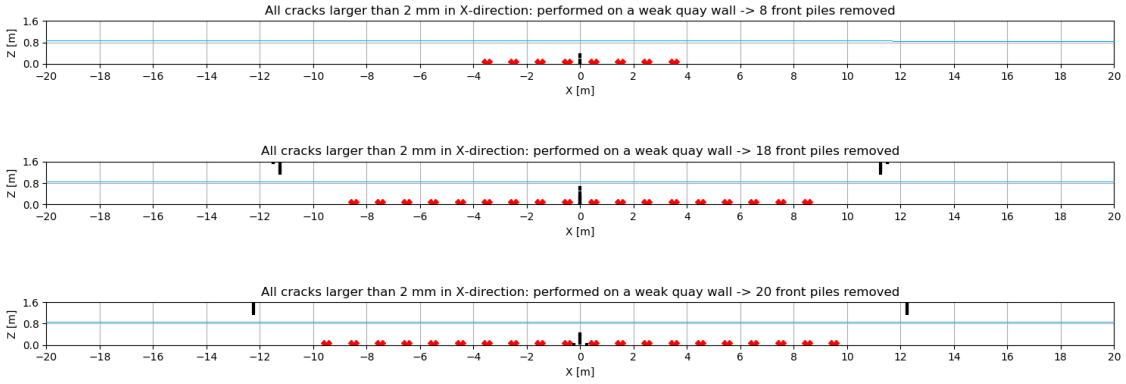

Figure 5.35: Cracking patterns when eight, eighteen and twenty front piles are removed. The quay wall is in a strong state.

Generally, it can be concluded that a stronger quay wall structure can withstand a larger amount of missing piles before the same cracks present itself as those of a weak wall. The amount of visible cracks are fairly limited if the masonry and the foundation structure is in relatively good quality.

5.4.3.3 Changing foundation quality

The effect of changing the foundation quality on the onset of cracking will be presented here. The case has been presented with the following properties:

- Baseline properties according to table 5.4.
- Six entire adjacent pile rows removed.
- Foundation E-modulus comparison: 3 GPa, 4 GPa, 5 GPa and 6 GPa.
- Pile diameter comparison: 160 mm, 170 mm and 180 mm.

Full results can be found in appendix C.1, only the lowest and highest property values are presented here (see figure 5.36).

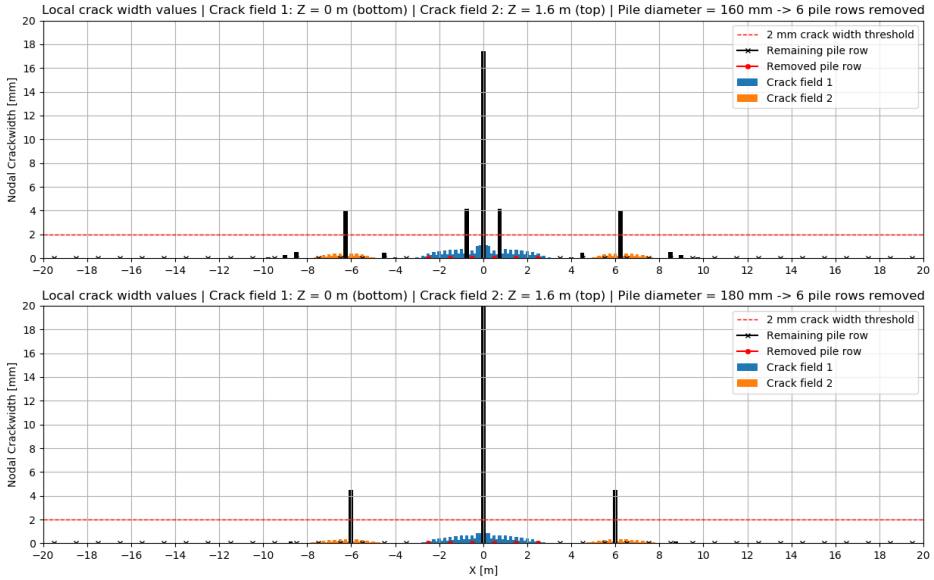

Figure 5.36: The upper graph presents the nodal crack widths at the top (crack field 2) and the bottom (crack field 1) of the masonry wall, with a global pile diameter of 160 mm. The lower graph presents the same, except with a global pile diameter of 180 mm.

According to figure 5.36, assigning a larger global pile diameter results into slightly larger secondary cracks. Also, the primary crack is represented by one large crack. In the case of a smaller global pile diameter, multiple smaller cracks represent the primary crack field. The overall primary crack field decreases in size as the pile diameter is increased, meaning that the accumulated primary crack width is smaller.

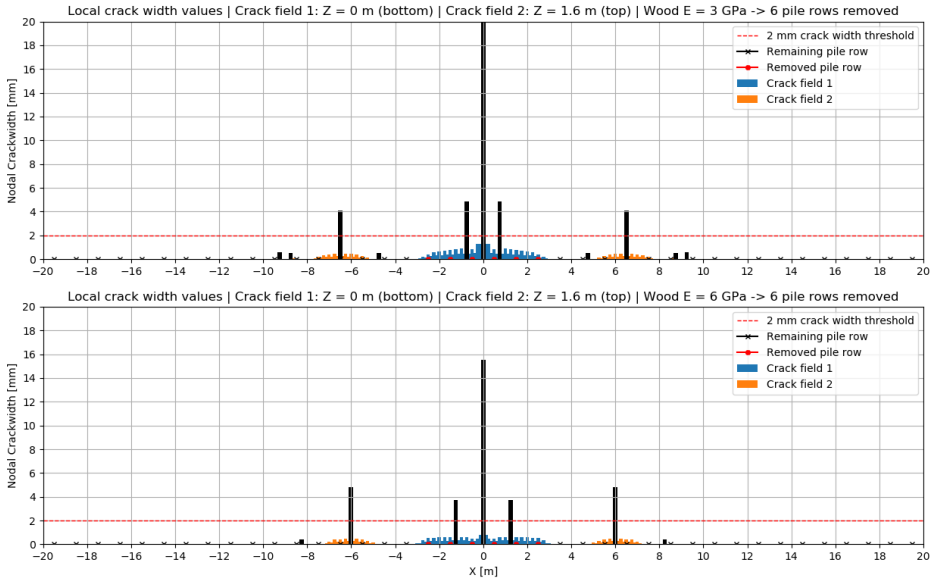

Figure 5.37: The upper graph presents the nodal crack widths at the top (crack field 2) and the bottom (crack field 1) of the masonry wall, with a wood E-modulus of 3 GPa. The lower graph presents the same, except with a wood E-modulus of 6 GPa.

According to figure 5.37, a larger foundation stiffness results into larger secondary cracks, but smaller primary cracks. The distance between individual primary cracks are larger when the foundation is stiffer.

Overall, decreasing the quality of the foundation structure leads to the following phenomena according to the model:

- An overall decrease in primary cracks, although it is difficult to establish whether a solitary crack will appear, or multiple cracks in this field. According to these results, it is more likely that the onset of visible cracks in this area is delayed when the foundation is in relatively good shape.
- An overall increase in secondary cracks. It is therefore likely that visible cracks in this area appear sooner when the foundation is in relatively good shape.

5.5. Non-uniform soil removal

In some cases, the quay wall structure loses horizontal soil support due to the possibility of the supporting soil to be washed away. This may contribute to the formation of a sinkhole, as it was the case at Grimburgwal (Korff et al., 2020). The effects of locally decreasing the soil embedding around the foundation piles will be discussed in this section.

5.5.1. Cracking patterns

This subsection presents and discusses the crack fields induced by loss of passive resistance of the soil surrounding the piles. The focus only lies on the location and direction of induced cracks. Two cases will be presented here:

- Strong foundation structure with a strong masonry wall.
- Strong foundation structure with a weak masonry wall.

In the upcoming analyses, an arbitrary healthy quay wall will be used as a baseline. These initial properties used in the analyses are summarised in table 5.6 below.

Property	**Value**	**Unit**
Strong masonry: Young's modulus	5000	N/mm^2
Strong masonry: Shear modulus	2000	N/mm^2
Strong masonry: Poisson's ratio	0.25	-
Strong masonry: Mass density	1800	kg/m^3
Strong masonry: Tensile strength	0.35	N/mm^2
Strong masonry: Tensile fracture energy	0.035	N/mm
Weak masonry: Young's modulus	3000	N/mm^2
Weak masonry: Shear modulus	1200	N/mm^2
Weak masonry: Poisson's ratio	0.25	-
Weak masonry: Mass density	1800	kg/m^3
Weak masonry: Tensile strength	0.21	N/mm^2
Weak masonry: Tensile fracture energy	0.021	N/mm
Pile: Young's modulus	6000	N/mm^2
Pile: Flexural strength	18	N/mm^2
Pile: Mass density	320	kg/m^3
Pile: Diameter	180	mm
Pile head connection	Hinged	-
Free height: Front pile	0	m
Free height: Middle pile	0	m
Free height: End pile	0	m
Sinkhole free height: Front pile	2.0	m
Sinkhole free height: Middle pile	1.5	m
Sinkhole free height: End pile	1.0	m

Table 5.6: Initial properties used in the upcoming analyses.

The same quay wall structure will be considered as the one mentioned in section 5.4. It is a section of 40 meters long, with free lateral and vertical movement at both sides. Movement in longitudinal direction, as well as rotation at the boundaries, are not permitted. Only half of the 40 meter wall is modelled due to the principle of symmetry (refer to figure 5.7). In the analyses, the quay wall structure will be assumed to be in a strong state. The model barely allows any form of soil removal if weak properties are assigned. Therefore, strong properties were assigned in order to study the effects of soil removal effectively. The following information will be extracted after each simulation:

- The damage/cracking patterns.
- The horizontal displacement of the masonry wall at ground surface level, at the location where the displacement is maximum. This location is indicated by the "X" in figure 5.7.
- The horizontal displacement of the masonry wall at the bottom of the masonry wall, at the same location.

- The vertical displacement of the masonry wall at ground surface level, at the same location.

The analyses will be performed with the following steps:

1. Lower the supporting soil at the two middle piles rows of the 40 meter long quay wall, and run the analysis. Removal must occur in pairs in order to retain symmetry.
2. Lower the supporting soil at the two neighboring pile rows (one at each side). Run the analysis.
3. Repeat step 2, until the model collapses.

Figure 5.38 illustrates how the model interprets non-uniform soil removal. Soil removal along a domain of 6 m in the model (or 12 m when accounting symmetry), results into the crack fields presented in figure 5.39. Each line represents the crack strain per element.

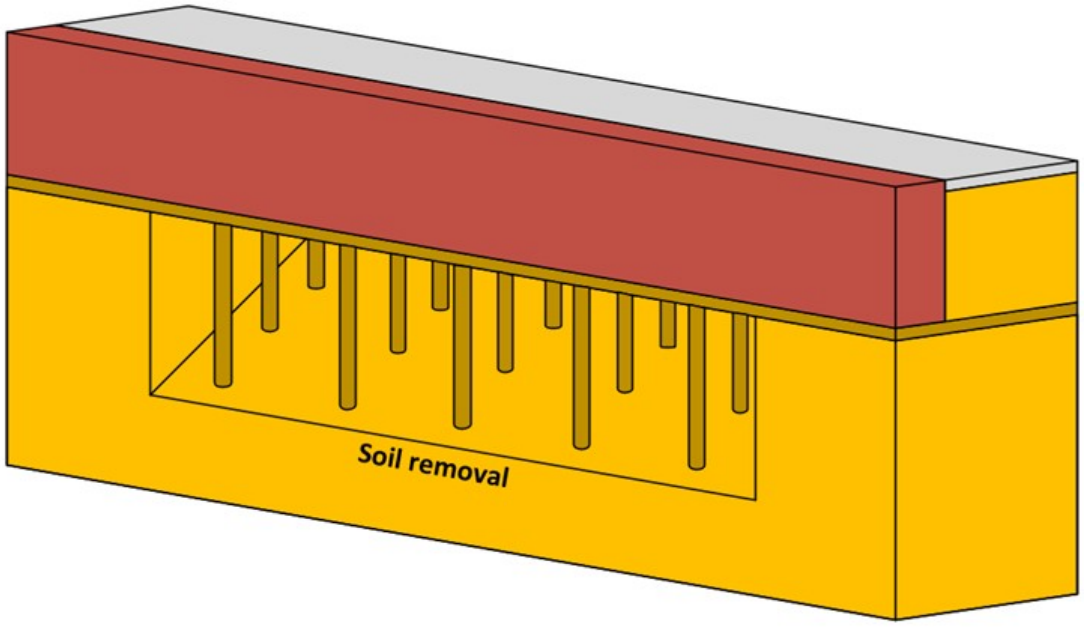

Figure 5.38: An illustration of the model interpretation of applying non-uniform soil removal.

Figure 5.39: Cracking patterns after applying soil removal along a domain of 6 m from the left.

According to the model output, increasing the domain of soil removal results into more or less the same cracking patterns shown in figure 5.39 above. These cracking patterns will be translated to generalised crack fields. In this case, only one crack field can be distinguished, which is located at the center of the domain where soil is removed (see figure 5.40 and 5.41).

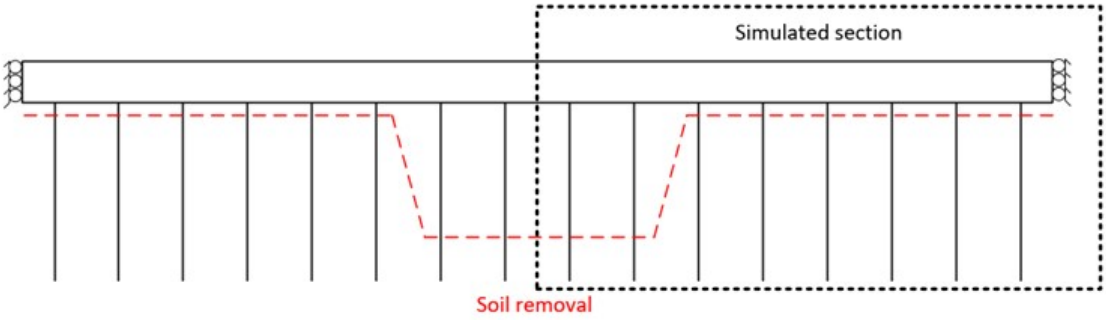

Figure 5.40: Soil removal modelling.

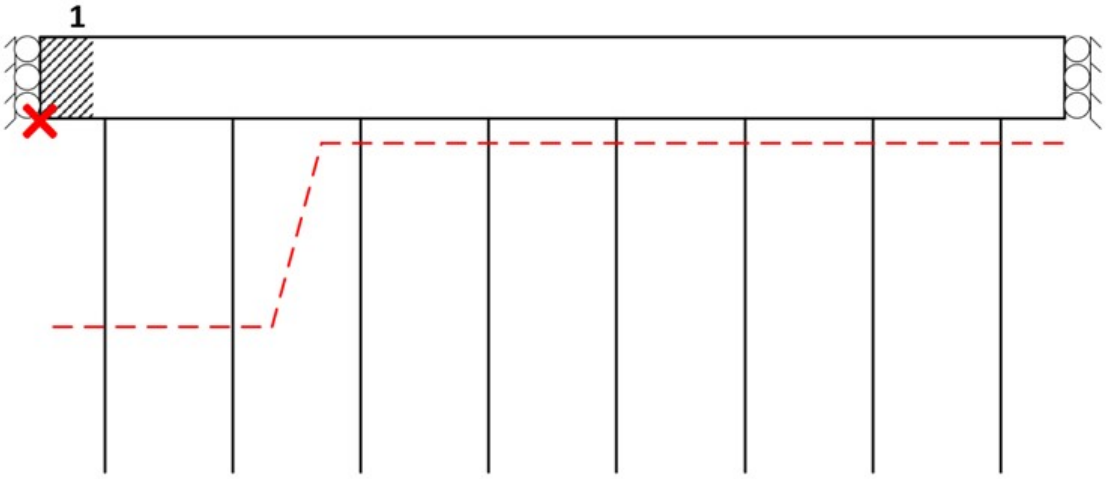

Figure 5.41: Schematic view of the cracking area induced by non-uniform soil removal. The point of maximum displacement (P.M.D.) is indicated by the red cross.

The effect of incrementally increasing the size of the area where soil is removed is presented in figures 5.42 (strong masonry) and 5.43 (weak masonry).

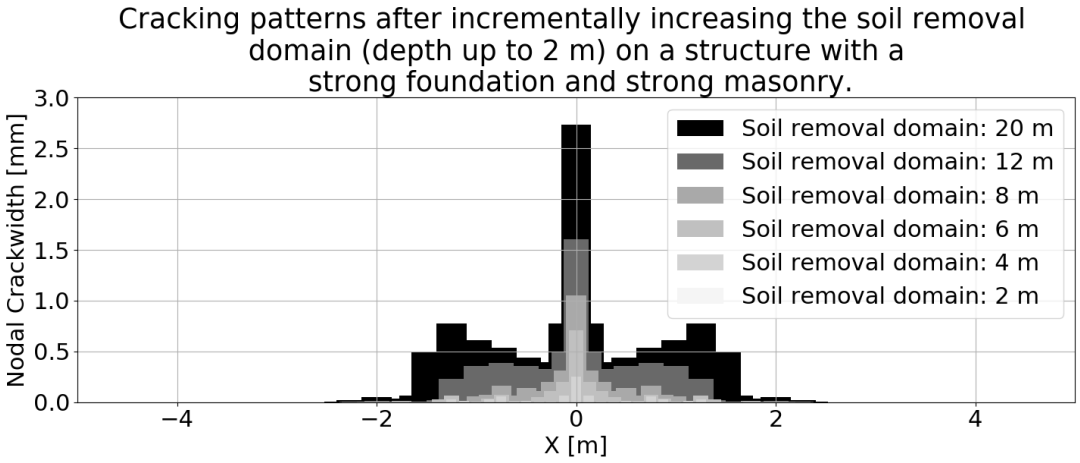

Figure 5.42: The effect of increasing the domain of soil removal around the piles on the nodal crack width values at the bottom nodes (healthy masonry combined with a healthy foundation structure).

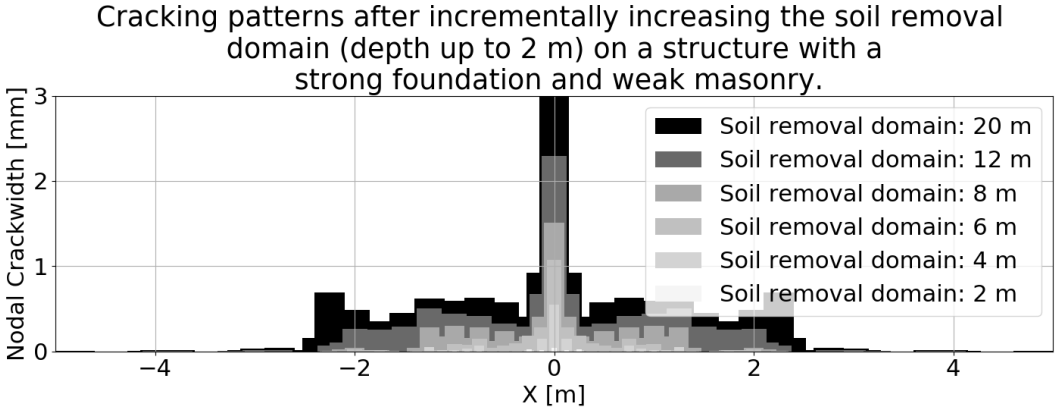

Figure 5.43: The effect of increasing the domain of soil removal around the piles on the nodal crack width values at the bottom nodes (degraded masonry combined with a healthy foundation structure).

Figures 5.42 and 5.43 show a single crack field with its maximum in the middle of the removed soil area (X = 0). The main conclusion is that increasing the domain of soil removal results into larger crack width values, and a larger spread of the crack area. The model output shows that these cracks have a mostly out-of-plane character, more so than the primary crack field induced by pile removal. The crack development at the point of maximum displacement in both cases can be compared (see figure 5.44). Both cross-sections have an in-plane component due to the higher crack values being present at the lower side of the wall. However, the in-plane component in the case of soil removal is less pronounced compared to the case of pile removal.

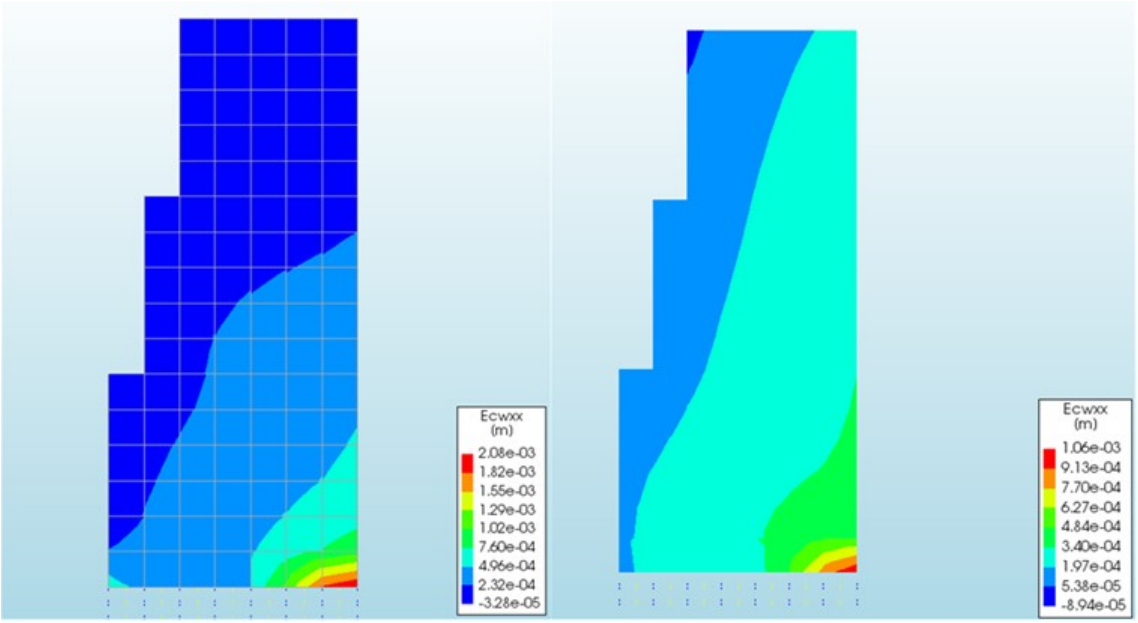

Figure 5.44: Crack development at P.M.D. after pile removal (left) and soil removal (right).

The cause of cracks can be summarised as follows:

- The primary crack field has an in-plane component, albeit less pronounced compared to pile removal, due to a reduction in vertical soil capacity. The cause of the in-plane component can be explained with the idea that lower soil levels lead to less pile shaft resistance according to the model code.
- The primary crack field has an out-of-plane component. The masonry wall bulges towards the canal, due to a lack of horizontal bearing capacity caused by a reduction of passive soil resistance.

In figure 5.45, the generalised cracking patterns are presented in 3D.

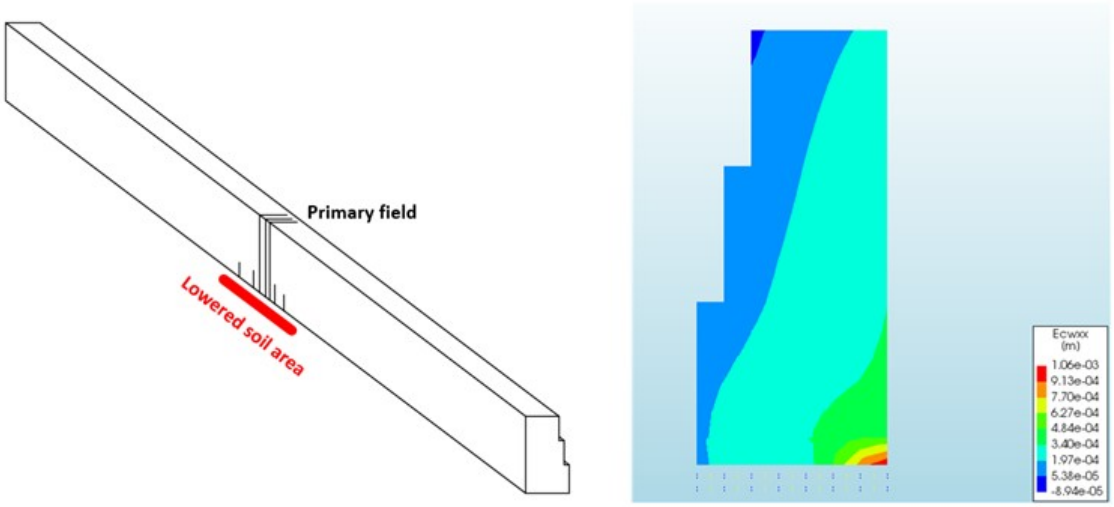

Figure 5.45: Left) Generalised cracking patterns due to soil removal — Right) Crack development in the middle of the primary crack field.

5.5.2. Displacement patterns

This subsection presents and discusses the displacement patterns induced by a reduction of passive soil resistance. Evidently, the largest displacements are found at the location where the soil has been lowered. The displacement output in that location will therefore be presented. The results have been obtained from the same simulations from which the cracking patterns have been determined. Therefore, the same model input has been used, which is given in table 5.6.

The graph in figure 5.46 displays the stance of the quay wall after incrementally increasing the domain in which the soil is removed.

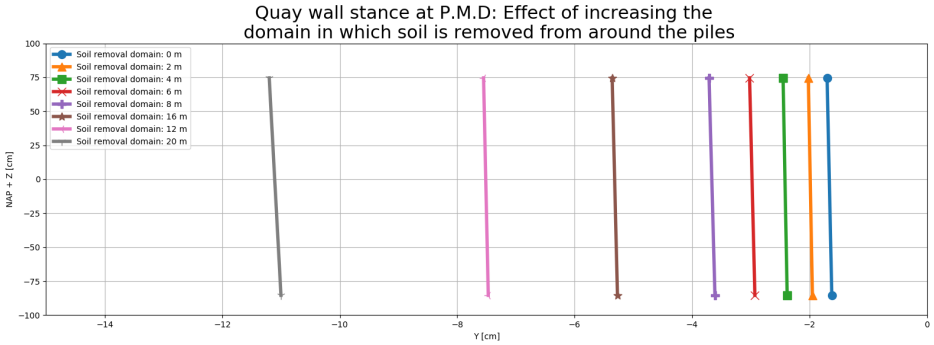

Figure 5.46: Quay wall stance at the P.M.D. after incrementally increasing the domain of soil removal.

A linear increase of the size of the area of removed soil causes an exponential increase in horizontal displacements towards the canal. The tilt of the quay wall is unaffected when accounting soil removal alone.

5.5.3. Visible cracks

This subsection is dedicated to providing an indication of masonry wall cracking visible to the naked eye. The previously mentioned disclaimer will be repeated: It is impossible to classify the simulation results as objective reality, but at least it gives a rough indication on how much a quay wall structure is able to degrade before any outward damage is visible.

Two cases will be presented here. One where the quality of the foundation and the masonry is strong. The other where the quality of the foundation is strong, but the quality of the masonry is weak. Figure 5.47 presents the onset of cracking in the case of a strong masonry wall.

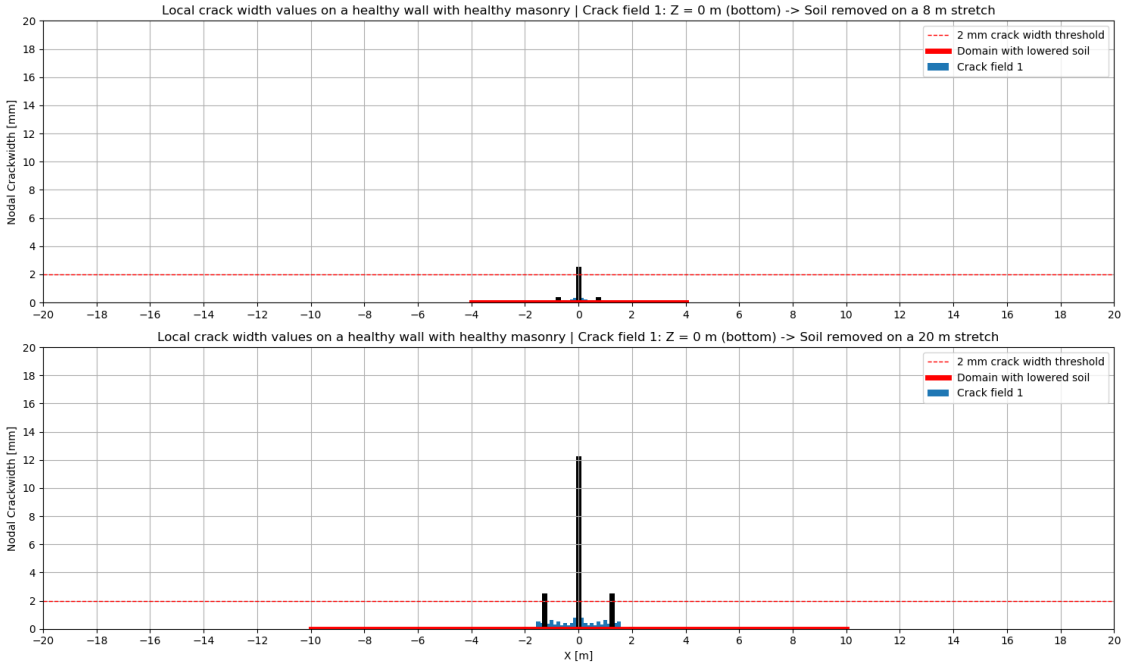

Figure 5.47: The onset of cracking when removing up to two meters of soil locally. Simulations have been performed using strong masonry properties. Full results can be found in appendix C.1

Figure 5.48 presents the onset of cracking in the case of a weak masonry wall.

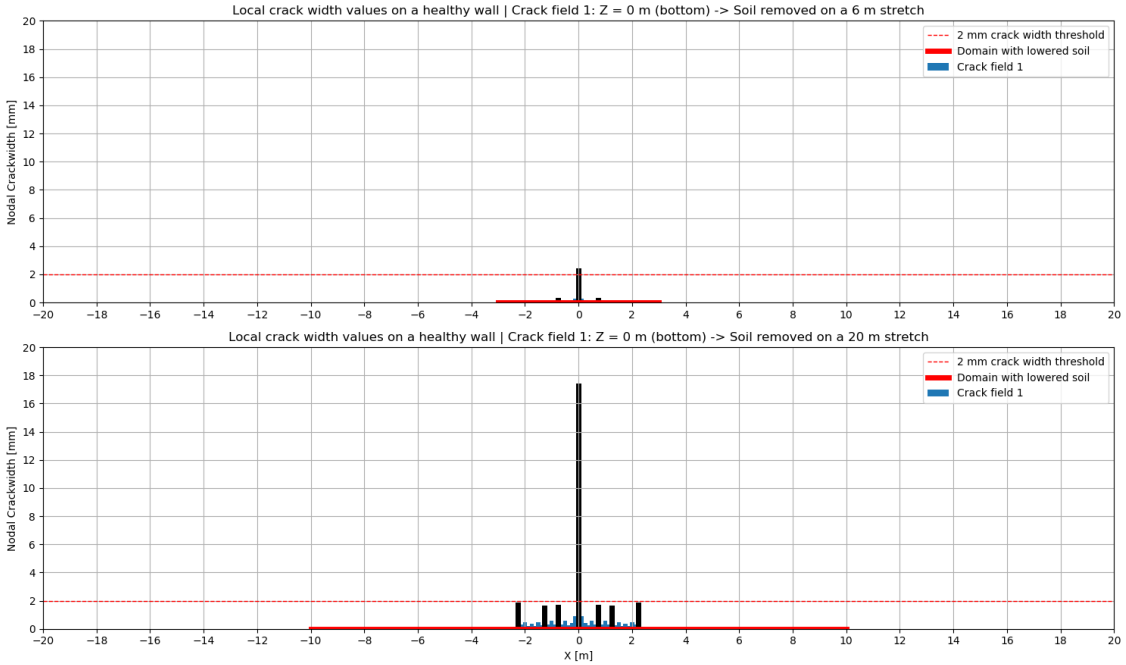

Figure 5.48: The onset of cracking when removing up to two meters of soil locally. Simulations have been performed using weak masonry properties. Full results can be found in appendix C.1

Cracking patterns remain the same when comparing both cases. As soil removal develops, weak masonry is more likely to show damage patterns sooner. The corresponding visible cracks are presented in figure 5.49 and 5.50 below. The mean water table is indicated by the blue line running through Z = 0.85 m.

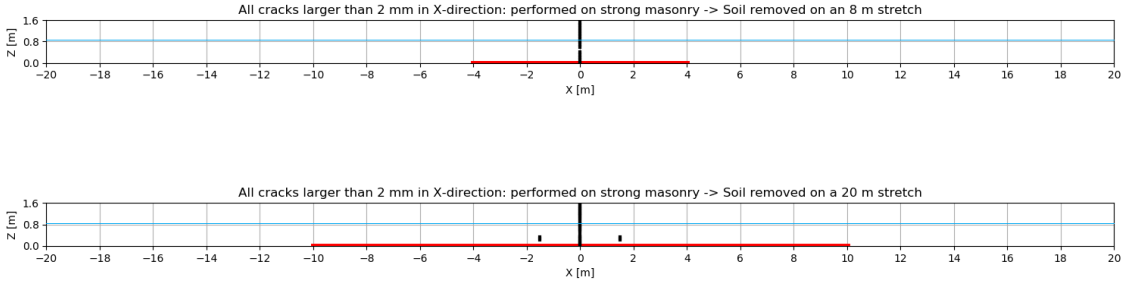

Figure 5.49: Corresponding cracking patterns at the onset of cracking (strong masonry).

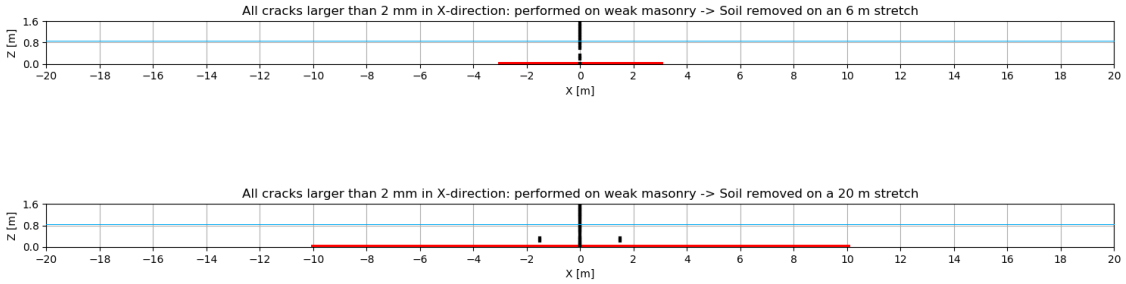

Figure 5.50: Corresponding cracking patterns at the onset of cracking (weak masonry).

The damage patterns remain the same regardless of the quality of the masonry. Figure 5.51 shows the generalised crack progression when the pile embedding is lowered locally.

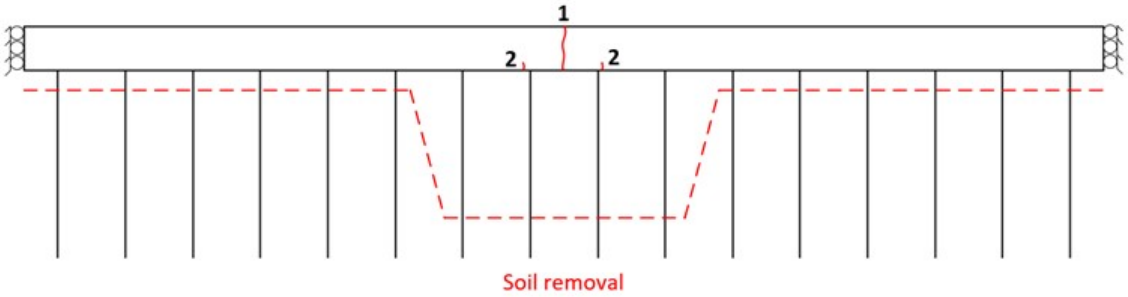

Figure 5.51: Crack progression caused by the incremental increase of the domain of soil removal.

5.6. General uniformity

In this section, simulations will be ran with complete uniformity over the entire length. The purpose is to document and to compare the effect each parameter has on the general displacement of the entire quay wall structure. Since the quay wall has uniform properties, there will be no induced cracks. For this reason, the masonry properties will be ignored in this section. Fixed boundaries will also be ignored, as they cause non-uniformity. By excluding these parameters, the following relevant parameters remain customisable in the model code:

- Wood stiffness
- Pile diameter
- Pile embedding
- Pile head connection
- Load behind the masonry
- Load behind the foundation

The base case will be used as a reference case, its properties are mentioned in section 5.3. In short, the base case is the case where no degradation has taken place yet. In other words, the most favourable parameters have been assigned. The listed parameters will be altered one at the time, after which the results will be compared to the base case. Notice that the strength parameter of wood has been excluded, as it has no impact on displacements in this case.

5.6.1. Pile degradation

Pile degradation is comprised of a reduction in stiffness and diameter. Reducing the wood stiffness and the pile diameter on a newly built quay wall has the following effect according to figures 5.52 and 5.53.

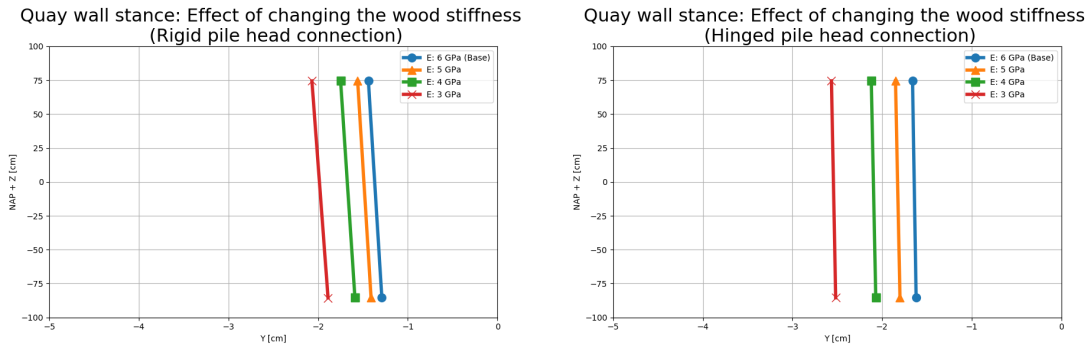

Figure 5.52: Stance of a strong uniform quay wall. Variable: Wood Young's Modulus. Comparison: Rigid pile head connection and hinged pile head connection.

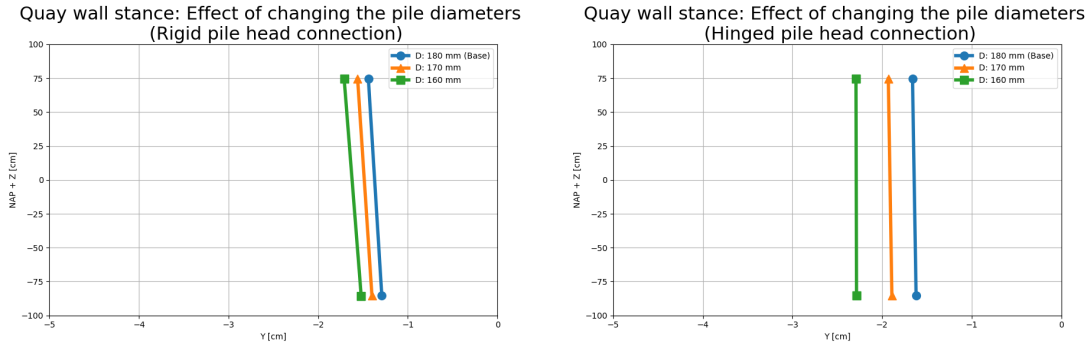

Figure 5.53: Stance of a strong uniform quay wall. Variable: Pile diameter. Comparison: Rigid pile head connection and hinged pile head connection.

In reality, a reduction in diameter and stiffness occur simultaneously. The combined effect is presented in figure 5.54.

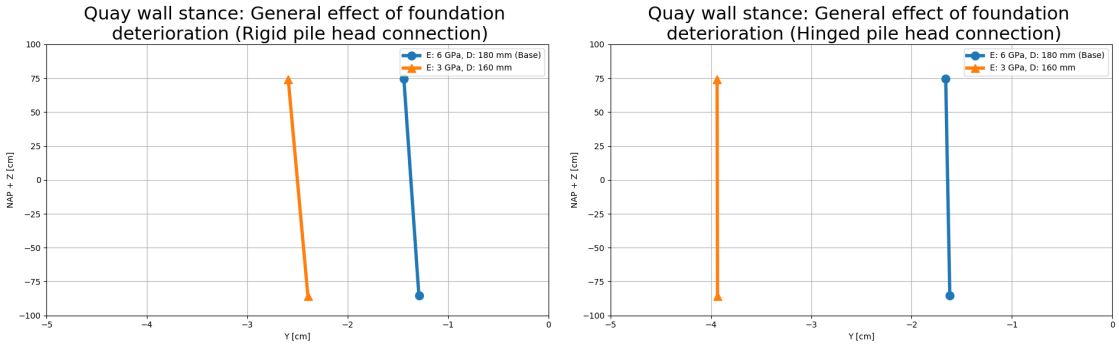

Figure 5.54: Stance of a strong uniform quay wall. Variable: Pile diameter and Young's Modulus. Comparison: Rigid pile head connection and hinged pile head connection.

If only pile reduction is taken into account, the entire masonry wall deflects less than 2.5 cm towards the water in the most unfavourable case (hinged pile head connection). In the same case, the vertical settlement is no more than 3 mm.

5.6.2. Pile embedding

In the model code, it is made possible to alter the soil level around the foundation piles. In the case of uniformly reducing the embedding of piles, four cases will be presented:

Cases	Free height: front pile	Free height: middle pile	Free height: end pile
Case 1	0 m	0 m	0 m
Case 2	0.5 m	0 m	0 m
Case 3	1.0 m	0.5 m	0 m
Case 4	1.5 m	1.0 m	0.5 m

Table 5.7: Soil reduction properties.

Reducing the soil level around the piles on a newly built quay wall has the following effect according to figure 5.55.

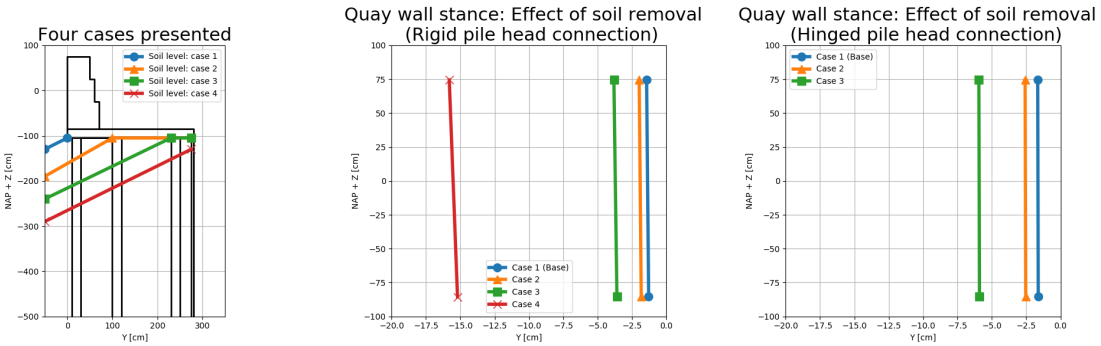

Figure 5.55: Stance of a strong uniform quay wall. Variable: Pile embedding. Comparison: Rigid pile head connection and hinged pile head connection.

Horizontal displacement towards the canal quickly develops as more soil is washed away. In the case of a hinged pile head connection, the 4th case leads to failure of the model. Horizontal displacements due to soil removal reach higher magnitudes compared to displacements due to pile degradation. However, the vertical settlement due to soil removal barely reaches 1 mm. Meaning that the effect of pile degradation on vertical settlement is larger. It has already been established in sections 5.4 and 5.5 that pile capacity reduction has the largest impact on the vertical settlement of the quay wall according to the model. It has also been established that the removal of pile embedding does not impact the vertical settlement of the wall as much according to the model.

As a final point, notice that the type of connection in the pile head has an impact on the displacement of the wall. A hinged connection causes about 1.5x more displacement compared to a rigid connection.

5.6.3. Adding surcharge

Adding uniform surcharge can be done in two ways according to the model code:

1. Adding surcharge directly behind the masonry wall (denoted by I).
2. Adding surcharge behind the foundation structure (denoted by II).

Its effect on the masonry wall is presented in figure 5.56.

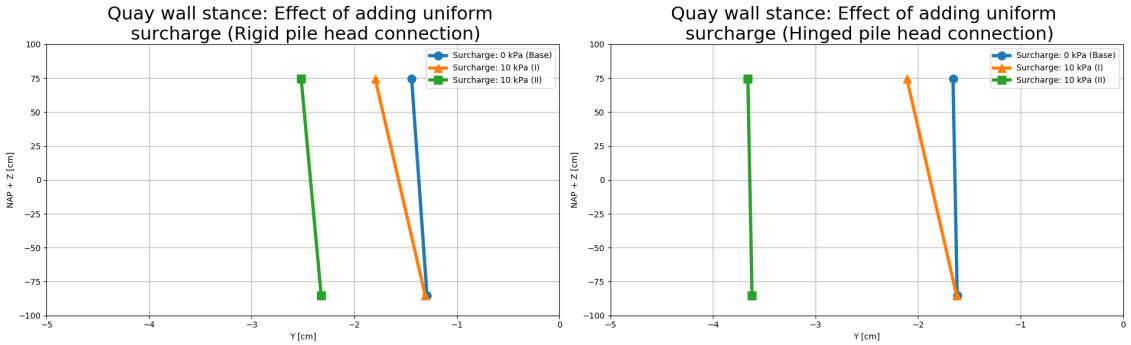

Figure 5.56: Stance of a strong uniform quay wall. Variable: Surcharge. Comparison: Rigid pile head connection and hinged pile head connection.

It has already been verified in section 4.4 that applying a load directly behind the wall does not contribute to any extra horizontal movement of the wall in the model code. The same results are visible in figure 5.56. Applying the surcharge behind the foundation does lead to larger horizontal movement. In the most unfavourable case, the net horizontal movement is approximately 2.5 cm when 10 kPa of surcharge is applied. However, this is more than three times the average load of a loaded truck. Therefore, adding a surcharge normally would give little direct contribution to the displacement of the quay wall. However, adding a surcharge may have a big indirect influence on the status of the quay wall, as it promotes faster degradation of the quay wall structure. This aspect is outside of the scope of this thesis, however.

5.7. Summary

Local pile failure is represented by a removal of a selection of piles from the model. In any case, two main crack areas will start to develop. These areas are referred to as the primary and the secondary crack field. The reasoning behind these names has to do with the likely order of appearance. The two crack fields are schematically presented in figure 5.57 below.

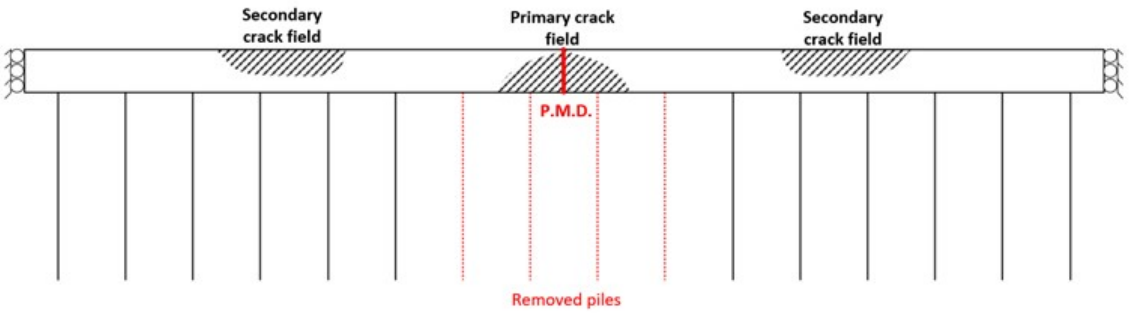

Figure 5.57: Quay wall schematisation with both crack fields induced by pile removal, including the display of the subsequent point of maximum displacement (P.M.D.).

The primary crack field has an in-plane and an out-of-plane component, while the secondary crack field is mostly in-plane. Although both crack fields appear around the area with minimal pile capacity, the crack orientations may vary depending on which piles are defected, especially in the secondary crack field. The primary crack field always appears sooner after running the

simulations. However, the onset of visibility of the primary crack does depend on the water table level (in case of assessing quay walls with the naked eye). Two cases will be presented:

1. Pile row removal: entire rows will be selected and deleted. The consequence on the masonry wall (crack-wise and displacement-wise) is schematically presented in figure 5.58.

2. Front pile removal: only front piles will be selected and deleted. The consequence on the masonry wall (crack-wise and displacement-wise) is schematically presented in figure 5.59.

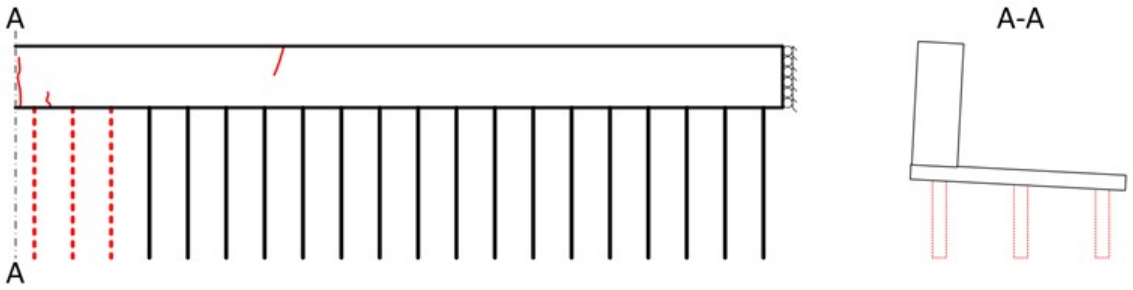

Figure 5.58: Schematisation of cracks induced by pile row removal and the tilt of the wall which follows as a consequence.

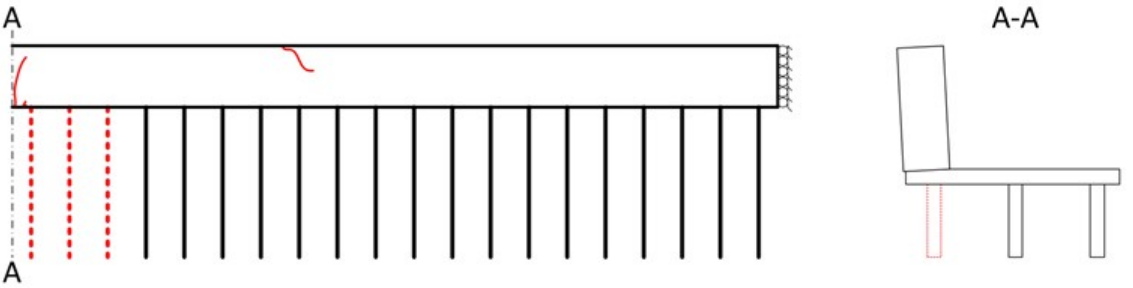

Figure 5.59: Schematisation of cracks induced by front pile removal and the tilt of the wall which follows as a consequence.

Removal of entire rows result into a slight backwards tilt of the wall, while removal of front piles result into a frontward tilt of the wall. These tilts are most pronounced at the P.M.D., while it decreases at locations situated further from the defected piles. This non-uniform tilting might be deciding factor of the orientation of the secondary cracks as it induces torsion in the wall. Notice that the secondary crack orientations are opposed when comparing both cases, just like the tilt orientation of the masonry wall.

Several parameters have been altered as well, in order to document the effect that each parameter has on the behaviour of the quay wall structure. The effect of each parameter is summarised in table 5.8 below.

Property	Cracking patterns	Displacement patterns
Pile removal	Removing more pile rows results into a larger cracking area in general, with larger crack width values. The crack width is largest at the bottom of the wall at the P.M.D., although it gradually decreases as the crack progresses upwards. Also, the secondary cracking area moves away from the point of maximum displacement as more piles are removed.	More pile removal results into larger displacements both laterally and vertically. The backwards tilt increases as more piles rows are removed in the case of total pile removal. The frontward tilt increases as more front piles are removed.
Pile and foundation degradation	Reducing the quality of the foundation structure leads mainly to a larger crack spread in both areas. The most significant increase in crack width occurs in the primary crack area, although cracks also develop further in the secondary area.	Bad foundation quality has a limited effect on the vertical displacement. It has a more significant effect on the horizontal displacement. The tilt of the quay wall is generally unaffected.
Soil bedding reduction	Reducing the soil bedding universally leads to smaller cracks.	The displacements at the point of maximum displacement is heavily affected when the soil bedding is decreased. The significant displacements occur mainly horizontally.
Masonry degradation	A lower quality in masonry results the secondary crack area to move towards the point of maximum displacement. Crack width also increases.	Barely an effect at all.

Table 5.8: Consequences of changing the parameters in the model code on the behaviour of the quay wall structure

Generally, altering the quality of the remaining foundation piles does not change much about the cracks in the wall. Changes in the magnitude of cracks are more significant when piles are removed from the model. However, altering the foundation quality does impact the absolute displacement of the wall significantly.

According to the model, the onset of cracks of at least 2 mm happens as follows:

- Pile row removal: on an already weak quay wall, the first primary crack of this magnitude occurs after removal of 2 pile rows, while the first secondary of this magnitude crack occurs after removal of 6 pile rows. When 6 pile rows are removed, the structure is on the brink of collapse. Healthy quay walls tolerate more pile damage before these cracks are induced.

- Front pile removal: on an already weak quay wall, the first primary crack of this magnitude occurs after removal of 6 front piles, while the first secondary crack of this magnitude occurs after removal of 12 pile rows. When 20 pile rows are removed, the structure is on the brink of collapse. Healthy quay walls tolerate more pile damage before these cracks are induced.
- Changing the quality of the remaining foundation piles results into little change when it comes to the formation of large cracks.

Local soil removal is represented by lowering the soil level around a selection of foundation piles (up to two meters). In this case, only one pronounced crack area forms. This crack field is schematically presented in figure 5.60 below.

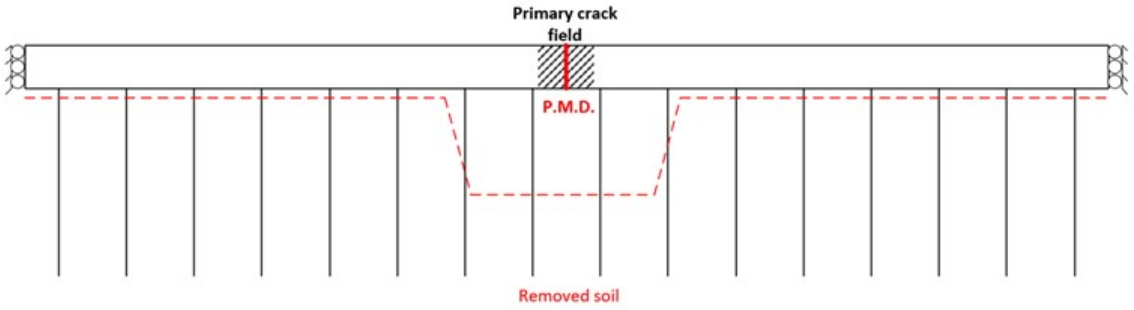

Figure 5.60: Quay wall schematisation with the crack field induced by local soil removal, including the display of the subsequent point of maximum displacement (P.M.D.).

The induced crack field has a mostly out-of-plane character. The crack fields appears around the area with minimal pile embedding. The consequence of soil removal on the masonry wall is schematically presented in figure 5.61.

Figure 5.61: Schematisation of cracks induced by soil removal and the tilt of the wall which follows as a consequence.

The tilt of the wall is generally unaffected by soil removal according to the model. The primary crack occurs at the same location as the one induced by pile removal. The main difference is that in the case of pile removal, the crack width decreases as it progresses vertically. While in the case of soil removal, the crack width stays consistent over the entire height of the wall. Displacements of the quay wall structure are relatively high in horizontal direction as more soil is removed from around the piles. The first 2 mm crack is induced when soil is removed on an 8 m stretch, with a depth of up to two meters from the pile head.

Modelling the quay wall with uniform conditions results in the following conclusions:

- Horizontal displacement is caused by both pile degradation and soil removal. However, the contribution of soil removal has the upper hand.
- Pile degradation causes more vertical settlement compared to soil removal.
- The type of pile head connection says much about the ability of the quay wall to displace. A hinged connection consistently causes about 1.5x more displacement compared to a rigid connection.
- Adding surcharge does not contribute much to the displacement of the wall directly.

Notice that an increase in local soil removal leads to an increase of the crack width. In the case of pile removal, decreasing the universal soil level leads to a decrease of the primary crack width. This sounds paradoxical, but it must be noted that the primary cracks in both cases are induced by different processes. Also, a uniform change in pile embedding does not cause cracking, while a local change does.

6

Qualitative Comparison Study

This chapter focuses on comparing the results in this thesis to other findings and cases. First of all, the results will be qualitatively compared to other performed numerical studies. Second of all, it will be attempted to relate the findings to real-life cases.

6.1. Other numerical studies

This research has focused on modelling a historical quay wall in three dimensions. Other numerical studies have already been performed on historical quay walls, where the focus has been put on two-dimensional modelling. Compared to 2D, the main advantage of 3D modelling is the fact that in-plane and out-of-plane behaviour can be simultaneously produced while applying non-uniform conditions. This includes both displacements and cracking patterns.

This section will focus on comparing the effect of 3D modelling to 2D modelling on the cracking patterns of the masonry wall. Two researches have been obtained which have performed two-dimensional analyses on historical quay walls. In this case, the important difference between the two is that one has used the Engineering Masonry Model (Grund, 2020) while the other has used the Total Strain Cracking Model (Voortman, 2020) to describe masonry. Cracks were only induced in in-plane analyses. The main cracking patterns are presented in figure 6.1 and 6.2 below.

Figure 6.1: Example of cracking patterns after inducing incrementally increasing in-plane loads, followed by local pile failure (Voortman, 2020). The used material model is the Total Strain Cracking Model. The center of the beam is at the right hand side.

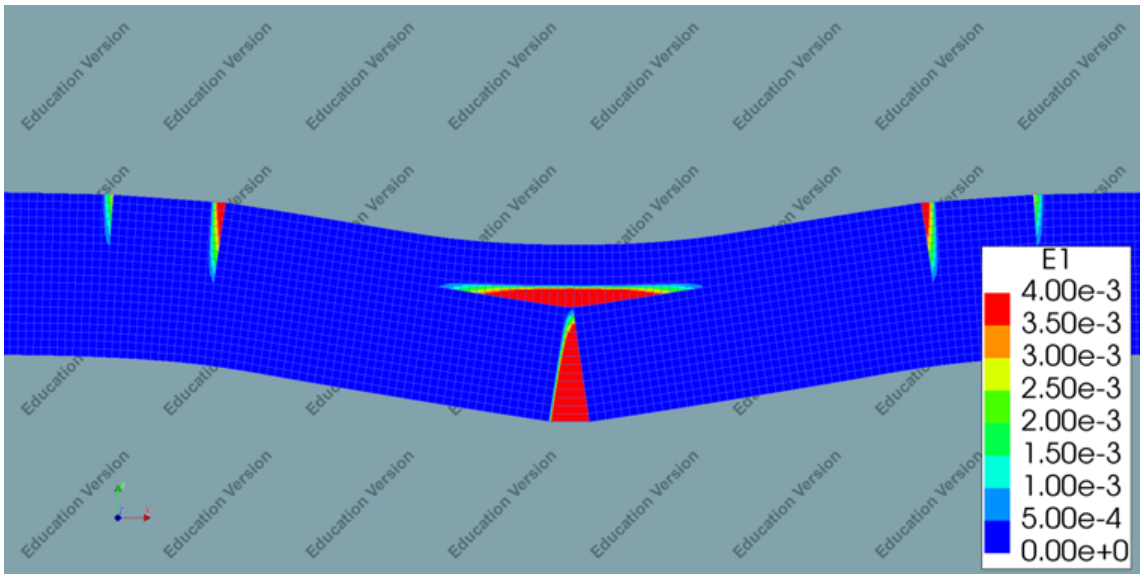

Figure 6.2: Example of cracking patterns after inducing incrementally increasing in-plane Gaussian deformations (Grund, 2020). The used material model is the Engineering Masonry Model.

It is important to address the used modelling prerequisites before comparing the cracking patterns to the ones produced in this research. In both studies, incrementally increasing load steps have been induced. Therefore, the results are progressive crack developments as a result of continuously increasing loads. In this research, only the permanent loads have been applied when it comes to studying cracking patterns. Also, the cracks in the provided research are all induced as a result of in-plane loading. With this in mind, the following similarities can be distinguished when comparing these results to the results in this research:

- The primary and secondary crack fields appear in all cases, with the primary field being significantly more pronounced.
- The primary crack tends to deviate sideways. This effect is also produced in this research after removing front piles only.

The following differences can also be distinguished:

- In this research, the primary crack does not progress sideways after removing entire pile rows.
- In the provided examples, the secondary cracks generally do not progress diagonally. This indicates the absence of torsion in those cases.

A striking finding is the sideways deviation of the primary crack in the provided examples. Given that these examples are two-dimensional, each pile should therefore represent an entire row. However, removing entire rows do not result into this crack progression according to the results produced in this research. These crack progressions are more resembling to those produced after removing the front piles only. One must keep in mind however, that the cracks produced in the example cases have been induced by incremental increases of loads, while the ones produced in this thesis are induced by permanent loads only (represented by a single load

step).

However, based on these findings, the most important limitation of 2D modelling is its inability to produce torsional behaviour. In this research, torsion is induced by non-uniform pile removal resulting into uneven tilting across the masonry wall.

6.2. Real-life cases

It is difficult to validate the results against real-life cases. In many cases, multiple factors are simultaneously at play which cause damage patterns. In this section, it is attempted to relate real-life cases to the crack and displacement patterns obtained in this research.

6.2.1. Nieuwe Herengracht

The quay wall at "Nieuwe Herengracht", on which the model dimensions are based, is known to be severely damaged. Several photographs have been taken of the structure, of which the most telling ones are presented here. The location of the photographs is indicated in figure 6.3.

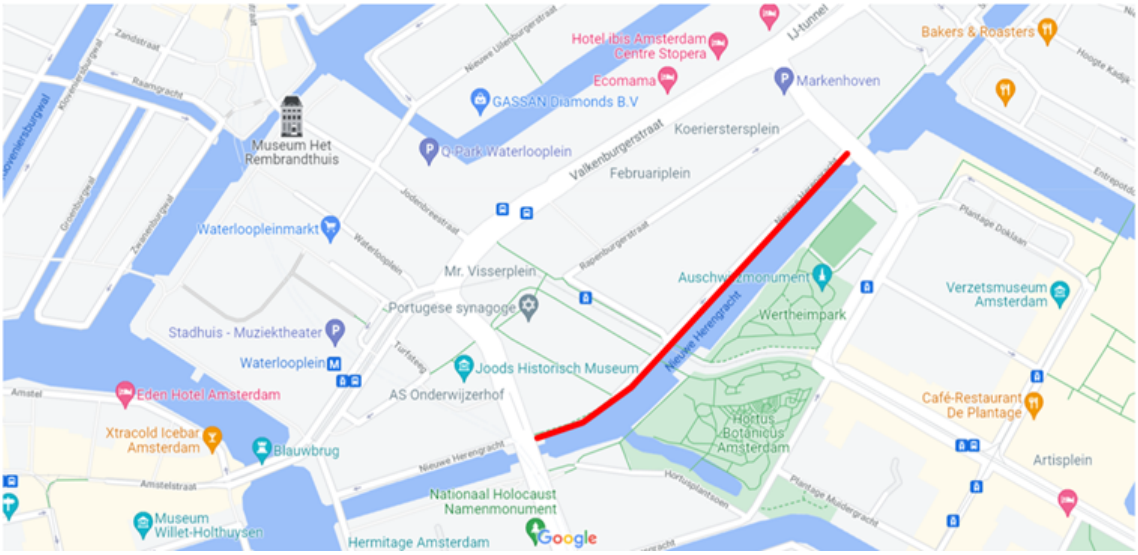

Figure 6.3: Location of the quay wall at "Nieuwe Herengracht", where the photographs have been taken.

In chapter 3, it is mentioned that critical damage at this quay wall is found at the foundation level. In the quay wall section indicated in figure 6.3, several damage patterns in the masonry have been observed. The photos are presented in order of location, starting from the North side, in appendix D. Some of them are presented below.

Figure 6.4: Photo of the quay wall at "Nieuwe Herengracht". Quay shows movement towards the water as the masonry sticks out at the dilation joint.

Notice that the masonry slides towards the water at the dilation joint. This effect has been incorporated into the model by applying a free sliding boundary condition.

Figure 6.5: Side view of the quay wall at "Nieuwe Herengracht". Masonry wall shows general forward tilting.

The photo in figure 6.5 shows the stance of the quay wall section. It is clear that the masonry wall shows a forward tilt. This is likely result of either numerous damaged front piles, or numerous front piles experiencing extreme settlements. However, other not-mentioned causes cannot be excluded. It is also visible that the tilt towards the water increases at locations further away from the dilation joint. There are two likely explanations:

1. The foundation quality at the dilation joint is comparatively higher than the quality further down the road.

2. There is sliding friction present at the dilation joint. In the model, it is assumed that the quay wall is able to slide freely along this joint. This implies that this assumption is too lenient when it comes to sliding. The dilation joint should therefore have some friction capacity.

Figure 6.6: Photo of the quay wall at "Nieuwe Herengracht". Vertical crack along with gaps between individual bricks at the lower side.

Multiple photos, particularly this one, shows a vertical crack along with gaps between individual bricks at the lower side. The vertical crack seems to get thinner as it progresses upwards. This might indicate an example of a primary crack. Indirectly, it might indicate a concentrated field of severely damaged piles, resulting to this crack.

Figure 6.7: Photo of the quay wall at "Nieuwe Herengracht". Shows the other side of the quay wall with damaged bricks and what appears to be a relatively thin diagonal crack moving up to the right, at the right-hand side of the dilation joint.

Figure 6.7 shows the Southern end of the quay wall. At this location, the masonry wall slides along the dilation joint (clearer photos found in appendix D). At the right-hand side, there appears to be a thin diagonal crack running upwards to the right. Given the forward tilt of the masonry wall, it might be the result of torsional loads within the wall. It could therefore be an example of a secondary crack.

Given that it is not exactly known what the pile quality is at each location, it is not easy to draw definitive conclusions. However, the crack orientations do match the cracking patterns produced by the finite element model, also in accordance to the perceived displacement (notably the forward tilt) of the masonry wall.

6.2.2. Grimburgwal

According to the case report of the Grimburgwal, the main cause of collapse was "the horizontal bending of the piles as a result of a locally deepening of the canal followed by breaking of the quay" (Korff et al., 2020). This will be referred to as "soil removal from around the piles" according to the terminology used in this thesis. This is a particular case, in which the masonry started showing cracks at a relatively late stage. However, horizontal and vertical displacements have been taking place. Figure 6.8 shows recent vertical settlement data obtained through remote sensing (satellites), up until the moment before collapse. The assumption that horizontal movement has taken place is deduced from the fact that the piles have fractured due to horizontal bending.

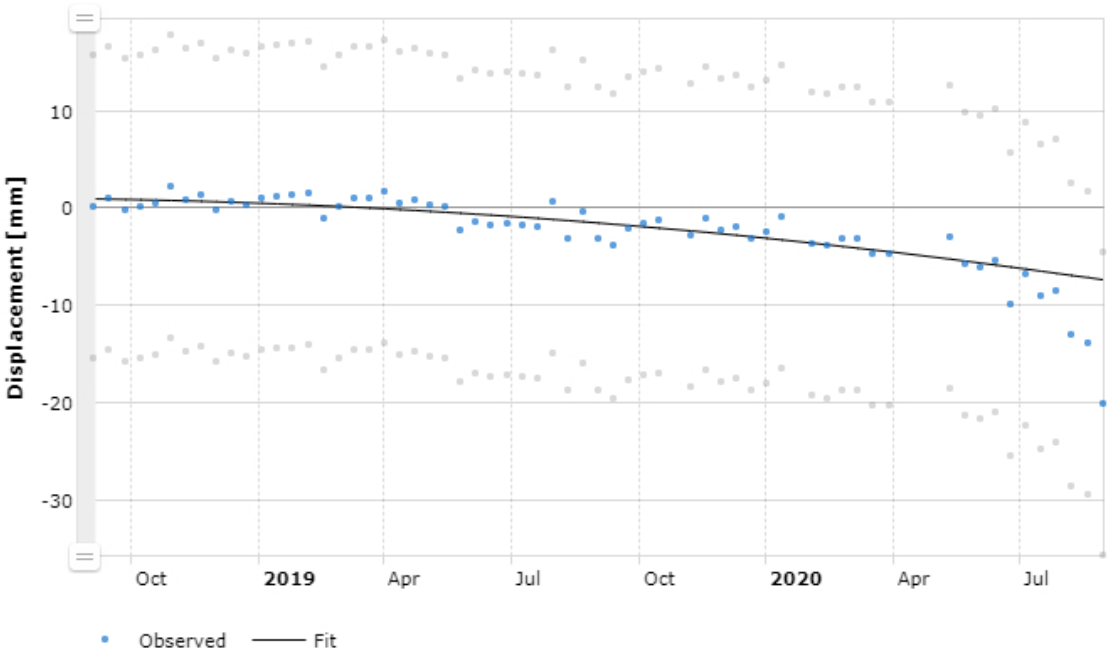

Figure 6.8: SkyGeo settlement data sample at the Grimburgwal; InSAR data ©SkyGeo.

The movement of the quay wall and the subsequent cracking patterns are shown in figure 6.9 and 6.10.

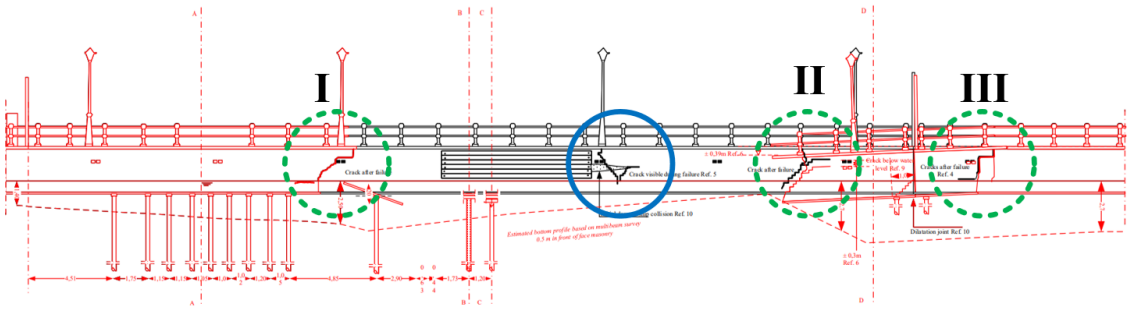

Figure 6.9: Cracks which appeared during and after the collapse of the Grimburgwal. The crack visible during failure is indicated by the blue circle. The cracks visible after failure are indicated by the green dotted circles (Korff et al., 2020).

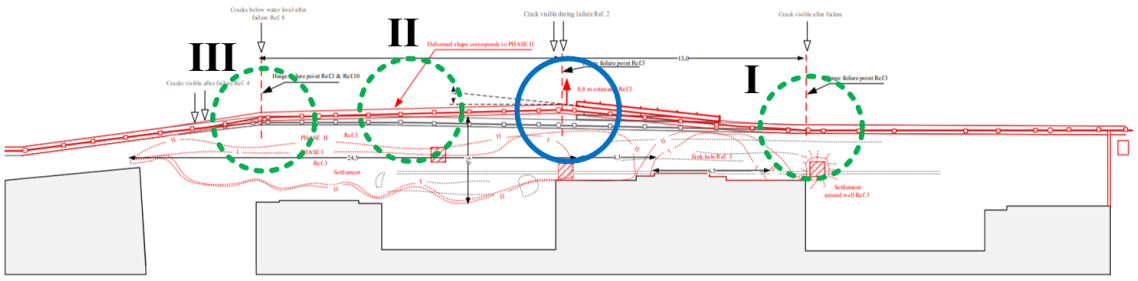

Figure 6.10: Top view of the Grimburgwal during failure. The same visible crack during failure is indicated by the blue circle. The cracks visible after failure are indicated by the green dotted circles (Korff et al., 2020).

During failure, the visible cracks appear at the location where the wall bulges maximally towards the water (indicated by the blue circle). These cracks appear to have progressed from the bottom side, this assumption is made given that the crack on the right does not reach the top. Both cracks appear to progress upwards and diagonally diverge from each other. If a relation is drawn between these cracks to the findings in this thesis, it is presumed that these could be classified as primary cracks. These primary cracks mostly resemble the primary cracks produced in the simulations in which the front piles have been removed. To clarify, the cracking patterns after removal of front piles are presented in figure 6.11 below, which can also be found in figure 5.31. The resemblance can be found at the crack indicated by the number "1".

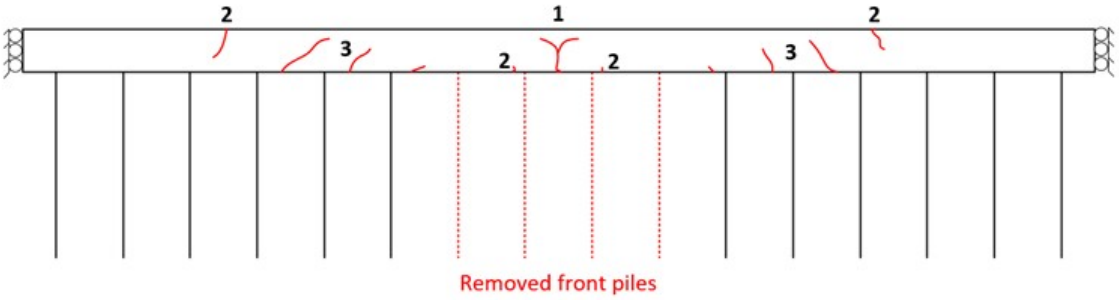

Figure 6.11: Crack progression caused by the incremental removal of front piles only.

This implies that the masonry wall of the Grimburgwal case must have experienced forward tilting, as it is required to form these cracks according to the results. This is the case, as the stance of the quay wall before failure is presented in figure 6.12. However, it must be pointed out that although the masonry wall tilts forwardly, it is not a result of broken piles in this case. It seems that it is a result of uneven settlements of the piles, in which the front piles have experienced the most settlement. Another observation is that in this case, the removal of soil has resulted in large settlements of piles (particularly the front row). According to the finite element model, the vertical settlements of piles are minimal when soil support is reduced, which in turn causes a different primary crack progression. Using the Grimburgwal case as a reference, it can be concluded that the finite element model works too favourably when it comes to vertical soil support.

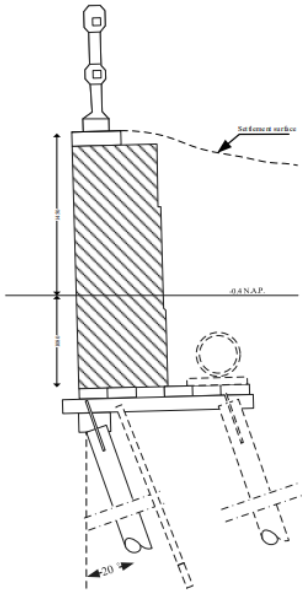

Figure 6.12: The stance of the quay wall at Grimburgwal according to a diver's interview (Korff et al., 2020).

At both sides of these "primary cracks", other cracks appeared as the wall collapsed (green dotted circles). These cracks have a diagonal progression, all of which point to the same direction. Because of their diagonal nature, it can be deduced that these cracks must be a result of torsion within the wall. It makes sense given the forward tilt of the wall before collapse relative to its neighbours. The crack indicated by "I" matches the expected torsional crack direction according to the output of the finite element model. However, the cracks indicated by "II" and "III" go opposite of the expected direction. This might indicate that they are a result of something else than torsion, which has not been incorporated into the model.

One caveat in comparing the results with the Grimburgwal case is the fact that the Grimburgwal quay wall has a different setup than the one used in the finite element model. It has different wall dimensions and a smaller number of pile rows. It is not known whether these differences affect the behaviour of the model in a significant way.

6.2.3. Conclusions

It is difficult to validate the model against real-life cases, as factors leading to a certain behaviour may be at play which are unknown or not incorporated into the model. However, some trends can be observed in real-life cases that closely match the output of the model when it comes to cracking patterns. Despite that it is practically impossible to predict every single crack accurately, the model still shows some degree of validity when it comes to predicting cracking patterns as a result of in-plane and out-of-plane displacements.

The "Nieuwe Herengracht" case is known for experiencing lots of damage at the foundation level (including the piles). Comparing the model output to the "Nieuwe Herengracht" yields the following conclusions:

- The quay wall experiences sliding at both boundaries (dilation joints). The model assumption is therefore correct in this case. The horizontal displacement of the wall

(towards the canal) is more pronounced at location further away from the dilation joints. The cause could perhaps lie with the idea that sliding friction is present at these dilation joints to some degree.

- The quay wall contains several vertical cracks throughout its domain, most of which progress to the top, in which the lower part shows a larger gap (larger crack width). This corresponds with the primary cracks produced by the finite element model, and is likely a result of a combination between out-of-plane and in-plane movement (both of which are present according to the photos).
- Close to the southern dilation joint, a relatively thin diagonal crack has been identified. This crack corresponds with the torsional cracks produced by the finite element model. It also progresses in the predicted direction given the forward tilt of the wall.

The Grimburgwal case is known for having experienced soil removal from around the piles. This is also proven to be the indirect cause of collapse. Comparing the model output to the "Grimburgwal" yields the following conclusions:

- The diagonal "primary cracks" presented in this case resemble the model output to some degree, corresponding the most with the case of front pile removal. Front pile removal causes a forward tilt of the wall. The Grimburgwal case shows a forward tilt as well, but the cause lies with large vertical settlements of the front piles, rather than pile fracture.
- Based on the Grimburgwal case, the vertical behaviour of piles after soil removal works too favourably in the model code.
- The cracking patterns appearing after failure have a diagonal progression. On one side it corresponds with the predicted torsional cracks as a result of forward tilting. However, the cracks on the other side progress in the opposite direction. This indicates that perhaps torsion is not the cause of these cracks, and that other factors are at play, which were not taken into account in the model. This shows the finite element models limitations.
- The quay wall in the model code have different dimensions and a different amount of pile positions (three, instead of two in the Grimburgwal case). It is not completely known how these differences affect the cracking pattern outcome of the model.

Lastly, a comparison will be made regarding the displacement patterns. Figure 6.8 shows the vertical settlement pattern of the quay wall at "Grimburgwal". The trend line shows that as time progresses, the rate of displacement increases. This proves that a continued deterioration process results into progressively increasing amounts of displacement. The finite element model shows a similar trend. However, the trend line shown in figure 6.8 only shows this process within a time frame of two years. One can only assume that the trend does not change when this line is extrapolated.

7

Discussion

7.1. Results discussion

In a three-dimensional model, both in-plane and out-of-plane behaviour of the quay wall can be illustrated after applying non-uniform deterioration. The main advantage compared to two-dimensional modelling is that the results can be produced in a single model, in which both effects can be simulated simultaneously. In the case of local pile fracture, it is clear that crack formation is a consequence of a combination between in-plane and out-of-plane displacements. The finite element model was able to show this effect quite well.

The results have found that the masonry wall shows great lateral and vertical deflection as a result of pile removal. This makes sense, given that the foundation piles provide both horizontal and vertical support for the masonry wall. If local support is diminished, one might expect such behaviour to occur. Suppose one symmetrical half is modelled, as a consequence of local pile removal, a cantilever-like structure starts to form. This is because the remaining piles still support the masonry wall. This causes a rise in bending moment further away from the point of maximum displacement, which explains the formation of secondary crack fields. Since the secondary crack fields develop at a later stage of deterioration, one might deduce that their presence indicates that a quay wall structure is in critical condition.

The model produces different crack orientations in the secondary crack field depending on how piles are removed. Front pile removal results in a forward tilt, while entire row removal results in a backward tilt. Given that this is the only difference between the two cases, it can be concluded that the tilt of the masonry wall indicates the crack direction of the secondary crack field. This can be explained by the idea that torsional loads develop within the masonry wall, causing cracks to propagate diagonally.

In this research, the effect of removal of soil support around the piles has been analysed independently. The results show that this causes more sensitivity towards horizontal deflection, more so than pile removal. This makes sense, given that removing soil support has a "double-effect" on the stability of the quay wall structure. Not only is the supporting length of the pile lower than before, but it also has an indirect effect on the passive-active soil balance. In the model code, this effect is incorporated as a reduction in soil capacity according to the Brinch

Hansen formulas.

Lowering the soil level has a relatively minimal effect on the vertical support capacity according to the model. From the standpoint of the model code, it makes sense that vertical settlements are therefore minimal as well. However, it is possible that certain processes take place in real life which drastically diminish the vertical capacity of the pile as a consequence of soil removal, which has not been taken into account in the model code. In practice, it does happen that the vertical bearing capacity is lost in piles due to poor soil quality. As a consequence, one might expect similar cracking patterns as those induced by pile removal. Theoretically, large vertical settlements of certain piles, in combination with horizontal deflection, in essence, produces the same effect as removing the pile from the model entirely. More research in this area is required to study these effects.

The results consistently show that cracks appear later when the masonry is of good quality. Qualities associated with strong masonry includes larger stiffness, tensile strength and tensile crack energy values (the same applies in compression, but compressive behaviour is not taken into account). A larger value in either of these properties results in a larger capability of the masonry to support itself before it shows signs of damage. Therefore, it makes sense that strong masonry is less likely to give early warning signs when it comes to the quality of the foundation structure underneath.

Lastly, the following notes have to be taken into account when it comes to interpreting the results. These are the most important limitations when it comes to the finite element model:

- Every simulation within every case is run from scratch. Suppose a pile stiffness of 6 GPa is assigned. Ideally, it would be more realistic if this stiffness value would decrease step by step in the same simulation. Instead, a new simulation had to be run with different values. It is unclear what difference it would have made in the final results, but it would have been more realistic.
- Second order bending moment effects have not been taken account into the simulations. Including these effects will likely cause the quay wall structure to fail sooner as stresses across the structure reach a high value sooner due to eccentricity. This leads automatically to the next bullet point.
- The capacity of the planks is likely overestimated due to a lack of plastic behaviour. Therefore, it is possible that the model would have failed sooner than the results might indicate. This would lead to fewer visible cracks in the wall before failure. Also, the fact that the quay wall model is able to withstand removal of six pile rows before collapse seems unreasonably high. This also indicates the that foundation strength is too optimistic.
- The obtained crack width values may be slightly different based on which mesh size and crack bandwidth is used. These two values compensate for each other, but this compensation is not exact. Therefore, the crack width values only serve as a rough indication.
- The crack width threshold is set to be 2 mm. However, it is likely that cracks might be visible sooner than that. This means that 2 mm is a conservative value.

- Due to the number of simplifications and assumptions. It is practically impossible to regard the displacement and crack results as factual. The numerical results obtained in this research only serve as an indication of how the quay wall can behave as a result of small parametric changes.
- The simulations use a symmetrical approach. However, it is unlikely that symmetrical damage patterns will occur in real life. Due to inconsistencies in the structure, damage may be larger on one side compared to the other.
- The quay wall structure is rarely uniform in real life. Small variations exist in for example: soil layer boundaries, centre-to-centre distances between piles, non-uniform permanent loads. Due to natural and human-caused inconsistencies, the quay wall may behave a certain way which is not described in this report.
- Every real-life quay wall situation is unique. This report described the response of the quay wall due to foundation degradation in the general sense. In real life, it is difficult to know precisely which piles are defected and by how much, because it differs on a case-by-case basis.
- The more complex a model is, the more insecurities arise. This statement reinforces the idea that the results are indicative and can only be interpreted as such.

7.2. Assumptions and simplifications

The finite element model contains several assumptions and simplifications. The main purpose of making assumptions is to reduce the complexity of the model. Using a numerical model to explain real-life behaviour also comes with its inherent limitations, especially when attempting to model an entire quay wall as realistically as possible. Each simplification affects the final results. The discussed topics are comprised of the following:

1. Assumptions and simplifications regarding the foundation structure.
2. Assumptions and simplifications regarding the behaviour of the surrounding soil.
3. Assumptions and simplifications regarding the masonry structure.
4. Final comments.

These are the most important simplifications and assumptions made when it comes to modelling the foundation structure:

- Lateral support beams ("kesp") have been omitted from the model. The thesis is mainly focused on the behaviour of the piles, which in turn dictates the behaviour of the masonry wall. The reasoning behind omitting these beams was to reduce the complexity of the model. Adding these beams may have contributed favourably to the strength and stiffness of the plank layer (depending on its quality).
- The soil retaining wall has been omitted from the model. However, its effect on the quay wall structure has been included in the model by replacing it with forces on the pile. The theory behind this behaviour has been obtained from the Grimburgwal report, although it is not precise and contains some degree of speculation.

- The planks have been assumed to be linear elastic. This choice is made to reduce complexity and to put the focus more on the behaviour of piles. However, excluding the non-linear behaviour of the planks likely overestimates the overall capacity of the planks.
- The pile head connection is assumed to be either rigid or hinged. In reality, these would be two extremities, as this connection is likely governed by a plastic moment (Korff et al., 2020).

These are the most important simplifications and assumptions made when it comes to modelling the soil:

- Soil acts as an external load, as well as external support. Soil loads have been modelled using attached loads, while passive soil support has been modelled using springs. Also, a virtual boundary has been applied to mimic the behaviour of soil. The effect that soil has on the quay wall may be more accurately portrayed if the soil is modelled as a complete medium, instead of separate loads and springs. Soil models do exist in DIANA FEA. However, modelling the soil as an entire continuum requires much more computing power as more elements are created, which is why these choices have been made.
- Soil parameters are approximations based on one CPT diagram. The angle of friction and cohesion values are deduced via a theoretical approach. A more thorough soil investigation would reduce inaccuracies in this regard.

These are the most important simplifications and assumptions made when it comes to modelling the masonry wall:

- The Total Strain Cracking Model is a macro-model, meaning that no distinction is made between bricks and mortar. Theoretically, making this distinction would be more realistic. However, it would require significantly more computing power. Besides, in this case, it is not required to produce accurate cracks up to the millimetre, as the interest lies more with the general orientation and the general magnitude of each crack. For this reason, it may not be worth it to apply a micro-model.
- The Total Strain Cracking Model is an isotropic model, while masonry is an anisotropic material. The stiffness of the material used is a somewhat average value between the stiffness in the vertical and horizontal directions. As the stiffness is larger in the in-plane direction and smaller in the out-of-plane direction, vertical deformations will likely be smaller in reality, while horizontal deformations will likely be larger.
- More accurate masonry models exist, such as the Engineering Masonry Model. The reason for choosing the Total Strain Crack Model is because it is the best available model which allows the modelling of masonry in 3D. Creating a 2D masonry wall with EMM may produce different crack results.
- The behaviour of masonry in compression is assumed to be linear static. This choice was made to reduce complexity. Also, the compressive strength is approximately 20 times larger than the tensile strength. However, it is unclear what the effect on the results would have been if non-linear compressive behaviour were included.

Simplifications that are difficult to overcome are summarised in these final comments:

- Quay wall structures are rarely uniform in real life. Small variations exist in for example: soil layer boundaries, centre-to-centre distances between piles and non-uniform permanent loads. Due to natural and human imperfections, the quay wall may behave a certain way which is not described in this report.
- Every real-life quay wall situation is unique. This report described the response of the quay wall due to foundation degradation in the general sense. In real life, it is difficult to know precisely which piles are defected and by how much, because it differs on a case-by-case basis. On top of that, every quay wall has different dimensions and properties. Some have more than three pile positions, thicker masonry walls, or have a different position of the soil retaining wall. It is expected that these factors greatly influence the displacement magnitudes and overall capacity.

8

Conclusions And Recommendations

Approximately 200 km worth of quay walls in Amsterdam require renovation. A thorough assessment of every quay wall is costly, labour-intensive and time-consuming, making it an unrealistic approach. For this reason, it is necessary to prioritize renovations based on the damage the quay walls are currently showing. In this research, it has been attempted to mimic the behaviour of a historical quay wall as realistically as possible, using a 3-dimensional finite element model. This model has been used to provide an indication of what the displacement and damage patterns can tell about the quality of the quay wall structure. The main advantage of the 3D model, is that more insight can be obtained on the combined effect of in-plane and out-of-plane movement on the cracking patterns in the masonry wall. This study contributes to improving the recognition of quay walls which find themselves in critical condition, which can then be prioritized for renovations. The main research objective will be stated before elaborating on the conclusions and recommendations. It reads as follows:

"How to recognize critically damaged quay wall structures using a three-dimensional finite element model."

The finite element model has provided indications on what kind of cracking and displacement patterns one might expect as a consequence of either pile group damage or soil removal from around the piles. The likely damage patterns resulting from different behaviour configurations are briefly summarised in table 8.1 below.

Behavioural phenomenon	**Pile removal: entire rows**	**Pile removal: front piles***	**Reduction of soil level around the piles**
Horizontal displacements	Yes	Yes, less than entire row removal.	Yes, more than entire row removal.
Vertical displacement	Yes	Yes, less than entire row removal.	Minimal**
Wall tilt	Yes, backwards	Yes, forwards	No
Primary cracks	Vertical cracks starting from the bottom, but slowly getting smaller as they propagate upwards. (out-of-plane and in-plane)	Vertical cracks starting from the bottom, but slowly getting smaller as they propagate upwards and sideways. (out-of-plane and in-plane)	Vertical crack with uniform thickness over the entire height. (out-of-plane)
Secondary cracks	Diagonal cracks starting from the top, which propagate towards the primary field. (in-plane and torsion)	Diagonal cracks starting from the top, which propagate away from the primary field. (in-plane and torsion)	None

Table 8.1: Summary of behavioural consequences of different cases, produced by the results.

* Front pile removal likely has the same effect on the masonry wall as front pile settlement.
** The vertical capacity of soil is likely overestimated (covered in the discussion).

Finally, uniform degradation does not cause cracks, but it does cause horizontal and vertical displacement, accompanied by a slight forward tilt in the masonry wall.

More elaborate answers will be given by answering the research questions separately.

8.1. Conclusions

"How do long-term phenomena affect the quality of the quay wall structure?"

Chapter 2 describes the theory behind material degradation. Many processes are at play that contribute to the loss of quality. In short, factors such as creep, mechanical and biological degradation and common physical processes lead to wear and tear of the used materials over a long time. In the finite element model, these processes have been taken into account by interpreting quay wall deterioration as follows:

- Wood strength reduction.
- Wood stiffness reduction.
- Pile diameter reduction.

- Masonry strength reduction.
- Masonry stiffness reduction.
- Masonry crack energy reduction.
- Reduction of the pile embedding soil level.

Each long-term process has its own unique way of affecting the health of the quay wall structure. Numerically, the deterioration of the structure has been modelled by reducing overall strength, stiffness and soil parameters.

"How should the numerical model be set up?"

In detail, the setup of the model has been described in chapter 3. This research aimed to model the quay wall as realistically as possible. An important realisation is that it is challenging to mimic reality using a numerical model. In the end, several simplifications and assumptions had to be made to reduce complexity and computation time.

However, the attempt has been made to understand the physical behaviour of a quay wall structure, using the theory from other research papers combined with information gathered from European norms. Eventually, it has been attempted to apply the theoretical behaviour of a quay wall structure in DIANA FEA as thoroughly as possible. A summary will follow, describing which physical processes and material behaviours have been applied to the model.

The behaviour of masonry is modelled using the Total Strain Cracking Model, using an exponential softening curve in tension and a linear elastic curve in compression. At the boundaries, no rotation or longitudinal displacement is permitted, while perpendicular sliding is permitted. The Coulomb Friction model has been used to define the interface between the masonry and the foundation layer.

The foundation can be divided into the plank layer and the piles. Support beams have been omitted from the model. The plank layer assumes linear elastic behaviour, while the piles assume non-linear behaviour. The piles behave ideally plastic in compression and brittle in tension. The pile head connection is either rigid or hinged depending on which analysis is ran. The soil retaining wall is not present in the model, but its effect is included by replacing it with a load directly behind the planks and loads behind every pile.

The soil acts as a load against the wall and planks and indirectly against the piles. The behaviour of soil is modelled as external loads with a virtual boundary. It has been found that it is a good alternative to modelling the soil as a continuous medium. The soil also acts as passive support for the piles. Horizontally, this support has been modelled by using Ménard springs with a maximum bearing capacity using the theory of Brinch Hansen. The shadowing effect of pile groups has also been taken into account. The pile tip is supported by a vertical spring, in which pile tip resistance, shaft resistance and adhesion are taken into account (Eurocode norms).

When it comes to obtaining results, three main cases have been assessed, of which the first two are used to induce cracks:

1. Non-uniform pile removal: modelled by locally removing piles from the model.
2. Non-uniform soil removal: modelled by locally altering the pile embedding.
3. Uniform conditions.

The model is made using a self-written parametric model written in Python. The Python programming language is well integrated into DIANA FEA. For this reason, it was possible to run a large number of simulations.

"Based on the numerical model, which tell-tale signs could be observed that can help better detect critical quay walls defects?"

To answer this question, the following output is of importance from the simulations: cracking patterns and displacement patterns. In the finite element model, cracks are induced either by locally removing piles or locally increasing the free height of the piles. When it comes to removing piles, two different situations are considered: one in which an entire row (front to back) is removed and one where only the front piles are removed. The expected cracking patterns and the stance of the quay wall are presented in figures 8.1, 8.2 and 8.3 below.

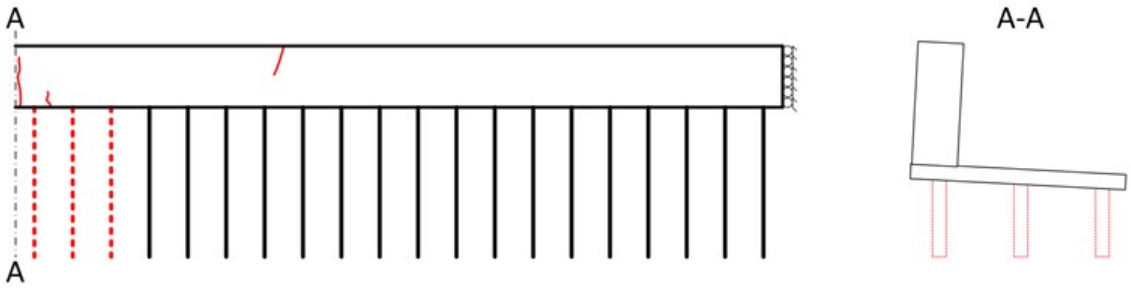

Figure 8.1: Schematisation of cracks induced by pile row removal (front to back) and the tilt of the wall which follows as a consequence.

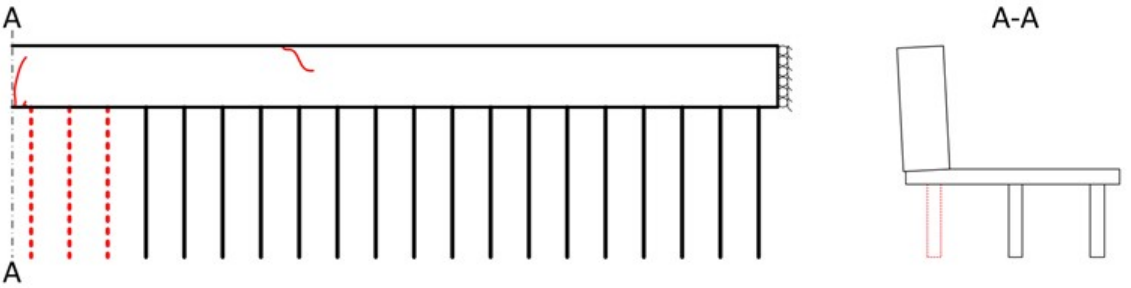

Figure 8.2: Schematisation of cracks induced by front pile removal and the tilt of the wall which follows as a consequence.

Figure 8.3: Schematisation of cracks induced by soil removal and the tilt of the wall which follows as a consequence.

Pile removal usually causes two crack fields. The primary crack field is situated at the location with pile damage, while the secondary crack field is located further away. The primary cracks are induced by a combination of out-of-plane and in-plane motion, and they propagate from the lower side of the wall. The secondary cracks are mainly a consequence of in-plane motion. These cracks propagate from the upper side of the wall. Once the secondary crack field becomes clearly visible, the model usually does not tolerate further deterioration. Therefore, it is concluded that the condition of the wall is critical when these secondary cracks show themselves. The appearance of the primary crack also depends on the level of the water in the canal if the masonry wall is assessed using the naked eye. The secondary crack orientation is governed by torsion within the masonry wall. Front pile removal causes a forward tilt in the masonry wall, which leads the secondary crack away from the primary field. Removal of entire rows leads to a backward tilt, leading to the opposite effect.

According to the model, one single crack field appears when assessing soil removal only. This field is situated at the location where the piles have the least support. These cracks are induced by mainly out-of-plane motion. The crack width is relatively consistent over the entire height of the wall. In other words, they do not progress from either the top or the bottom of the wall. This behaviour is expected given that vertical soil support is still relatively strong.

Excessive vertical displacements are usually accompanied by pile removal, while excessive horizontal displacements are usually a consequence of soil removal. Pile removal also leads to horizontal displacements, but a lesser degree. These displacement patterns directly explain the in-plane and out-of-plane components in the primary crack fields in both cases.

"To what extent can the quay wall deteriorate before it starts to portray visually detectable signs of damage?"

This question is difficult to answer accurately with numbers, as the deterioration process of every quay wall is unique. However, it is possible to do a comparative study, to see which factors influence the likelihood of observing dangerous cracks early. Also, the threshold of visible cracks is set to be 2 mm, this number is arbitrary to some degree, as it might be possible to see thinner cracks clearly as well. Based on the results in chapter 5, the following conclusions can be drawn:

- Even weak quay wall structures require some degree of non-uniform degradation for cracks to appear.

- In any case, the primary cracks appear before the secondary cracks. Once the secondary cracks reach 2 mm in width, the quay wall is usually in a vulnerable state, meaning that it does not tolerate much more deterioration.
- Pile fracture on an otherwise strong masonry wall will also cause cracks. However, cracks will appear later compared to a weak quay wall structure. In other words, foundation defects are more difficult to detect if the masonry is strong. This only applies if the quality of the quay wall is assessed only by looking for damage in the masonry.
- If pile fracture is present next to an otherwise strong foundation structure, primary cracks will likely appear later compared to a weak foundation structure. However, secondary cracks will likely appear sooner in the same situation. The difference is minimal, but it is there.
- The onset of cracking is also dependent on the pile embedding when it comes to local pile fracture. If the surrounding non-broken piles lose embedding (horizontal support), the onset of cracking is delayed compared to when the piles are completely embedded.

The degree of crack formation is dependent on many factors. The most important factor is the degree of local environmental differences surrounding the quay wall. An area with lots of broken piles is more likely to induce cracks, just like in an area where lots of supporting soil are lost. As conditions are more uniform, the likelihood of crack formation decreases. In that case, looking at displacements might be a more sensible approach.

"Which factor contributes the most to cause the displacement of quay walls?"

According to the model, an increase in displacements are induced by either a loss of pile capacity or soil capacity. A loss of pile embedding causes a decrease in horizontal and vertical soil capacity. Vertical settlements are relatively minimal according to the model, while horizontal displacements are significant. A loss of pile capacity leads to horizontal and vertical displacements. Vertical settlements of the masonry wall are most pronounced at the location of broken piles. In the end, horizontal displacements reach the highest magnitude when passive soil support is reduced, while vertical displacements reach the highest magnitude due to a loss of pile capacity.

8.2. Recommendations

This section covers suggestions on which to improve the model and ways in which further interesting results may be obtained.

First of all, it is possible to add lateral support beams (or "kespen") into the model. Adding these beams may affect the force and displacement distribution of the planks, and thus of the masonry wall as well. It is unclear whether this change is noticeable, but it could be tested.

If a future researcher is purely interested in in-plane and out-of-plane displacement patterns resulting from non-uniform conditions, one could consider modelling the quay wall structure in a two-dimensional model with a cross-sectional view. However, the 2D plane should include a boundary friction interface to simulate the extra capacity resulting from the longitudinal direction (due to non-uniformity). Modelling in 2D is a quicker approach which could be applied

in this case.

In this research, the program DIANA FEA was used to run the simulations. However, the educational version was used, which comes with limitations compared to the full version. Limitations include a limit on how many elements can be used, but also changing material properties through time, or reading results files. If a researcher would use the full version, the following improvements could be made:

- Model the soil as a continuous medium. Since the number of elements that can be used is virtually limitless, it is possible to achieve this.
- Instead of changing a parameter after every single simulation, it should be interesting to see what difference it makes if materials can degrade through time during the same simulation.
- In this research, all results have been manually obtained. Many more simulations could be run if the results files could be programmatically accessed. This way, more cases could be analysed relatively quickly.

Another recommendation is to replace the solid wall object with a 2D plane, after which the Engineering Masonry Model can be applied. This material model is better suited for masonry. The cracking patterns which are produced should be compared to those produced in this research, to see whether they are similar.

Another possible way to discover tell-tale signs of a failing quay wall is to analyse the displacement rate of the wall. To achieve this, it is important to know how fast the materials degrade over time. After which, these properties can be assigned using time-dependent analyses.

References

Brannan, N. (2020). Reconstructie: Hoe achterstallig onderhoud aan kades en bruggen de stad op palen doet wankelen. *AT5*.

de Baar, P.-P. (2009). Amsterdam heeft verraderlijke bodem. *Ons Amsterdam*.

de Gans, W. (2011). *De bodem onder amsterdam: Een geologische stadswandeling*. TNO (Nederlandse Organisatie voor toegepast-natuurwetenschappelijk onderzoek).

de Gijt, J. (2010). *A history of quay walls: Techniques, types, costs and future* (Master's thesis). Delft University of Technology.

de Gijt, J., Roubos, A., & Grotegoed, D. (2013). *Binnenstedelijke kademuren*. SBRCURnet.

de Vent, I. (2011). *Structural damage in masonry: Developing diagnostic decision support* (Master's thesis). Delft University of Technology.

DIANA. (2017). Diana fea user's manual. https://dianafea.com/manuals/d102/Diana.html

Dijksma, S. (2019). Aanpak civiele constructies. https://rolfuhlhorn.amsterdam/wp-content/uploads/2019/12/Aanpak-civiele-constructies.pdf

Dijstelbloem, J. (2020). *Herstellen en verbinden: Bouwen aan het fundament van de stad (programmaplan bruggen en kademuren)*. Gemeente Amsterdam.

Dijstelbloem, J., ten Hulsen, E., & Hilgers, T. (2019). *Actieplan bruggen en kademuren*. Gemeente Amsterdam.

Eurocode. (2017). Nen-en 1995 1-1 houteigenschappen: Sterktegegevens van gezaagd en gelamineerd hout. https://www.houtdatabase.nl/infobladen/Infoblad_Houteigenschappen-Sterktegegevens.pdf

Fayyazi, M. S., Taiebat, M., & Finn, W. L. (2014). Group reduction factors for analysis of laterally loaded pile groups. *NRC Research Press*.

Granello, G., & Palermo, A. (2019). *Creep in timber: Research overview and comparison between code provisions*. New Zealand Timber Design.

Grund, M. (2020). *Urban quay walls: A numerical study to recognize foundation defects via masonry damage patterns* (Master's thesis). Delft University of Technology.

Hamakareem, M. (n.d.). Negative skin friction on piles and pile groups. *The Constructor*.

Hoefsloot, F. (2008). *Door grond horizontaal belaste palen: Bestaande ontwerpmodellen*. Fugro Ingenieursbureau B.V.

Hoekstra, T. (2020). *Multiwaterwerk: Materialisatie sluisdeuren: Houten sluisdeuren*. Ingenieursbureau Boorsma.

Jafari, S., Rots, J., Esposito, R., & Messali, F. (2017). Characterizing the material properties of dutch unreinforced masonry. *Elsevier*.

Kasprick, S. (2019). Winter is coming: The effects of frost on structural elements. *CEP Forensic inc.*

Klaassen, R. (2007). Water flow through wooden foundation piles: A preliminary study. *Elsevier*.

Korff, M., Esposito, R., & Hemel, M. (2020). *Bezwijken grimburgwal: Leerpunten voor het amsterdamse areaal*. Municipality of Amsterdam.

Kruidhof, J. (2019). *Wethouder dijksma: Bij bruggenonderhoud is de link met veiligheid niet direct gelegd*. Retrieved July 2, 2019, from https://www.trouw.nl/nieuws/wethouder-dijksma-bij-bruggenonderhoud-is-de-link-met-veiligheid-niet-direct-gelegd~b8bdb4ea/

Lourenço, P. (1996). *Computational strategies for masonry structures* (Master's thesis). Delft University of Technology.

Lourenço, P., Rots, J., & Blaauwendraad, J. (1995). *Two approaches for the analysis of masonry structures: Micro and macro-modeling*. Delft University of Technology.

Maljaee, H., Ghiassi, B., Lourenço, P. B., & Oliveira, D. V. (2013). *Moisture-induced degradation of interfacial bond in frp-strengthened masonry*. ISISE, University of Minho, Department of Civil Engineering, Guimarães, Portugal.

Molenaar, W., & Voorendt, M. (2017). *Manual Hydraulic Structures*. TU Delft.

Nematollahi, B., Voo, Y. L., & Rashid, R. S. (2014). Structural behavior of precast ultra-high performance fiber reinforced concrete (uhpfrc) cantilever retaining walls: Part i - analysis and design procedures and environmental impact calculations (eic). *KSCE Journal of Civil Engineering 18(5). DOI:10.1007/s12205-014-0411-8*.

NPR9998. (2020). *Assessment of structural safety of buildings in case of erection, reconstruction and disapproval – induced earthquakes – basis of design, actions and resistances*. Nederlands Normalisatie Instituut (NEN).

Pande, G., Kralj, B., & Middleton, J. (1994). *Analysis of the compressive strength of masonry given by the equation fk = k(fb) a (fb) b*. The Institution of Structural Engineers.

RTLNieuws. (2020). *Kademuur ingestort in centrum amsterdam, vermoedelijk door sinkhole*. Retrieved September 1, 2020, from https://www.rtlnieuws.nl/nieuws/nederland/artikel/5180850/kade-ingestort-centrum-amsterdam

Sas, F. (2007). *De houten paalfundering doorgezaagd*.

Sayed-Ahmed, E. Y., Shrive, N. G., & Tilleman, D. (1997). *Creep deformation of clay masonry structures: A parametric study*. Department of Civil Engineering, The University of Calgary, Calgary, AB T2N 1N4, Canada.

Schol-Calingacion, L., & Bosveld, M. (2016). *Integrale beoordeling walmuren nieuwe herengracht te amsterdam*. Royal Haskoning DHV.

Slobbe, A. (2015). *Propagation and band width of smeared cracks*. Delft University of Technology.

Strikvoort, I. (2014). *Old quay walls: Proposal for a method for analysing the remaining lifespan.* (Master's thesis). Delft University of Technology.

van der Linde, L. (2018). Oude assets beheren met nieuwe technieken. *iMaintain*.

van Kasteren, J. (2009). Vloeibaar mengsel houdt amsterdam rechtop. *Delft Integraal*.

van Noort, J. (2012). *Computational modelling of masonry structures* (Master's thesis). Delft University of Technology.

Vecchio, F. J., & Collins, M. P. (1986). The modified compression-field theory for reinforced concrete elements subjected to shear. *American Concrete Institute*.

Voortman, R. (2020). *The historic quay walls of amsterdam: A study into the hidden structural capacity of masonry quay walls under the condition of a partly failing foundation* (Master's thesis). Delft University of Technology.

Walsh, J. (2005). *Full scale lateral load test of a 3x5 pile group in sand* (Master's thesis). Brigham Young University, Department of Civil and Environmental Engineering.

Willis, C. (2004). *Design of unreinforced masonry walls for out-of-plane loading* (Master's thesis). The University of Adelaide.

Appendix

A

Element Properties

A.1. Wood properties

All softwood properties described by Eurocode 5 are shown in figure A.1. Softwood class C18 is highlighted in red.

Property	C14	C16	C18	C20	C22	C24	C27	C30	C35	C40	C45	C50	Unit
$f_{m,k}$	14	16	18	20	22	24	27	30	35	40	45	50	N/mm^2
$E_{0,mean}$	7	8	9	9,5	10	11	11,5	12	13	14	15	16	kN/mm^2
ρ_{mean}	350	370	380	400	410	420	430	460	470	480	520	520	kg/m^3
ρ_k	290	310	320	330	340	350	360	380	390	400	440	430	kg/m^3
$f_{t;0;k}$	7,2	8,5	10	11,5	13	14,5	16,5	19	22,5	26	30	33,5	N/mm^2
$f_{t;90;k}$	0,4	0,4	0,4	0,4	0,4	0,4	0,4	0,4	0,4	0,4	0,4	0,4	N/mm^2
$f_{c;0;k}$	16	17	18	19	20	21	22	24	25	27	29	30	N/mm^2
$f_{c;90;k}$	2,0	2,2	2,2	2,3	2,4	2,5	2,5	2,7	2,7	2,8	2,9	3,0	N/mm^2
$f_{v;k}$	3,0	3,2	3,4	3,6	3,8	4,0	4,0	4,0	4,0	4,0	4,0	4,0	N/mm^2
$E_{0,05}$	4,7	5,4	6,0	6,4	6,7	7,4	7,7	8,0	8,7	9,4	10,1	10,7	kN/mm^2
$E_{90,mean}$	0,23	0,27	0,30	0,32	0,33	0,37	0,38	0,40	0,43	0,47	0,50	0,53	kN/mm^2
G_{mean}	0,44	0,50	0,56	0,59	0,63	0,69	0,72	0,75	0,81	0,88	0,94	1,00	kN/mm^2
$G_{0,05}$	0,29	0,34	0,38	0,40	0,42	0,46	0,48	0,50	0,54	0,59	0,63	0,67	kN/mm^2

Figure A.1: Characteristic properties of Class C18 wood, retrieved from Eurocode, 2017

A.2. Soil properties

The soil properties used in this thesis are based on the sounding received from the performed cone penetration test at "Nieuwe Herengracht".

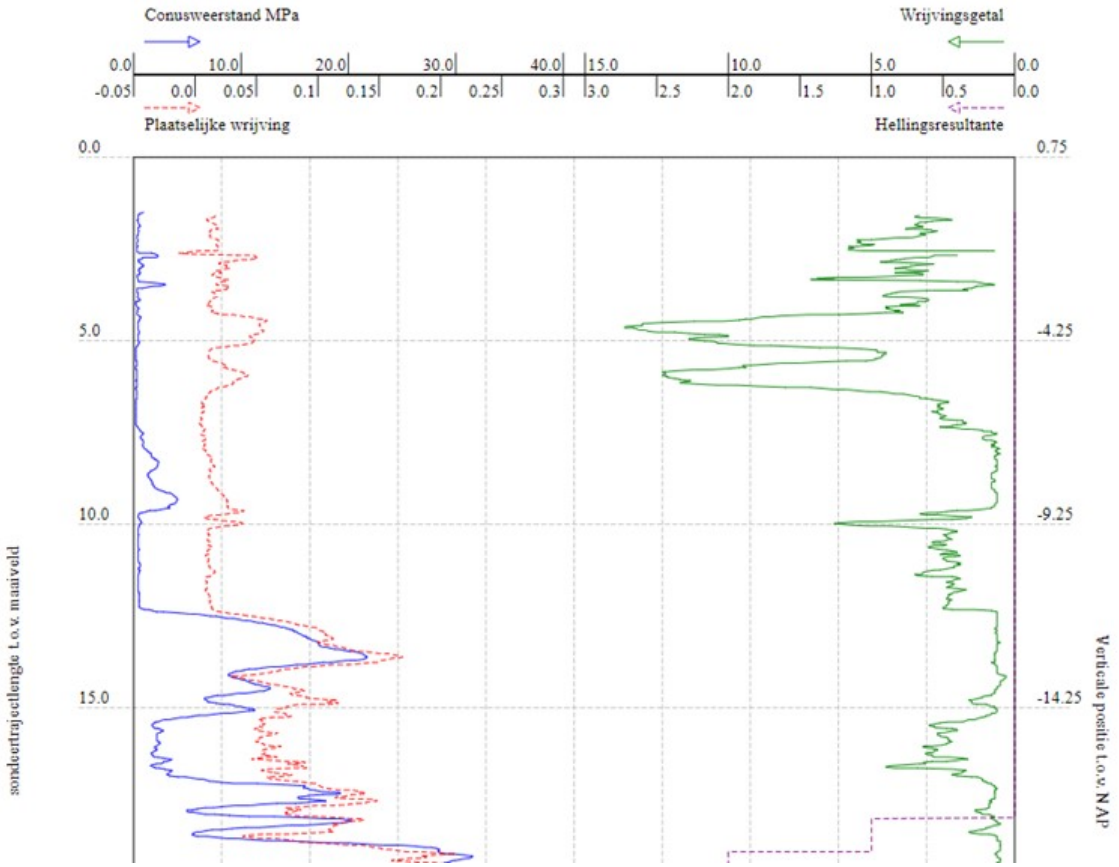

Figure A.2: CPT diagram at "Nieuwe Herengracht", retrieved from DINOloket.

The soil type is determined using the classification chart developed by Peter Robertson in 2010.

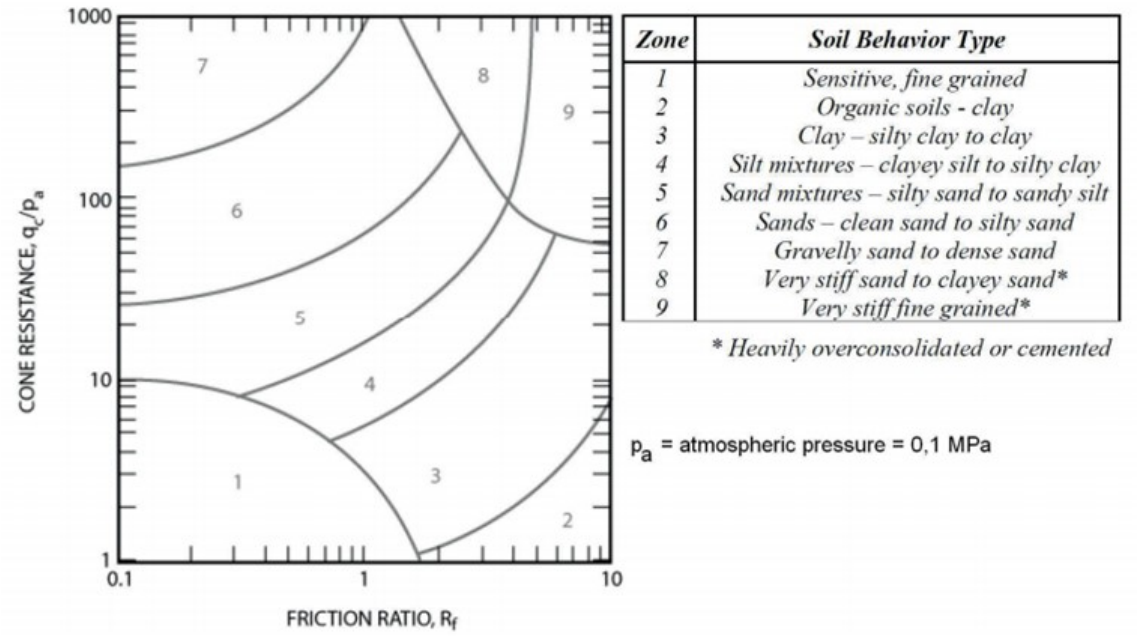

Zone	Soil Behavior Type
1	Sensitive, fine grained
2	Organic soils - clay
3	Clay – silty clay to clay
4	Silt mixtures – clayey silt to silty clay
5	Sand mixtures – silty sand to sandy silt
6	Sands – clean sand to silty sand
7	Gravelly sand to dense sand
8	Very stiff sand to clayey sand*
9	Very stiff fine grained*

* Heavily overconsolidated or cemented

Figure A.3: Soil type classification chart based on cone resistance vs friction ratio, developed by Peter Robertson. Retrieved from Molenaar and Voorendt, 2017.

The cone resistance parameters used to calculate the maximum pile tip bearing capacity is calculated using the Koppejan method. The calculation process is illustrated here.

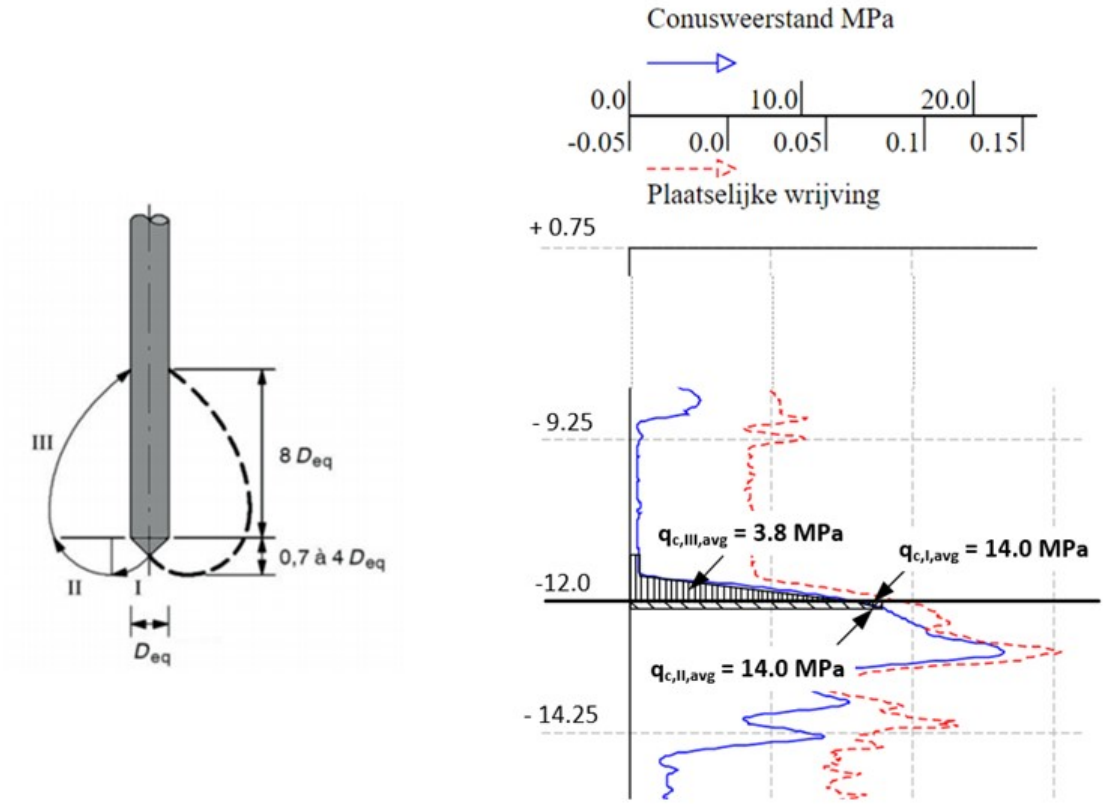

Figure A.4: Left: Slip plane definition according to Koppejan, retrieved from Molenaar and Voorendt, 2017. Right: Determination of average cone resistance values around the pile tip (NAP - 12.0 m).

A.3. Brinch Hansen formulas

The complete approach as formulated by Brinch Hansen is elaborated here.

$$K_q = \frac{K_q^0 + K_q^\infty \cdot \alpha_q \frac{D}{B}}{1 + \alpha_q \cdot \frac{D}{B}}$$

$$K_c = \frac{K_c^0 + K_c^\infty \cdot \alpha_c \frac{D}{B}}{1 + \alpha_c \frac{D}{B}}$$

$$\alpha_q = \left(\frac{K_q^0}{K_q^\infty - K_q^0} \right) \left(\frac{K_0 \sin\varphi}{\sin\left(45° + \frac{1}{2}\varphi\right)} \right)$$

$$\alpha_c = \left(\frac{K_c^0}{K_c^\infty - K_c^0} \right) \cdot 2\sin\left(45° + \frac{1}{2}\varphi\right)$$

$$K_0 = 1 - \sin\varphi$$

$$\sigma'_p = K_q \cdot \sigma_v' + K_c \cdot c$$

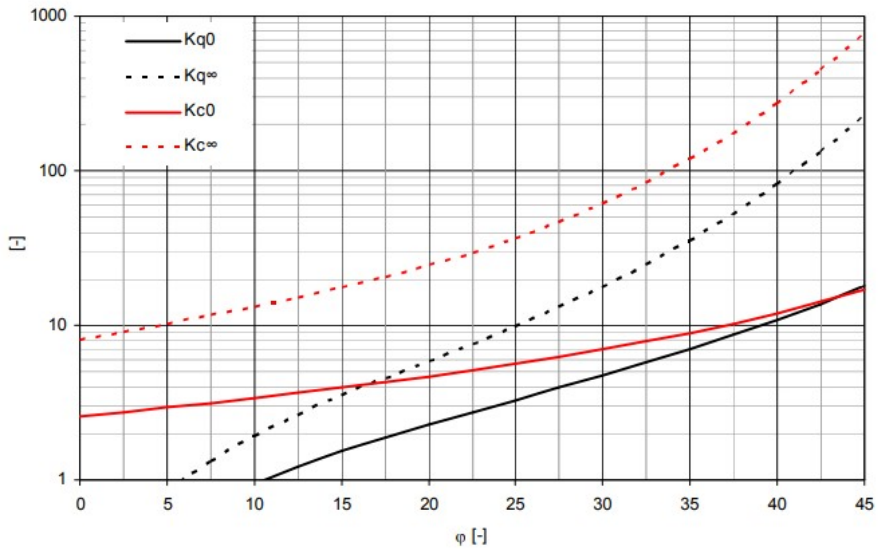

φ	K_q^0	K_q^∞	K_c^0	K_c^∞
1E-07	0.0	0.0	2.6	8.1
2.5	0.2	0.4	2.7	9.1
5.0	0.5	0.8	2.9	10.3
7.5	0.7	1.3	3.1	11.6
10.0	1.0	1.9	3.4	13.2
12.5	1.2	2.6	3.6	15.2
15.0	1.5	3.5	3.9	17.6
17.5	1.9	4.5	4.3	20.6
20.0	2.3	5.9	4.7	24.5
22.5	2.7	7.6	5.1	29.7
25.0	3.3	9.9	5.6	36.7
27.5	3.9	13.1	6.2	46.7
30.0	4.8	17.7	7.0	61.3
32.5	5.8	24.6	7.9	83.4
35.0	7.0	35.3	8.9	118.2
37.5	8.7	52.6	10.3	175.1
40.0	10.9	81.4	11.9	271.7
42.5	13.8	131.6	14.1	442.8
45.0	17.9	222.3	17.0	759.1

B

DIANA FEA

All predefined tension softening curves offered by DIANA for the Total Strain Crack Model are shown in figure B.1.

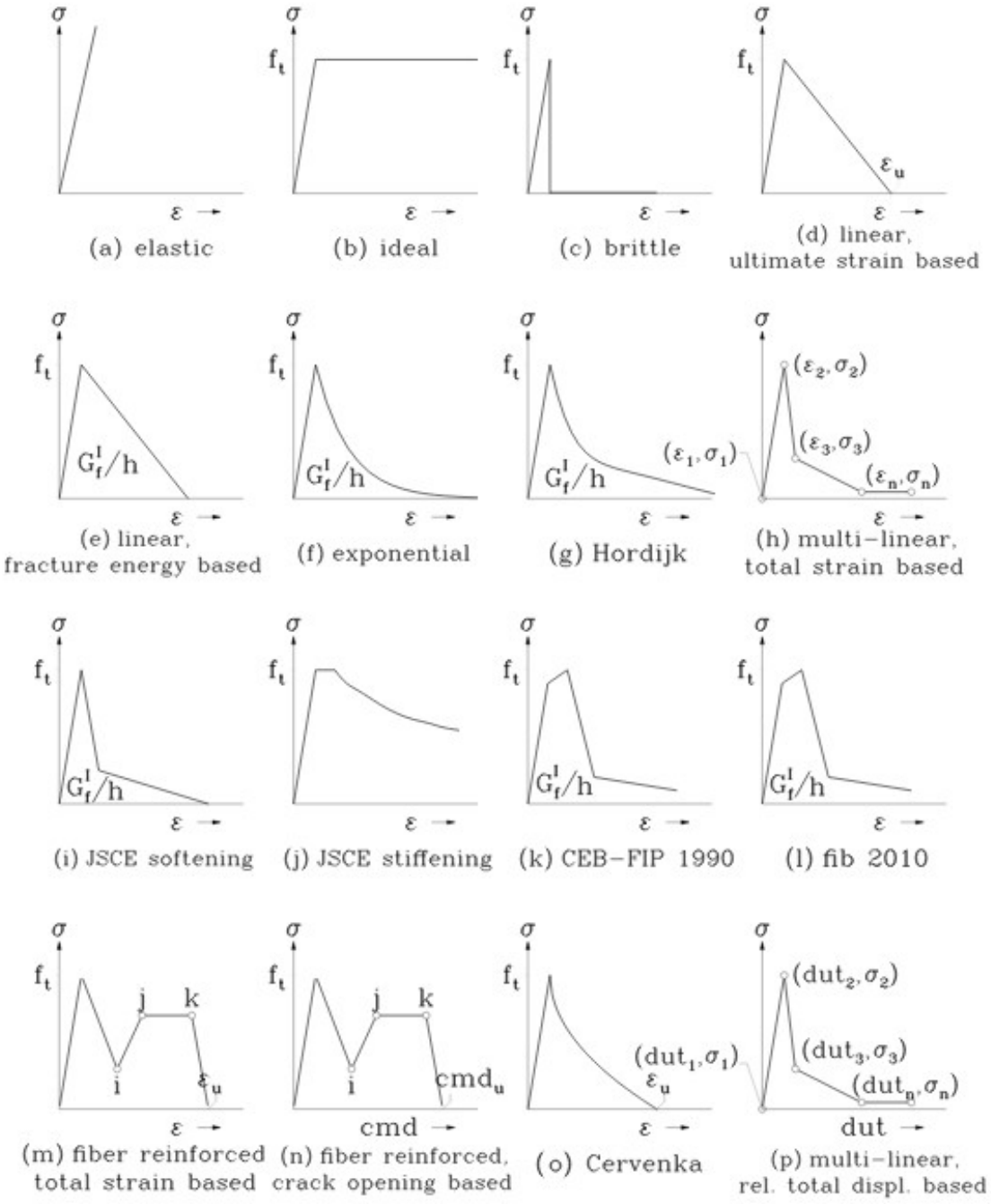

Figure B.1: All predefined tension softening curves, acquired from the DIANA manual.

All predefined compression softening curves offered by DIANA for the Total Strain Crack Model are shown in figure B.2.

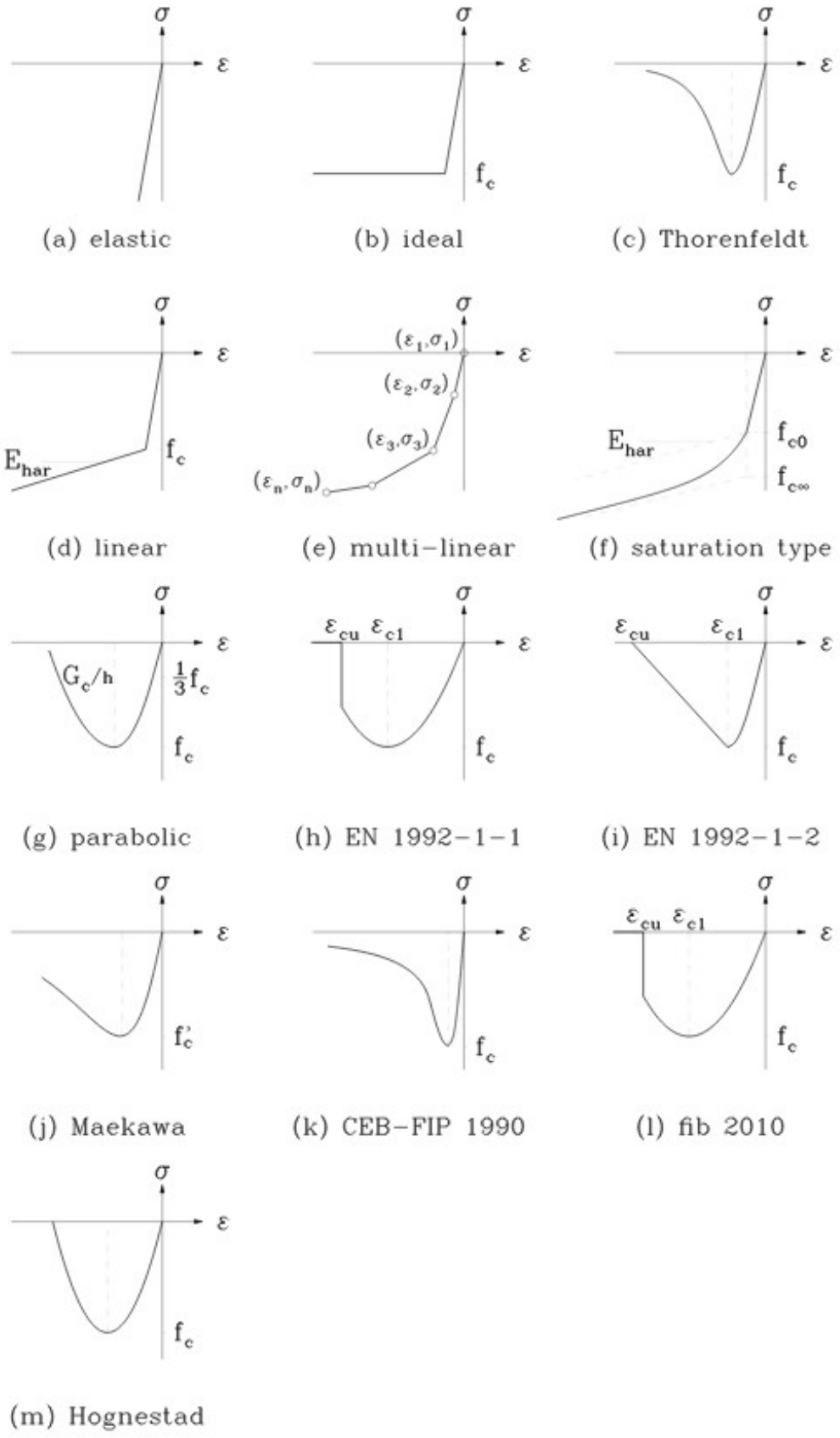

Figure B.2: All predefined compression softening curves, acquired from the DIANA manual.

C

Results (Extended)

C.1. Crack development

In this section, all results regarding crack progression will be presented. The results are presented in the following order:

- Removal of entire pile rows on a weak quay wall.
- Removal of front piles on a weak quay wall.
- Removal of entire pile rows on a strong quay wall.
- Removal of front piles on a strong quay wall.

Removal of entire pile rows on a weak quay wall. With the baseline properties presented in table C.1 below.

Property	**Value**	**Unit**
Masonry: Young's modulus	3000	N/mm^2
Masonry: Shear modulus	1200	N/mm^2
Masonry: Poisson's ratio	0.25	-
Masonry: Mass density	1800	kg/m^3
Masonry: Tensile strength	0.21	N/mm^2
Masonry: Tensile fracture energy	0.021	N/mm
Pile: Young's modulus	4000	N/mm^2
Pile: Flexural strength	16	N/mm^2
Pile: Mass density	320	kg/m^3
Pile: Diameter	160	mm
Pile head connection	Hinged	-
Free height: Front pile	0	m
Free height: Middle pile	0	m
Free height: End pile	0	m

Table C.1: Initial properties used in the upcoming analyses (degraded properties).

Generalised crack fields induced by the removal of entire rows are presented in figure C.1. The output is retrieved from DIANA. The corresponding crack interpretation is presented in figure C.2.

Figure C.1: Generalised crack fields induced by removal of entire rows, output produced in DIANA FEA.

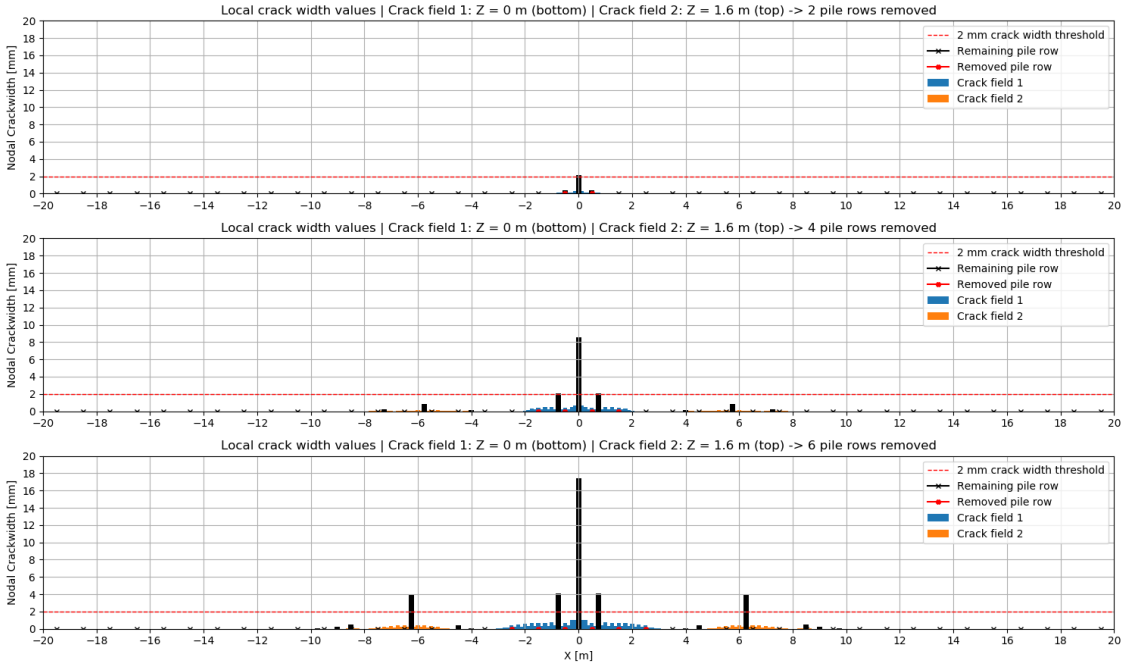

Figure C.2: Crack width values at the bottom (1st crack area) and the top (2nd crack area) of the masonry wall. Pile rows have been incrementally removed on a weak quay wall structure.

Removal of front piles on a weak quay wall, using the same baseline properties.

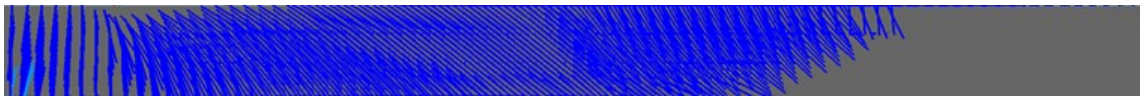

Figure C.3: Generalised crack fields induced by removal of front piles, output produced in DIANA FEA.

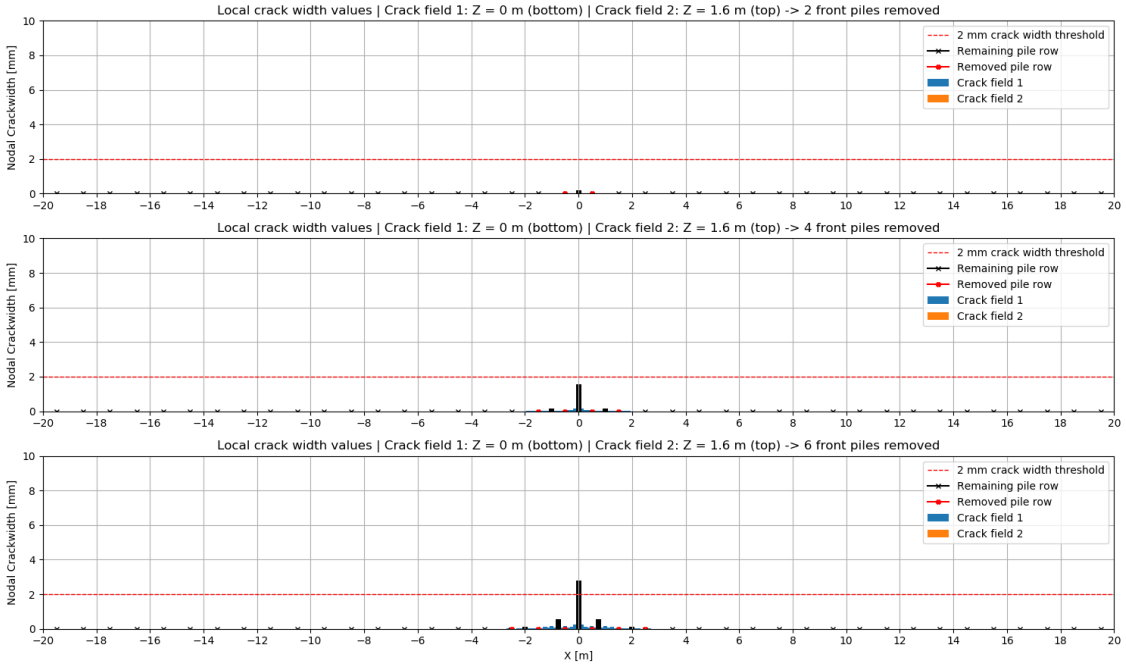

Figure C.4: Crack width values at the bottom (1st crack area) and the top (2nd crack area) of the masonry wall. Front piles have been incrementally removed on a weak quay wall structure. [PART 1/3]

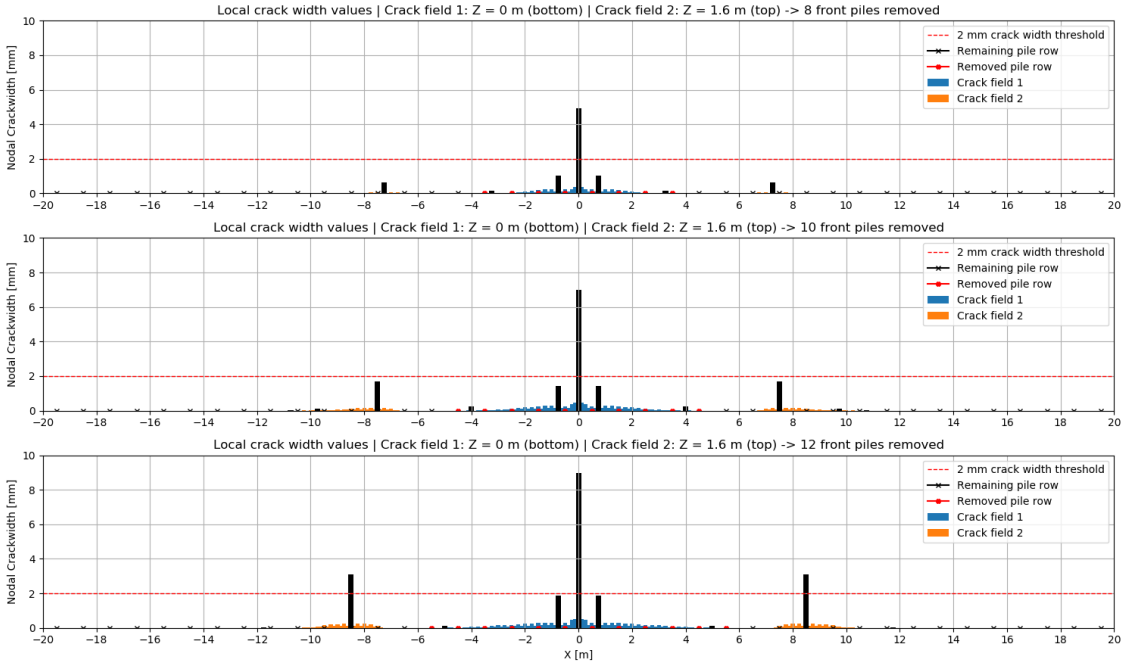

Figure C.5: Crack width values at the bottom (1st crack area) and the top (2nd crack area) of the masonry wall. Front piles have been incrementally removed on a weak quay wall structure. [PART 2/3]

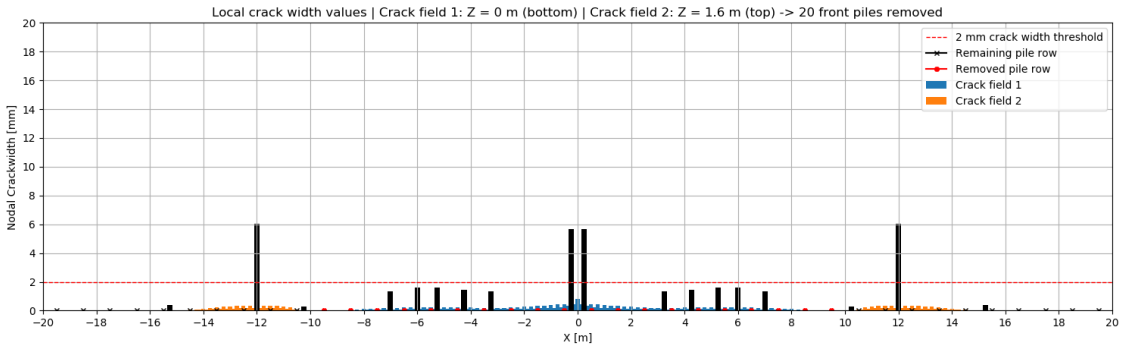

Figure C.6: Crack width values at the bottom (1st crack area) and the top (2nd crack area) of the masonry wall. Front piles have been incrementally removed on a weak quay wall structure. [PART 3/3]

Removal of entire pile rows on a strong quay wall. With the baseline properties presented in table C.2 below.

Property	**Value**	**Unit**
Masonry: Young's modulus	5000	N/mm^2
Masonry: Shear modulus	2000	N/mm^2
Masonry: Poisson's ratio	0.25	-
Masonry: Mass density	1800	kg/m^3
Masonry: Tensile strength	0.35	N/mm^2
Masonry: Tensile fracture energy	0.035	N/mm
Pile: Young's modulus	6000	N/mm^2
Pile: Flexural strength	18	N/mm^2
Pile: Mass density	320	kg/m^3
Pile: Diameter	180	mm
Pile head connection	Rigid	-
Free height: Front pile	0	m
Free height: Middle pile	0	m
Free height: End pile	0	m

Table C.2: Initial properties used in the upcoming analyses (healthy properties).

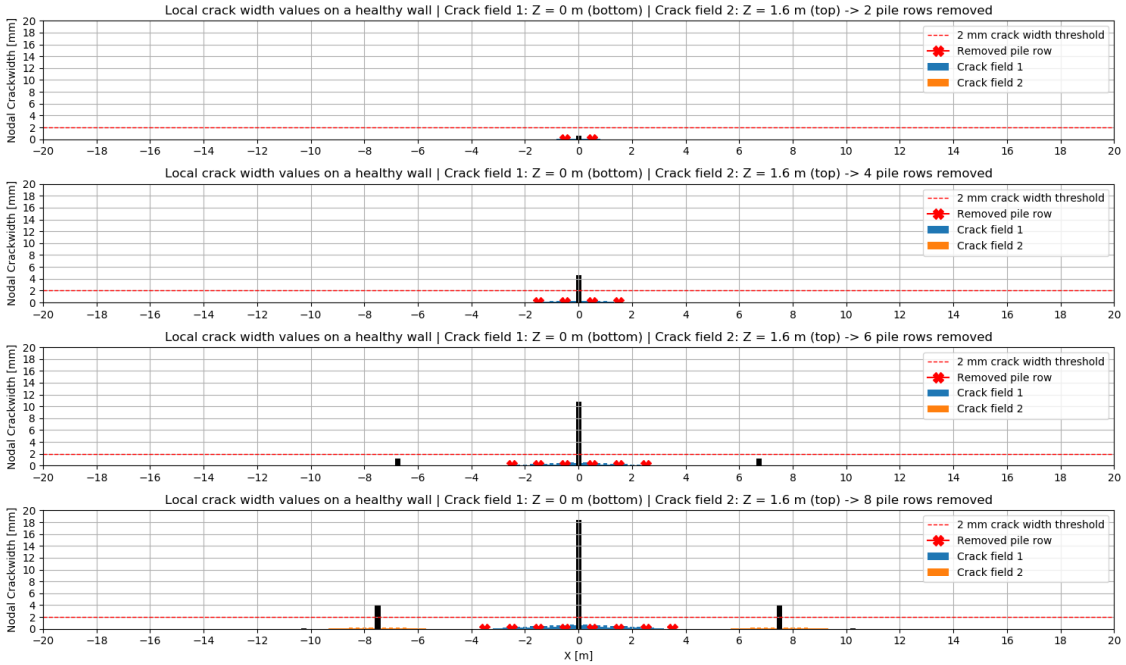

Figure C.7: Crack width values at the bottom (1st crack area) and the top (2nd crack area) of the masonry wall. Pile rows have been incrementally removed on a strong quay wall structure.

Removal of front piles on a strong quay wall, using the same baseline properties.

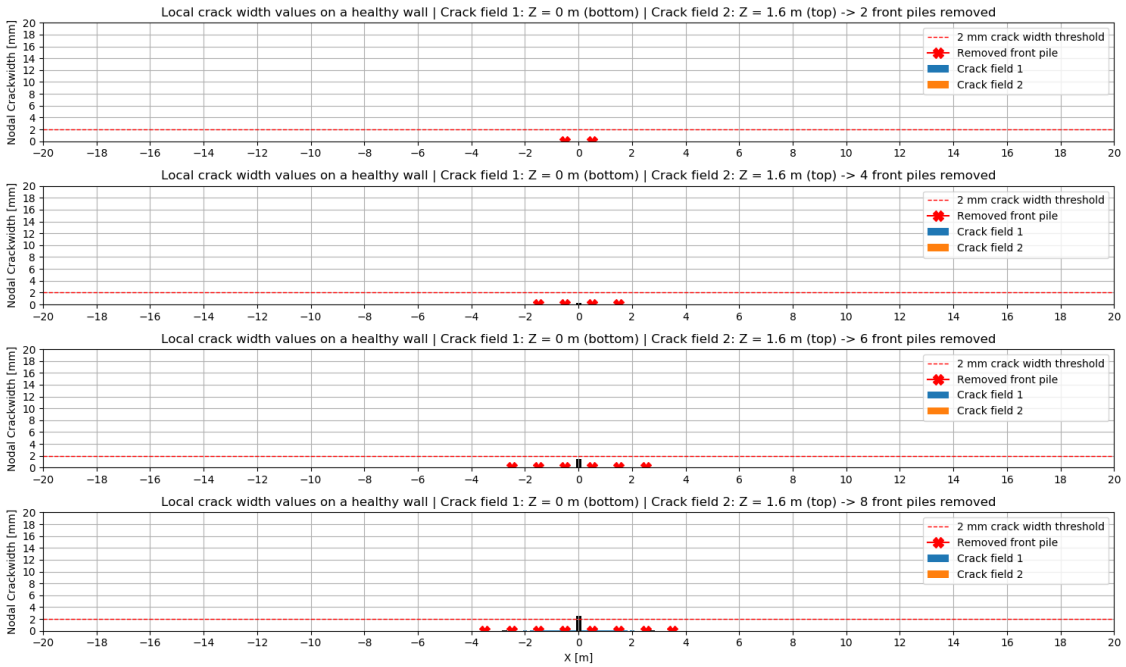

Figure C.8: Crack width values at the bottom (1st crack area) and the top (2nd crack area) of the masonry wall. Front piles have been incrementally removed on a strong quay wall structure. [PART 1/3]

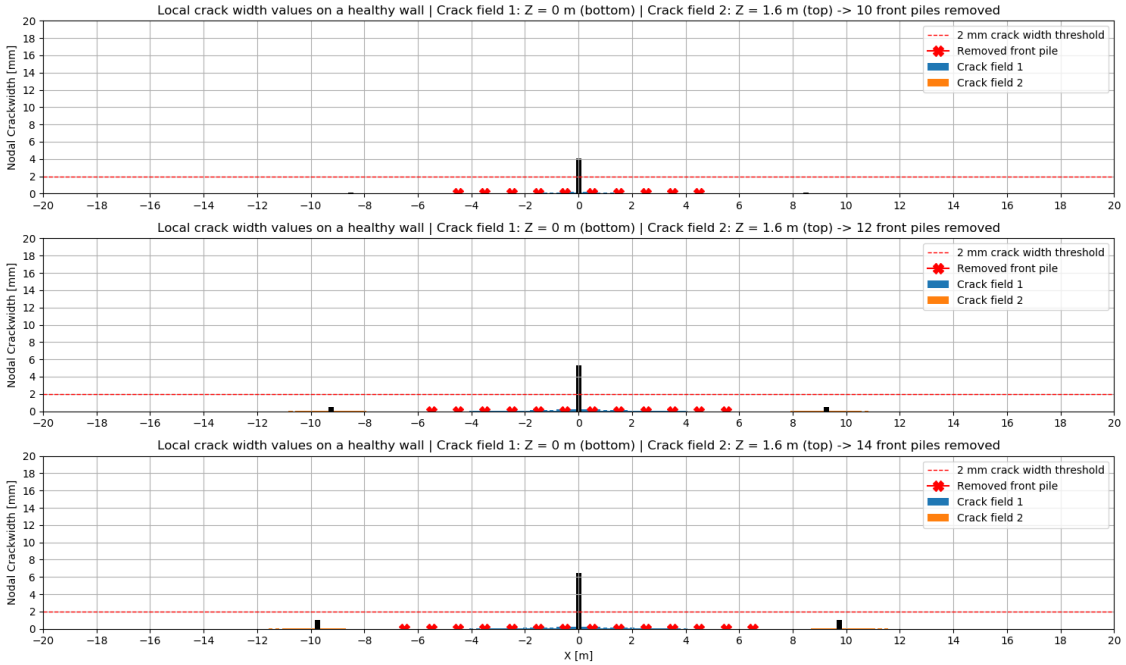

Figure C.9: Crack width values at the bottom (1st crack area) and the top (2nd crack area) of the masonry wall. Front piles have been incrementally removed on a strong quay wall structure. [PART 2/3]

Figure C.10: Crack width values at the bottom (1st crack area) and the top (2nd crack area) of the masonry wall. Front piles have been incrementally removed on a strong quay wall structure. [PART 3/3]

The effect of changing the foundation quality on the onset of cracking will be presented here.

The case has been presented with the following properties:

- Baseline properties according to table 5.4.
- Six entire adjacent pile rows removed.
- Foundation E-modulus comparison: 3 GPa, 4 GPa, 5 GPa and 6 GPa.
- Pile diameter comparison: 160 mm, 170 mm and 180 mm.

The effect of changing pile diameters of the remaining piles.

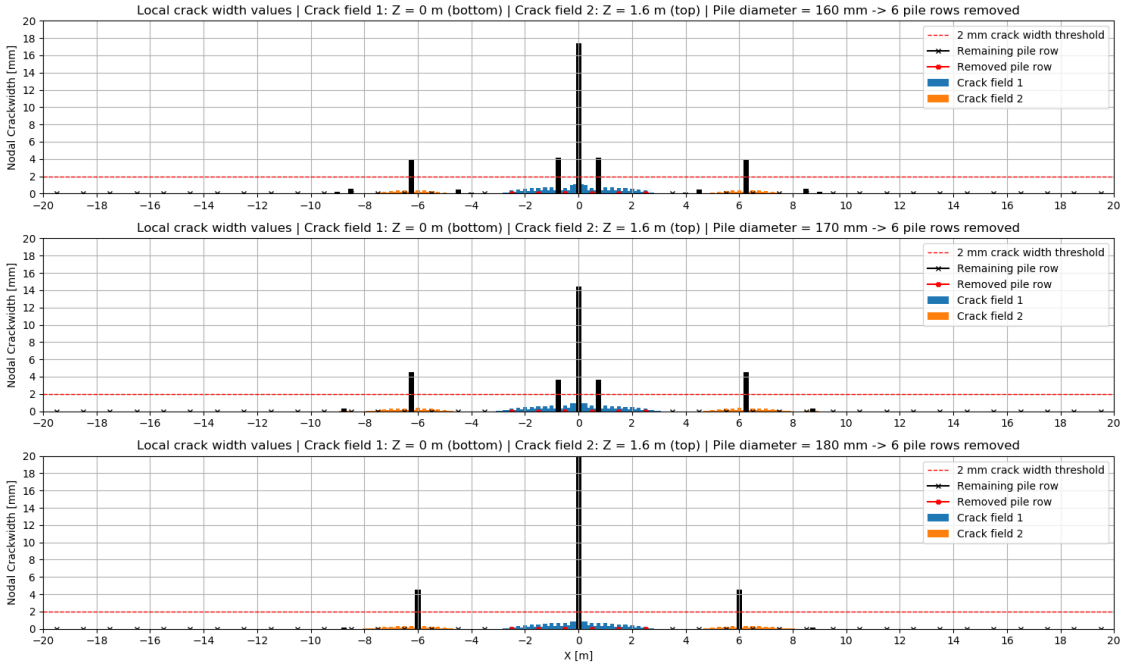

Figure C.11: The upper graph presents the nodal crack widths at the top (crack field 2) and the bottom (crack field 1) of the masonry wall, with a global pile diameter of 160 mm. The lower graph presents the same, except with a global pile diameter of 180 mm. The middle graph uses a pile diameter of 170 mm.

The effect of changing foundation stiffness.

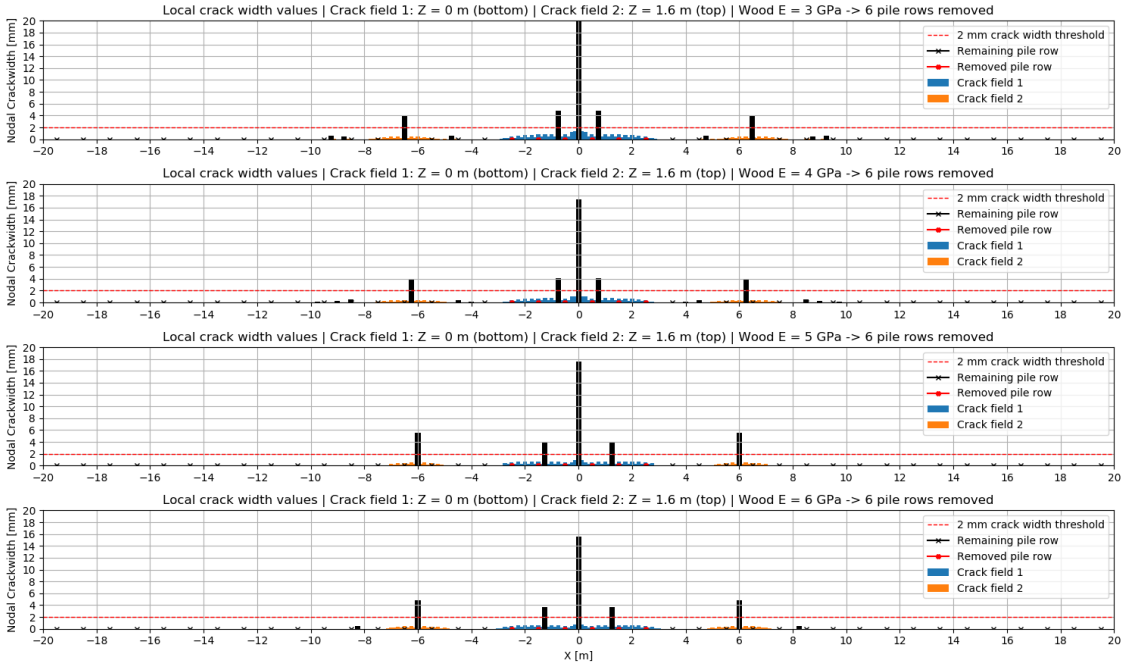

Figure C.12: The upper graph presents the nodal crack widths at the top (crack field 2) and the bottom (crack field 1) of the masonry wall, with a wood E-modulus of 3 GPa. The lower graph presents the same, except with a wood E-modulus of 6 GPa. Stiffness values of 4 GPa and 5 GPa are represented by the second and third graph respectively.

C.2. Non-uniform soil removal

This section presents the full results regarding crack progression from section 5.5. The baseline properties are presented below.

Property	Value	Unit
Strong masonry: Young's modulus	5000	N/mm^2
Strong masonry: Shear modulus	2000	N/mm^2
Strong masonry: Poisson's ratio	0.25	-
Strong masonry: Mass density	1800	kg/m^3
Strong masonry: Tensile strength	0.35	N/mm^2
Strong masonry: Tensile fracture energy	0.035	N/mm
Weak masonry: Young's modulus	3000	N/mm^2
Weak masonry: Shear modulus	1200	N/mm^2
Weak masonry: Poisson's ratio	0.25	-
Weak masonry: Mass density	1800	kg/m^3
Weak masonry: Tensile strength	0.21	N/mm^2
Weak masonry: Tensile fracture energy	0.021	N/mm
Pile: Young's modulus	6000	N/mm^2
Pile: Flexural strength	18	N/mm^2
Pile: Mass density	320	kg/m^3
Pile: Diameter	180	mm
Pile head connection	Hinged	-
Free height: Front pile	0	m
Free height: Middle pile	0	m
Free height: End pile	0	m
Sinkhole free height: Front pile	2.0	m
Sinkhole free height: Middle pile	1.5	m
Sinkhole free height: End pile	1.0	m

Table C.3: Initial properties used in the upcoming analyses.

Generalised crack fields induced by the removal of supporting soil are presented in figure C.1. The output is retrieved from DIANA. The corresponding crack interpretation is presented in figure after that.

Figure C.13: Generalised crack fields induced by removal of supporting soil, output produced in DIANA FEA.

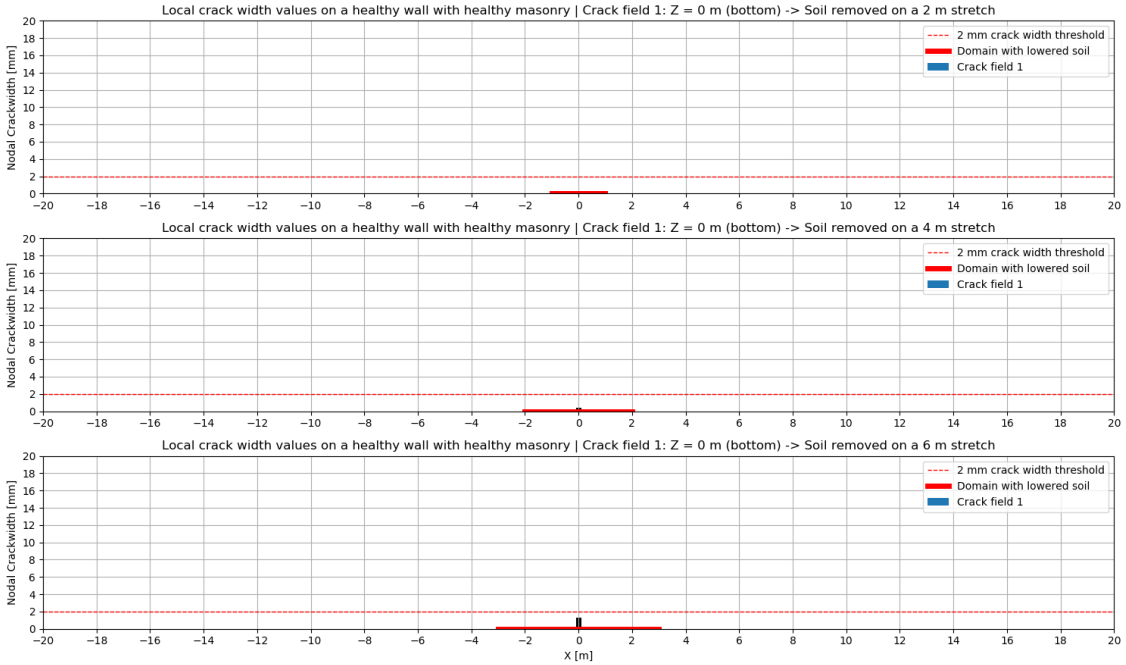

Figure C.14: The onset of cracking when removing up to two meters of soil locally. Simulations have been performed using strong masonry properties. [PART 1/2]

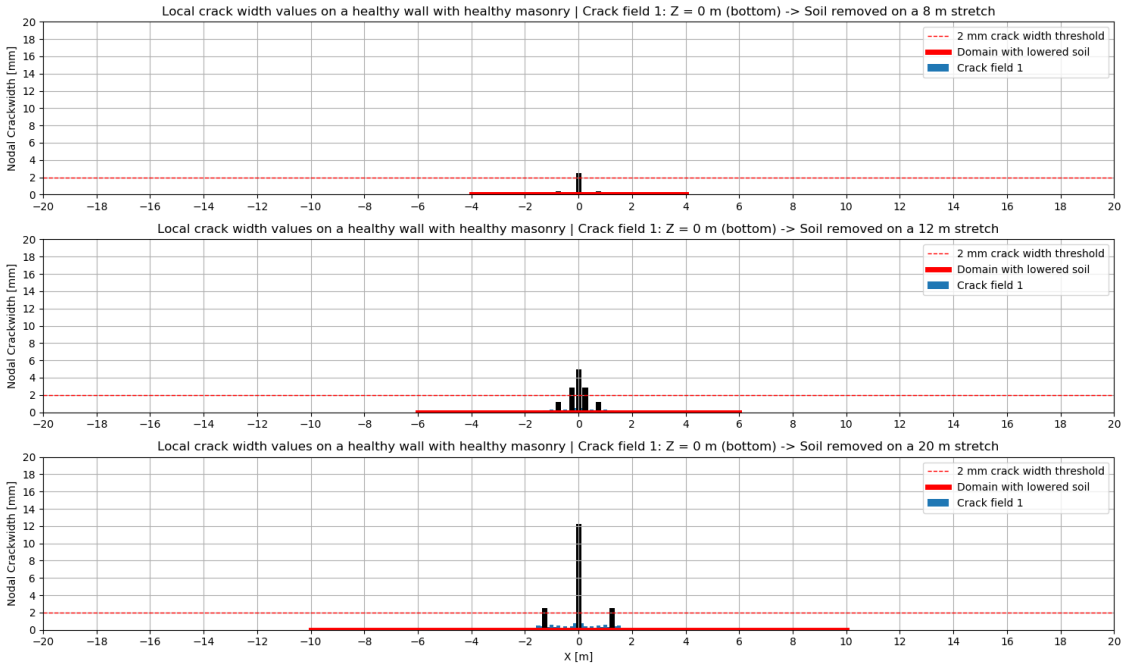

Figure C.15: The onset of cracking when removing up to two meters of soil locally. Simulations have been performed using strong masonry properties. [PART 2/2]

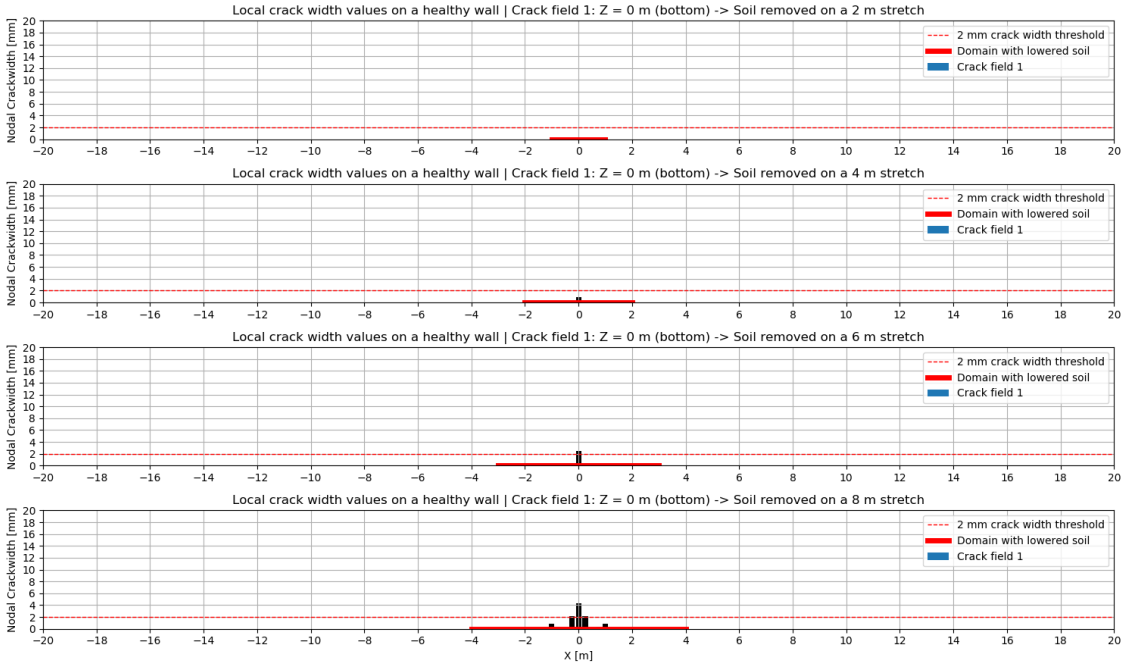

Figure C.16: The onset of cracking when removing up to two meters of soil locally. Simulations have been performed using weak masonry properties. [PART 1/2]

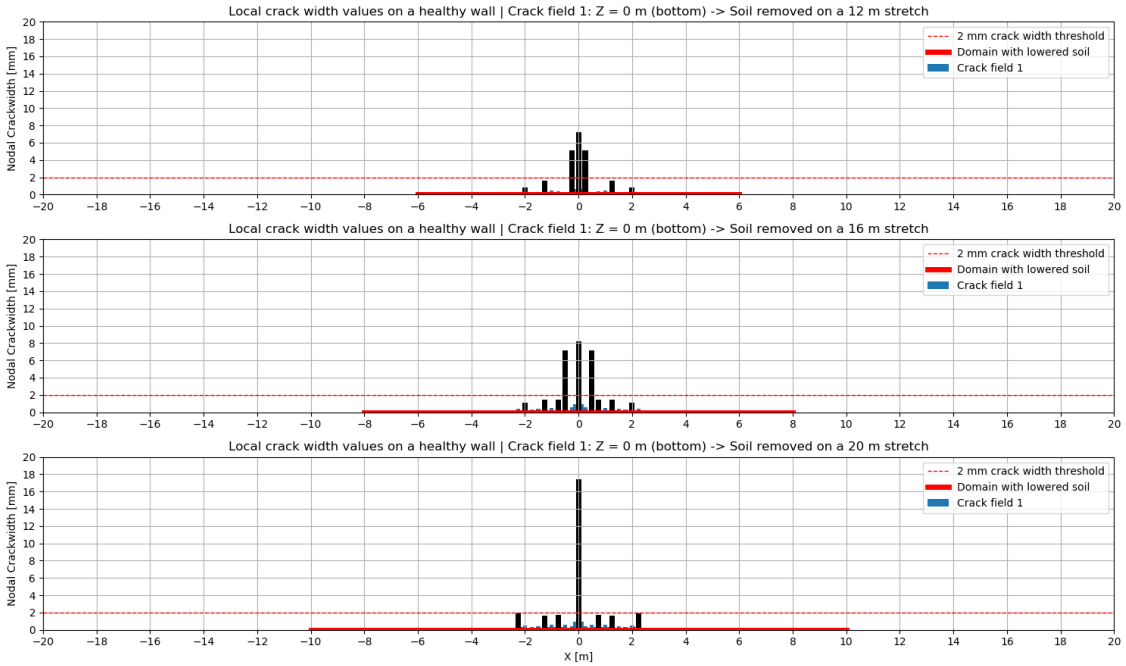

Figure C.17: The onset of cracking when removing up to two meters of soil locally. Simulations have been performed using weak masonry properties. [PART 2/2]

D

Nieuwe Herengracht Photos

This appendix contains all relevant photos of the current state of the "Nieuwe Herengracht" quay wall. The order is presented by location, starting from the North side.

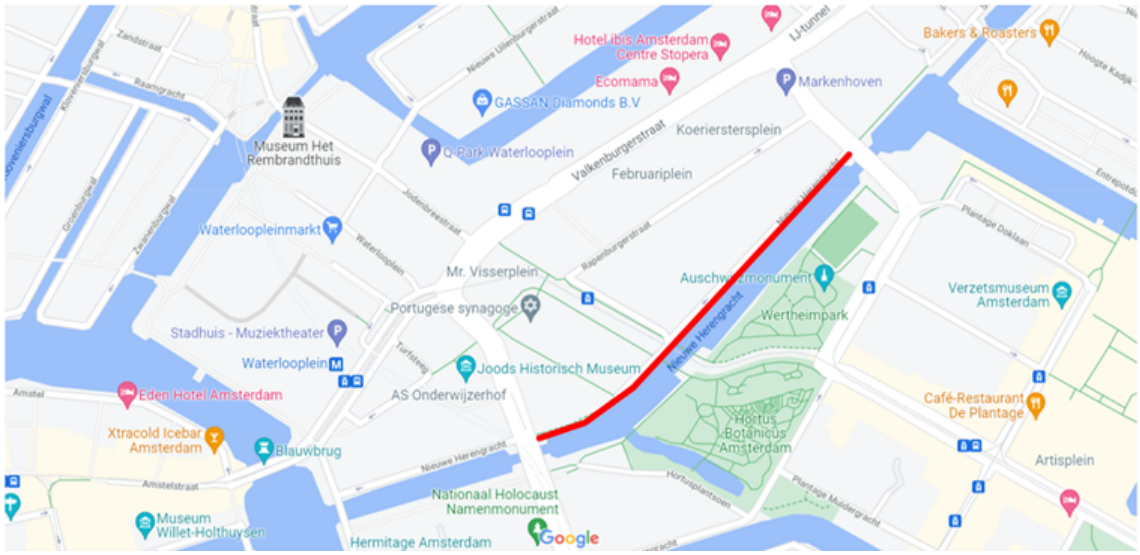

Figure D.1: Location of the quay wall at "Nieuwe Herengracht", where the photographs have been taken.

Figure D.2: First photo of the quay wall at "Nieuwe Herengracht". Quay shows movement towards the water as the masonry sticks out at the dilation joint.

Figure D.3: Second photo of the quay wall at "Nieuwe Herengracht". Vertical crack along with gaps between individual bricks at the lower side.

Figure D.4: Third photo of the quay wall at "Nieuwe Herengracht". Vertical crack along with gaps between individual bricks at the lower side.

Figure D.5: Fourth photo of the quay wall at "Nieuwe Herengracht". Vertical crack along with gaps between individual bricks at the lower side.

Figure D.6: Fifth photo of the quay wall at "Nieuwe Herengracht". Relatively uniform vertical crack along with relatively small gaps between individual bricks at the lower side.

Figure D.7: Sixth photo of the quay wall at "Nieuwe Herengracht". Shows the other side of the quay wall with damaged bricks and what appears to be a relatively thin diagonal crack moving up to the right, at the right-hand side of the dilation joint.

Figure D.8: Sixth photo of the quay wall at "Nieuwe Herengracht". Quay shows movement towards the water as the masonry sticks out at the dilation joint at the Southern end.

Figure D.9: Side view of the quay wall at "Nieuwe Herengracht". Street lanterns all tilt towards the water, indicating a forward tilt of the entire structure.

Figure D.10: Side view of the quay wall at "Nieuwe Herengracht". Masonry wall shows general forward tilting.

E

Python Code (Parametric Model)

This appendix contains only the parametric model code used to run simulations in DIANA FEA.

```
# -*- coding: utf-8 -*-
"""
Created on Tue Nov 23 2021

@author: Chris van Hulten
"""

import math

Mesh = 0.25 #m

Masonry_E = 3e+09 #N/m2 E-modulus
Masonry_TS = 210000 #N/m2 #Tensile Strength
Masonry_CE = 21 #N/m #Tensile Cr. Energy

Wood_E = 4e+09 #N/m2 E-modulus
Wood_S = 16e+06 #N/m2 Bending Strength

D = 0.16 #m PILE DIAMETER
D_Alter = 0.15 #m

Fu_diagram_Front = [-0.1, -55545.55175766722, -0.010254834494002175,
    -55545.55175766722, -0.003877852436341293, -37779.11155343931,
    -0.0018916911016798154, -19709.993795903036, -0.00080187910362499,
    -1539.1223000505706, -0.00019926687997969683, -0.0001, -0.0, -0.0]
K_ver_Front = Fu_diagram_Front[7]/Fu_diagram_Front[8]
Fu_diagram_Mid = [-0.1, -55545.55175766722, -0.010254834494002175,
    -55545.55175766722, -0.003877852436341293, -37779.11155343931,
    -0.0018916911016798154, -19709.993795903036, -0.00080187910362499,
    -1539.1223000505706, -0.00019926687997969683, -0.0001, -0.0, -0.0]
K_ver_Mid = Fu_diagram_Mid[7]/Fu_diagram_Mid[8]
Fu_diagram_End = [-0.1, -55545.55175766722, -0.010254834494002175,
    -55545.55175766722, -0.003877852436341293, -37779.11155343931,
    -0.0018916911016798154, -19709.993795903036, -0.00080187910362499,
```

```
    -1539.1223000505706, -0.00019926687997969683, -0.0001, -0.0, -0.0]
K_ver_End = Fu_diagram_End[7]/Fu_diagram_End[8]

Fu_diagram_Front_alter = [-0.1, -822.5301630399743, -0.01026488783321323,
    -822.5301630399743, -0.0041244771048613675, -589.0014499926849,
    -0.001992016308724927, -355.4763464149055, -0.0008437844684262449,
    -121.95025843635056, -0.0002196501348399889, -0.0001, -0.0, -0.0]
K_ver_Front_alter = Fu_diagram_Front_alter[7]/Fu_diagram_Front_alter[8]
Fu_diagram_Mid_alter = [-0.1, -83784.54272262246, -0.01026488783321323,
    -83784.54272262246, -0.0041244771048613675, -60125.42924560399,
    -0.001992016308724927, -36466.24282441756, -0.0008437844684262449,
    -12807.076297095125, -0.0002196501348399889, -0.0001, -0.0, -0.0]
K_ver_Mid_alter = Fu_diagram_Mid_alter[7]/Fu_diagram_Mid_alter[8]
Fu_diagram_End_alter = [-0.1, -85316.06914124746, -0.01026488783321323,
    -85316.06914124746, -0.0041244771048613675, -61370.523154294984,
    -0.001992016308724927, -37325.83677193826, -0.0008437844684262449,
    -13381.028181931295, -0.0002196501348399889, -0.0001, -0.0, -0.0]
K_ver_End_alter = Fu_diagram_End_alter[7]/Fu_diagram_End_alter[8]

#SPACE DEPENDENT VARIABLES
pile_y = [0.2,1.1,2.4] # Y-COORD PILES
p = [0.9, 0.8, 0.7] #- GROUP REDUCTION FACTOR

n = 20 #Quay wall length = no. of 1 m segments
x_alter = [1,2,3] # Between 1 and n
boundarycondition = 0 #0: Slide, 1: Rigid
pileconnection = 0 #0: Hinge, 1: Rigid
removed = []

removed = [x-1 for x in removed]

B = 0.7
L_plank = 2.8

forceloc = 1 #-1: behind, 1: front
q = 0 # Added surcharge
q_behind = 0
qwall = q*0
qx = [0,n] # Domain along quay wall with added surcharge: >= 0 and <= n

thick_front = [2.5,3.0,2.5,2.5,0.5]
thick_mid = [2.5,3.0,2.5,2.5,0.5]
thick_end = [2.5,3.0,2.5,2.5,0.5]
thick = [thick_front,thick_mid,thick_end]

cohesion = 200000

thick_front_alter = [0.5,3.0,2.5,2.5,0.5]
thick_mid_alter = [1.0,3.0,2.5,2.5,0.5]
thick_end_alter = [1.5,3.0,2.5,2.5,0.5]
thick_alter = [thick_front_alter,thick_mid_alter,thick_end_alter]

#GLOBAL
x_alter = [x-1 for x in x_alter]
x_main = list(range(n))

for i in range(len(x_alter)):
    if x_alter[i] >= n:
        break
    x_main.remove(x_alter[i])
```

```
77
78 piles_front_main = ["PileFrontMain"+str(i+1) for i in x_main]
79 piles_mid_main = ["PileMidMain"+str(i+1) for i in x_main]
80 piles_end_main = ["PileEndMain"+str(i+1) for i in x_main]
81
82 piles_front_alter = ["PileFrontAlter"+str(i+1) for i in x_alter]
83 piles_mid_alter = ["PileMidAlter"+str(i+1) for i in x_alter]
84 piles_end_alter = ["PileEndAlter"+str(i+1) for i in x_alter]
85
86 def ProjectSettings(): #Sets Project
87     newProject( "./KadePaal/KadePaal.dpf", 100 )
88     setModelAnalysisAspects( [ "STRUCT" ] )
89     setModelDimension( "3D" )
90     setDefaultMeshOrder( "QUADRATIC" )
91     setDefaultMesherType( "HEXQUAD" )
92     setDefaultMidSideNodeLocation( "LINEAR" )
93     setModelAnalysisAspects( [ "STRUCT" ] )
94     setModelDimension( "3D" )
95     setDefaultMeshOrder( "QUADRATIC" )
96     setDefaultMesherType( "HEXQUAD" )
97     setDefaultMidSideNodeLocation( "LINEAR" )
98
99 def Shapes(): #Creates Shapes
100
101     #1. MASONRY WALL (3D)
102     #createSheet( "Masonry", [[ 0, 0, 0 ],[ 0, 0, 1.6 ],[ 0, B-0.2, 1.6 ],[
        0, B-0.2, 1.1 ],[ 0, B-0.1, 1.1 ],[ 0, B-0.1, 0.6 ],[ 0, B, 0.6 ],[ 0,
        B, 0 ]] )
103     #extrudeProfile( [ "Masonry" ], [ n, 0, 0 ] )
104     createBlock( "Masonry", [ 0, 0, 0 ], [ n, B, 0.6 ] )
105     createBlock( "Masonry2", [ 0, 0, 0.6 ], [ n, B-0.1, 0.5 ] )
106     createBlock( "Masonry3", [ 0, 0, 1.1 ], [ n, B-0.2, 0.5 ] )
107     #unite( "Masonry", [ "Block 2", "Block 3" ], False, True )
108     createLine( "Line 1", [ 0, B-0.1, 0.6 ], [ n, B-0.1, 0.6 ] )
109     projection( "Masonry", [ "Line 1" ], [ 0, 0, -1 ], True )
110     removeShape( [ "Line 1" ] )
111     createLine( "Line 1", [ 0, B-0.2, 1.1 ], [ n, B-0.2, 1.1 ] )
112     projection( "Masonry2", [ "Line 1" ], [ 0, 0, -1 ], True )
113     removeShape( [ "Line 1" ] )
114
115     lines = ["Line "+str(i+1) for i in range(n+1)]
116
117     X = [[[ 0, pile_y[0], 0 ], [ 0.5, pile_y[0], 0 ]]]
118     for i in range(0,n-1):
119         X.append([[ 0.5 + i, pile_y[0], 0 ], [ 1.5 + i, pile_y[0], 0 ]])
120     X.append([[ n-0.5, pile_y[0], 0 ], [ n, pile_y[0], 0 ]])
121
122     for i in range(len(lines)):
123         createLine( lines[i], X[i][0], X[i][1] )
124
125     projection( "Masonry", lines, [ 0, 0, -1 ], True )
126     removeShape( lines )
127     setShapeColor( "#990000", [ "Masonry", "Masonry2", "Masonry3" ] )
128
129     setViewPoint( "ISO1" )
130
131     #2. FOUNDATION PLANKS DIRECTLY UNDERNEATH WALL (2D)
132     createSheet( "Planks1", [[ 0, 0, -0.1 ],[ 0, B, -0.1 ],[ n, B, -0.1 ],[
        n, 0, -0.1 ]] )
133
```

```
    X = [[[ 0, pile_y[0], -0.1 ], [ 0.5, pile_y[0], -0.1 ]]]
    for i in range(0,n-1):
        X.append([[ 0.5 + i, pile_y[0], -0.1 ], [ 1.5 + i, pile_y[0], -0.1 ]])
    X.append([[ n-0.5, pile_y[0], -0.1 ], [ n, pile_y[0], -0.1 ]])

    for i in range(len(lines)):
        createLine( lines[i], X[i][0], X[i][1] )

    projection( "Planks1", lines, [ 0, 0, -1 ], True )
    removeShape( lines )
    setShapeColor( "#f1c232", [ "Planks1" ] )

    #3. FOUNDATION PLANKS DIRECTLY UNDERNEATH SOIL (2D)
    createSheet( "Planks2", [[ 0, B, -0.1 ],[ 0, 2.8, -0.1 ],[ n, 2.8, -0.1 ],[ n, B, -0.1 ]] )

    for j in [1,2]:
        X = [[[ 0, pile_y[j], -0.1 ], [ 0.5, pile_y[j], -0.1 ]]]
        for i in range(0,n-1):
            X.append([[ 0.5 + i, pile_y[j], -0.1 ], [ 1.5 + i, pile_y[j], -0.1 ]])
        X.append([[ n-0.5, pile_y[j], -0.1 ], [ n, pile_y[j], -0.1 ]])

        for i in range(len(lines)):
            createLine( lines[i], X[i][0], X[i][1] )

        projection( "Planks2", lines, [ 0, 0, -1 ], True )
        removeShape( lines )

    setShapeColor( "#f1c232", [ "Planks2" ] )

    virtualpoints = ["Point body "+str(i) for i in range(1,int(n/Mesh)+1)] #Because two points

    X = -Mesh #Point 0: Because Point 1 must be at x = 0.5 m
    for i in range(len(virtualpoints)):
        X += Mesh #Add pile row every 1 meter
        createPointBody( virtualpoints[i], [ X, L_plank, -0.1 ])

    projection( "SHAPEFACE", "Planks2", [[ 0.5, L_plank-0.01, -0.1 ]], virtualpoints, [ 0, 0, -1 ], True )
    removeShape( virtualpoints )

    #4. VIRTUAL BOUNDARY

    createSheet( "VirtualBoundary", [[ 0, 2.8, -0.0 ],[ 0, 2.8, 1.6 ],[ n, 2.8, 1.6 ],[ n, 2.8, -0.0 ]] )

    virtuallines = ["Line "+str(i) for i in range(1,int(n/Mesh)+1)]

    X = -Mesh #Point 0: Because Point 1 must be at x = 0.5 m
    for i in range(len(virtuallines)):
        X += Mesh #Add pile row every 1 meter
        createLine( virtuallines[i], [ X, L_plank, 0 ],[ X, L_plank, 1.6 ])

    projection( "VirtualBoundary", virtuallines, [ 0, 1, 0 ], True )
    removeShape( virtuallines )

    #PILES
```

```
188
189     pile_row = [piles_front_main, piles_mid_main, piles_end_main]
190
191     X = [x+0.5 for x in x_main] #Point 0: Because Point 1 must be at x =
    0.5 m
192     for j in range(len(pile_row)):
193         for i in range(len(pile_row[j])):
194             #X += 1 #Add pile row every 1 meter
195             createLine( pile_row[j][i], [ X[i], pile_y[j], -11.2 ], [ X[i],
     pile_y[j], -0.2 ] )
196             createPointBody( "Point body 1", [ X[i], pile_y[j], -10.7 ] )
197             createPointBody( "Point body 2", [ X[i], pile_y[j], -8.2 ] )
198             createPointBody( "Point body 3", [ X[i], pile_y[j], -5.7 ] )
199             createPointBody( "Point body 4", [ X[i], pile_y[j], -2.7 ] )
200             createPointBody( "Point body 5", [ X[i], pile_y[j], -11.2 + sum
    (thick[j]) ] )
201             projection( "SHAPEEDGE", pile_row[j][i], [[ X[i], pile_y[j],
    -5.7 ]], [ "Point body 1", "Point body 2", "Point body 3", "Point body
    4", "Point body 5" ], [ 1, 0, 0 ], True )
202             removeShape( [ "Point body 1", "Point body 2", "Point body 3",
    "Point body 4", "Point body 5" ] )
203
204 def ShapeMaterials(): #Creates Materials for Shapes
205
206     #MASONRY
207     addMaterial( "Masonry_Cracking", "CONCR", "TSCR", [] )
208     setParameter( "MATERIAL", "Masonry_Cracking", "LINEAR/ELASTI/YOUNG",
    Masonry_E )
209     setParameter( "MATERIAL", "Masonry_Cracking", "LINEAR/ELASTI/POISON",
    0.25 )
210     setParameter( "MATERIAL", "Masonry_Cracking", "LINEAR/MASS/DENSIT",
    1800 )
211     setParameter( "MATERIAL", "Masonry_Cracking", "MODTYP/TOTCRK", "ROTATE"
     )
212     setParameter( "MATERIAL", "Masonry_Cracking", "TENSIL/TENCRV", "EXPONE"
     )
213     setParameter( "MATERIAL", "Masonry_Cracking", "TENSIL/TENSTR",
    Masonry_TS )
214     setParameter( "MATERIAL", "Masonry_Cracking", "TENSIL/GF1", Masonry_CE
    )
215     setParameter( "MATERIAL", "Masonry_Cracking", "TENSIL/CBSPEC", "GOVIND"
     )
216     setParameter( "MATERIAL", "Masonry_Cracking", "TENSIL/RESTST", 0 )
217
218     #setParameter( "MATERIAL", "Masonry_Cracking", "COMPRS/COMCRV", "THOREN
    " )
219     #setParameter( "MATERIAL", "Masonry_Cracking", "COMPRS/COMSTR", 8500000
     )
220     #setParameter( "MATERIAL", "Masonry_Cracking", "COMPRS/NTHORE", 0.85 )
221     #setParameter( "MATERIAL", "Masonry_Cracking", "COMPRS/KTHORE", 0.85 )
222     #setParameter( "MATERIAL", "Masonry_Cracking", "COMPRS/LTHORE", 0 )
223     #setParameter( "MATERIAL", "Masonry_Cracking", "COMPRS/RESCST", 1000000
     )
224
225     #PLANKS
226     addMaterial( "Planks", "MCSTEL", "ISOTRO", [] )
227     setParameter( "MATERIAL", "Planks", "LINEAR/ELASTI/YOUNG", Wood_E )
228     setParameter( "MATERIAL", "Planks", "LINEAR/ELASTI/POISON", 0.3 )
229     setParameter( "MATERIAL", "Planks", "LINEAR/MASS/DENSIT", 320 )
230
```

```
231     #PILE
232     epsilon = Wood_S/Wood_E
233     epsilon2 = epsilon + 0.1*epsilon
234     addMaterial( "Wood", "MCSTEL", "UNIAXI", [] )
235     setParameter( "MATERIAL", "Wood", "ELASTI/ELASTI/YOUNG", Wood_E )
236     setParameter( "MATERIAL", "Wood", "ELASTI/MASS/DENSIT", 320 )
237     setParameter( "MATERIAL", "Wood", "ELASTI/EPSSIG", [ -1.0, 0, -epsilon2
        , 0, -epsilon, -Wood_S, 0, 0, epsilon, Wood_S, epsilon2, 0, 1.0, 0 ] )
238     setParameter( "MATERIAL", "Wood", "ELASTI/EPSSIG", [ -5.0, -Wood_S, -
        epsilon, -Wood_S, 0, 0, epsilon, Wood_S, epsilon2, 0, 5.0, 0 ] )
239
240     #BROKEN PILE
241     epsilon = Wood_S/Wood_E
242     epsilon2 = epsilon + 0.1*epsilon
243     addMaterial( "WoodBroken", "MCSTEL", "UNIAXI", [] )
244     setParameter( "MATERIAL", "WoodBroken", "ELASTI/ELASTI/YOUNG", 0.1*
        Wood_E )
245     setParameter( "MATERIAL", "WoodBroken", "ELASTI/MASS/DENSIT", 320 )
246     setParameter( "MATERIAL", "WoodBroken", "ELASTI/EPSSIG", [ -5.0, 0, -
        epsilon2, 0, -epsilon, -0.1*Wood_S, 0, 0, epsilon, 0.1*Wood_S, epsilon2
        , 0, 5.0, 0 ] )
247     setParameter( "MATERIAL", "WoodBroken", "ELASTI/EPSSIG", [ -5.0, -0.1*
        Wood_S, -epsilon, -0.1*Wood_S, 0, 0, epsilon, 0.1*Wood_S, epsilon2, 0,
        5.0, 0 ] )
248
249     #VIRTUAL BOUNDARY
250     addMaterial( "VirtualMaterial", "MCSTEL", "ISOTRO", [] )
251     setParameter( "MATERIAL", "VirtualMaterial", "LINEAR/ELASTI/YOUNG", 1e
        +12 )
252     setParameter( "MATERIAL", "VirtualMaterial", "LINEAR/ELASTI/POISON",
        0.3 )
253     setParameter( "MATERIAL", "VirtualMaterial", "LINEAR/MASS/DENSIT", 1 )
254
255     #MASONRY-PLANKS1 INTERFACE CONDITION (SLIDING)
256     addMaterial( "Masonry-Planks1 Interface", "INTERF", "ELASTI", [] )
257     setParameter( "MATERIAL", "Masonry-Planks1 Interface", "LINEAR/ELAS6/
        DSNZ", 5000000 )
258     setParameter( "MATERIAL", "Masonry-Planks1 Interface", "LINEAR/ELAS6/
        DSSX", 1e+09 )
259     setParameter( "MATERIAL", "Masonry-Planks1 Interface", "LINEAR/ELAS6/
        DSSY", 1e+09 )
260
261
262     addMaterial( "Masonry-Planks1 Interface NL", "INTERF", "FRICTI", [] )
263     setParameter( "MATERIAL", "Masonry-Planks1 Interface NL", "LINEAR/ELAS6
        /DSNZ", 1e+09 )
264     setParameter( "MATERIAL", "Masonry-Planks1 Interface NL", "LINEAR/ELAS6
        /DSSX", 1e+09 )
265     setParameter( "MATERIAL", "Masonry-Planks1 Interface NL", "LINEAR/ELAS6
        /DSSY", 1e+09 )
266     setParameter( "MATERIAL", "Masonry-Planks1 Interface NL", "COULOM/
        COHESI", cohesion )
267     setParameter( "MATERIAL", "Masonry-Planks1 Interface NL", "COULOM/PHI",
         0.7 )
268     setParameter( "MATERIAL", "Masonry-Planks1 Interface NL", "COULOM/PSI",
         0 )
269     #setParameter( "MATERIAL", "Masonry-Planks1 Interface NL", "COULOM/
        OPNTYP", "GAP" )
270     #setParameter( "MATERIAL", "Masonry-Planks1 Interface NL", "COULOM/
        GAPVAL", 20000 )
```

```
271
272     #SOIL MATERIALS
273     no = 1 #SOIL MULTIPLIER
274     pi = 3.141592653589793
275
276     #Order: Clay, Peat, Silt, Clay, Sand
277     Soiltype = ["Clay1","Peat","Silt","Clay2","Sand"]
278     qc = [0.5, 0.5, 2.0, 0.5, 15.0]
279     alpha = [2/3, 1, 1/2, 2/3, 1/3]
280     beta = [2.0, 3.0, 1.0, 2.0, 0.7]
281     R = D/2
282
283     Stiffness = [[],[],[]]
284
285     for i in range(len(qc)):
286         for j in range(3): #ROW
287             Stiffness[j].append((((2*R)/(qc[i]*beta[i]))*((4.0*(2.65)**
    alpha[i]+alpha[i]*3)/18))**-1*10**6 * no * p[j]) #N/m3
288             #Stiffness[j].append(((1/(3*qc[i]*beta[i]))*(1.3*0.3*(2.65*(R
    /0.3))**alpha[i]+alpha[i]*R))**-1*10**6 * no)
289
290     phi = [17.5, 15, 27.5, 17.5, 32.5]
291     phi = [x*2*pi/360 for x in phi]
292     c = [5, 2.5, 1, 5, 0] #kPa
293
294     Kq0 = [1.9, 1.5, 3.9, 1.9, 5.8]
295     Kqinf = [4.5, 3.5, 13.1, 4.5, 24.6]
296     Kc0 = [4.3, 3.9, 6.2, 4.3, 7.9]
297     Kcinf = [20.6, 17.6, 46.7, 20.6, 83.4]
298     K0 = [1-math.sin(x) for x in phi]
299
300     aq = []
301     ac = []
302
303     for i in range(len(phi)):
304
305         aq.append((Kq0[i]/(Kqinf[i]-Kq0[i]))*((K0[i]*math.sin(phi[i]))/
306                                                 math.sin(0.25*pi+0.5*phi[i
    ])))
307
308         ac.append((Kc0[i]/(Kcinf[i]-Kc0[i]))*2*math.sin(0.25*pi+0.5*phi[i])
    )
309
310     thick_front.insert(0,0)
311     thick_mid.insert(0,0)
312     thick_end.insert(0,0)
313     def accumu(lis):
314         total = 0
315         for x in lis:
316             total += x
317             yield total
318
319     Depth_bnd_front = list(accumu(thick_front))
320     Depth_bnd_mid = list(accumu(thick_mid))
321     Depth_bnd_end = list(accumu(thick_end))
322
323     Depth_mid_front = []
324     Depth_mid_mid = []
325     Depth_mid_end = []
326
```

```
    for i in range(len(thick[0])-1):
        Depth_mid_front.append(0.5*(Depth_bnd_front[i+1]-Depth_bnd_front[i])+Depth_bnd_front[i])
        Depth_mid_mid.append(0.5*(Depth_bnd_mid[i+1]-Depth_bnd_mid[i])+Depth_bnd_mid[i])
        Depth_mid_end.append(0.5*(Depth_bnd_end[i+1]-Depth_bnd_end[i])+Depth_bnd_end[i])

    Depth = [Depth_mid_front,Depth_mid_mid,Depth_mid_end]

    gamma = [12, 17, 20, 20] #kN/m3
    gamma = [x-10 for x in gamma]

    sig = [0,0,0]
    thick_front.pop(0)
    thick_mid.pop(0)
    thick_end.pop(0)
    for i in range(3): #ROW
        layer = thick[i]
        sig1 = layer[0]*gamma[1]*0.5
        sig2 = layer[0]*gamma[1]+layer[1]*gamma[0]*0.5
        sig3 = layer[0]*gamma[1]+layer[1]*gamma[0]+layer[2]*gamma[2]*0.5
        sig4 = layer[0]*gamma[1]+layer[1]*gamma[0]+layer[2]*gamma[2]+layer[3]*gamma[1]*0.5
        sig5 = layer[0]*gamma[1]+layer[1]*gamma[0]+layer[2]*gamma[2]+layer[3]*gamma[1]+layer[4]*gamma[3]*0.5
        sig[i] = [sig1,sig2,sig3,sig4,sig5]

    Kq =[[],[],[]]
    Kc =[[],[],[]]

    for i in range(len(phi)):
        for j in range(3): #ROW
            Kq[j].append((Kq0[i] +Kqinf[i]*aq[i]*(Depth[j][i]/D))/(1+aq[i]*(Depth[j][i]/D)))
            Kc[j].append((Kc0[i] +Kcinf[i]*ac[i]*(Depth[j][i]/D))/(1+ac[i]*(Depth[j][i]/D)))

    sigp = [[],[],[]]

    for i in range(len(phi)):
        for j in range(3):
            if Depth[j][i] != 0:
                sigp[j].append(Kq[j][i]*sig[j][i] + Kc[j][i]*c[i])
            else:
                sigp[j].append(0)
                Stiffness[j][i] = 1

    for i in range(3):
        sigp[i] = [1000*p[i]*x for x in sigp[i]] #N/m2

    u = [0,0,0]
    for i in range(3):
        u[i]  = [x / y for x, y in zip(sigp[i], Stiffness[i])] #m

    row = ["FrontMain", "MidMain", "EndMain"]

    for j in range(3):
        for i in range(len(Soiltype)):
            addMaterial( Soiltype[i]+row[j], "INTERF", "NONLIF", [] )
```

```
            addMaterial( Soiltype[i]+row[j], "INTERF", "ELASTI", [] )
            setParameter( "MATERIAL", Soiltype[i]+row[j], "LINEAR/IFTYP", "LIN3D3" ) #Normal = 3, Shell = None
            setParameter( "MATERIAL", Soiltype[i]+row[j], "LINEAR/ELAS7/DSNY", Stiffness[j][i] ) #7; 4
            setParameter( "MATERIAL", Soiltype[i]+row[j], "LINEAR/ELAS7/DSSX", Stiffness[j][i] ) #7; 4
            setParameter( "MATERIAL", Soiltype[i]+row[j], "LINEAR/ELAS7/DSSZ", 0 ) #7; 4
            setParameter( "MATERIAL", Soiltype[i]+row[j], "NONLIN/IFNOTE", "DIAGRM" )
            setParameter( "MATERIAL", Soiltype[i]+row[j], "NONLIN/NLEL10/DUSTNY", [ -5, -sigp[j][i], -u[j][i], -sigp[j][i], 0, 0, u[j][i], sigp[j][i], 5, sigp[j][i] ] ) #10; 4

    addMaterial( "Pile_Ver_Front", "SPRING", "LINETR", [] )
    setParameter( "MATERIAL", "Pile_Ver_Front", "LINETR/SPRING", K_ver_Front )
    setParameter( "MATERIAL", "Pile_Ver_Front", "LINETR/SPTYPE", "DIAGRA" )
    setParameter( "MATERIAL", "Pile_Ver_Front", "LINETR/DIAGRA/DUFX", Fu_diagram_Front )

    addMaterial( "Pile_Ver_Mid", "SPRING", "LINETR", [] )
    setParameter( "MATERIAL", "Pile_Ver_Mid", "LINETR/SPRING", K_ver_Mid )
    setParameter( "MATERIAL", "Pile_Ver_Mid", "LINETR/SPTYPE", "DIAGRA" )
    setParameter( "MATERIAL", "Pile_Ver_Mid", "LINETR/DIAGRA/DUFX", Fu_diagram_Mid )

    addMaterial( "Pile_Ver_End", "SPRING", "LINETR", [] )
    setParameter( "MATERIAL", "Pile_Ver_End", "LINETR/SPRING", K_ver_End )
    setParameter( "MATERIAL", "Pile_Ver_End", "LINETR/SPTYPE", "DIAGRA" )
    setParameter( "MATERIAL", "Pile_Ver_End", "LINETR/DIAGRA/DUFX", Fu_diagram_End )

def ElementGeometries(): #Creates Element Geometries

    #PLANK THICKNESS
    addGeometry( "Planks", "SHEET", "CURSHL", [] )
    setParameter( "GEOMET", "Planks", "THICK", 0.05 )

    #PILE DIAMETER
    addGeometry( "Paal_Diameter", "LINE", "CLS3B3", [] )
    setParameter( "GEOMET", "Paal_Diameter", "SHAPE/BESHAP", "CIRCLE" )
    setParameter( "GEOMET", "Paal_Diameter", "SHAPE/ROUND/CIRCLE", D )

    #SOIL SPRING SUPPORT THICKNESS
    addGeometry( "Soil_Geometry", "LINE", "LIN3DS", [] )
    setParameter( "GEOMET", "Soil_Geometry", "THICK", D )
    #setParameter( "GEOMET", "Soil_Geometry", "ZAXIS", [ 0, 1, 0 ] ) #for SHLLIF
    setParameter( "GEOMET", "Soil_Geometry", "LOCAXS", True )
    setParameter( "GEOMET", "Soil_Geometry", "LOCAXS/ZAXIS", [ 1, 0, 0 ] )

    #PILE DIAMETER ALTER
    addGeometry( "Paal_Diameter_Alter", "LINE", "CLS3B3", [] )
    setParameter( "GEOMET", "Paal_Diameter_Alter", "SHAPE/BESHAP", "CIRCLE" )
    setParameter( "GEOMET", "Paal_Diameter_Alter", "SHAPE/ROUND/CIRCLE", D_Alter )

```

```
    #SOIL SPRING SUPPORT THICKNESS ALTER
    addGeometry( "Soil_Geometry_Alter", "LINE", "LIN3DS", [] )
    setParameter( "GEOMET", "Soil_Geometry_Alter", "THICK", D_Alter )
    #setParameter( "GEOMET", "Soil_Geometry", "ZAXIS", [ 0, 1, 0 ] ) #for SHLLIF
    setParameter( "GEOMET", "Soil_Geometry_Alter", "LOCAXS", True )
    setParameter( "GEOMET", "Soil_Geometry_Alter", "LOCAXS/ZAXIS", [ 1, 0, 0 ] )

    #VERTICAL SPRING DIRECTION (Z)
    addGeometry( "Pile_Ver", "POINT", "SPRING", [] )
    setParameter( "GEOMET", "Pile_Ver", "AXIS", [ 0, 0, 1 ] )

    #VIRTUAL GEOMETRY
    addGeometry( "VirtualGeometry", "SHEET", "CURSHL", [] )
    setParameter( "GEOMET", "VirtualGeometry", "THICK", 0.1 )

def MaterialAssign(): #Assign properties to Shapes
    setElementClassType( "SHAPE", [ "Masonry","Masonry2","Masonry3" ], "STRSOL" )
    assignMaterial( "Masonry_Cracking", "SHAPE", [ "Masonry","Masonry2","Masonry3" ] )
    setElementClassType( "SHAPE", [ "Planks1" ], "CURSHL" )
    assignMaterial( "Planks", "SHAPE", [ "Planks1" ] )
    assignGeometry( "Planks", "SHAPE", [ "Planks1" ] )
    setElementClassType( "SHAPE", [ "Planks2" ], "CURSHL" )
    assignMaterial( "Planks", "SHAPE", [ "Planks2" ] )
    assignGeometry( "Planks", "SHAPE", [ "Planks2" ] )

    setElementClassType( "SHAPE", [ "VirtualBoundary" ], "CURSHL" )
    assignMaterial( "VirtualMaterial", "SHAPE", [ "VirtualBoundary" ] )
    assignGeometry( "VirtualGeometry", "SHAPE", [ "VirtualBoundary" ] )

    for i in range(len(piles_front_main)):
        setElementClassType( "SHAPE", [ piles_front_main[i] ], "CLS3B3" )
        assignMaterial( "Wood", "SHAPE", [ piles_front_main[i] ] )
        assignGeometry( "Paal_Diameter", "SHAPE", [ piles_front_main[i] ] )
    for i in range(len(piles_mid_main)):
        setElementClassType( "SHAPE", [ piles_mid_main[i] ], "CLS3B3" )
        assignMaterial( "Wood", "SHAPE", [ piles_mid_main[i] ] )
        assignGeometry( "Paal_Diameter", "SHAPE", [ piles_mid_main[i] ] )
    for i in range(len(piles_end_main)):
        setElementClassType( "SHAPE", [ piles_end_main[i] ], "CLS3B3" )
        assignMaterial( "Wood", "SHAPE", [ piles_end_main[i] ] )
        assignGeometry( "Paal_Diameter", "SHAPE", [ piles_end_main[i] ] )

    #MASONRY-PLANKS1 INTERFACE CONDITION
    createConnection( "Masonry-Planks1 Interface", "INTER", "SHAPEFACE", "SHAPEFACE" )
    setParameter( "GEOMETRYCONNECTION", "Masonry-Planks1 Interface", "MODE", "MANUAL" )
    attachTo( "GEOMETRYCONNECTION", "Masonry-Planks1 Interface", "SOURCE", "Planks1", [[ 0.232135, 0.5*pile_y[0], -0.1 ],[ 0.232135, pile_y[0]+0.01, -0.1 ]] )
    attachTo( "GEOMETRYCONNECTION", "Masonry-Planks1 Interface", "TARGET", "Masonry", [[ 0.232135, 0.5*pile_y[0], 0 ],[ 0.232135, pile_y[0]+0.01, 0 ]] )
    setElementClassType( "GEOMETRYCONNECTION", "Masonry-Planks1 Interface", "STPLIF" )
```

```
474     assignMaterial( "Masonry-Planks1 Interface NL", "GEOMETRYCONNECTION", "
        Masonry-Planks1 Interface" )
475     resetGeometry( "GEOMETRYCONNECTION", "Masonry-Planks1 Interface" )
476     setParameter( "GEOMETRYCONNECTION", "Masonry-Planks1 Interface", "FLIP"
        , False )
477     attachTo( "GEOMETRYCONNECTION", "Masonry-Planks1 Interface", "SRCANC",
        "Planks1", [[ 0, 0, -0.1 ]] )
478     attachTo( "GEOMETRYCONNECTION", "Masonry-Planks1 Interface", "SRCANC",
        "Planks1", [[ 0, pile_y[0], -0.1 ]] )
479     attachTo( "GEOMETRYCONNECTION", "Masonry-Planks1 Interface", "TRGANC",
        "Masonry", [[ 0, 0, 0 ]] )
480     attachTo( "GEOMETRYCONNECTION", "Masonry-Planks1 Interface", "TRGANC",
        "Masonry", [[ 0, pile_y[0], 0 ]] )
481     resetElementData( "GEOMETRYCONNECTION", "Masonry-Planks1 Interface" )
482
483 def Loads(): #Sets Loads
484
485     #LINEAR FUNCTION FOR HORIZONTAL SOIL LOAD
486     setFunctionValues( "Soil_Hor", [  ], [  ], [ 0, 0.85, 1.6 ], [ 6600,
        4050, 0 ] )
487
488     #HORIZONTAL SOIL LOAD
489     addSet( "GEOMETRYLOADSET", "Permanent" )
490     createSurfaceLoad( "Soil_Hor", "Permanent" )
491     setParameter( "GEOMETRYLOAD", "Soil_Hor", "FORCE/VALUE", -1 )
492     setParameter( "GEOMETRYLOAD", "Soil_Hor", "FORCE/DIRECT", 2 )
493     attach( "GEOMETRYLOAD", "Soil_Hor", "Masonry", [[ 0.573573, B, 0.1 ]] )
494     attach( "GEOMETRYLOAD", "Soil_Hor", "Masonry2", [[ 0.573573, B-0.1,
        0.9177168 ]] )
495     attach( "GEOMETRYLOAD", "Soil_Hor", "Masonry3", [[ 0.573573, B-0.2, 1.5
         ]] )
496     setValueFunction( "GEOMETRYLOAD", "Soil_Hor", "Soil_Hor" )
497
498     #VERTICAL LOADS (1: Dead-weight; 2: Soil column)
499     #createModelLoad( "Deadweight", "Permanent" ) #1
500
501     createSurfaceLoad( "Soil_Ver", "Permanent" ) #2
502     setParameter( "GEOMETRYLOAD", "Soil_Ver", "FORCE/VALUE", -22000 )
503     setParameter( "GEOMETRYLOAD", "Soil_Ver", "FORCE/DIRECT", 3 )
504     attach( "GEOMETRYLOAD", "Soil_Ver", "Planks2", [[ 0.426427, pile_y
        [1]-0.01, -0.1 ],[ 0.426427, pile_y[1]+0.01, -0.1 ],[ 0.426427, pile_y
        [2]+0.01, -0.1 ]] )
505     createSurfaceLoad( "Soil_Ver.a", "Permanent" ) #2
506     setParameter( "GEOMETRYLOAD", "Soil_Ver.a", "FORCE/VALUE", -16000 )
507     setParameter( "GEOMETRYLOAD", "Soil_Ver.a", "FORCE/DIRECT", 3 )
508     attach( "GEOMETRYLOAD", "Soil_Ver.a", "Masonry", [[ 0.426427, B-0.05,
        0.6 ]] )
509     createSurfaceLoad( "Soil_Ver.b", "Permanent" ) #2
510     setParameter( "GEOMETRYLOAD", "Soil_Ver.b", "FORCE/VALUE", -9000 )
511     setParameter( "GEOMETRYLOAD", "Soil_Ver.b", "FORCE/DIRECT", 3 )
512     attach( "GEOMETRYLOAD", "Soil_Ver.b", "Masonry2", [[ 0.426427, B-0.15,
        1.1 ]] )
513
514     #DELTA_Q
515     addSet( "GEOMETRYLOADSET", "Surcharge" )
516
517     q_xfunction = [ 0, qx[0]-0.001, qx[0]+0.001, qx[1]-0.001, qx[1]+0.001,
        n ]
518     q_zfunction = [ 0, 0, 1, 1, 0, 0 ]
519
```

```
    if qx[0] == 0 and qx[1] == n:
        q_xfunction = [ 0, n ]
        q_zfunction = [ 1, 1 ]
    elif qx[0] == 0:
        del q_xfunction[1:3]
        del q_zfunction[0:2]
    elif qx[1] == n:
        del q_xfunction[3:5]
        del q_zfunction[4:6]

    setFunctionValues( "DeltaQ", q_xfunction, [  ], [  ], q_zfunction )

    createSurfaceLoad( "DeltaQ_Hor", "Surcharge" )
    setParameter( "GEOMETRYLOAD", "DeltaQ_Hor", "FORCE/VALUE", -0.3*q )
    setParameter( "GEOMETRYLOAD", "DeltaQ_Hor", "FORCE/DIRECT", 2 )
    attach( "GEOMETRYLOAD", "DeltaQ_Hor", "Masonry", [[ 0.573573, B, 0.1 ]]
    )
    attach( "GEOMETRYLOAD", "DeltaQ_Hor", "Masonry2", [[ 0.573573, B-0.1,
    0.9177168 ]] )
    attach( "GEOMETRYLOAD", "DeltaQ_Hor", "Masonry3", [[ 0.573573, B-0.2,
    1.5 ]] )
    setValueFunction( "GEOMETRYLOAD", "DeltaQ_Hor", "DeltaQ" )

    #createLineLoad( "DeltaQ_Hor2", "Surcharge" )
    #setParameter( "GEOMETRYLOAD", "DeltaQ_Hor2", "FORCE/VALUE", -0.3*q*0.2
    )
    #setParameter( "GEOMETRYLOAD", "DeltaQ_Hor2", "FORCE/DIRECT", 2 )
    #attach( "GEOMETRYLOAD", "DeltaQ_Hor2", "Planks2", [[ 0.5, L_plank,
    -0.1 ]] )
    #setValueFunction( "GEOMETRYLOAD", "DeltaQ_Hor", "DeltaQ" )

    createSurfaceLoad( "DeltaQ_Ver", "Surcharge" )
    setParameter( "GEOMETRYLOAD", "DeltaQ_Ver", "FORCE/VALUE", -q )
    setParameter( "GEOMETRYLOAD", "DeltaQ_Ver", "FORCE/DIRECT", 3 )
    attach( "GEOMETRYLOAD", "DeltaQ_Ver", "Planks2", [[ 1.279281,
    1.8587676, -0.1 ]] )
    attach( "GEOMETRYLOAD", "DeltaQ_Ver", "Masonry", [[ 0.426427, B-0.05,
    0.6 ]] )
    attach( "GEOMETRYLOAD", "DeltaQ_Ver", "Masonry2", [[ 0.426427, B-0.15,
    1.1 ]] )
    setValueFunction( "GEOMETRYLOAD", "DeltaQ_Ver", "DeltaQ" )

    createSurfaceLoad( "DeltaQ_Ver_Wall", "Surcharge" )
    setParameter( "GEOMETRYLOAD", "DeltaQ_Ver_Wall", "FORCE/VALUE", -qwall
    )
    setParameter( "GEOMETRYLOAD", "DeltaQ_Ver_Wall", "FORCE/DIRECT", 3 )
    attach( "GEOMETRYLOAD", "DeltaQ_Ver_Wall", "Masonry2", [[ 0.426427,
    0.3, 1.6 ]] )
    setValueFunction( "GEOMETRYLOAD", "DeltaQ_Ver_Wall", "DeltaQ" )

def Retaining_Wall():
    weight = [0,18,10,10,7,2] #1 = q
    thick = [0,0.75,0.85,0.2,2.5,1.5] #1 = 1
    phi = [0,32.5,32.5,32.5,17.5,15.0]
    phi = [x*2*math.pi/360.0 for x in phi]
    phi_a = [(1-math.sin(x))/(1+math.sin(x)) for x in phi]
    Q = q_behind/1000

    Q_A = []

```

```
    for i in range(len(weight)):
        Q_A.append(weight[i]*thick[i])

    for i in range(len(Q_A)-1):
        Q_A[i+1] = Q_A[i+1] + Q_A[i]

    Q_A = Q_A[2:]
    Q_A = [val for val in Q_A for _ in (0, 1)]
    Q_A.pop(0)
    Q_A.pop(-1)

    phi_a = phi_a[3:]
    phi_a = [val for val in phi_a for _ in (0, 1)]

    S_r = [x*y for x,y in zip(Q_A, phi_a)]

    force = 0.5*(S_r[2]+S_r[3])*2.5 + 0.5*(S_r[4]+S_r[5])*1.5
    moment = (0.5*2.5*(S_r[3]-S_r[2])*(2.5*(2/3)) + 0.5*1.5*(S_r[5]-S_r[4])*(1.5*(2/3)+2.5)
                    + 2.5*S_r[2]*(2.5*(1/2)) + 1.5*S_r[4]*(1.5*(1/2)+2.5))
    force_q = Q*phi_a[4]*2.5 + Q*phi_a[5]*1.5
    moment_q = Q*phi_a[4]*2.5*(2.5*(1/2)) + Q*phi_a[5]*1.5*(1.5*(1/2)+2.5)

    q_pile = moment/(5*4.0*4.0/18)
    F_kesp = force - moment/(5*4.0/6) + 0.5*(S_r[0]+S_r[1])*0.2
    q_pile_q = moment_q/(5*4.0*4.0/18)
    F_kesp_q = force_q - moment_q/(5*4.0/6) + Q*phi_a[3]*0.2

    global q_piles
    global q_piles_q

    q_piles = [0.2*q_pile, 0.3*q_pile, 0.5*q_pile]
    q_piles_q = [0.2*q_pile_q, 0.3*q_pile_q, 0.5*q_pile_q]

    if thick_front[1] <= 2.0:
        q_piles = [0, 0.35*q_pile, 0.65*q_pile]
        q_piles_q = [0, 0.35*q_pile_q, 0.65*q_pile_q]
    if thick_front[1] and thick_mid[1] <= 2.0:
        q_piles = [0, 0, q_pile]
        q_piles_q = [0, 0, q_pile_q]

    p_main = [(x * Mesh) for x in range(0, int(n/Mesh))]

    sourceplanks = []
    for i in range(len(p_main)):
        sourceplanks.append([0.5*Mesh + p_main[i],2.8,-0.1])

    createLineLoad( "SoilToPlanks", "Permanent" )
    setParameter( "GEOMETRYLOAD", "SoilToPlanks", "FORCE/VALUE", -1000*F_kesp )
    setParameter( "GEOMETRYLOAD", "SoilToPlanks", "FORCE/DIRECT", 2 )
    attach( "GEOMETRYLOAD", "SoilToPlanks", "Planks2", sourceplanks )
    createLineLoad( "SurchargeToPlanks", "Surcharge" )
    setParameter( "GEOMETRYLOAD", "SurchargeToPlanks", "FORCE/VALUE", -1000*F_kesp_q )
    setParameter( "GEOMETRYLOAD", "SurchargeToPlanks", "FORCE/DIRECT", 2 )
    attach( "GEOMETRYLOAD", "SurchargeToPlanks", "Planks2", sourceplanks )

    setFunctionValues( "SoilToPile", [  ], [  ], [ -4.2, -2.8667 ], [ 1, 1 ] ) #-4.2, -2.8667
```

```
626
627     pos = ["Front","Mid","End"]
628     for j in range(3):
629         createLineLoad( "SoilToPile"+pos[j], "Permanent" )
630         setParameter( "GEOMETRYLOAD", "SoilToPile"+pos[j], "FORCE/VALUE",
    -1000*q_piles[j] )
631         setParameter( "GEOMETRYLOAD", "SoilToPile"+pos[j], "FORCE/DIRECT",
    2 )
632         for i in x_main:
633             attach( "GEOMETRYLOAD", "SoilToPile"+pos[j], "Pile"+pos[j]+"
    Main"+str(i+1), [[ i + 0.5, pile_y[j], -4.1999 ]] ) #-4.1999
634             #attach( "GEOMETRYLOAD", "SoilToPile"+pos[j], "Pile"+pos[j]+"
    Main"+str(i+1), [[ i + 0.5, pile_y[j], -5.6999 ]] )
635             setValueFunction( "GEOMETRYLOAD", "SoilToPile"+pos[j], "
    SoilToPile" )
636
637     for j in range(3):
638         createLineLoad( "QToPile"+pos[j], "Surcharge" )
639         setParameter( "GEOMETRYLOAD", "QToPile"+pos[j], "FORCE/VALUE",
    -1000*q_piles_q[j] )
640         setParameter( "GEOMETRYLOAD", "QToPile"+pos[j], "FORCE/DIRECT", 2 )
641         for i in x_main:
642             attach( "GEOMETRYLOAD", "QToPile"+pos[j], "Pile"+pos[j]+"Main"+
    str(i+1), [[ i + 0.5, pile_y[j], -4.1999 ]] )
643             #attach( "GEOMETRYLOAD", "QToPile"+pos[j], "Pile"+pos[j]+"Main
    "+str(i+1), [[ i + 0.5, pile_y[j], -2.8668 ]] )
644             setValueFunction( "GEOMETRYLOAD", "QToPile"+pos[j], "SoilToPile
    " )
645
646
647 def Supports(): #Sets supports for piles
648
649     #UNDERNEATH PILES
650     addSet( "GEOMETRYSUPPORTSET", "Pile_Support" )
651     createPointSupport( "Pile_Support", "Pile_Support" )
652     setParameter( "GEOMETRYSUPPORT", "Pile_Support", "AXES", [ 1, 2 ] )
653     setParameter( "GEOMETRYSUPPORT", "Pile_Support", "TRANSL", [ 1, 0, 0 ]
    )
654     setParameter( "GEOMETRYSUPPORT", "Pile_Support", "ROTATI", [ 0, 0, 0 ]
    )
655
656     for i in range(len(x_main)):
657         attach( "GEOMETRYSUPPORT", "Pile_Support", piles_front_main[i], [[
    0.5+i, pile_y[0], -11.2 ]] )
658         attach( "GEOMETRYSUPPORT", "Pile_Support", piles_mid_main[i], [[
    0.5+i, pile_y[1], -11.2 ]] )
659         attach( "GEOMETRYSUPPORT", "Pile_Support", piles_end_main[i], [[
    0.5+i, pile_y[2], -11.2 ]] )
660
661     #SOIL SUPPORT SET
662     addSet( "GEOMETRYSUPPORTSET", "Soil Support" )
663     createLineSupport( "Soil Support", "Soil Support" )
664     setParameter( "GEOMETRYSUPPORT", "Soil Support", "AXES", [ 1, 2 ] )
665     setParameter( "GEOMETRYSUPPORT", "Soil Support", "TRANSL", [ 1, 1, 0 ]
    )
666     setParameter( "GEOMETRYSUPPORT", "Soil Support", "ROTATI", [ 0, 0, 0 ]
    )
667
668 def Boundary():
669     if boundarycondition == 0:
```

```
        rot = [1,0,0]
    else:
        rot = [1,1,1]
    addSet( "GEOMETRYSUPPORTSET", "BC" )
    createSurfaceSupport( "Wall_BC", "BC" )
    setParameter( "GEOMETRYSUPPORT", "Wall_BC", "AXES", [ 1, 2 ] )
    setParameter( "GEOMETRYSUPPORT", "Wall_BC", "TRANSL", rot ) #1 0 0 default
    setParameter( "GEOMETRYSUPPORT", "Wall_BC", "ROTATI", [ 1, 1, 1 ] )
    attach( "GEOMETRYSUPPORT", "Wall_BC", "Masonry", [[ n, 0.01, 0.3 ]] )
    attach( "GEOMETRYSUPPORT", "Wall_BC", "Masonry2", [[ n, 0.01, 0.85 ]] )
    attach( "GEOMETRYSUPPORT", "Wall_BC", "Masonry3", [[ n, 0.01, 1.35 ]] )
    createLineSupport( "Planks_BC", "BC" )
    setParameter( "GEOMETRYSUPPORT", "Planks_BC", "AXES", [ 1, 2 ] )
    setParameter( "GEOMETRYSUPPORT", "Planks_BC", "TRANSL", rot ) #1 0 0 default
    setParameter( "GEOMETRYSUPPORT", "Planks_BC", "ROTATI", [ 1, 1, 1 ] )
    attach( "GEOMETRYSUPPORT", "Planks_BC", "Planks1", [[ n, 0.33, -0.1 ]] )
    attach( "GEOMETRYSUPPORT", "Planks_BC", "Planks2", [[ n, 1.705, -0.1 ]] )

    addSet( "GEOMETRYSUPPORTSET", "BC_FREE" )
    createSurfaceSupport( "Wall_BC_FREE", "BC_FREE" )
    setParameter( "GEOMETRYSUPPORT", "Wall_BC_FREE", "AXES", [ 1, 2 ] )
    setParameter( "GEOMETRYSUPPORT", "Wall_BC_FREE", "TRANSL", [ 1, 0, 0 ] )
    setParameter( "GEOMETRYSUPPORT", "Wall_BC_FREE", "ROTATI", [ 1, 1, 1 ] )
    attach( "GEOMETRYSUPPORT", "Wall_BC_FREE", "Masonry", [[ 0, 0.01, 0.3 ]] )
    attach( "GEOMETRYSUPPORT", "Wall_BC_FREE", "Masonry2", [[ 0, 0.01, 0.85 ]] )
    attach( "GEOMETRYSUPPORT", "Wall_BC_FREE", "Masonry3", [[ 0, 0.01, 1.35 ]] )
    createLineSupport( "Planks_BC_FREE", "BC_FREE" )
    setParameter( "GEOMETRYSUPPORT", "Planks_BC_FREE", "AXES", [ 1, 2 ] )
    setParameter( "GEOMETRYSUPPORT", "Planks_BC_FREE", "TRANSL", [ 1, 0, 0 ] ) #1 0 0 default
    setParameter( "GEOMETRYSUPPORT", "Planks_BC_FREE", "ROTATI", [ 1, 1, 1 ] ) #1 0 0 default
    attach( "GEOMETRYSUPPORT", "Planks_BC_FREE", "Planks1", [[ 0, 0.33, -0.1 ]] )
    attach( "GEOMETRYSUPPORT", "Planks_BC_FREE", "Planks2", [[ 0, 1.705, -0.1 ]] )

def BoundarySprings(): #Horizontal Springs
    row = ["FrontMain", "MidMain", "EndMain"]
    Soiltype = ["Clay1","Peat","Silt","Clay2","Sand"]
    Z = [-2.6999, -5.6999, -8.1999, -10.6999, -11.1999]

    for k in range(5): #Z
        for j in range(3): #Y
            createConnection( Soiltype[k]+"_Springs_"+row[j], "BOUNDA", "SHAPEEDGE" )
            for i in x_main: #X
                attachTo( "GEOMETRYCONNECTION", Soiltype[k]+"_Springs_"+row[j], "SOURCE", "Pile"+row[j]+str(i+1), [[ 0.5+i, pile_y[j], Z[k] ]] )
            setElementClassType( "GEOMETRYCONNECTION", Soiltype[k]+"_Springs_"+row[j], "LIN3DS" ) # SHLLIF for Shells LIN3DS
```

```
            assignMaterial( Soiltype[k]+row[j], "GEOMETRYCONNECTION", Soiltype[k]+"_Springs_"+row[j] )
            assignGeometry( "Soil_Geometry", "GEOMETRYCONNECTION", Soiltype[k]+"_Springs_"+row[j] )
            setParameter( "GEOMETRYCONNECTION", Soiltype[k]+"_Springs_"+row[j], "FLIP", False )
            resetElementData( "GEOMETRYCONNECTION", Soiltype[k]+"_Springs_"+row[j] )
            for i in x_main: #X
                attach( "GEOMETRYSUPPORT", "Soil Support", "Pile"+row[j]+str(i+1), [[ 0.5+i, pile_y[j], Z[k] ]] )

    createConnection( "Pile_Ver_Front", "BNDSPR", "SHAPEVERTEX" )

    for i in x_main: #X
        attachTo( "GEOMETRYCONNECTION", "Pile_Ver_Front", "SOURCE", "Pile"+row[0]+str(i+1), [[ 0.5+i, pile_y[0], -11.2 ]] )
    setElementClassType( "GEOMETRYCONNECTION", "Pile_Ver_Front", "SPRING" )
    assignMaterial( "Pile_Ver_Front", "GEOMETRYCONNECTION", "Pile_Ver_Front" )
    assignGeometry( "Pile_Ver", "GEOMETRYCONNECTION", "Pile_Ver_Front" )
    setParameter( "GEOMETRYCONNECTION", "Pile_Ver_Front", "FLIP", False )

    createConnection( "Pile_Ver_Mid", "BNDSPR", "SHAPEVERTEX" )

    for i in x_main: #X
        attachTo( "GEOMETRYCONNECTION", "Pile_Ver_Mid", "SOURCE", "Pile"+row[1]+str(i+1), [[ 0.5+i, pile_y[1], -11.2 ]] )
    setElementClassType( "GEOMETRYCONNECTION", "Pile_Ver_Mid", "SPRING" )
    assignMaterial( "Pile_Ver_Mid", "GEOMETRYCONNECTION", "Pile_Ver_Mid" )
    assignGeometry( "Pile_Ver", "GEOMETRYCONNECTION", "Pile_Ver_Mid" )
    setParameter( "GEOMETRYCONNECTION", "Pile_Ver_Mid", "FLIP", False )

    createConnection( "Pile_Ver_End", "BNDSPR", "SHAPEVERTEX" )
    for i in x_main: #X
        attachTo( "GEOMETRYCONNECTION", "Pile_Ver_End", "SOURCE", "Pile"+row[2]+str(i+1), [[ 0.5+i, pile_y[2], -11.2 ]] )
    setElementClassType( "GEOMETRYCONNECTION", "Pile_Ver_End", "SPRING" )
    assignMaterial( "Pile_Ver_End", "GEOMETRYCONNECTION", "Pile_Ver_End" )
    assignGeometry( "Pile_Ver", "GEOMETRYCONNECTION", "Pile_Ver_End" )
    setParameter( "GEOMETRYCONNECTION", "Pile_Ver_End", "FLIP", False )

    #PILE-PLANKS HINGE
    if pileconnection == 0:
        rot = [0,0,0]
    else:
        rot = [1,1,1]
    createConnection( "Pile_Wood_Connection", "HINGE", "SHAPEVERTEX", "SHAPEVERTEX" )
    setParameter( "GEOMETRYCONNECTION", "Pile_Wood_Connection", "MODE", "MANUAL" )
    setParameter( "GEOMETRYCONNECTION", "Pile_Wood_Connection", "DOF/AXES", [ 1, 2 ] )
    setParameter( "GEOMETRYCONNECTION", "Pile_Wood_Connection", "DOF/TRANSL", [ 1, 1, 1 ] )
    setParameter( "GEOMETRYCONNECTION", "Pile_Wood_Connection", "DOF/ROTATI", rot )

    planks1 = []
    for i in x_main: #X
```

```
        planks1.append([0.5+i, pile_y[0], -0.1])
    planks2 = []
    for j in range(2): #Y
        for i in x_main: #X
            planks2.append([0.5+i, pile_y[j+1], -0.1])

    attachTo( "GEOMETRYCONNECTION", "Pile_Wood_Connection", "SOURCE", "Planks1", planks1 )
    attachTo( "GEOMETRYCONNECTION", "Pile_Wood_Connection", "SOURCE", "Planks2", planks2 )

    for j in range(3): #Y
        for i in x_main: #X
            attachTo( "GEOMETRYCONNECTION", "Pile_Wood_Connection", "TARGET", "Pile"+row[j]+str(i+1), [[ 0.5+i, pile_y[j], -0.2 ]] )

def Test():
    sourceplanks = []
    sourcebnd = []
    for i in range(1,int(n/Mesh)+1):
        sourceplanks.append([ -0.5*Mesh + Mesh*i, 2.8, -0.1 ])
        sourcebnd.append([ -0.5*Mesh + Mesh*i, 2.8, 0 ])

    createConnection( "VirtualConnection", "RIGID", "SHAPEEDGE", "SHAPEEDGE" )
    setParameter( "GEOMETRYCONNECTION", "VirtualConnection", "MODE", "MANUAL" )
    setParameter( "GEOMETRYCONNECTION", "VirtualConnection", "DOF/AXES", [ 1, 2 ] )
    setParameter( "GEOMETRYCONNECTION", "VirtualConnection", "DOF/TRANSL", [ 1, 1, 1 ] )
    setParameter( "GEOMETRYCONNECTION", "VirtualConnection", "DOF/ROTATI", [ 1, 1, 1 ] )
    attachTo( "GEOMETRYCONNECTION", "VirtualConnection", "SOURCE", "Planks2", sourceplanks )
    attachTo( "GEOMETRYCONNECTION", "VirtualConnection", "TARGET", "VirtualBoundary", sourcebnd )
    setParameter( "GEOMETRYCONNECTION", "VirtualConnection", "FLIP", False )
    for i in range(1,int(n/Mesh)+1):
        attachTo( "GEOMETRYCONNECTION", "VirtualConnection", "SRCANC", "Planks2", [[ -Mesh+Mesh*i, 2.8, -0.1 ]] )
    for i in range(1,int(n/Mesh)+1):
        attachTo( "GEOMETRYCONNECTION", "VirtualConnection", "TRGANC", "VirtualBoundary", [[ -Mesh+Mesh*i, 2.8, 0 ]] )

    slide = []
    slide1 = []
    for i in range(2,int(n/Mesh)+2):
        slide.append([ -Mesh+Mesh*i, 2.8, 0.8 ])
        slide1.append([ -Mesh+Mesh*i, 2.8, 1.6 ])

    createConnection( "VirtualSlide", "RIGID", "SHAPEEDGE", "SHAPEEDGE" )
    setParameter( "GEOMETRYCONNECTION", "VirtualSlide", "MODE", "MANUAL" )
    setParameter( "GEOMETRYCONNECTION", "VirtualSlide", "DOF/AXES", [ 1, 2 ] )
    setParameter( "GEOMETRYCONNECTION", "VirtualSlide", "DOF/TRANSL", [ 0, 0, 0 ] )
    setParameter( "GEOMETRYCONNECTION", "VirtualSlide", "DOF/ROTATI", [ 0, 0, 0 ] )
```

```
804     attachTo( "GEOMETRYCONNECTION", "VirtualSlide", "SOURCE", "
    VirtualBoundary", slide )
805     attachTo( "GEOMETRYCONNECTION", "VirtualSlide", "TARGET", "
    VirtualBoundary", slide )
806     setParameter( "GEOMETRYCONNECTION", "VirtualSlide", "FLIP", False )
807     for i in range(2,int(n/Mesh)+2):
808         attachTo( "GEOMETRYCONNECTION", "VirtualSlide", "SRCANC", "
    VirtualBoundary", [[ -Mesh+Mesh*i, 2.8, 1.6 ]] )
809     for i in range(2,int(n/Mesh)+2):
810         attachTo( "GEOMETRYCONNECTION", "VirtualSlide", "TRGANC", "
    VirtualBoundary", [[ -Mesh+Mesh*i, 2.8, 1.6 ]] )
811
812     createModelLoad( "Deadweight", "Permanent" )
813
814     forcebnd = []
815     for i in range(1,int(n/Mesh)+1):
816         forcebnd.append([ -0.5*Mesh + Mesh*i, 2.8, 0.8 ])
817
818     qbnd = []
819     p = [(x * Mesh) for x in range(int(qx[0]/Mesh), int(qx[1]/Mesh))]
820     for i in range(len(p)):
821         qbnd.append([0.5*Mesh + p[i],2.8,0.8])
822
823     forcebnd_comp = []
824     for i in range(1,int(n/Mesh)+1):
825         forcebnd_comp.append([ -0.5*Mesh + Mesh*i, 2.8, 0.0 ])
826
827     qbnd_comp = []
828     p_comp = [(x * Mesh) for x in range(int(qx[0]/Mesh), int(qx[1]/Mesh))]
829     for i in range(len(p_comp)):
830         qbnd_comp.append([0.5*Mesh + p_comp[i],2.8,0.0])
831
832     createSurfaceLoad( "Soil_Hor_Vir", "Permanent" )
833     setParameter( "GEOMETRYLOAD", "Soil_Hor_Vir", "FORCE/VALUE", 1 )
834     setParameter( "GEOMETRYLOAD", "Soil_Hor_Vir", "FORCE/DIRECT", 2 )
835     attach( "GEOMETRYLOAD", "Soil_Hor_Vir", "VirtualBoundary", forcebnd )
836     setValueFunction( "GEOMETRYLOAD", "Soil_Hor_Vir", "Soil_Hor" )
837
838     createSurfaceLoad( "DeltaQ_Hor_Vir", "Surcharge" )
839     setParameter( "GEOMETRYLOAD", "DeltaQ_Hor_Vir", "FORCE/VALUE", forceloc
    *0.3*q )
840     setParameter( "GEOMETRYLOAD", "DeltaQ_Hor_Vir", "FORCE/DIRECT", 2 )
841     attach( "GEOMETRYLOAD", "DeltaQ_Hor_Vir", "VirtualBoundary", qbnd )
842     #setValueFunction( "GEOMETRYLOAD", "DeltaQ_Hor_Vir", "DeltaQ" )
843
844     #createLineLoad( "Soil_Hor_Comp", "Permanent" )
845     #setParameter( "GEOMETRYLOAD", "Soil_Hor_Comp", "LODTYP", "MOMENT" )
846     #setParameter( "GEOMETRYLOAD", "Soil_Hor_Comp", "MOMENT/VALUE", 2071 )
847     #setParameter( "GEOMETRYLOAD", "Soil_Hor_Comp", "MOMENT/DIRECT", 1 )
848     #attach( "GEOMETRYLOAD", "Soil_Hor_Comp", "VirtualBoundary",
    forcebnd_comp )
849
850     createLineLoad( "DeltaQ_Hor_Comp", "Surcharge" )
851     setParameter( "GEOMETRYLOAD", "DeltaQ_Hor_Comp", "LODTYP", "MOMENT" )
852     setParameter( "GEOMETRYLOAD", "DeltaQ_Hor_Comp", "MOMENT/VALUE",
    forceloc * 0.3*q*1.6*0.8 )
853     setParameter( "GEOMETRYLOAD", "DeltaQ_Hor_Comp", "MOMENT/DIRECT", 1 )
854     attach( "GEOMETRYLOAD", "DeltaQ_Hor_Comp", "VirtualBoundary", qbnd_comp
     )
855
```

```
    createSurfaceLoad( "Soil_Hor_Vir2", "Permanent" )
    setParameter( "GEOMETRYLOAD", "Soil_Hor_Vir2", "FORCE/VALUE", -1 )
    setParameter( "GEOMETRYLOAD", "Soil_Hor_Vir2", "FORCE/DIRECT", 2 )
    attach( "GEOMETRYLOAD", "Soil_Hor_Vir2", "VirtualBoundary", forcebnd )
    setValueFunction( "GEOMETRYLOAD", "Soil_Hor_Vir2", "Soil_Hor" )

def Sinkhole():
    def AffectedPiles():
        pile_row = [piles_front_alter, piles_mid_alter, piles_end_alter]

        X = [x+0.5 for x in x_alter] #Point 0: Because Point 1 must be at x = 0.5 m
        for j in range(len(pile_row)):
            for i in range(len(pile_row[j])):
                #X += 1 #Add pile row every 1 meter
                createLine( pile_row[j][i], [ X[i], pile_y[j], -11.2 ], [ X[i], pile_y[j], -0.2 ] )
                createPointBody( "Point body 1", [ X[i], pile_y[j], -10.7 ] )
                createPointBody( "Point body 2", [ X[i], pile_y[j], -8.2 ] )
                createPointBody( "Point body 3", [ X[i], pile_y[j], -5.7 ] )
                createPointBody( "Point body 4", [ X[i], pile_y[j], -2.7 ] )
                createPointBody( "Point body 5", [ X[i], pile_y[j], -11.2 + sum(thick_alter[j]) ] )
                projection( "SHAPEEDGE", pile_row[j][i], [[ X[i], pile_y[j], -5.7 ]], [ "Point body 1", "Point body 2", "Point body 3", "Point body 4", "Point body 5" ], [ 1, 0, 0 ], True )
                removeShape( [ "Point body 1", "Point body 2", "Point body 3", "Point body 4", "Point body 5" ] )

    def RemainingSoil():
        #SOIL MATERIALS
        no = 1 #SOIL MULTIPLIER
        pi = 3.141592653589793

        #Order: Clay, Peat, Silt, Clay, Sand
        Soiltype = ["Clay1","Peat","Silt","Clay2","Sand"]
        qc = [0.5, 0.5, 2.0, 0.5, 15.0]
        alpha = [2/3, 1, 1/2, 2/3, 1/3]
        beta = [2.0, 3.0, 1.0, 2.0, 0.7]
        R = D/2

        Stiffness = [[],[],[]]

        for i in range(len(qc)):
            for j in range(3): #ROW
                Stiffness[j].append((((2*R)/(qc[i]*beta[i]))*((4.0*(2.65)**alpha[i]+alpha[i]*3)/18))**-1*10**6 * no * p[j]) #N/m3

        phi = [17.5, 15, 27.5, 17.5, 32.5]
        phi = [x*2*pi/360 for x in phi]
        c = [5, 2.5, 1, 5, 0] #kPa

        Kq0 = [1.9, 1.5, 3.9, 1.9, 5.8]
        Kqinf = [4.5, 3.5, 13.1, 4.5, 24.6]
        Kc0 = [4.3, 3.9, 6.2, 4.3, 7.9]
        Kcinf = [20.6, 17.6, 46.7, 20.6, 83.4]
```

```
        K0 = [1-math.sin(x) for x in phi]

        aq = []
        ac = []

        for i in range(len(phi)):

            aq.append((Kq0[i]/(Kqinf[i]-Kq0[i]))*((K0[i]*math.sin(phi[i]))/
                                                  math.sin(0.25*pi+0.5*
    phi[i])))

            ac.append((Kc0[i]/(Kcinf[i]-Kc0[i]))*2*math.sin(0.25*pi+0.5*phi
    [i]))

        thick_front_alter.insert(0,0)
        thick_mid_alter.insert(0,0)
        thick_end_alter.insert(0,0)
        def accumu(lis):
            total = 0
            for x in lis:
                total += x
                yield total

        Depth_bnd_front = list(accumu(thick_front_alter))
        Depth_bnd_mid = list(accumu(thick_mid_alter))
        Depth_bnd_end = list(accumu(thick_end_alter))

        Depth_mid_front = []
        Depth_mid_mid = []
        Depth_mid_end = []

        for i in range(len(thick_alter[0])-1):
            Depth_mid_front.append(0.5*(Depth_bnd_front[i+1]-
    Depth_bnd_front[i])+Depth_bnd_front[i])
            Depth_mid_mid.append(0.5*(Depth_bnd_mid[i+1]-Depth_bnd_mid[i])+
    Depth_bnd_mid[i])
            Depth_mid_end.append(0.5*(Depth_bnd_end[i+1]-Depth_bnd_end[i])+
    Depth_bnd_end[i])

        Depth = [Depth_mid_front,Depth_mid_mid,Depth_mid_end]

        gamma = [12, 17, 20, 20] #kN/m3
        gamma = [x-10 for x in gamma]

        sig = [0,0,0]
        thick_front_alter.pop(0)
        thick_mid_alter.pop(0)
        thick_end_alter.pop(0)
        for i in range(3): #ROW
            layer = thick_alter[i]
            sig1 = layer[0]*gamma[1]*0.5
            sig2 = layer[0]*gamma[1]+layer[1]*gamma[0]*0.5
            sig3 = layer[0]*gamma[1]+layer[1]*gamma[0]+layer[2]*gamma
    [2]*0.5
            sig4 = layer[0]*gamma[1]+layer[1]*gamma[0]+layer[2]*gamma[2]+
    layer[3]*gamma[1]*0.5
            sig5 = layer[0]*gamma[1]+layer[1]*gamma[0]+layer[2]*gamma[2]+
    layer[3]*gamma[1]+layer[4]*gamma[3]*0.5
            sig[i] = [sig1,sig2,sig3,sig4,sig5]

```

```
        Kq =[[],[],[]]
        Kc =[[],[],[]]

        for i in range(len(phi)):
            for j in range(3): #ROW
                Kq[j].append((Kq0[i] +Kqinf[i]*aq[i]*(Depth[j][i]/D))/(1+aq[i]*(Depth[j][i]/D)))
                Kc[j].append((Kc0[i] +Kcinf[i]*ac[i]*(Depth[j][i]/D))/(1+ac[i]*(Depth[j][i]/D)))

        sigp = [[],[],[]]

        for i in range(len(phi)):
            for j in range(3):
                if Depth[j][i] != 0:
                    sigp[j].append(Kq[j][i]*sig[j][i] + Kc[j][i]*c[i])
                else:
                    sigp[j].append(0)
                    Stiffness[j][i] = 1

        for i in range(3):
            sigp[i] = [1000*p[i]*x for x in sigp[i]] #N/m2

        u = [0,0,0]
        for i in range(3):
            u[i]  = [x / y for x, y in zip(sigp[i], Stiffness[i])] #m

        row = ["FrontAlter", "MidAlter", "EndAlter"]

        for j in range(3):
            for i in range(len(Soiltype)):
                addMaterial( Soiltype[i]+row[j], "INTERF", "NONLIF", [] )
                addMaterial( Soiltype[i]+row[j], "INTERF", "ELASTI", [] )
                setParameter( "MATERIAL", Soiltype[i]+row[j], "LINEAR/IFTYP", "LIN3D3" ) #Normal = 3, Shell = None
                setParameter( "MATERIAL", Soiltype[i]+row[j], "LINEAR/ELAS7/DSNY", Stiffness[j][i] ) #7; 4
                setParameter( "MATERIAL", Soiltype[i]+row[j], "LINEAR/ELAS7/DSSX", Stiffness[j][i] ) #7; 4
                setParameter( "MATERIAL", Soiltype[i]+row[j], "LINEAR/ELAS7/DSSZ", 0 ) #7; 4
                setParameter( "MATERIAL", Soiltype[i]+row[j], "NONLIN/IFNOTE", "DIAGRM" )
                setParameter( "MATERIAL", Soiltype[i]+row[j], "NONLIN/NLEL10/DUSTNY", [ -1, -sigp[j][i], -u[j][i], -sigp[j][i], 0, 0, u[j][i], sigp[j][i], 1, sigp[j][i] ] ) #10; 4

        addMaterial( "Pile_Ver_Front_alter", "SPRING", "LINETR", [] )
        setParameter( "MATERIAL", "Pile_Ver_Front_alter", "LINETR/SPRING", K_ver_Front_alter )
        setParameter( "MATERIAL", "Pile_Ver_Front_alter", "LINETR/SPTYPE", "DIAGRA" )
        setParameter( "MATERIAL", "Pile_Ver_Front_alter", "LINETR/DIAGRA/DUFX", Fu_diagram_Front_alter )

        addMaterial( "Pile_Ver_Mid_alter", "SPRING", "LINETR", [] )
        setParameter( "MATERIAL", "Pile_Ver_Mid_alter", "LINETR/SPRING", K_ver_Mid_alter )
        setParameter( "MATERIAL", "Pile_Ver_Mid_alter", "LINETR/SPTYPE", "DIAGRA" )
```

```
        setParameter( "MATERIAL", "Pile_Ver_Mid_alter", "LINETR/DIAGRA/DUFX", Fu_diagram_Mid_alter )

        addMaterial( "Pile_Ver_End_alter", "SPRING", "LINETR", [] )
        setParameter( "MATERIAL", "Pile_Ver_End_alter", "LINETR/SPRING", K_ver_End_alter )
        setParameter( "MATERIAL", "Pile_Ver_End_alter", "LINETR/SPTYPE", "DIAGRA" )
        setParameter( "MATERIAL", "Pile_Ver_End_alter", "LINETR/DIAGRA/DUFX", Fu_diagram_End_alter )



    def MaterialAssign():
        piles = [piles_front_alter, piles_mid_alter, piles_end_alter]
        for j in range(len(piles)):
            for i in range(len(piles[j])):
                setElementClassType( "SHAPE", [ piles[j][i] ], "CLS3B3" )
                assignMaterial( "Wood", "SHAPE", [ piles[j][i] ] )
                assignGeometry( "Paal_Diameter", "SHAPE", [ piles[j][i] ] )

    def Supports(): #Sets supports for piles
        for i in range(len(x_alter)):
            attach( "GEOMETRYSUPPORT", "Pile_Support", piles_front_alter[i], [[ 0.5+i, pile_y[0], -11.2 ]] )
            attach( "GEOMETRYSUPPORT", "Pile_Support", piles_mid_alter[i], [[ 0.5+i, pile_y[1], -11.2 ]] )
            attach( "GEOMETRYSUPPORT", "Pile_Support", piles_end_alter[i], [[ 0.5+i, pile_y[2], -11.2 ]] )

    def BoundarySprings(): #Horizontal Springs
        row = ["FrontAlter", "MidAlter", "EndAlter"]
        Soiltype = ["Clay1","Peat","Silt","Clay2","Sand"]
        Z = [-2.6999, -5.6999, -8.1999, -10.6999, -11.1999]

        for k in range(5): #Z
            for j in range(3): #Y
                createConnection( Soiltype[k]+"_Springs_"+row[j], "BOUNDA", "SHAPEEDGE" )
                for i in x_alter: #X
                    attachTo( "GEOMETRYCONNECTION", Soiltype[k]+"_Springs_"+row[j], "SOURCE", "Pile"+row[j]+str(i+1), [[ 0.5+i, pile_y[j], Z[k] ]] )
                setElementClassType( "GEOMETRYCONNECTION", Soiltype[k]+"_Springs_"+row[j], "LIN3DS" ) # SHLLIF for Shells
                assignMaterial( Soiltype[k]+row[j], "GEOMETRYCONNECTION", Soiltype[k]+"_Springs_"+row[j] )
                assignGeometry( "Soil_Geometry", "GEOMETRYCONNECTION", Soiltype[k]+"_Springs_"+row[j] )
                setParameter( "GEOMETRYCONNECTION", Soiltype[k]+"_Springs_"+row[j], "FLIP", False )
                resetElementData( "GEOMETRYCONNECTION", Soiltype[k]+"_Springs_"+row[j] )
                for i in x_alter: #X
                    attach( "GEOMETRYSUPPORT", "Soil Support", "Pile"+row[j]+str(i+1), [[ 0.5+i, pile_y[j], Z[k] ]] )

        createConnection( "Pile_Ver_Front_alter", "BNDSPR", "SHAPEVERTEX" )

        for i in x_alter: #X
```

```
            attachTo( "GEOMETRYCONNECTION", "Pile_Ver_Front_alter", "SOURCE", "Pile"+row[0]+str(i+1), [[ 0.5+i, pile_y[0], -11.2 ]] )
        setElementClassType( "GEOMETRYCONNECTION", "Pile_Ver_Front_alter", "SPRING" )
        assignMaterial( "Pile_Ver_Front_alter", "GEOMETRYCONNECTION", "Pile_Ver_Front_alter" )
        assignGeometry( "Pile_Ver", "GEOMETRYCONNECTION", "Pile_Ver_Front_alter" )
        setParameter( "GEOMETRYCONNECTION", "Pile_Ver_Front_alter", "FLIP", False )

        createConnection( "Pile_Ver_Mid_alter", "BNDSPR", "SHAPEVERTEX" )

        for i in x_alter: #X
            attachTo( "GEOMETRYCONNECTION", "Pile_Ver_Mid_alter", "SOURCE", "Pile"+row[1]+str(i+1), [[ 0.5+i, pile_y[1], -11.2 ]] )
        setElementClassType( "GEOMETRYCONNECTION", "Pile_Ver_Mid_alter", "SPRING" )
        assignMaterial( "Pile_Ver_Mid_alter", "GEOMETRYCONNECTION", "Pile_Ver_Mid_alter" )
        assignGeometry( "Pile_Ver", "GEOMETRYCONNECTION", "Pile_Ver_Mid_alter" )
        setParameter( "GEOMETRYCONNECTION", "Pile_Ver_Mid_alter", "FLIP", False )

        createConnection( "Pile_Ver_End_alter", "BNDSPR", "SHAPEVERTEX" )
        for i in x_alter: #X
            attachTo( "GEOMETRYCONNECTION", "Pile_Ver_End_alter", "SOURCE", "Pile"+row[2]+str(i+1), [[ 0.5+i, pile_y[2], -11.2 ]] )
        setElementClassType( "GEOMETRYCONNECTION", "Pile_Ver_End_alter", "SPRING" )
        assignMaterial( "Pile_Ver_End_alter", "GEOMETRYCONNECTION", "Pile_Ver_End_alter" )
        assignGeometry( "Pile_Ver", "GEOMETRYCONNECTION", "Pile_Ver_End_alter" )
        setParameter( "GEOMETRYCONNECTION", "Pile_Ver_End_alter", "FLIP", False )

        #PILE-PLANKS HINGE
        planks1 = []
        for i in x_alter: #X
            planks1.append([0.5+i, pile_y[0], -0.1])
        planks2 = []
        for j in range(2): #Y
            for i in x_alter: #X
                planks2.append([0.5+i, pile_y[j+1], -0.1])

        attachTo( "GEOMETRYCONNECTION", "Pile_Wood_Connection", "SOURCE", "Planks1", planks1 )
        attachTo( "GEOMETRYCONNECTION", "Pile_Wood_Connection", "SOURCE", "Planks2", planks2 )

        for j in range(3): #Y
            for i in x_alter: #X
                attachTo( "GEOMETRYCONNECTION", "Pile_Wood_Connection", "TARGET", "Pile"+row[j]+str(i+1), [[ 0.5+i, pile_y[j], -0.2 ]] )

        global q_piles
        global q_piles_q

```

```
        if thick_front_alter[1] <= 2.0:
            q_piles = [0, 0.35*sum(q_piles), 0.65*sum(q_piles)]
            q_piles_q = [0, 0.35*sum(q_piles_q), 0.65*sum(q_piles_q)]
        if thick_front_alter[1] and thick_mid[1] <= 2.0:
            q_piles = [0, 0, sum(q_piles)]
            q_piles_q = [0, 0, sum(q_piles_q)]

        pos = ["Front","Mid","End"]
        for j in range(3):
            createLineLoad( "SoilToPile1"+pos[j], "Permanent" )
            setParameter( "GEOMETRYLOAD", "SoilToPile1"+pos[j], "FORCE/
    VALUE", -1000*q_piles[j] )
            setParameter( "GEOMETRYLOAD", "SoilToPile1"+pos[j], "FORCE/
    DIRECT", 2 )
            for i in x_alter:
                attach( "GEOMETRYLOAD", "SoilToPile1"+pos[j], "Pile"+pos[j
    ]+"Alter"+str(i+1), [[ i + 0.5, pile_y[j], -4.1999 ]] ) #-4.1999
                #attach( "GEOMETRYLOAD", "SoilToPile1"+pos[j], "Pile"+pos[j
    ]+"Alter"+str(i+1), [[ i + 0.5, pile_y[j], -5.6999 ]] )
                setValueFunction( "GEOMETRYLOAD", "SoilToPile1"+pos[j], "
    SoilToPile" )

        for j in range(3):
            createLineLoad( "QToPile1"+pos[j], "Surcharge" )
            setParameter( "GEOMETRYLOAD", "QToPile1"+pos[j], "FORCE/VALUE",
     -1000*q_piles_q[j] )
            setParameter( "GEOMETRYLOAD", "QToPile1"+pos[j], "FORCE/DIRECT"
    , 2 )
            for i in x_alter:
                attach( "GEOMETRYLOAD", "QToPile1"+pos[j], "Pile"+pos[j]+"
    Alter"+str(i+1), [[ i + 0.5, pile_y[j], -4.1999 ]] )
                #attach( "GEOMETRYLOAD", "QToPile1"+pos[j], "Pile"+pos[j]+"
    Alter"+str(i+1), [[ i + 0.5, pile_y[j], -2.8668 ]] )
                setValueFunction( "GEOMETRYLOAD", "QToPile1"+pos[j], "
    SoilToPile" )

    AffectedPiles()
    RemainingSoil()
    MaterialAssign()
    Supports()
    BoundarySprings()

def Frontpiles():
    remain = list(range(n))

    for i in range(len(removed)):
        if removed[i] >= n:
            break
        remain.remove(removed[i])

    for i in removed:
        removeShape( [ "PileFrontMain"+str(i+1) ] )

    remove( "GEOMETRYLOAD", "SoilToPileFront" )
    createLineLoad( "SoilToPileFront", "Permanent" )
    setParameter( "GEOMETRYLOAD", "SoilToPileFront", "FORCE/VALUE", -1000*
    q_piles[0] )
    setParameter( "GEOMETRYLOAD", "SoilToPileFront", "FORCE/DIRECT", 2 )

    for i in remain:
```

```
1138        attach( "GEOMETRYLOAD", "SoilToPileFront", "PileFrontMain"+str(i+1)
    , [[ i + 0.5, pile_y[0], -4.1999 ]] ) #-4.1999
1139        #attach( "GEOMETRYLOAD", "SoilToPile"+pos[j], "Pile"+pos[j]+"Main"+
    str(i+1), [[ i + 0.5, pile_y[j], -5.6999 ]] )
1140        setValueFunction( "GEOMETRYLOAD", "SoilToPileFront", "SoilToPile" )
1141
1142    setValueFunction( "GEOMETRYLOAD", "SoilToPileFront", "SoilToPile" )
1143
1144    remove( "GEOMETRYLOAD", "QToPileFront" )
1145    createLineLoad( "QToPileFront", "Surcharge" )
1146    setParameter( "GEOMETRYLOAD", "QToPileFront", "FORCE/VALUE", -1000*
    q_piles_q[0] )
1147    setParameter( "GEOMETRYLOAD", "QToPileFront", "FORCE/DIRECT", 2 )
1148
1149    for i in remain:
1150        attach( "GEOMETRYLOAD", "QToPileFront", "PileFrontMain"+str(i+1),
    [[ i + 0.5, pile_y[0], -4.1999 ]] ) #-4.1999
1151        #attach( "GEOMETRYLOAD", "SoilToPile"+pos[j], "Pile"+pos[j]+"Main"+
    str(i+1), [[ i + 0.5, pile_y[j], -5.6999 ]] )
1152        setValueFunction( "GEOMETRYLOAD", "QToPileFront", "SoilToPile" )
1153
1154    setValueFunction( "GEOMETRYLOAD", "QToPileFront", "SoilToPile" )
1155
1156    remove( "GEOMETRYSUPPORT", "Pile_Support" )
1157    createPointSupport( "Pile_Support", "Pile_Support" )
1158    setParameter( "GEOMETRYSUPPORT", "Pile_Support", "AXES", [ 1, 2 ] )
1159    setParameter( "GEOMETRYSUPPORT", "Pile_Support", "TRANSL", [ 1, 0, 0 ]
    )
1160    setParameter( "GEOMETRYSUPPORT", "Pile_Support", "ROTATI", [ 0, 0, 0 ]
    )
1161    for i in remain:
1162        attach( "GEOMETRYSUPPORT", "Pile_Support", "PileFrontMain"+str(i+1)
    , [[ i+0.5, pile_y[0], -11.2 ]] )
1163    for i in range(n):
1164        attach( "GEOMETRYSUPPORT", "Pile_Support", "PileMidMain"+str(i+1),
    [[ i+0.5, pile_y[1], -11.2 ]] )
1165    for i in range(n):
1166        attach( "GEOMETRYSUPPORT", "Pile_Support", "PileEndMain"+str(i+1),
    [[ i+0.5, pile_y[2], -11.2 ]] )
1167
1168    remove( "GEOMETRYSUPPORT", "Soil Support" )
1169    createLineSupport( "Soil Support", "Soil Support" )
1170    setParameter( "GEOMETRYSUPPORT", "Soil Support", "AXES", [ 1, 2 ] )
1171    setParameter( "GEOMETRYSUPPORT", "Soil Support", "TRANSL", [ 1, 1, 0 ]
    )
1172    setParameter( "GEOMETRYSUPPORT", "Soil Support", "ROTATI", [ 0, 0, 0 ]
    )
1173
1174    Z = [-2.6999, -5.6999, -8.1999, -10.6999, -11.1999]
1175
1176    for k in range(5): #Z
1177        for i in remain: #X
1178            attach( "GEOMETRYSUPPORT", "Soil Support", "PileFrontMain"+str(
    i+1), [[ 0.5+i, pile_y[0], Z[k] ]] )
1179        for i in range(n): #X
1180            attach( "GEOMETRYSUPPORT", "Soil Support", "PileMidMain"+str(i
    +1), [[ 0.5+i, pile_y[1], Z[k] ]] )
1181        for i in range(n): #X
1182            attach( "GEOMETRYSUPPORT", "Soil Support", "PileEndMain"+str(i
    +1), [[ 0.5+i, pile_y[2], Z[k] ]] )
```

```
1183
1184     remove( "GEOMETRYCONNECTION", "Pile_Wood_Connection" )
1185     createConnection( "Pile_Wood_Connection", "HINGE", "SHAPEVERTEX", "
         SHAPEVERTEX" )
1186     setParameter( "GEOMETRYCONNECTION", "Pile_Wood_Connection", "MODE", "
         MANUAL" )
1187     setParameter( "GEOMETRYCONNECTION", "Pile_Wood_Connection", "DOF/AXES",
          [ 1, 2 ] )
1188     setParameter( "GEOMETRYCONNECTION", "Pile_Wood_Connection", "DOF/TRANSL
         ", [ 1, 1, 1 ] )
1189     setParameter( "GEOMETRYCONNECTION", "Pile_Wood_Connection", "DOF/ROTATI
         ", [ 0, 0, 0 ] )
1190
1191     planks1 = []
1192     for i in remain: #X
1193         planks1.append([0.5+i, pile_y[0], -0.1])
1194     planks2 = []
1195     for j in range(2): #Y
1196         for i in range(n): #X
1197             planks2.append([0.5+i, pile_y[j+1], -0.1])
1198
1199     attachTo( "GEOMETRYCONNECTION", "Pile_Wood_Connection", "SOURCE", "
         Planks1", planks1 )
1200     attachTo( "GEOMETRYCONNECTION", "Pile_Wood_Connection", "SOURCE", "
         Planks2", planks2 )
1201
1202     for i in remain:
1203         attachTo( "GEOMETRYCONNECTION", "Pile_Wood_Connection", "TARGET", "
         PileFrontMain"+str(i+1), [[ i+0.5, pile_y[0], -0.2 ]] )
1204     for i in range(n):
1205         attachTo( "GEOMETRYCONNECTION", "Pile_Wood_Connection", "TARGET", "
         PileMidMain"+str(i+1), [[ i+0.5, pile_y[1], -0.2 ]] )
1206     for i in range(n):
1207         attachTo( "GEOMETRYCONNECTION", "Pile_Wood_Connection", "TARGET", "
         PileEndMain"+str(i+1), [[ i+0.5, pile_y[2], -0.2 ]] )
1208
1209 def SetMesh1(): #Sets Mesh
1210
1211     setElementSize( [ "Masonry", "Masonry2", "Masonry3", "Planks1", "
         Planks2", "VirtualBoundary"], Mesh, -1, True )
1212     clearMesherType( [ "Masonry", "Masonry2", "Masonry3", "Planks1", "
         Planks2", "VirtualBoundary" ] )
1213     clearMidSideNodeLocation( [ "Masonry", "Masonry2", "Masonry3", "Planks1
         ", "Planks2", "VirtualBoundary" ] )
1214
1215     setElementSize( "Masonry", 1, [[ 0.5*n, 0, 0 ],[ 0.5*n, B, 0 ],[ 0.5*n,
          B, 0.6 ],[ 0.5*n, B-0.1, 0.6 ],[ 0.5*n, 0, 0.6 ]], Mesh, 0, True )
1216     setElementSize( "Masonry2", 1, [[ 0.5*n, B-0.1, 0.6 ],[ 0.5*n, 0, 0.6
         ],[ 0.5*n, B-0.1, 1.1 ],[ 0.5*n, B-0.2, 1.1 ],[ 0.5*n, 0, 1.1 ]], Mesh,
          0, True )
1217     setElementSize( "Masonry3", 1, [[ 0.5*n, B-0.2, 1.1 ],[ 0.5*n, 0, 1.1
         ],[ 0.5*n, B-0.2, 1.6 ],[ 0.5*n, 0, 1.6 ]], Mesh, 0, True )
1218
1219     setElementSize( "Masonry", 1, [[ 0, 0.3, 0.6 ],[ 0, 0.65, 0.6 ],[ 0,
         pile_y[0]+0.01, 0 ],[ 0, 0.5*pile_y[0], 0 ],[ n, 0.65, 0.6 ],[ n, 0.3,
         0.6 ],[ n, pile_y[0]+0.01, 0 ],[ n, 0.5*pile_y[0], 0 ]], 0.1, 0, True )
1220     setElementSize( "Masonry2", 1, [[ 0, 0.25, 1.1 ],[ 0, 0.55, 1.1 ],[ 0,
         pile_y[0]+0.01, 0.6 ],[ n, pile_y[0]+0.01, 0.6 ],[ n, 0, 0.85 ],[ n,
         0.6, 0.85 ],[ n, 0.55, 1.1 ],[ n, 0.25, 1.1 ]], 0.1, 0, True )
```

```
    setElementSize( "Masonry3", 1, [[ 0, 0.25, 1.6 ],[ 0, 0.25, 1.1 ],[ n, 0.25, 1.1 ],[ n, 0, 1.35 ],[ n, 0.5, 1.35 ],[ n, 0.25, 1.6 ]], 0.1, 0, True )

    setElementSize( "Masonry", 1, [[ n, 0.7, 0.3 ],[ n, 0, 0.3 ],[ 0, 0.7, 0.3 ],[ 0, 0, 0.3 ]], 0.1, 0, True )
    setElementSize( "Masonry2", 1, [[ n, 0.6, 0.85 ],[ n, 0, 0.85 ],[ 0, 0.6, 0.85 ],[ 0, 0, 0.85 ]], 0.1, 0, True )
    setElementSize( "Masonry3", 1, [[ n, 0.5, 1.35 ],[ n, 0, 1.35 ],[ 0, 0.5, 1.35 ],[ 0, 0, 1.35 ]], 0.1, 0, True )

    setElementSize( "Planks1", 1, [[ 0.5*n, B, -0.1 ],[ 0.5*n, 0, -0.1 ]], Mesh, 0, True )

    virtual = []

    for i in range(0,int(n/Mesh)+1):
        virtual.append([ i * Mesh, 2.8, 0.8 ])

    setElementSize( "VirtualBoundary", 1, virtual, 0.1, 0, True )

    setElementSize( "Planks2", 1, [[ 0, 0.85, -0.1 ],[ 0, 1.7, -0.1 ],[ 0, 2.6, -0.1 ],[ n, 2.6, -0.1 ],[ n, 1.7, -0.1 ],[ n, 0.85, -0.1 ]], 0.1, 0, True )

    piles = piles_front_main+piles_mid_main+piles_end_main+piles_front_alter+piles_mid_alter+piles_end_alter
    setElementSize( piles, 0.1, -1, True )
    clearMesherType( piles )
    clearMidSideNodeLocation( piles )

    generateMesh( [] )

def SetMesh(): #Sets Mesh
    setElementSize( [ "Masonry", "Planks1", "Planks2", "VirtualBoundary"], 0.1, -1, True )
    clearMesherType( [ "Masonry", "Planks1", "Planks2", "VirtualBoundary" ] )
    clearMidSideNodeLocation( [ "Masonry", "Planks1", "Planks2", "VirtualBoundary" ] )
    generateMesh( [] )

def Analysis(): #Sets Analysis parameters

    #STRUCTURAL LINEAR STATIC
    addAnalysis( "Linear" )
    addAnalysisCommand( "Linear", "LINSTA", "Structural linear static" )

    #STRUCTURAL NON-LINEAR
    addAnalysis( "Non-Linear" )
    addAnalysisCommand( "Non-Linear", "NONLIN", "Structural nonlinear" )
    addAnalysisCommandDetail( "Non-Linear", "Structural nonlinear", "EXECUT(1)/LOAD/LOADNR" )
    setAnalysisCommandDetail( "Non-Linear", "Structural nonlinear", "EXECUT(1)/LOAD/LOADNR", 1 )
    setAnalysisCommandDetail( "Non-Linear", "Structural nonlinear", "EXECUT(1)/ITERAT/MAXITE", 100 )
    setAnalysisCommandDetail( "Non-Linear", "Structural nonlinear", "EXECUT(1)/ITERAT/METHOD/METNAM", "SECANT" )
```

```
1264     setAnalysisCommandDetail( "Non-Linear", "Structural nonlinear", "EXECUT
    (1)/ITERAT/CONVER/SIMULT", True )
1265     setAnalysisCommandDetail( "Non-Linear", "Structural nonlinear", "EXECUT
    (1)/ITERAT/CONVER/FORCE", False )
1266     addAnalysisCommandDetail( "Non-Linear", "Structural nonlinear", "EXECUT
    (1)/ITERAT/CONVER/ENERGY" )
1267     setAnalysisCommandDetail( "Non-Linear", "Structural nonlinear", "EXECUT
    (1)/ITERAT/CONVER/ENERGY", True )
1268     setAnalysisCommandDetail( "Non-Linear", "Structural nonlinear", "EXECUT
    (1)/ITERAT/CONVER/ENERGY/TOLCON", 0.01 )
1269     setAnalysisCommandDetail( "Non-Linear", "Structural nonlinear", "EXECUT
    /EXETYP", "LOAD" )
1270     addAnalysisCommandDetail( "Non-Linear", "Structural nonlinear", "EXECUT
    (2)/LOAD/LOADNR" )
1271     setAnalysisCommandDetail( "Non-Linear", "Structural nonlinear", "EXECUT
    (2)/LOAD/LOADNR", 2 )
1272     setAnalysisCommandDetail( "Non-Linear", "Structural nonlinear", "EXECUT
    (2)/LOAD/STEPS/EXPLIC/SIZES", "1" )
1273     setAnalysisCommandDetail( "Non-Linear", "Structural nonlinear", "EXECUT
    (2)/ITERAT/MAXITE", 100 )
1274     setAnalysisCommandDetail( "Non-Linear", "Structural nonlinear", "EXECUT
    (2)/ITERAT/METHOD/METNAM", "SECANT" )
1275     setAnalysisCommandDetail( "Non-Linear", "Structural nonlinear", "EXECUT
    (2)/ITERAT/CONVER/FORCE", False )
1276     addAnalysisCommandDetail( "Non-Linear", "Structural nonlinear", "EXECUT
    (2)/ITERAT/CONVER/ENERGY" )
1277     setAnalysisCommandDetail( "Non-Linear", "Structural nonlinear", "EXECUT
    (2)/ITERAT/CONVER/ENERGY", True )
1278     setAnalysisCommandDetail( "Non-Linear", "Structural nonlinear", "EXECUT
    (2)/ITERAT/CONVER/ENERGY/TOLCON", 0.01 )
1279     addAnalysisCommandDetail( "Non-Linear", "Structural nonlinear", "EXECUT
    (2)/ITERAT/LINESE" )
1280     setAnalysisCommandDetail( "Non-Linear", "Structural nonlinear", "EXECUT
    (2)/ITERAT/LINESE", True )
1281     setAnalysisCommandDetail( "Non-Linear", "Structural nonlinear", "EXECUT
    (2)/ITERAT/MAXITE", 100 )
1282     setAnalysisCommandDetail( "Non-Linear", "Structural nonlinear", "EXECUT
    (2)/ITERAT/CONVER/SIMULT", False )
1283     setAnalysisCommandDetail( "Non-Linear", "Structural nonlinear", "OUTPUT
    /SELTYP", "PRIMAR" )
1284     setAnalysisCommandDetail( "Non-Linear", "Structural nonlinear", "OUTPUT
    (2)/SELTYP", "USER" )
1285     addAnalysisCommandDetail( "Non-Linear", "Structural nonlinear", "OUTPUT
    (2)/USER" )
1286     addAnalysisCommandDetail( "Non-Linear", "Structural nonlinear", "OUTPUT
    (2)/USER/STRAIN(1)/CRACK/GREEN" )
1287     addAnalysisCommandDetail( "Non-Linear", "Structural nonlinear", "OUTPUT
    (2)/USER/STRAIN(2)/CRKWDT/GREEN/LOCAL" )
1288     addAnalysisCommandDetail( "Non-Linear", "Structural nonlinear", "OUTPUT
    (2)/USER/STRAIN(3)/CRKWDT/GREEN/GLOBAL" )
1289     addAnalysisCommandDetail( "Non-Linear", "Structural nonlinear", "OUTPUT
    (2)/USER/STRAIN(4)/CRKWDT/GREEN/PRINCI" )
1290     addAnalysisCommandDetail( "Non-Linear", "Structural nonlinear", "OUTPUT
    (2)/USER/STRAIN(5)/CRKWDT/GREEN/VONMIS" )
1291     addAnalysisCommandDetail( "Non-Linear", "Structural nonlinear", "OUTPUT
    (2)/USER/STRESS(1)/CRACK/CAUCHY/LOCAL" )
1292     removeAnalysisCommandDetail( "Non-Linear", "Structural nonlinear", "
    EXECUT(2)" )
1293     #addAnalysisCommandDetail( "Non-Linear", "Structural nonlinear", "TYPE/
    GEOMET" )
```

```
    #setAnalysisCommandDetail( "Non-Linear", "Structural nonlinear", "TYPE/
    GEOMET", True )


def Execute(): #Runs analysis
    runSolver( "Non-Linear" )
    showView( "RESULT" )
    setResultPlot( "contours", "Displacements/node", "DtY" )

ProjectSettings()
Shapes()
ShapeMaterials()
ElementGeometries()
MaterialAssign()
Loads()
Retaining_Wall()
Supports()
Boundary()
BoundarySprings()
Test()
Sinkhole()
Frontpiles()
SetMesh1()
Analysis()
Execute()
```

Listing E.1: 3D quay wall code in DIANA FEA.